Novel

{1,2-*closo*-C_2B_{10}} Carbaborane Compounds

Bruce D. Reid

Thesis Presented for the Degree of

Doctor of Philosophy

University of Edinburgh

1992

Declaration

Except where specific reference is made to other sources, the work presented in this thesis is the original work of the author. It has not been submitted, in whole or in part, for any other degree. Certain of the results have been accepted for publication.

This thesis is dedicated to Marion, Douglas and Lesley, for their unconditional love and support.

From the dawn of time we came, moving silently down through the centuries. Living many secret lives, struggling to reach the time of the gathering, when the few that remain will battle to the last. No one has ever known we were among you...until now...

From the film "*Highlander*", released by Warner Bros., 1986.

Acknowledgements

Firstly, I would like to thank my supervisor, Dr. Alan Welch, for his advice, inspiration and zest which has always been forthcoming during the past three years; and for providing a certain *je ne sais quoi* to research (and the golf course !).

I am also grateful to Scott Aitken for his valuable contribution to part of the work in chapter 4, to Dr. David Reed for running the COSY NMR spectrum, to John Millar and Heather Grant for running many NMR spectra, and to the various technical staff who performed the microanalyses.

The various personalities who have graced labs. 86, 107 and 293 in my time at Edinburgh have meant that life has never been dull. Their advice, encouragement and friendly banter has been thoroughly appreciated. Restrictions of space prevent a full roll-call of those involved but you know who you are!!

Finally, thanks are due to the University of Edinburgh for use of facilities, and to the SERC for financial support.

Abstract

Chapter 1 outlines the development of carbaborane and carbametallaborane chemistries and is consequently background to the work described in this thesis. Brief descriptions of the chemistry and bonding capability of the tertiary gold(I) fragment and of chemical studies related to BNCT are also presented.

Chapter 2 describes the synthesis and characterisation of a series of σ-bonded phosphine and arsine gold(I) carbaborane compounds, 1-R'-2-{ER_3Au}-1,2-*closo*-$C_2B_{10}H_{10}$ (R' = Ph [**3**] or CH_3OCH_2 [**4**], ER_3 = PPh_3 [**a**], P(*o*-tol)$_3$ [**b**], PCy_3 [**c**], PEt_3 [**d**] or $AsPh_3$ [**e**]) by reaction between ER_3AuCl and the appropriate lithium carbaborane. The $^{11}B\{^1H\}$ NMR spectrum of 1-CH_3OCH_2-2-{PPh_3Au}-1,2-*closo*-$C_2B_{10}H_{10}$ (**4a**) is assigned by an ^{11}B-^{11}B COSY NMR experiment and by comparison with the (assigned) $^{11}B\{^1H\}$ NMR spectrum of 1-CH_3OCH_2-1,2-*closo*-$C_2B_{10}H_{11}$ (**1**). Consideration of the $^{11}B\{^1H\}$ NMR and (where appropriate) $^{31}P\{^1H\}$ NMR chemical shifts of compounds **3** and **4** by comparison with related species implies that the *closo*-carbaborane ligands function as efficient electron donating groups. Comparison of the Au-C distance in 1-CH_3OCH_2-2-{$AsPh_3Au$}-1,2-*closo*-$C_2B_{10}H_{10}$ (**4e**) and $AsPh_3AuMe$ (**5**) suggests that the gold-carbon bond in the former is stronger. This is supported by analysis of the results from EHMO calculations on model compounds. Consequently, *closo*-carbaboranes bonded to metal atoms *via* a metal-carbon σ-bond are shown to be good σ-donor ligands.

Chapter 3 discusses the synthesis and characterisation of thermally stable σ-bonded titanium(IV) carbaborane compounds by reaction of $TiCl_4$ or $CpTiCl_3$ with lithium carbaborane. Reaction of Cp_2TiCl_2 with one or two equivalents of lithium

carbaborane yielded the decomposition product Cp_2TiCl (**9**), though the latter reaction afforded a transient deep green species which is tentatively suggested as being a titanocene carbaborane compound. The molecular structure of 1-CH_3OCH_2-2-{$CpTiCl_2$}-1,2-*closo*-$C_2B_{10}H_{10}$ (**8**) was determined by X-ray crystallography and the Ti^{IV} centre was found to be 7-coordinate as a result of intramolecular coordination by the oxygen atom of the substituent ether group. Comparison of the $^{11}B\{^1H\}$ and ^1H NMR spectra of 1-CH_3OCH_2-2-{$TiCl_3$}-1,2-*closo*-$C_2B_{10}H_{10}$ (**6**) and **8** allows the structure of **6** to be proposed.

Chapter 4 details the synthesis and characterisation of a series of phosphine carbaborane compounds, starting from the new species 1-CH_3OCH_2-2-PPh_2-1,2-*closo*-$C_2B_{10}H_{10}$ (**11**), formed by reaction between PPh_2Cl and lithium carbaborane. Also synthesised were 1-CH_3OCH_2-2-{PPh_2AuCl}-1,2-*closo*-$C_2B_{10}H_{10}$ (**12**), 1-CH_3OCH_2-2-{PPh_2AuMe}-1,2-*closo*-$C_2B_{10}H_{10}$ (**13**), 1-CH_3OCH_2-2-(1'-CH_3OCH_2-2'-{PPh_2Au}-1',2'-*closo*-$C_2B_{10}H_{10}$)-1,2-*closo*-$C_2B_{10}H_{10}$ (**14**) and 1-CH_3OCH_2-2-(5',6'-{μ-PPh_2Au}-*nido*-$B_{10}H_{13}$)-1,2-*closo*-$C_2B_{10}H_{10}$ (**15**). X-ray crystallographic studies of **12** and **14** and detailed NMR studies of **11-15** are discussed. Finally, (unsuccessful) attempts to synthesise possible new BNCT reagents by linkage of carbaborane to an amino-acid through gold are also described.

Chapter 5 describes the experimental techniques employed in the synthesis, characterisation and structural analysis of the compounds described in the main part of the research. The synthetic methods used in the preparation of the compounds, including their spectroscopic and analytical data, are detailed. Crystallographic methods and experimental details of the structure determinations are also outlined and the chapter concludes with a brief description of the EHMO method.

Appendix A details the synthesis of two π-carbaruthenaborane compounds,

1-CH_3OCH_2-3-(η^6-*p*-cym)-3,1,2-*closo*-$RuC_2B_{10}H_{10}$ (**20**) and 1-Ph-3-(η^6-mes)-3,1,2-*closo*-$RuC_2B_9H_{10}$ (**23**). The characterisation of **20** and **23** is accomplished by detailed NMR studies. Furthermore, the molecular structure of **23** was determined by X-ray crystallographic methods.

Appendix B lists supplementary crystallographic data derived from the structure determinations of **4e**, **5**, **8**, **12**, **14** and **23**.

Abbreviations

AO	atomic orbital
bipy	2,2'-bipyridyl
BNCT	boron neutron capture therapy
BSH	$Na_2[B_{12}H_{11}SH]$
Bu	butyl
carb'	9-SMe_2-7,8-*nido*-$C_2B_9H_{10}$
Cp	cyclopentadiene
Cp^*	pentamethylcyclopentadiene
Cy	*cyclo*-hexyl
COSY	correlated spectroscopy
EHMO	extended Hückel molecular orbital
Et	ethyl
Et_2O	diethyl ether
FTIR	fourier transform infra-red
h	hour(s)
HOMO	highest occupied molecular orbital
hy	hybrid
IR	infra-red
LCAO	linear combination of atomic orbitals
Me	methyl
mes	mesitylene
MO	molecular orbital
NCCS	neutron capture cross-section
NMR	nuclear magnetic resonance
o-tol	*ortho*-tolyl
p-cym	*para*-cymene
p	page
Ph	phenyl
ppm	parts per million
PSEP	polyhedral skeletal electron pair
RI	relative integral
SEP	skeletal electron pairs
THF	tetrahydrofuran
tht	tetrahydrothiophene
TLC	thin layer chromatography

Abbreviations for Specific Compounds

1 1-CH_3OCH_2-1,2-*closo*-$C_2B_{10}H_{11}$

2 1-Ph-1,2-*closo*-$C_2B_{10}H_{11}$

3a 1-Ph-2-{PPh_3Au}-1,2-*closo*-$C_2B_{10}H_{10}$

3b 1-Ph-2-{$P(o\text{-tol})_3Au$}-1,2-*closo*-$C_2B_{10}H_{10}$

3c 1-Ph-2-{PCy_3Au}-1,2-*closo*-$C_2B_{10}H_{10}$

3e 1-Ph-2-{$AsPh_3Au$}-1,2-*closo*-$C_2B_{10}H_{10}$

4a 1-CH_3OCH_2-2-{PPh_3Au}-1,2-*closo*-$C_2B_{10}H_{10}$

4b 1-CH_3OCH_2-2-{$P(o\text{-tol})_3Au$}-1,2-*closo*-$C_2B_{10}H_{10}$

4c 1-CH_3OCH_2-2-{PCy_3Au}-1,2-*closo*-$C_2B_{10}H_{10}$

4d 1-CH_3OCH_2-2-{PEt_3Au}-1,2-*closo*-$C_2B_{10}H_{10}$

4e 1-CH_3OCH_2-2-{$AsPh_3Au$}-1,2-*closo*-$C_2B_{10}H_{10}$

5 $AsPh_3AuMe$

6 1-CH_3OCH_2-2-{$TiCl_3$}-1,2-*closo*-$C_2B_{10}H_{10}$

7 1-CH_3OCH_2-2-{(bipy)$TiCl_3$}-1,2-*closo*-$C_2B_{10}H_{10}$

8 1-CH_3OCH_2-2-{$CpTiCl_2$}-1,2-*closo*-$C_2B_{10}H_{10}$

9 Cp_2TiCl

10 1-$CH_3CH_2OCH_2$-2-{MeHg}-1,2-*closo*-$C_2B_{10}H_{10}$

11 1-CH_3OCH_2-2-PPh_2-1,2-*closo*-$C_2B_{10}H_{10}$

12 1-CH_3OCH_2-2-{PPh_2AuCl}-1,2-*closo*-$C_2B_{10}H_{10}$

13 1-CH_3OCH_2-2-{PPh_2AuMe}-1,2-*closo*-$C_2B_{10}H_{10}$

14 1-CH_3OCH_2-2-(1'-CH_3OCH_2-2'-{PPh_2Au}-1',2'-*closo*-$C_2B_{10}H_{10}$)-1,2-*closo*-$C_2B_{10}H_{10}$

15 1-CH_3OCH_2-2-(5',6'-{μ-PPh_2Au}-*nido*-$B_{10}H_{13}$)-1,2-*closo*-$C_2B_{10}H_{10}$

16 $CH_3S(AuCl)CH_2CH_2CH(COOH)NHCOCH_3$

17 $PPh_3AuSCH_2CH(COOCH_3)NH_2$

18 Tl_2[7-Ph-7,8-*nido*-$C_2B_9H_{10}$]

19 Tl_2[7-CH_3OCH_2-7,8-*nido*-$C_2B_9H_{10}$]

20 1-CH_3OCH_2-3-(η^6-*p*-cym)-3,1,2-*closo*-$RuC_2B_9H_{10}$

21 1,2-$(CH_3OCH_2)_2$-3-(η^6-*p*-cym)-3,1,2-*closo*-$RuC_2B_9H_9$

22 3-(η^6-C_6Me_6)-3,1,2-*closo*-$RuC_2B_9H_{11}$

23 1-Ph-3-(η^6-mes)-3,1,2-*closo*-$RuC_2B_9H_{10}$

Contents

CHAPTER 1
BACKGROUND

1.1 Introduction

Through their isolation of a series of boron hydrides (or boranes), the pioneering research of Alfred Stock and co-workers[1] was the genesis of an area of chemistry of considerable scope and variety.

These boranes, of general formula B_nH_{n+m}, were initially thought to have hydrocarbon chain-like structures, but their electron deficiency, in terms of classical electron counting, could not be rationalised without unequivocal structural data. For example, the 22 valence electrons in B_4H_{10} are insufficient for a 13 bond-26 electron butane-type structure. As structural characterisation techniques, such as X-ray crystallography, developed, it was established that these boranes formed regular polyhedra with a {BH} fragment at each of the vertices. The rationalisation of the structure of boranes and related polyhedra is discussed in **Section 1.2.**

A series of stable polyhedral neutral carbaboranes ($C_2B_{n-2}H_n$) was suggested from molecular orbital calculations performed by Lipscomb and Hoffmann[2, 3], these being derived from the isoelectronic analogue, $[B_nH_n]^{2-}$, by replacement of two $\{BH\}^-$ vertices with two {CH} vertices. The first published carbaboranes were $C_2B_nH_{n+2}$ where n = 3, 4 and 5[4]. The development of carbaborane chemistry is discussed in **Section 1.3.**

Following the emergence of carbaboranes in the 1960's, the synthesis of the ferrocene-like species $[(C_2B_9H_{11})_2Fe]^{2-}$ was reported by Hawthorne and co-workers[5]. This first example of a carbametallaborane complex opened up a vast new area of carbaborane chemistry which has been extensively developed. **Section 1.4** gives an

overview of two distinct areas of carbametallaborane chemistry: Firstly, complexes with a transition metal π-bonded to the open face of a *nido*-carbaborane; and secondly *closo*-carbaborane ligands σ-bonded to a transition metal.

The main bulk of this research uses the late transition metal gold in the form of a tertiary phosphine gold(I) fragment and, consequently, a brief overview of this fragment's chemistry and bonding capability is discussed in **Section 1.5**.

The properties of boron within polyhedral species have some practical applications. For example, the fact that the ^{10}B isotope (20% abundance) has an unusually high neutron capture cross-section (NCCS) has been exploited with the development of the boron neutron capture therapy (BNCT) treatment of (brain) tumours. **Section 1.6** outlines the theory and practicalites behind BNCT.

This introductory chapter concludes with details of the scope of work covered by the thesis (**Section 1.7**).

1.2 Polyhedral Structures and Bonding

The boranes and carbaboranes form polyhedral structures and classification of these structures has been made in terms of their geometry. As the boranes and carbaboranes are isoelectronic the classification applies to both species. There are four main classes: *Closo* (greek meaning "closed") which describes regular polyhedra consisting entirely of triangulated faces. For example, 2,3-$C_2B_9H_{11}$ (**Figure 1.1a**) has a *closo* geometry; *nido* ("nest") is a *closo* structure with one vertex removed revealing an open face, for example, 5,7-$C_2B_8H_{12}$ (**Figure 1.1b**); *arachno* ("web") is a *closo* structure with two vertices removed, for example 1,3-$C_2B_7H_{13}$ (**Figure 1.1c**); finally, *hypho* ("network") is a *closo* structure with three vertices removed, $[B_5H_{12}]^-$ (**Figure 1.1d**) being an example of a *hypho*-borane.

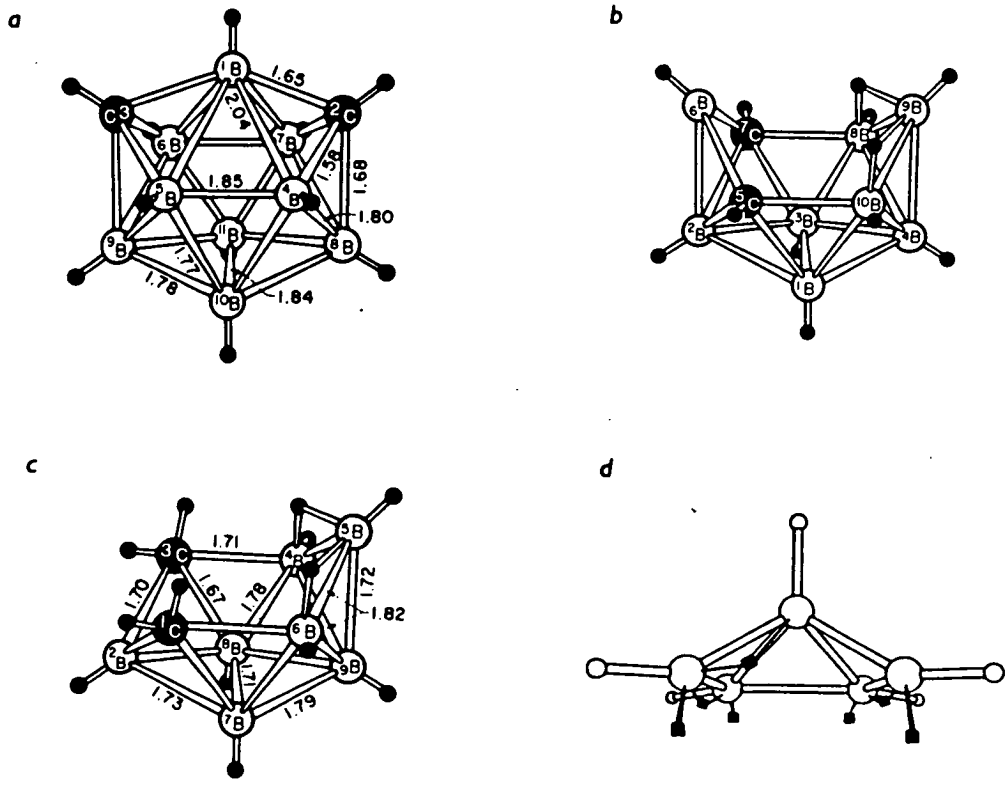

Figure 1.1 Examples of (a) *closo*, (b) *nido*, (c) *arachno* and (d) *hypho* Structures.

As the total number of valence electrons is less than the total number of valence atomic orbitals (AOs) available for bonding, the boranes and carbaboranes, in terms of classical electron counting, appear to be electron deficient. Their molecular structures cannot be represented entirely in terms of classical 2 centre-2 electron bonding because there are insufficient electrons for the required (classical) bonds. The existence of such species therefore signifies that the nature of their bonding must extend beyond the concept of a 2 centre-2 electron bond. Indeed, the rationalisation of the structures and bonding of the boranes has transformed the ways in which chemists think about bonding.

The first attempt to clarify the bonding in polyhedral boranes was made by Lipscomb[6] who developed the concept of the multicentre bond; localised valence-bond structures incorporating 2- and 3- centre-2 electron bonds. The 3 centre-2 electron bond approach to describe BHB, open BBB and closed BBB interactions (**Figure 1.2**) was useful for the small and more open cage boranes but, for more symmetrical species and for large polyhedral boranes, the localised approach becomes tremendously intricate.

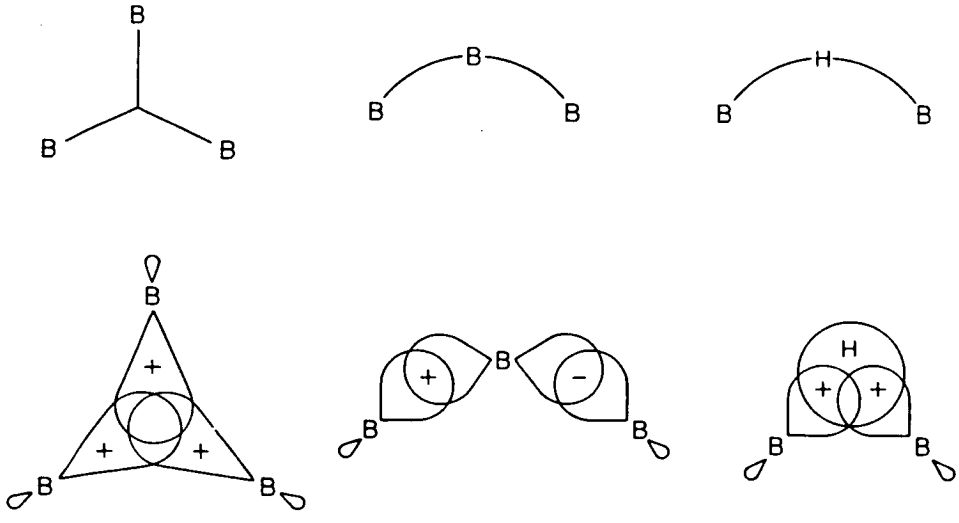

Figure 1.2 Borane 3 centre-2 electron Bonding Arrangements.

Another approach, using quantitative molecular orbital calculations on individual polyhedral systems, has been used for a number of boranes and carbaboranes, but the introduction of a metal atom into the polyhedral framework (of which there are numerous examples, *vide infra*) complicates the calculations immensely.

The structures of polyhedral boranes and carbaboranes have been most successfully rationalised by polyhedral skeletal electron pair (PSEP) theory[7, 8]. This set of electron counting rules considers the total number of skeletal electrons involved in the polyhedral framework and takes into account its overall size, charge and atomic composition: The total number of electrons available for skeletal bonding is counted, this being the sum of the number of electrons each vertex fragment (for example {BH} or {CH}) has available for cluster bonding plus electrons associated with "extra", usually bridging, hydrogen atoms and/or the overall charge on the molecule. This total is divided by 2 to give the number of skeletal electron pairs (SEP). The relationship between the number of SEP and geometry for a cluster with *n* vertices is summarised in **Figure 1.3**. For carbaboranes of general formula $[(CH)_a(BH)_mH_b]^{c-}$ these rules can be adapted to give a relationship between the sum of *a*, *b* and *c* and the molecular geometry as outlined in **Figure 1.3**.

No. SEP	*a*+*b*+*c*	Geometry
n+1	2	*closo*
n+2	4	*nido*
n+3	6	*arachno*
n+4	8	*hypho*

Figure 1.3 Rationalisation of Geometry from PSEP Theory.

The number of electrons a {BH} vertex contributes to cluster bonding is determined by consideration of its frontier molecular orbitals (MOs) (**Figure 1.4**). A

boron atom has 3 valence electrons in the $2s$ and $2p$ atomic orbitals and a hydrogen atom has 1 electron in the $1s$ orbital. Combination of the hydrogen atom $1s$ AO with a boron atom $2sp_z$ hybrid orbital (formed by mixing of the $2s$ and $2p_z$ AOs) produces a (filled) bonding MO and an (empty) anti-bonding MO, thus forming a 2 electron boron-hydrogen bond. The remaining (filled) $2sp_z$ and (empty) $2p_x$ and $2p_y$ orbitals are available for cluster bonding and, consequently, a {BH} fragment contributes 3 orbitals and 2 electrons to cluster bonding. Similarily, a {CH} vertex has 3 electrons and 3 orbitals available for cluster bonding.

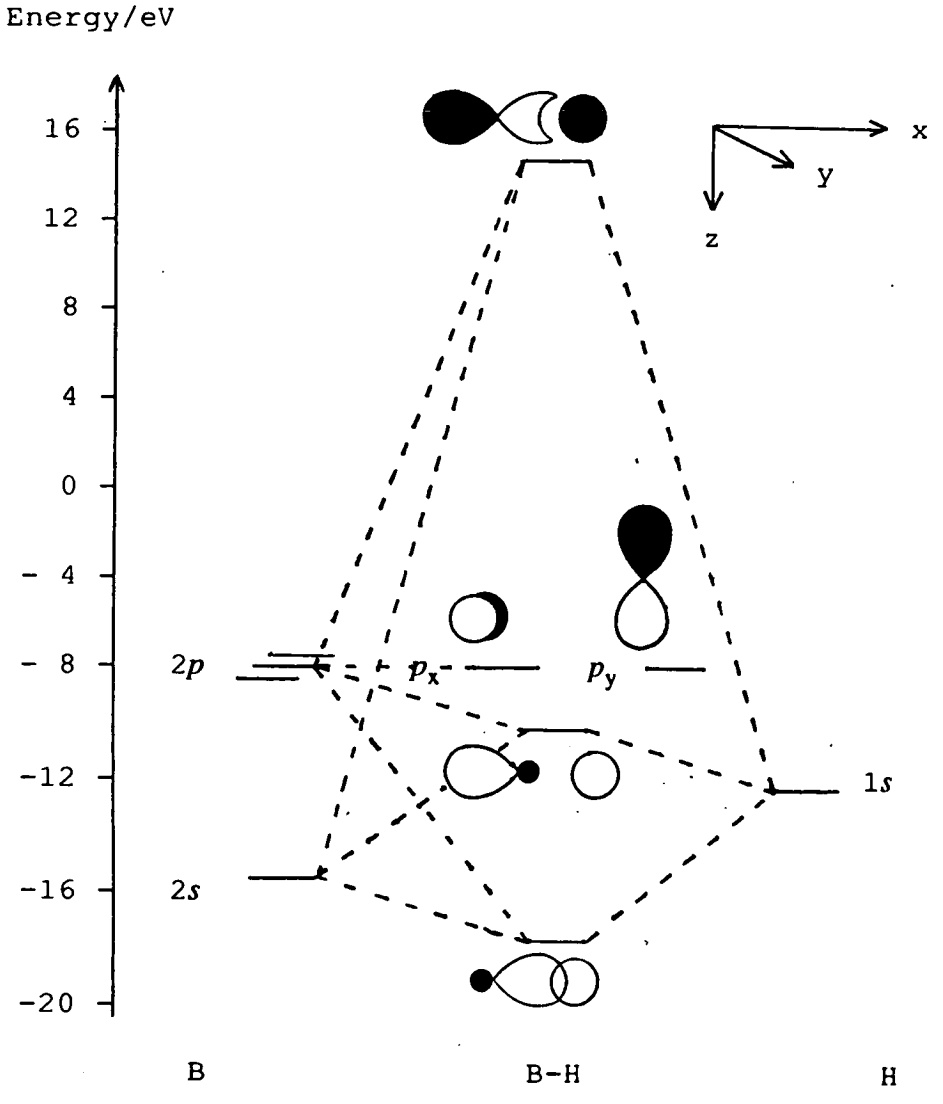

Figure 1.4 Frontier Molecular Orbitals of a {BH} Fragment.

Therefore, using PSEP theory, the structure of $[C_2B_{10}H_{13}]^-$, for example, can be rationalised in the following way:

Skeletal electron source	No. electrons
2 x {CH}	6
10 x {BH}	20
1 x H	1
-ve charge	1
Total =	28
∴ No. SEP =	14

n+2 SEP corresponds to a *nido* structure, as observed by crystallographic determination[9]. Also, $a + b + c = 4$ (2+1+1), again corresponding to a *nido* structure.

Significantly, the rules defined by PSEP theory can be applied to boranes and carbaboranes containing other heteroatoms, in particular transition metals, in order to predict their structure. For a transition metal vertex the number of electrons available for cluster bonding, e, is given by $e = v + x - 12$, where v is the number of valence electrons of the metal and x is the number of electrons contributed by the ligands bonded to the metal.

The structure of (for example) 1-Ph-3-(η^6-$C_6H_3Me_3$)-3,1,2-$RuC_2B_9H_{10}$ can therefore be rationalised by PSEP theory as follows:

Skeletal electron source	No. electrons
1 x {CH}	3
1 x {CPh}	3
9 x {BH}	18
1 x {arene Ru}	2*
Total =	26
∴ No. SEP =	13

* $e = 8 + 6 - 12$ for {(η^6-arene Ru^{II}}

n+1 SEP corresponds to a *closo* structure, a prediction which is consistent with the crystallographic determination of its molecular structure (see **Appendix A**).

The determination of *e*, the number of electrons contributed to cluster bonding by a transition metal fragment, allows the expansion of PSEP theory to the prediction of the molecular geometry of metal clusters. For example, $[Ru_6(CO)_{18}]^{2-}$ contains *n*+1 SEP (6 x $\{Ru(CO)_3\}$ where $e = 2$ for each fragment plus the dianionic charge gives 14 skeletal electrons) and exhibits the predicted *closo* structure.

As with any set of rules there are exceptions and a notable example in PSEP theory is B_8H_{12} which has *n*+2 (10) SEP predicting a *nido* geometry but, in reality, exhibits an *arachno* structure. Although the anomaly has yet to be fully rationalised it has been observed[10] that the neutral *arachno*-B_8H_{12} is more stable than the PSEP-precise [*arachno*-B_8H_{12}]$^{2-}$. The relative stability of these *arachno* species was determined by analysis of the frontier MOs of the related $\{B_8H_{10}\}^{2-}$ and $\{B_8H_{12}\}^{4-}$ fragments with imposed *arachno* geometry: The highest occupied molecular orbital (HOMO) in {*arachno*-B_8H_{10}}$^{2-}$ is bonding, but in {*arachno*-B_8H_{10}}$^{4-}$ it is strongly antibonding. It was observed that introduction of $2H^+$ (to produce *arachno*-B_8H_{12} and [*arachno*-B_8H_{12}]$^{2-}$ respectively) would stabilise the former but, because of the occupation of a strongly antibonding MO, would not stabilise the latter. Consequently, it appears that *arachno*-B_8H_{12} is more stable than [*arachno*-B_8H_{12}]$^{2-}$ and this may partly explain the anomalous (with respect to PSEP theory) structure of B_8H_{12}.

In summary, the boranes and carbaboranes are polyhedral molecules, adopting unusual structures with multicentre bonding to overcome their apparent electron deficiency. Their structures can generally be predicted from PSEP theory, a theory which can also be applied to polyhedral frameworks not necessarily containing boron, for example low valent metal clusters.

1.3 *closo*-Carbaboranes

The neutral *closo*-carbaboranes have the general formula $C_2B_nH_{n+2}$ (except CB_5H_7) where n is mostly 3 to 10, and are generally more stable than their air- and moisture- sensitive neutral borane precursors. This stability has seen the rapid development of carbaborane chemistry since its inception in 1963[11, 12]. Such was the meteoric rise of carbaborane chemistry that by 1970 an extensive review had been published[13]. The research in this thesis uses carbon-substituted derivatives of the icosahedral 1,2-*closo*-$C_2B_{10}H_{12}$ (*ortho*-carbaborane) and consequently this section concentrates on the synthesis and chemistry of *ortho*-carbaborane and its derivatives.

At this point it is worth noting the standard atom numbering procedure used for an icosahedral carbaborane: For all cage systems, heteroatoms take the lowest possible numbers with established rules of precedence applying (with carbon always first) when two or more different heteroatoms are present. In {*closo*-C_2B_{10}} cage systems, numbering begins with one of the carbon atoms and in {*nido*-C_2B_9} systems, the boron atom opposite the open C_2B_3 face is assigned atom 1. In both, numbering proceeds in a clockwise direction around successive pentagonal faces taking account of the heteroatom requirement. In moving from one pentagonal ring to the other in an icosahedron, a connectivity is crossed. **Figure 1.5** illustrates the numbering used for a mono carbon-substituted derivative of *ortho*-carbaborane, the substituted carbon being assigned position 1. *Ortho*-carbaborane has C_{2v} symmetry its mono-carbon-substituted derivatives have C_s symmetry. The plane of symmetry lies on the C(1)-C(2) vector [and the B(9)-B(12) vector since B(9) and B(12) are opposite C(2) and C(1) respectively]. Consequently, B(9) and B(12) are symmetry unique boron atoms while B(3), B(4), B(7) and B(8) are related by symmetry to B(6), B(5), B(11) and B(10) respectively.

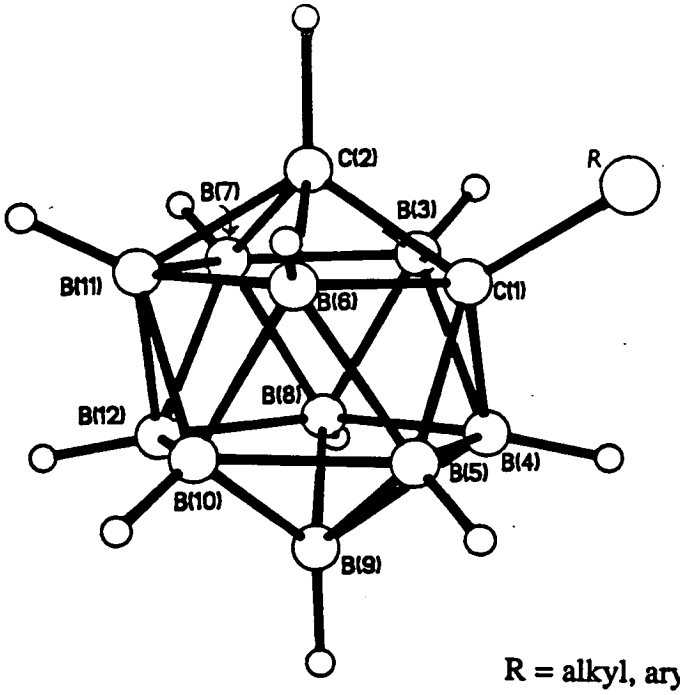

Figure 1.5 1-R-1,2-*closo*-$C_2B_{10}H_{11}$ Illustrating Numbering Scheme Adopted.

1.3.1 Synthesis of Icosahedral 1,2-*closo*-Carbaboranes

The icosahedral 1,2-*closo*-carbaboranes are readily synthesised from decaborane(14) in a two-step synthesis as illustrated in **Figure 1.6**. *Nido*-$B_{10}H_{14}$ reacts with the Lewis base to form the more open *arachno*-$B_{10}H_{12}(base)_2$, alkyne subsequently inserting into the open face of this to form the icosahedral *closo*-carababorane with loss of base. The substituted alkynes RC≡CH and RC≡CR' (R, R' = alkyl, aryl and alkenyl) are used to prepare a number of carbon-substituted *ortho*-carbaborane derivatives[13]. Furthermore, ester, ether, halogen, sulphur and nitrogen derivatives have been prepared in this way using the appropriate alkyne[13].

Although less common than carbon-substituted derivatives, boron-substituted derivatives of *ortho*-carbaborane are known, for example an ethyl boron-substituted

ortho-carbaborane has been prepared from ethyldecaborane(13) and acetylene[11].

The stability and ease of preparation of the carbaboranes in good yields has meant that their chemistry has been extensively, though not exhaustively, studied[13, 14].

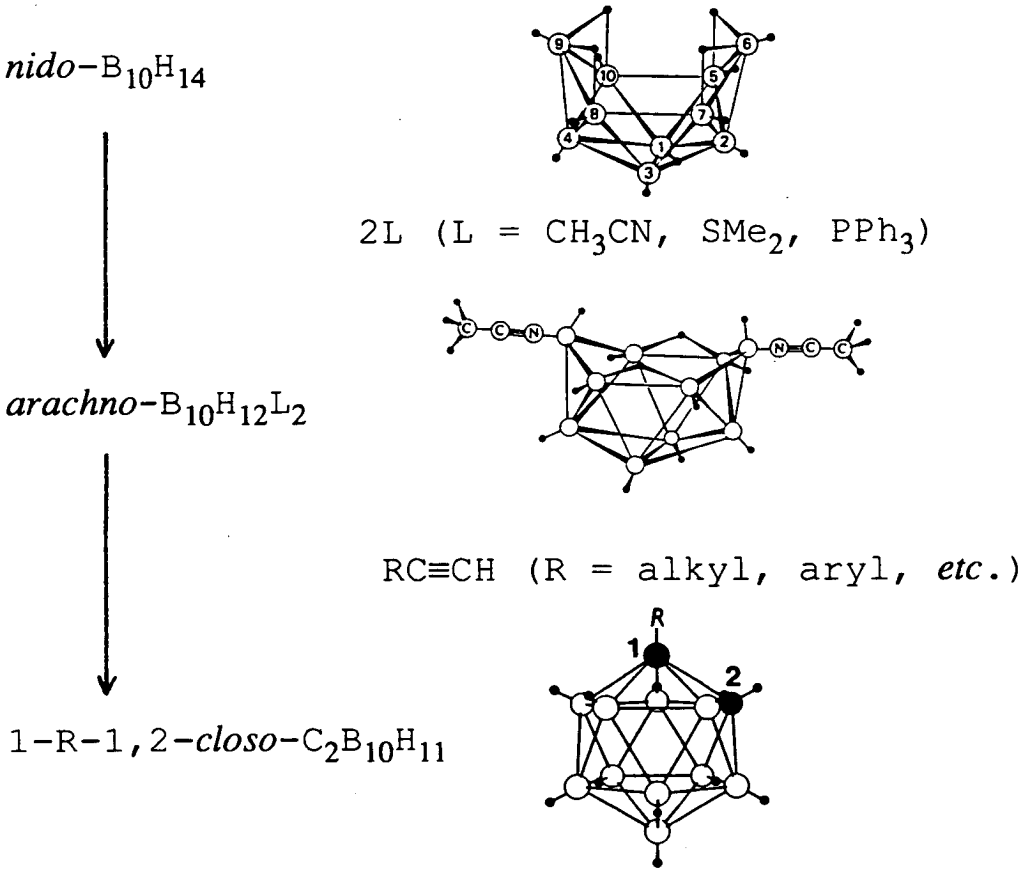

Figure 1.6 Synthesis of Icosahedral 1,2-*closo*-Carbaboranes from *nido*-$B_{10}H_{14}$.

1.3.2 Chemistry of *ortho*-Carbaborane

The chemistry of *ortho*-carbaborane has been thoroughly explored and some of the reactions are displayed in **Figure 1.7**. The basis for all these reactions involves the abstraction of hydrogen terminally bonded to the cage carbons. The hydrogen atoms on the carbon atoms are readily and preferentially abstracted by alkyl lithium reagents (RLi), for example MeLi, because they are more (weakly) acidic than the hydrogen atoms bonded to cage boron atoms: Simply, carbon is more electronegative than boron and consequently induces a greater δ+ on the hydrogen atom. Removal of the

hydrogen atom(s) forms the reactive (di)lithium salt of the carbaborane and the formation of LiCl is the driving force for the reactions detailed in **Figure 1.7**. For 1,2-*closo*-$C_2B_{10}H_{12}$, the preparation of the monolithium derivative (1 equivalent of RLi) is complicated by an equilibrium between the monolithium and dilithium species in Et_2O or Et_2O-C_6H_6 solution[15] (**Figure 1.8**). However, in benzene solution the equilibrium remains to the left and so the monolithium species is predominant. On addition of a second equivalent of RLi the dilithium carbaborane is exclusively produced.

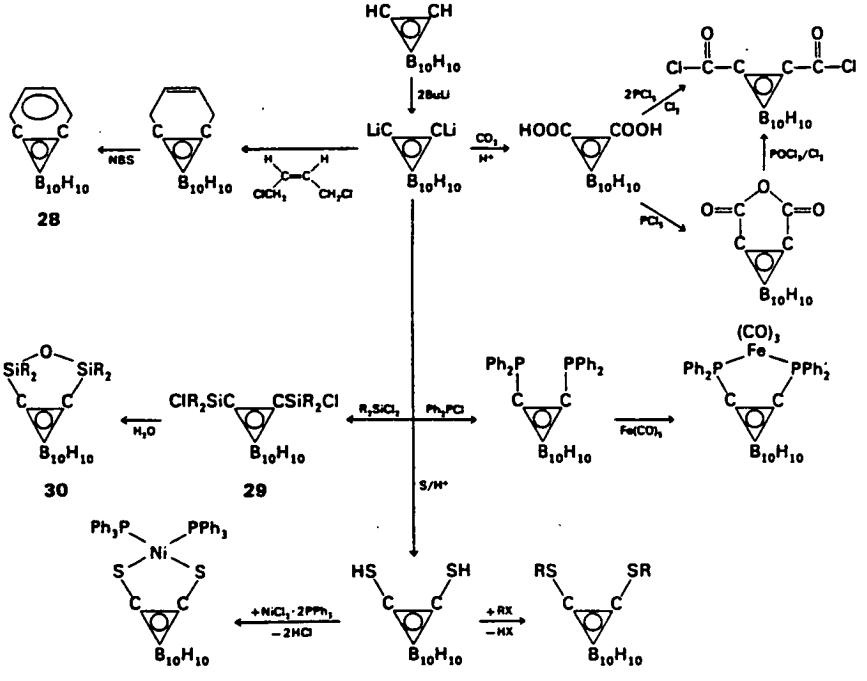

Figure 1.7 Some Representative Reactions of 1,2-*closo*-$C_2B_{10}H_{12}$.

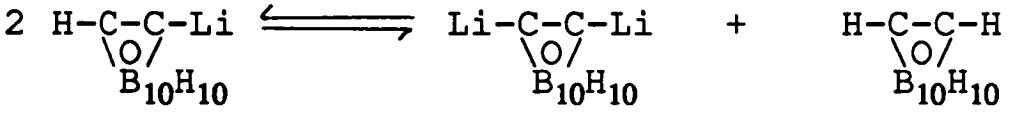

Figure 1.8 Equilibrium on Lithiation of 1,2-*closo*-$C_2B_{10}H_{12}$ in Ethereal Solvents.

1.3.3 Characterisation of 1,2-*closo*-Carbaboranes

Carbaboranes are readily characterised by a number of techniques. A common non-spectroscopic method used is microanalysis with results generally consistent with the expected (calculated) formulations. Microanalysis results have been used as the only characterisation for some derivatised carbaboranes[11, 12].

However, the majority of techniques employed for characterisation are spectroscopic. Infra-red spectra of carbaboranes have a distinctive strong broad band between 2500 and 2660 cm^{-1} attributed to $B\text{-}H_{terminal}$ vibrations and, when present, the $C\text{-}H_{terminal}$ stretch is found in the region 2900-3160 cm^{-1} [16].

Boron-11 NMR spectroscopy has been extensively used for the characterisation of carbaboranes and can be used to determine the number and connectivities of the boron atoms present in a cage system. ^{11}B NMR spectra give resonances due to the boron atoms present and include coupling to the bound hydrogen atoms. Broad band decoupling produces a standard decoupled spectrum. Using these one-dimensional spectra to assign specific resonances to specific boron atoms is not a trivial task since the geometrical relationships between one atom and another in the cage can produce 'peculiarities' in the ^{11}B NMR spectrum. For example, the antipodal effect is the effect upon an atom due to the one directly opposite it (e.g. atoms 1 and 12 or 2 and 9 in **Figure 1.5**). Empirical rules for predicting ^{11}B NMR spectra of polyboron species which take into account these relationships have been discussed by Teixidor *et al*[17].

Assignment of the resonances to specific boron atoms in the cage system is currently (and effectively) achieved using $^{11}B\text{-}^{11}B$ COSY NMR spectroscopy[18]. By showing cross peaks between coupled boron atoms, the COSY NMR spectrum allows a connectivity map of peak positions to be determined, and thus assignment of the peaks is generally possible.

Carbaboranes have been structurally characterised using electron diffraction methods, for example *ortho*-carbaborane[19], but X-ray crystallography is regarded as the ultimate analytical technique. Certainly, complete (except occasionally hydrogen atom positions, especially in presence of heavy atoms) structural information (atom positions, interatomic bonds and distances *etc.*) is obtained from the results of X-ray diffraction studies, but a restriction is that the compound must, of course, be crystalline. However, this seems not to be a problem in carbaborane chemistry with numerous carbaboranes and their derivatives structurally characterised by X-ray diffraction studies.

1.3.4 Parent *closo*-Carbaboranes

The "parent" *closo* carbaboranes refers to the mono- (carbon) substituted derivatives of *ortho*-carbaborane used in the research described in this thesis: 1-CH_3OCH_2-1,2-*closo*-$C_2B_{10}H_{11}$[20] (**1**) and 1-Ph-1,2-*closo*-$C_2B_{10}H_{11}$[11] (**2**).

The reasons for using these carbaboranes are three-fold: Firstly, they are stable solids readily produced in high yield and purity from *nido*-$B_{10}H_{14}$, $2CH_3CN$ and the appropriate alkyne RC≡CH [R = CH_3OCH_2 (**1**) or Ph (**2**)] as in **Figure 1.6.** Moreover, the alkynes used are stable liquids at room temperature and are therefore easier to handle than HC≡CH; secondly, one cage carbon carries the weakly acidic hydrogen atom and can be readily deprotonated by alkyl lithium reagents. The abstraction of this proton forms the basis of the research. Furthermore, an organic substituent on the other cage carbon has the advantage over *ortho*-carbaborane in that only the monolithium salt is formed whereas with *ortho*-carbaborane an equilibrium between the mono- and dilithium salt can occur; finally, with the lone pair of electrons on the oxygen atom of the ether substituent there is the possibility of oxygen interaction with other substituents (*vide infra*). Geometrical calculations[21]

with a metal in the B(3) position approximately 2.7 Å above the C_2B_3 face and a $ROCH_2$- group on C(1) have shown that a metal-oxygen interaction can be achieved with sensible bond lengths, angles and torsions (actual examples from the literature are discussed in **Section 1.4**). As no such interaction can occur with the phenyl derivative, it can be used as a comparison.

Compound **1** has been fully characterised[20]: The solid state structure in **Figure 1.9** shows two molecules of **1** in the asymmetric fraction of the unit cell which are reciprocally hydrogen-bonded, the bond between the ether oxygen atom of one molecule and the cage C-*H* of the other. The ^{11}B NMR spectrum of **1** was fully assigned by ^{11}B-^{11}B COSY NMR spectroscopy (**Figure 1.10**). The ^1H NMR spectrum showed two sharp peaks and one broad peak of relative integral 3:2:1 (δ 3.36, 3.79 and 4.00 ppm) corresponding to OCH_3, OCH_2 and C_{cage}-*H* respectively.

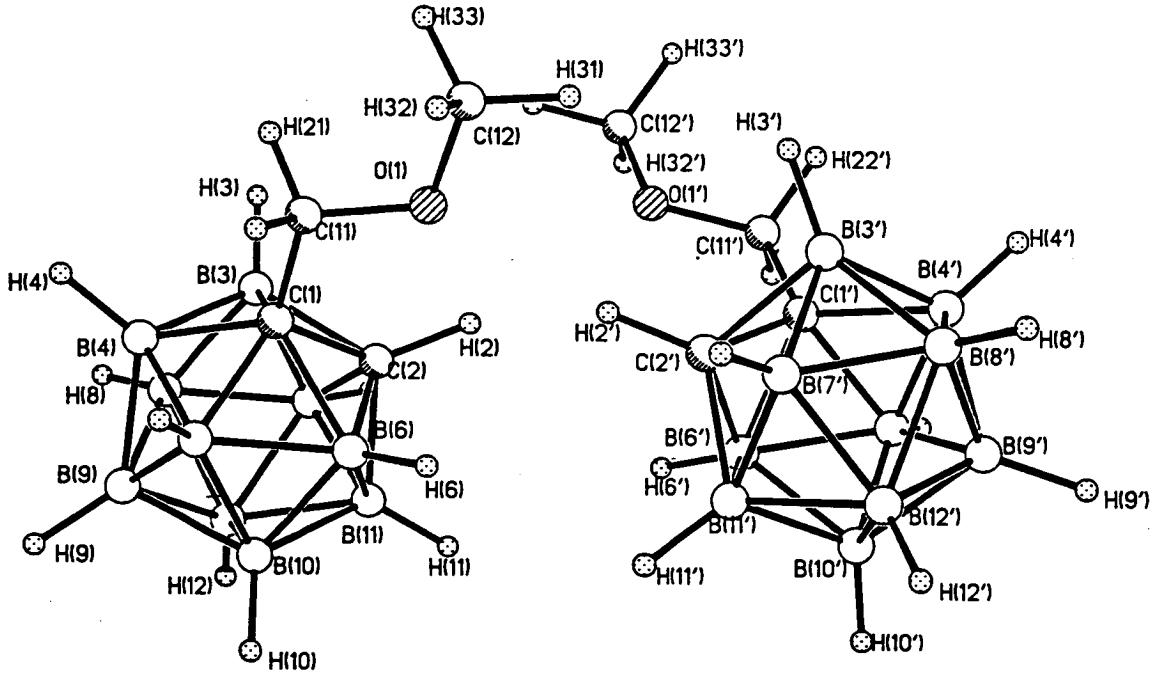

Figure 1.9 Molecular Structure of 1-CH_3OCH_2-1,2-*closo*-$C_2B_{10}H_{11}$.

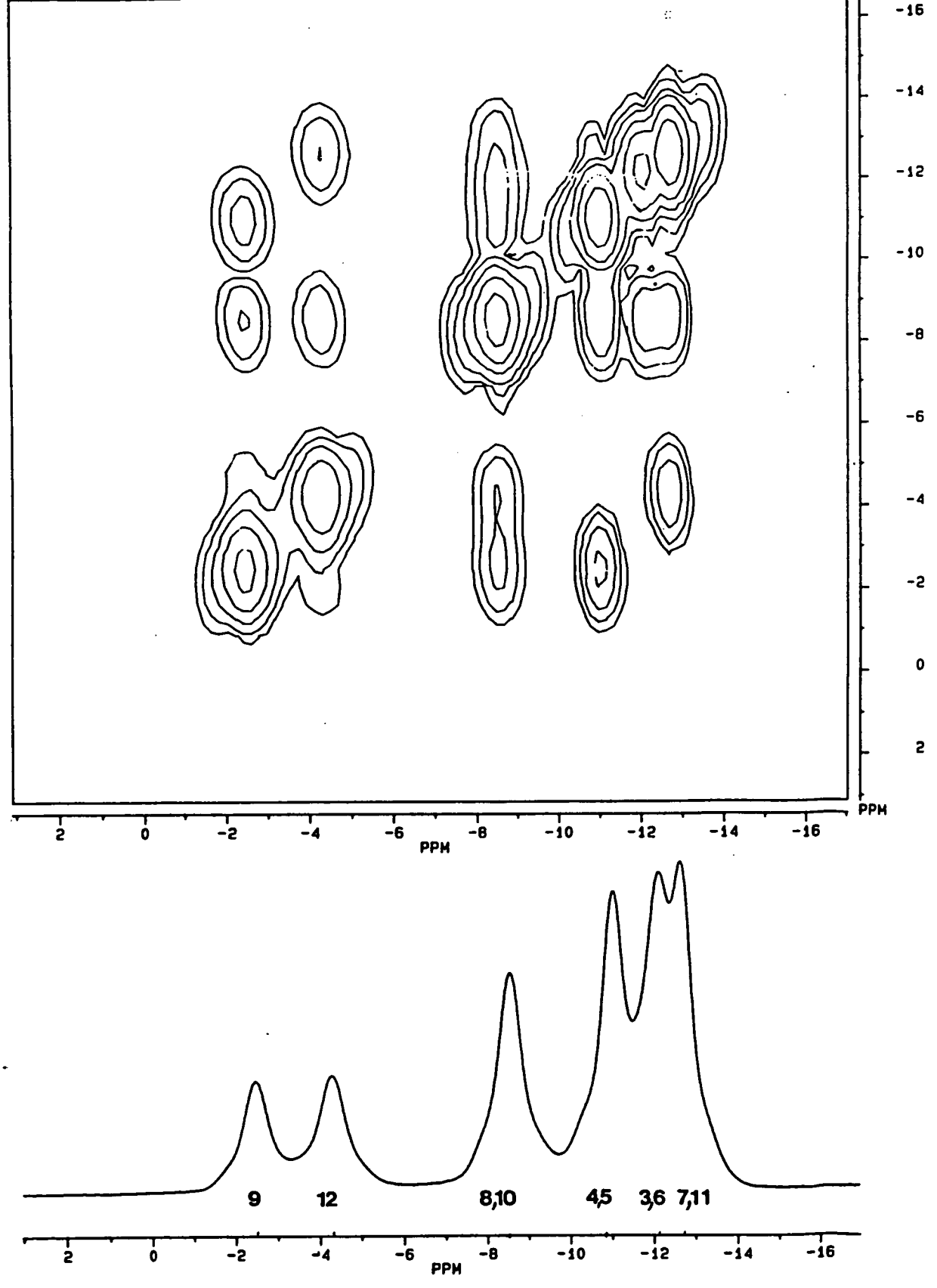

Figure 1.10 ^{11}B-^{11}B NMR Spectrum and Assignment of 1-CH_3OCH_2-1,2-*closo*-$C_2B_{10}H_{11}$.

The full characterisation of **2** has not been reported in the literature and so relevant details appear in the main part of the thesis when appropriate, for example $^{11}B\{^1H\}/^{11}B$ NMR and ^1H NMR spectra appear in **Figures 2.3** and **2.4** in **Chapter 2.**

The CH_3OCH_2- and Ph- groups are both electron withdrawing with respect to the carbaborane. The effect of the electron withdrawal on the electron density distribution within the carbaborane cage has been studied by consideration of the shift in the boron resonances in the ^{11}B NMR spectra of a number of carbaboranes. For example, it was found that successive substitution of H by CH_3OCH_2-[21] or by Ph- at the carbon atoms of 1,2-*closo*-$C_2B_{10}H_{12}$ resulted in an overall shift of the boron resonances in the ^{11}B NMR spectra to higher frequency, and a narrowing of the spectrum width (highest-lowest frequency resonance), consistent with electron density removal from the cage (**Figure 1.11**).

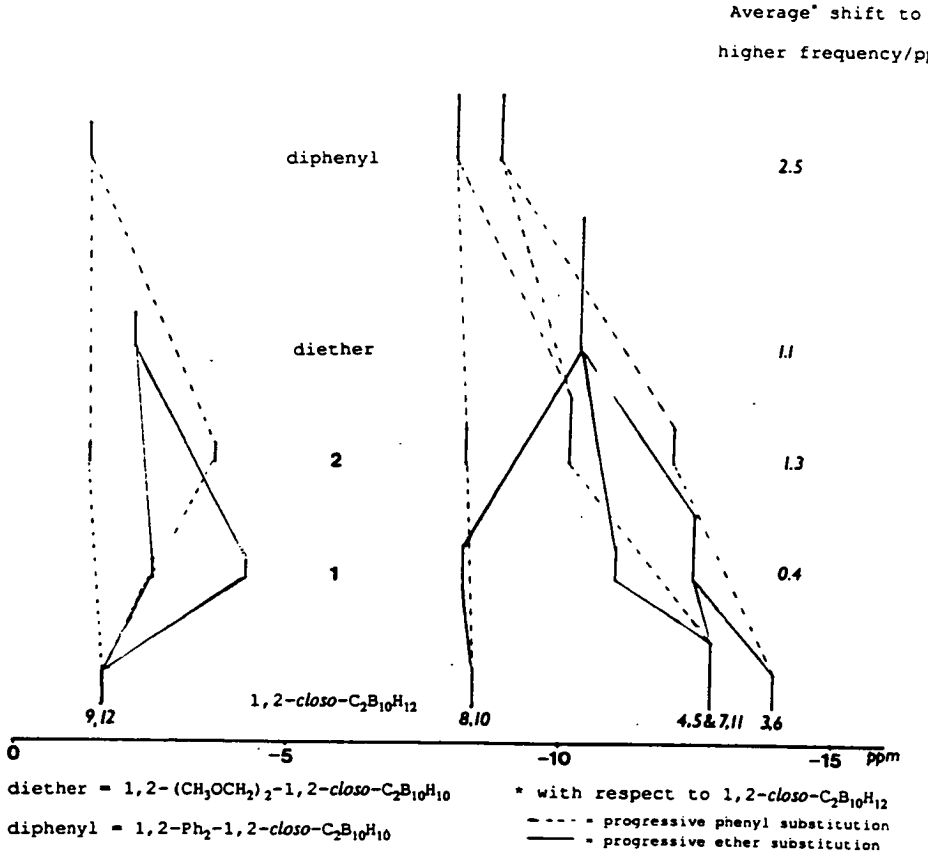

Figure 1.11 Comparison of $^{11}B\{^1H\}$ NMR Spectra of 1,2-*closo*-$C_2B_{10}H_{12}$ and its Mono- and Di- Ether and Phenyl Derivatives.

1.4 Carbametallaboranes

The relative stability and high synthetic yields of *ortho*-carbaborane and its derivatives has meant that many carbametallaborane species have been synthesised and characterised[22]. Indeed, the first carbametallaborane reported, $[(C_2B_9H_{11})_2Fe]^{2-}$[5], is a derivative of *ortho*-carbaborane, the two [7,8-*nido*-$C_2B_9H_{11}]^{2-}$ cages coordinating the iron(II) metal centre are produced by selective removal of a $\{BH\}^{2+}$ vertex (deboronation) from 1,2-*closo*-$C_2B_{10}H_{12}$. By using a strong base, the deboronation of *ortho*-carbaborane and its *closo*-derivatives occurs readily and in good yields[23].

This section gives an overview of two distinct areas of carbametallaborane chemistry: Firstly, π-carbametallaboranes where the metal is π-bonded to the open face of the {*nido*-C_2B_9} species; and secondly, σ-carbametallaboranes where the metal is σ-bonded (*i.e. via* a 2 centre-2 electron bond) to one of the cage atoms (usually carbon) of the {*closo*-C_2B_{10}} species.

Carbametallaboranes have recently[24] been classified into three groups: Class 1 refers to a carbametallaborane where the metal occupies a polyhedral vertex; class 2 refers to those where the metal atom bridges a polyhedral edge; and class 3 are those in which the metal and cage are connected *via* a single 2 centre-2 electron bond. This classification is used throughout this thesis to define the type of carbametallaborane under discussion.

1.4.1 π-Carbametallaboranes

By far the most extensive area of carbametallaborane chemistry involves carbametallaboranes in which the metal occupies a central vertex position to produce a class 1 *closo*-carbametallaborane (or a distorted *closo* structure in "slipped" species; *vide infra*). This continues to be a widely researched area because of the analogy

between $[C_2B_9H_{11}]^{2-}$ and $[C_5H_5]^-$ (Cp^-)[25], and latterly $[C_5Me_5]^-$ (Cp^{*-})[26], whereby both ions have similar frontier molecular orbitals containing 6 π-electrons and therefore have similar bonding capabilities. As a result a plethora of carbametallaborane analogues of Cp have been synthesised, including those of all the first row transition metals between Cr and Cu. An important difference between the *nido*-carbaborane and Cp anions is demonstrated by the ability of the *nido*-carbaborane to stabilise high oxidation states of late transition metals (for example, Ni^{IV}) and low oxidation states of early transition metals (for example, Ti^{II}). These enhanced donor properties exhibited by $\{nido\text{-}C_2B_9\}^{2-}$ over Cp^- have also resulted in the formation of carbaborane sandwich complexes of $Pd^{II\text{-}IV}$, $Cu^{II\text{-}III}$ and $Au^{II\text{-}III}$ whereas the Cp analogues are not known.

Structurally these sandwich complexes fall into two categories: The symmetrical sandwich (**Figure 1.12a**); and the slipped sandwich where the metal does not occupy the central vertex position (**Figure 1.12b**). The slippage can be explained by the metal atom avoiding the adoptance of an electron configuration greater than 18 electrons. The structures of the latter have been the subject of much discussion[27, 28].

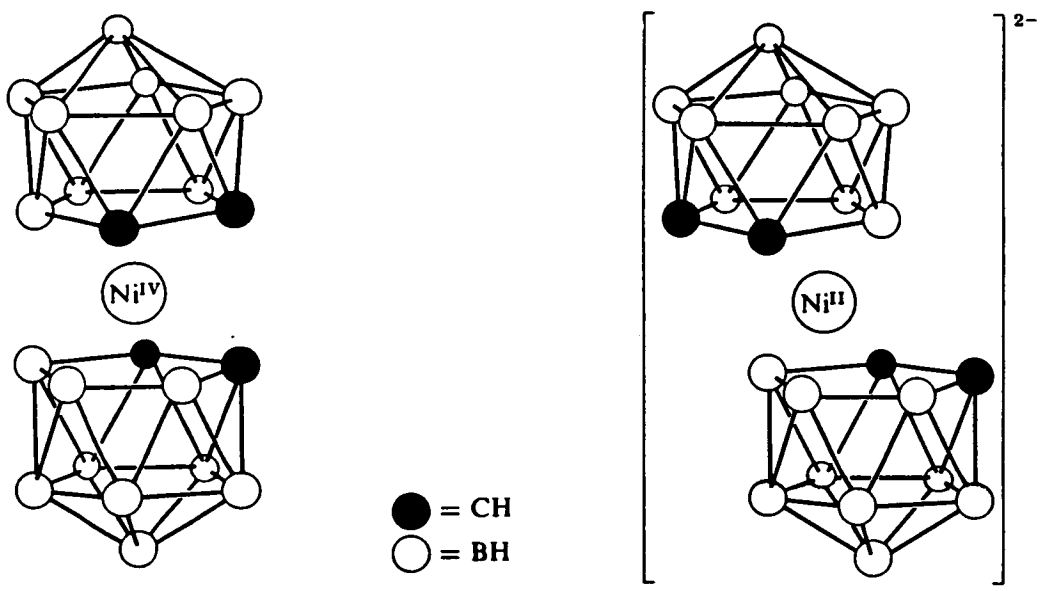

Figure 1.12 π-Carbametallaborane Sandwich Complexes: (a) Ni^{IV}; (b) Ni^{II}.

The Cp^- / {*nido*-C_2B_9}$^{2-}$ analogy has been further explored through the synthesis of charge compensated species such as [9-SMe_2-7,8-*nido*-$C_2B_9H_{10}$]$^-$ ([carb']$^-$)[29]. In this the SMe_2 group reduces the formal negative charge on the open C_2B_3 face from 2- to 1-, thus making it more comparable to the monoanionic Cp^-. **Figure 1.13** shows the structure of a class 1 transition metal carb' species, 3,3,3-$(OC)_3$-4-SMe_2-3,1,2-*closo*-$MnC_2B_9H_{10}$, formed by the reaction of $[Mn(CO)_3(NCMe)_3][BPh_4]$ and Tl[carb'][30].

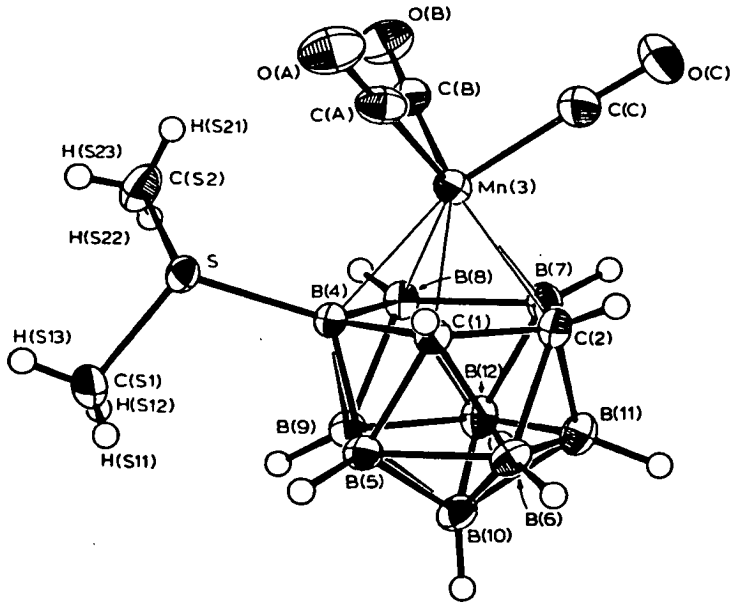

Figure 1.13 Molecular Structure of 3,3,3-$(OC)_3$-4-SMe_2-3,1,2-*closo*-$MnC_2B_9H_{10}$.

Other examples of the capping of the C_2B_3 face by an organometallic transition metal fragment include 3-(η^6-C_6Me_6)-3,1,2-*closo*-$RuC_2B_9H_{11}$[31] and 1-Ph-3-(η-C_9H_7)-3,1,2-*closo*-$CoC_2B_9H_{10}$[32]. The latter is an example of a carbon-substituted derivative of a $MC_2B_9H_{11}$ species with a phenyl ring bound to one of the cage carbon atoms.

Recent literature concentrates on using the substituents on the cage either to produce structural changes in the polyhedron or for coordination with the metal. An

example of the former is 1,2-Ph_2-3-Cp^*-3,1,2-*pseudocloso*-$RhC_2B_9H_9$ **(Figure 1.14)** in which the steric influences of the two phenyl rings and the Cp^* result in the cage carbon atoms [C(1) and C(2)] being pushed apart leaving a non-bonding interaction of 2.51(3) Å. As a result of the deformation, B(6) is pulled out of the plane of atoms B(5), B(9), B(11) and B(12) resulting in generally long connectivities to B(6) and short C-B connectivities to C(1) and C(2)[33].

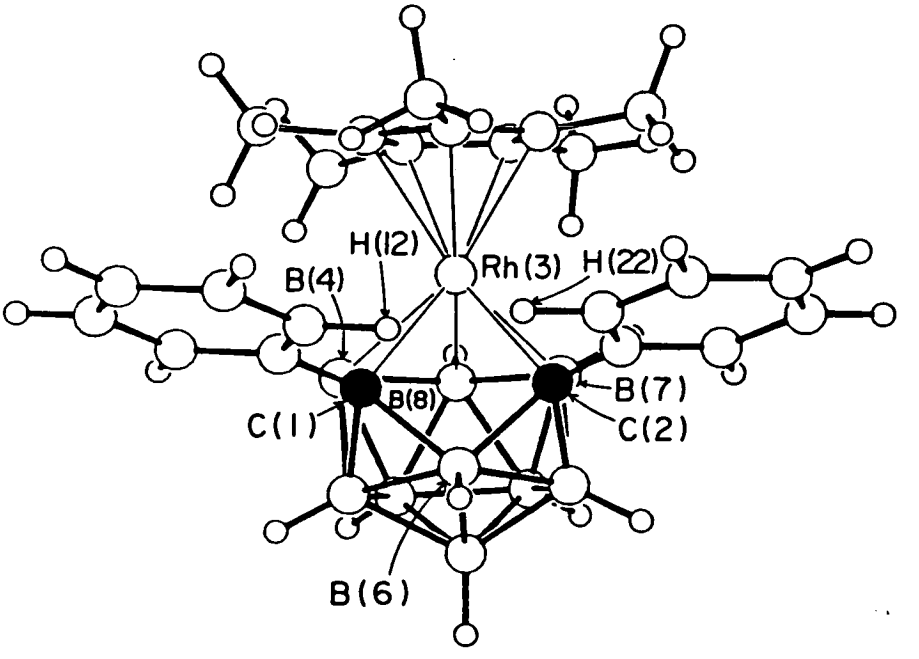

Figure 1.14 Molecular Structure of 1,2-Ph_2-3-Cp^*-3,1,2-*pseudocloso*-$RhC_2B_9H_9$.

In 7,8-$(CH_3OCH_2)_2$-10-*endo*-{PPh_3Hg}-7,8-*nido*-$C_2B_9H_9$ **(Figure 1.15)**, the two ether groups adopt an orientation such that the O(1)-Hg and O(2)-Hg distances are 3.065(4) Å and 3.070(4) Å respectively, both strongly intimating Hg-O interaction with oxygen lone-pairs of electrons donating into the empty $6p_x$ and $6p_y$ orbitals of the mercury atom[34].

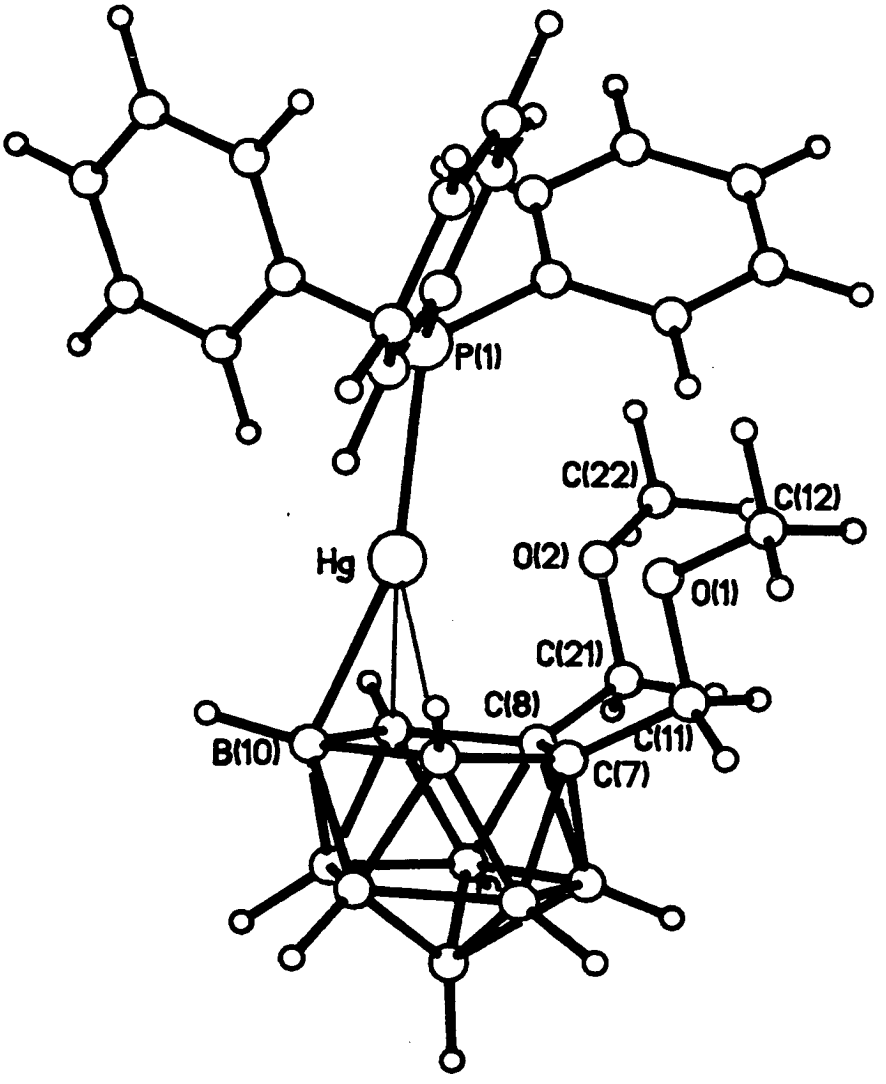

Figure 1.15 Molecular Structure of 7,8-$(CH_3OCH_2)_2$-10-*endo*-{PPh_3Hg}-7,8-*nido*-$C_2B_9H_9$.

Reaction of PPh_3AuCl with Tl_2[7,8-*nido*-$C_2B_9H_{11}$] produces the structurally similar (in terms of metal-carbaborane ligation) species 10-*endo*-{PPh_3Au}-7,8-*nido*-$C_2B_9H_{11}$[35] but reaction of PPh_3AuCl with Tl[carb'] yields a class 2 carbauraborane with the gold fragment bridging two boron atoms on the C_2B_3 face[36]. These highlight an important difference between the {*nido*-C_2B_9}$^{2-}$ (and Cp^-) and the [carb']$^-$ ligands: {PPh_3Au}$^+$ (and H^+) add to {*nido*-C_2B_9}$^{2-}$ (and Cp^-) to give

σ-bonded (*endo*) substituents in comparison to the preferred bridging modes of the [carb']$^-$ species.

Such is the interest in carbametallaborane chemistry that recent literature has included some other novel species including macrocyclic ligands incorporated into carbaborane cages. The sodium ion in 7,8-[$SCH_2CH_2(OCH_2CH_2)_3Na$]-7,8-*nido*-$C_2B_9H_{10}$ (**Figure 1.16**) is coordinated by the three oxygen and two sulphur atoms of the macrocycle but not by the cage[37]. A series of carbametallaborane species containing two metals, one π-bonded to the C_2B_3 face the other σ-bonded either directly to a boron or *via* a hydrogen bridge have also featured in recent literature[38, 39], for example [$CoRh(CO)_2(PPh_3)(\eta^4\text{-}C_4Me_4)(\eta^5\text{-}C_2B_9H_{11})$] (**Figure 1.17**)[38].

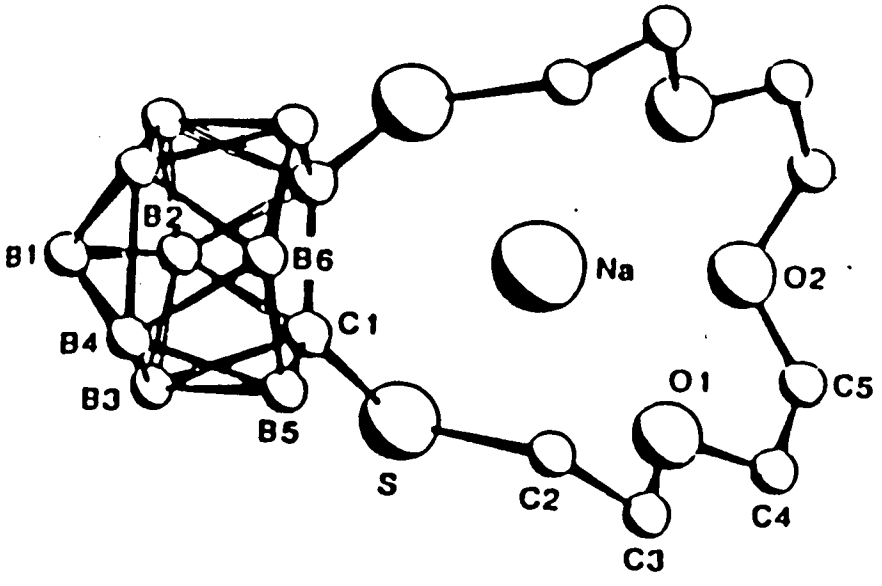

Figure 1.16 Molecular Structure of 7,8-[$SCH_2CH_2(OCH_2CH_2)_3Na$]-7,8-*nido*-$C_2B_9H_{10}$.

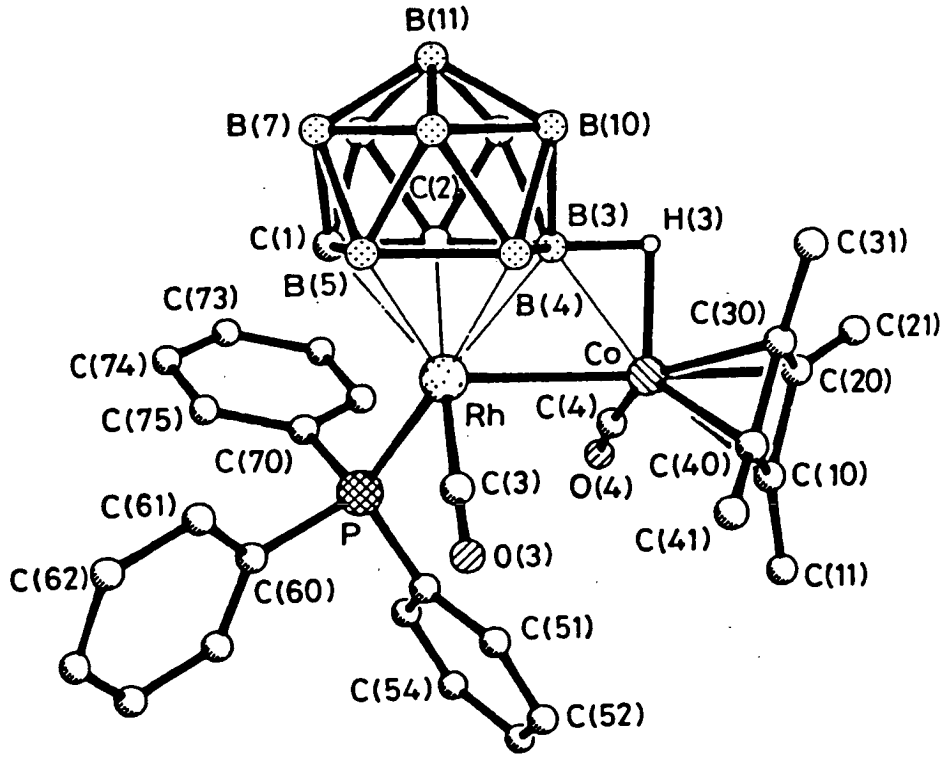

Figure 1.17 Molecular Structure of $[CoRh(CO)_2(PPh_3)(\eta^4\text{-}C_4Me_4)(\eta^5\text{-}C_2B_9H_{11})]$.

Furthermore, π-carbametallaborane complexes have not been restricted to transition metals, 3,1,2-*closo*-$SnC_2B_9H_{11}$[40] and $[Cl_2U(C_2B_9H_{11})_2]^{2-}$ [41] representing examples of *p*- and *f*- block metal complexes respectively.

The prolific amount of research in this area during the past 30 years has produced a seemingly endless list of new complexes, a full catalogue of which is beyond the scope of this section. This is in contrast to σ-carbametallaboranes, very much an underdeveloped area with only a comparative few complexes reported. Indeed, a recent overview[42] of boron chemistry notes that since a 1982 review of (carba)metallaborane chemistry[43] practically no research has been reported from this area.

1.4.2 σ-Carbametallaboranes

The synthesis of *closo*-carbametallaboranes containing a cage carbon-metal σ-bond is achieved using 3 similar preparative methods as outlined in **Figure 1.18**: The most widely employed method is *via* the lithium salt of the *closo*-carbaborane, the C_{cage}-*H* bond readily cleaved by alkyl lithium reagents (**Section 1.3.2**); metallation can also be accomplished *via* alkali metal or Grignard σ-carbaborane derivatives. These three reactive species are useful intermediates, undergoing many of the common reactions of organometallic chemistry[13, 44] and, furthermore, reaction with the appropriate metal halide yields the desired σ-carbametallaborane.

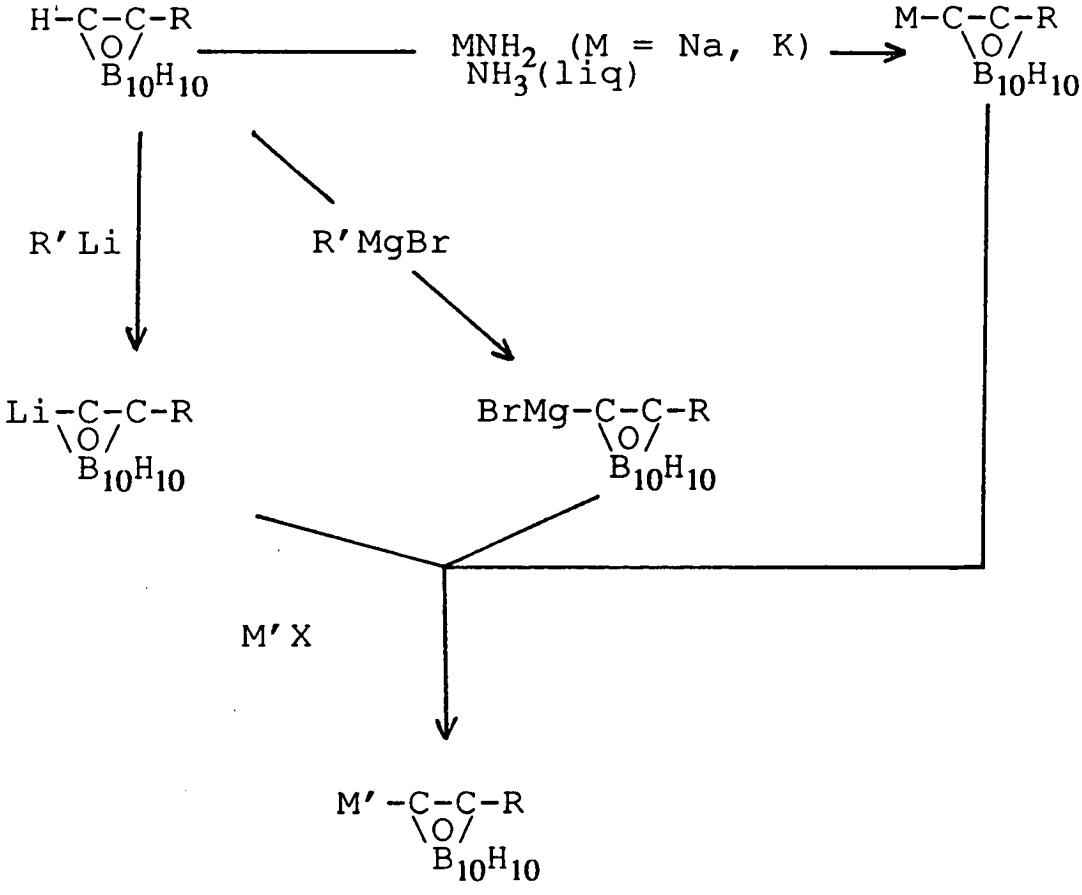

R, R' = alkyl, aryl, *etc.*; M'X = (transition) metal halide.

Figure 1.18 Preparative Routes for σ-Carbametallaboranes.

The driving force behind the reactions involving these intermediates is the formation of the group 1 or group 2 halide, the high lattice energy and low solubility (in the reaction solvent - Et_2O, THF or benzene) of which pushes the reaction to completion. Although merely used as an intermediate to other carbametallaborane compounds (and various substituted carbaborane compounds as outlined in **Figure 1.7** previously), lithium carbaborane has been studied structurally as the pentamethyldiethylenetriamine adduct of Li[1-Me-1,2-*closo*-$C_2B_{10}H_{10}$][45] (**Figure 1.19**). This first structural study of a group 1 metal σ-bonded to a *closo*-carbaborane yielded a Li-C_{cage} distance of 2.176(8) Å which is at the limit of what can realistically be regarded as covalent. Consequently, the interaction between Li^+ and the carbaborane anion is probably best regarded as strongly ionic.

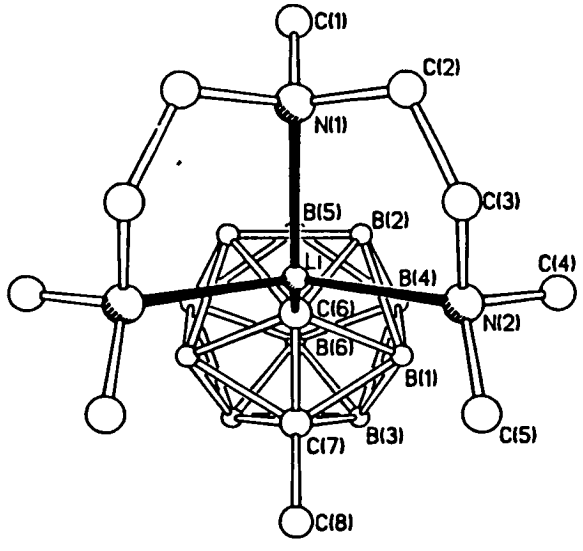

Figure 1.19 Molecular Structure of 1-{$MeN(CH_2CH_2NMe_2)_2$}Li-2-Me-1,2-*closo*-$C_2B_{10}H_{10}$.

Lithiation of 1,2-*closo*-$C_2B_{10}H_{12}$ produces the mono- or dilithium reagent or an equilibrium between the two (see **Section 1.3.2**). However, with one of the cage carbon atoms bound to an organic substituent, only the monolithium carbaborane complex is produced. As might be expected, this difference leads to contrasting

chemistries. For example reaction of $(n\text{-}C_4H_9)_2SnCl_2$ with Li[1-Ph-1,2-*closo*-$C_2B_{10}H_{10}$] and Li_2[1,2-*closo*-$C_2B_{10}H_{10}$] respectively results in structurally different products[46] **(Figure 1.20)**.

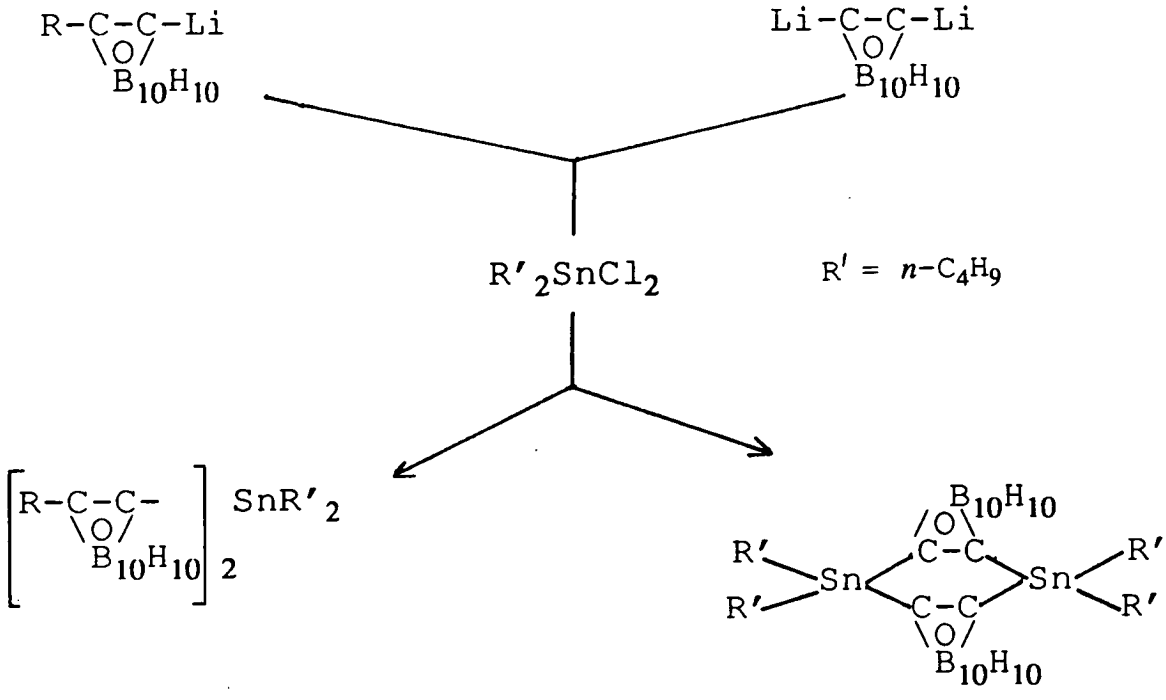

Figure 1.20 Reaction of $(n\text{-}C_4H_9)_2SnCl_2$ with Mono- and Dilithium Carbaboranes.

There are several more examples of main group metals (and non-metals) σ-bonded to *closo*-carbaboranes and these have been widely reviewed in the literature[42, 43]. However, transition metal carbaboranes are of most relevance to the research undertaken for this thesis and appropriate examples are discussed in the main text as required.

The first transition metal carbametallaborane containing a cage carbon-metal σ-bond was a Pt^{II} complex reported by Bresadola in 1968[47]. A flurry of activity in this area until *ca.* 1982 yielded several other interesting transition metal complexes. However, all the work concentrated on the synthesis and characterisation of late (d^6, for example Fe^{II} [48] **[Figure 1.21]**, or greater) transition metal species although a Ti^{IV}

centre σ-bonded to a carbaborane cage, albeit through a methylene group has been reported[49] ($Cp_2Ti[CH_2\text{-}C_2B_{10}H_{11}]_2$) - see **Figure 3.3**, p 88 in **Section 3.1**).

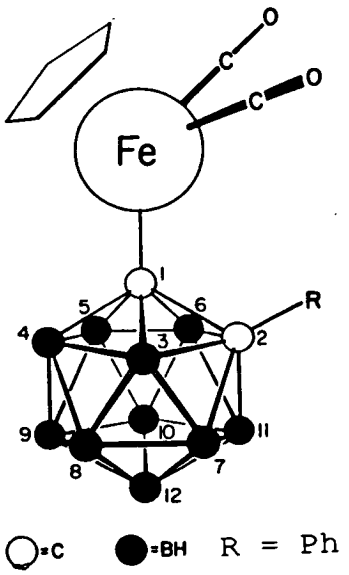

Figure 1.21 Proposed Structure of 1-Ph-2-{$CpFe(CO)_2$}-1,2- *closo*-$C_2B_{10}H_{10}$.

The carbaborane anion is a highly unusual carbanion in that the carbon carrying the negative charge is highly connected (bonded to one carbon and four boron atoms in {1,2-*closo*-C_2B_{10}} species) and the cage structure means substantial steric demands. Indeed, the steric bulk of the icosahedral carbaborane has allowed some unusual transition metal derivatives to be produced: For example, when $Rh(PPh_3)_3Cl$ reacts with Li[1-Ph-1,2-*closo*-$C_2B_{10}H_{10}$] one PPh_3 ligand is lost to give what was initially thought to be the first example of a 3-coordinate Rh^I complex[50]. The presence of the large carbaborane ligand does not allow the coordination of more than two of the bulky PPh_3 groups. The molecular structure of the complex (**Figure 1.22**) revealed that although there are only three ligands the Rh^I centre is still 4-coordinate because of an agostic interaction between the metal and the hydrogen atom bound to B(1)[51].

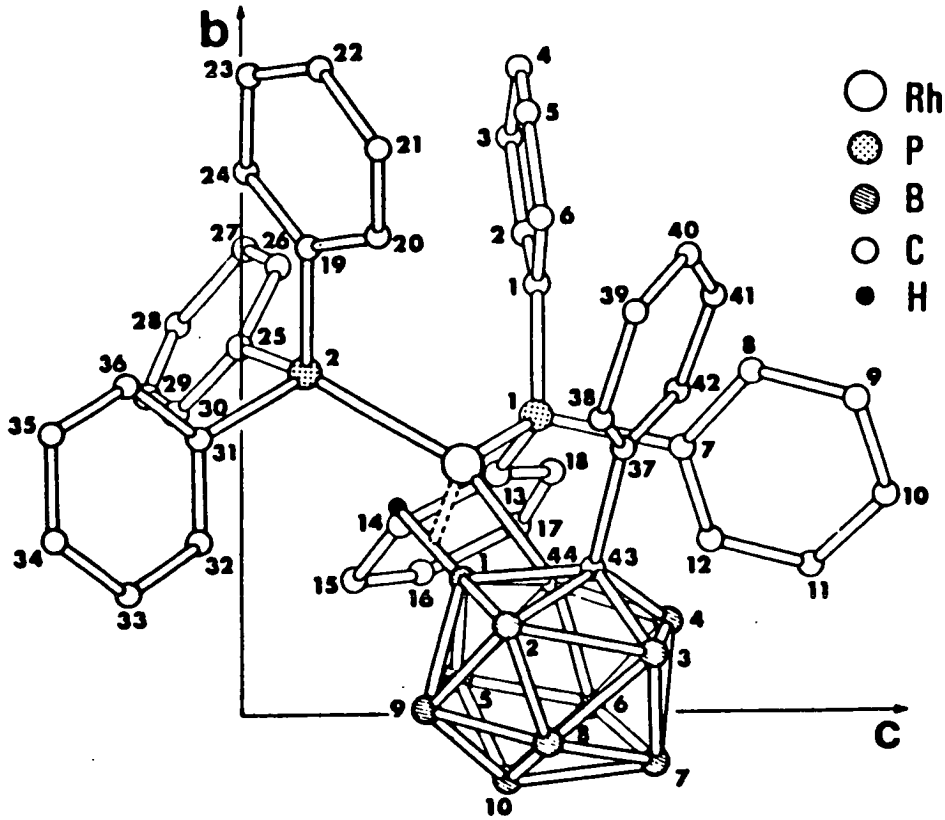

Figure 1.22 Molecular Structure of 1-Ph-2-{$(PPh_3)_2Rh$}-1,2-*closo*-$C_2B_{10}H_{10}$.

Complexes with Ir, Pd, Ni, Pt, Mn, Co, Cu, Hg and Au have been synthesised and charcterised in the years up to 1982. The research of the late 1970's and early 1980's concentrated on modifications to the organic substituent on the adjacent cage carbon atom so that coordination to the metal could occur. The stability of the transition metal *closo*-carbaborane complexes previously reported had been relatively low with facile cleavage of the M-C_{cage} σ-bond. Attempts to stabilise the complexes included chelation with 2,2'-bipyridyl (*cf* Ti^{IV} organometallic chemistry[52]) as in the Pd^{II} complex 1-Ph-2-{(bipy)Pd}-1,2-*closo*-$C_2B_{10}H_{10}$[53].

Zakharkin and co-workers in Moscow have synthesised a series of complexes where the nitrogen or oxygen atom in the organic substituent on one cage carbon coordinates to the metal atom σ-bonded to an adjacent cage carbon, as in the proposed structure of the Cu^{I} [54] and the molecular structure of the Hg^{II} [55] species in

Figure 1.23. No marked increase in the stability of the metal-carbon σ-bond was reported. The relative instability of the metal-carbon σ-bond has meant that the chemistry of such complexes has, in general, not been thoroughly investigated.

a

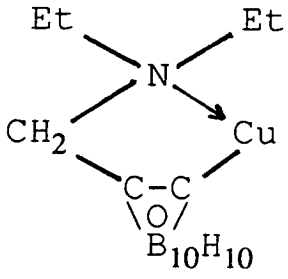

b

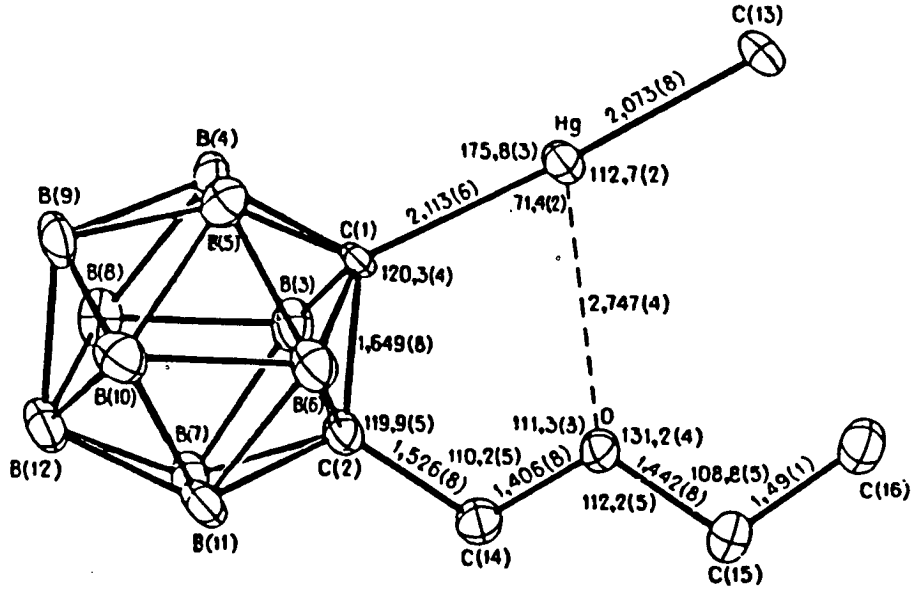

Figure 1.23 Structure of (a) 1-CH_2NEt_2-2-Cu-1,2-*closo*-$C_2B_{10}H_{10}$ (proposed) and (b) 1-$CH_2OCH_2CH_3$-2-{MeHg}-1,2-*closo*-$C_2B_{10}H_{10}$ (molecular).

Finally, it is worth noting that transition metal derivatives with cage boron-metal σ-bonds are known and are synthesised by reacting the boron substituted (carboxcylic

acid or acid chloride) carbaborane with a sodium salt of the transition metal anion. Several Fe^{II} compounds have been produced in this way[56].

Overall, it is clear that π-carbametallaborane chemistry has been studied far more extensively than σ-carbametallaborane chemistry. Probable reasons for this could be, firstly, the analogy between the extensively studied Cp^- and the $\{nido\text{-}C_2B_9\}^{2-}$ species in the former and secondly, the relative instability of the metal-carbaborane bond in the latter. As a result, π-carbametallaborane chemistry continues to move rapidly forward whereas σ-carbametallaborane chemistry remains very much an underdeveloped field.

1.5 Tertiary Phosphine Gold(I) Compounds

Gold chemistry is dominated by the oxidation states (I) and (III). Gold(I) complexes are usually 2-coordinate, linear complexes, the 14 electron configuration of the gold resulting in coordinatively unsaturated compounds. Gold(III) complexes are generally 4 coordinate, square planar, with a 16 electron configuration. Most of the research described in this thesis involves the synthesis of organogold(I) carbaborane complexes, in particular tertiary phosphine gold(I) compounds. This section briefly describes the synthesis, chemistry and bonding capability of the tertiary phosphine gold(I) fragment although appropriate examples are included in the main text as required. Organogold chemistry in general has been extensively reviewed in the literature[57].

1.5.1 Synthesis of Tertiary Phosphine Gold(I) Complexes

The syntheses of organometallic gold(I) complexes of the type PR_3AuL involve many of the reactions common to organometallic chemistry[57]. However, the range of PR_3AuL complexes is limited because the phosphine exerts a high *trans* effect and unless the ligand, L, has a particularily high affinity for gold it will readily dissociate leaving the reactive $\{PR_3Au\}^+$ species.

The most useful starting material for synthesising organogold(I) complexes of this type is the chloride, PR_3AuCl. This is obtained in high yield from the reaction of $HAuCl_4.3H_2O$ and two equivalents of PR_3. One equivalent of PR_3 reduces the gold(III) in the chloroauric acid to gold(I), it being oxidised to PR_3Cl_2[58] and the other equivalent of phosphine coordinates to the gold(I) centre. If the phosphine reduces gold(III) to gold(0) in this reaction a less direct method is possible: Reaction of two equivalents of AsR_3[59] or three equivalents of tetrahydrothiophene (tht)[60] with

chloroauric acid yields AsR_3AuCl and thtAuCl respectively. The more weakly gold-bound AsR_3 and tht are readily displaced by phosphine when stirred in stoichiometric amounts in an appropriate solvent[61].

The reaction of PR_3AuCl with various ligand salts is reviewed in **Figure 1.24**. The driving force for these reactions is again the formation of the alkali (or thallium) metal chloride. Alkyl gold(I) complexes (Equation 1 in **Figure 1.24**) are generally stable and do not decompose by β-elimination. It is interesting to note that the alkyl ligand labilises the *trans* phosphine such that, for example, PMe_3 can readily be replaced by other less volatile phosphines.

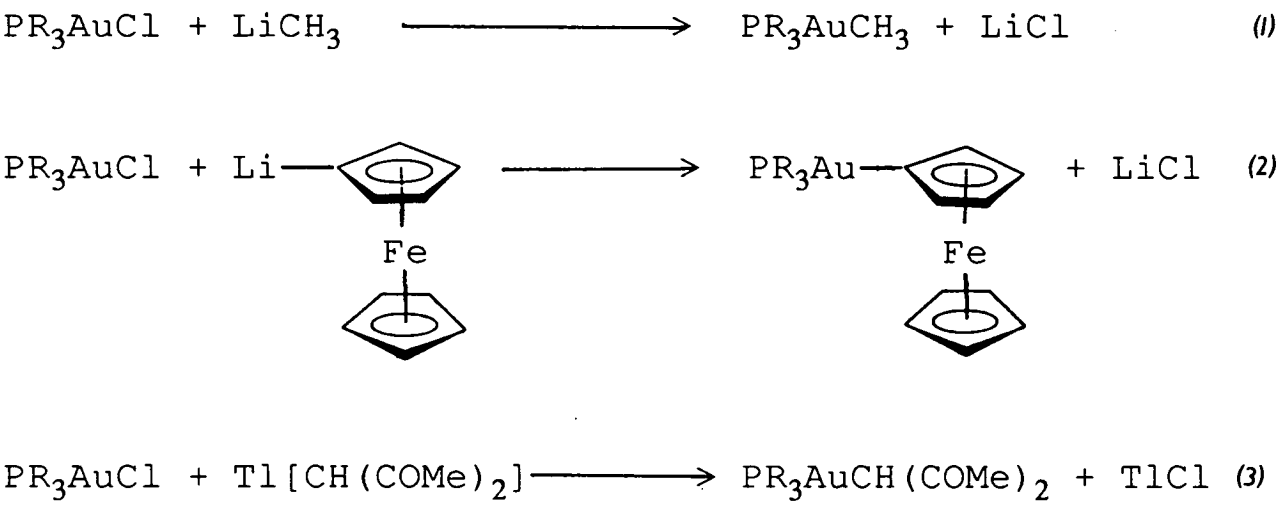

Figure 1.24 Some Representative Reactions of PR_3AuCl.

The $\{PR_3Au\}^+$ fragment is also found in metal cluster compounds, for example $Au_6(PPh_3)_6^{2+}$ [62]. Rationalisation of the structures of clusters such as this has lead to the greater understanding of the $\{PR_3Au\}^+$ fragments' bonding capability.

1.5.2 Bonding Capability of the $\{PR_3Au\}^+$ Fragment

In the cluster compound described above the phosphine ligands have been shown[63] to play an important role in the stabilisation of the cluster by encouraging a more favourable hybridisation of the gold valence orbitals. Interestingly, PSEP theory is not valid in prediciting the geometry of these gold cluster compounds: The poor $6p_\pi$-$6p_\pi$ overlap for gold atoms separated by 2.8 to 3.0 Å means that the gold valence orbitals do not generate a set of strongly bonding molecular orbitals which are tangential to the polyhedral surface.

Arising from these studies, the bonding capability of the $\{PR_3Au\}^+$ fragment has emerged[64]. The frontier molecular orbitals of $\{PR_3Au\}^+$ as derived from extended Hückel molecular orbital calculations are shown in **Figure 1.25**. The orbitals with a predominance of *d* orbital character are filled and are low lying in energy such that they can essentially be considered as core. In essence this demonstrates that the gold *d* electrons are not available for bonding and so the $\{PR_3Au\}^+$ fragment cannot be assumed to be electron donating as might be expected with a transition metal fragment with a high d^n configuration. The bonding characteristics are therefore determined primarily by the (vacant) hy(*s*-*z*) and the higher energy p_x and p_y orbitals.

In terms of the *isolobal* analogy[65] (i.e. the number, symmetry properties, extent in space and energies of the frontier MOs of isolobal fragments are similar) the $\{PR_3Au\}^+$ fragment could therefore be identified with either a $\{CH\}^{3+}$ fragment or the $\{Mn(CO)_3\}^+$ fragment both of which have frontier MOs related to those of $\{PR_3Au\}^+$. However, the hy(*s*-*z*) and especially the p_x and p_y MOs in $\{PR_3Au\}^+$ are significantly less stable than the corresponding orbitals of the $\{Mn(CO)_3\}^+$ fragment and so the $\{PR_3Au\}^+$ can essentially be considered as having only one frontier MO available for bonding. Therefore, to a first approximation, $\{PR_3Au\}^+$ is isolobal with H^+, CH_3^+, $\{Mn(CO)_5\}^+$ and $\{Co(CO)_4\}^+$ all of which only have one frontier MO

available for bonding.

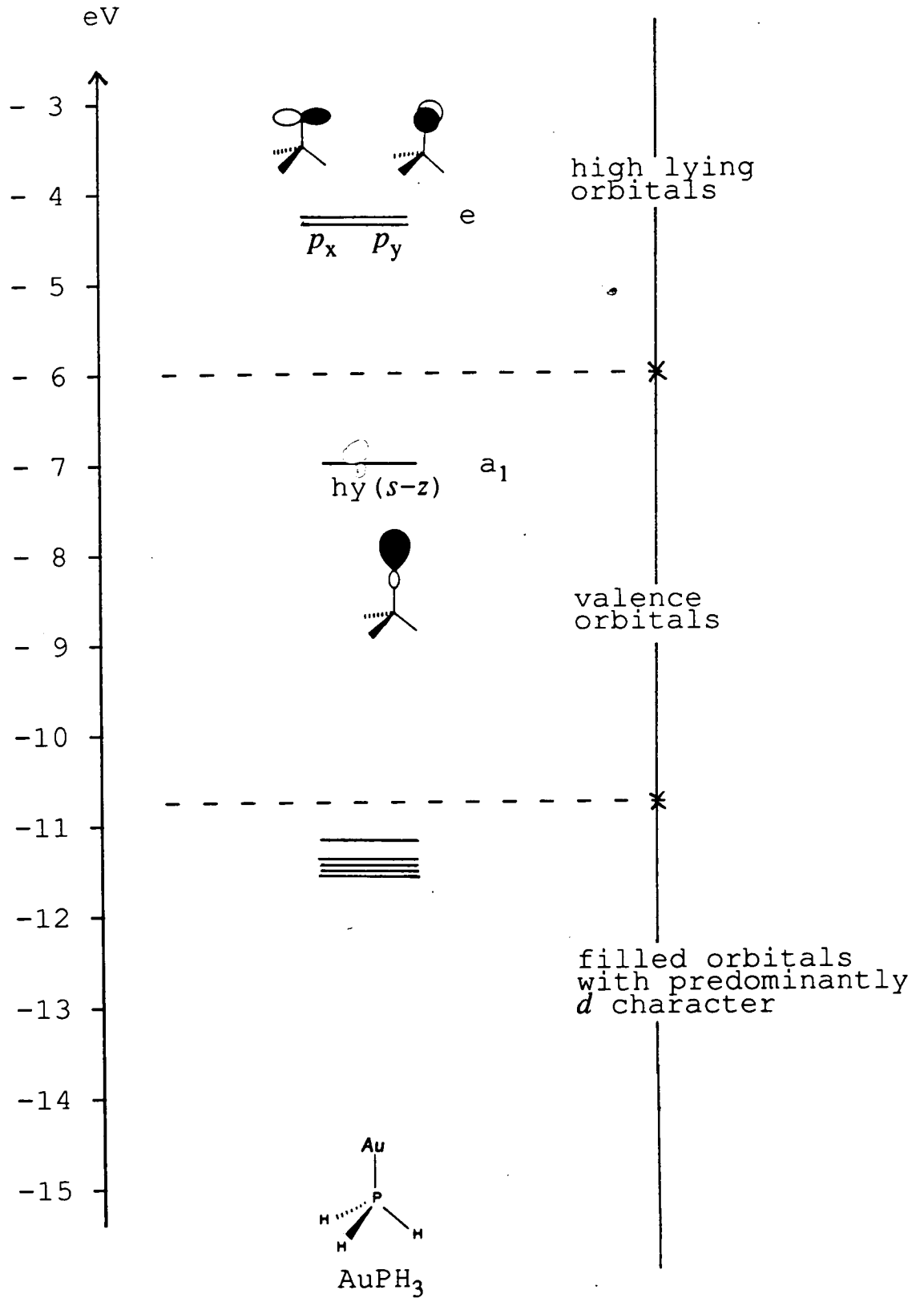

Figure 1.25 Frontier MOs of $\{PR_3Au\}^+$ Fragment.

1.6 BNCT

Boron neutron capture therapy (BNCT) is currently undergoing new clinical trials as part of the treatment of severe brain tumours, but is still in the early stages of development even though the basic strategy was conceived[66] only 4 years after the discovery of the neutron in 1932. The process relies on the high neutron capture cross section (NCCS) of the 20% abundance ^{10}B isotope which, when bombarded by a stream of epithermal neutrons, undergoes a nuclear reaction, releasing an α-particle with 2.7 MeV of kinetic energy: $^{10}B + {}^{1}n \text{ ------> } {}^{4}\alpha + {}^{7}Li$. The α-particle will destroy any material within its flight distance of about 10μm (equivalent to the dimensions of one cell) and, therefore, if a reagent containing ^{10}B can be localised on a tumour then this application can be used to destroy tumour cells.

The concepts of BNCT are extremely difficult to put into practice and they still have not been been satisfactorily resolved[67]. The development of BNCT has consequently been sporadic: In the 1960's the Brookman National Laboratory undertook unsuccessful trials on patients with highly malignant brain tumours using borax as the BNCT reagent. The failure of these and other trials at that time lead to the abandonment of BNCT research in the United States. However, in the late 1960's, Hatanaka used $Na_2[B_{12}H_{11}SH]$ (BSH) in clinical trials in Japan and found that this non-toxic compound gave high and persistent concentrations of boron in the tumour: Concentrations of BSH averaged 26.3mg per 1g of tumour and an average BSH_{tumour} to BSH_{blood} concentration of 1.69:1 was achieved[68].

BSH has been shown to bind to the tumour *via* a disulphide link[69] and therefore binds only to the surface of the tumour. As the α-particles produced only penetrate and destroy up to one cell depth, BNCT using BSH requires prior removal of most of the tumour by surgery and then repetition of the traumatic BNCT process to ensure

complete irradication of the tumour. This highlights the fact that BNCT is a multidisciplinary field: Extensive cooperation of surgeons, biochemists, chemists, and nuclear physicists is required to ensure success. BSH is still being used in clinical trials while research continues into synthesising better (more tumour specific) BNCT reagents.

Research into synthesising new reagents is problematic in that any reagent must satisfy certain stringent conditions: They must be able to be synthesised pure and in good yield, be ^{10}B enriched to a high degree (>90%), be water soluble and stable at physiological pH and under physiological conditions, be non-toxic, not contain heteroatoms with a large NCCS, be to some degree tumour specific, and they must bind to the tumour without crossing the blood-brain barrier in excessive amounts. Nevertheless, three major classes of borane derivatives have been identified as being particularly useful as BNCT reagents[70]: Functionalised polyhedral boranes which are not tumour specific; boronated organic compounds (tumour area seeking); and boronated monoclonal antibodies (tumour seeking).

Polyhedral (carba)boranes have the advantage of generally being non-toxic due to their inertness to biochemical reactions. To attach the (carba)borane to the tumour cells, they need to be functionalised with a substituent capable of interaction with the biochemical system, for example HS-. BSH is an example of a molecule in this class. Other examples include HS-, MeS-, and HOOC- derivatives of $[closo\text{-}CB_{11}H_{12}]^-$ [71] but these compounds have not been used in clinical trials, probably because they are not tumour specific.

Boronated organic species take advantage of the fact that a variety of physiologically active organic compounds tend to accumulate in specific areas, for example, porphyrin derivatives prefer brain tissue. After appropriate boronation such compounds may concentrate in these specific areas and eventually accumulate in

malignant tissue localised there. An extensive study of boronated porphyrins for use in brain tumours is currently proceeding[70]. Compounds are also being developed for other tumours, for example, promazine has an affinity for melanin pigments and boronated promazines have been synthesised and suggested for the BNCT treatment of melanoma[72].

Boronated monoclonal antibodies rely on the principle that the antibodies to any tumour can be cultivated and isolated. This adopts the most sophisticated and precise approach of the BNCT reagents because these compounds bind specifically to the tumour cells. The main problem is that only a few antibody molecules bind to an individual cell and so a large concentration of boron per molecule is required to ensure cell destruction. This must be achieved by attaching as many icosahedral boranes to the biomolecule without damaging its essential functionality. The linkage between the borane derivative and the antibody is achieved using reactive organic groups such as SCN and COOH. Applications of, among others, BSH[73] and [7,8-*nido*-$C_2B_9H_{12}$]$^-$ [74] have been tested, and research to overcome the problem of requiring a high boron concentration per molecule continues[75].

BNCT has been recently reviewed [70, 76, 77] and continues to be a developing area of practical interest in polyhedral borane chemistry.

1.7 Scope of Work

Section 1.4.2 briefly describes the interesting and underdeveloped area of σ-carbametallaborane chemistry where a transition metal is σ-bonded to a cage carbon atom in {1,2-*closo*-C_2B_{10}} derivatives. This review of the literature identified that no transition metal with a d^n configuration of less than 6 had been used in such complexes and, of those that had been reported, the majority showed relative instability *via* facile cleavage of the metal-carbon σ-bond.

The research concentrates on the synthesis of σ-carbauraboranes alledged to be unusually stable. Structural and theoretical studies were undertaken in order to understand the ligand function of icosahedral *closo*-carbaborane derivatives and to quantify and clarify the observed degree of stability in the complexes. The conclusions arising from the work directed the research into the synthesis of σ-carbametallaborane complexes containing early transition metals in a high oxidation state.

The ease of derivatisation of *ortho*-carbaborane and the results obtained in the early part of the research lead to the synthesis of some unusual carbaborane complexes containing a *closo*-carbaborane σ-bonded or σ-linked to gold. Also, the use of gold in the synthesis of biomolecules, for example gold-amino acid and anti-rheumatic gold-sugar complexes, stimulated research into possible reagents for use in BNCT which contain a gold atom σ-linked to a carbaborane and an active biochemical site.

CHAPTER 2
σ-BONDED GOLD CARBABORANES

2.1 Introduction

Without exception all the reported transition metal *closo*-carbaboranes where the metal is σ-bonded to a cage carbon involve transiton metals with a d^6 or greater valence electron configuration, in particular Fe^{II} [48] (d^6), Pt^{II} [47, 78] (d^8) and Rh^{I} [50] (d^8). The reason for concentrating on these late transition metals probably stems from previous[43] (and indeed current[79]) thinking that the carbaborane ligand has electron withdrawing properties brought about by its electron 'deficiency' and so requires a metal in low oxidation state and with a high number of available valence electrons in order to form stable complexes. However, this rationale is flawed because the carbaboranes (and boranes) are only electron deficient in terms of classical electron counting and adopt their unusual geometries to overcome this electron deficiency. The complexes that have been synthesised are, in general, relatively unstable, degrading by cleavage of the metal-carbon σ-bond. For example 1-Ph-2-{$CpFe(CO)_2$}-1,2-*closo*-$C_2B_{10}H_{10}$ is stable in aromatic solvents[48] but decomposes to $[CpFe(CO)_2]_2$ and 1-Ph-1,2-*closo*-$C_2B_{10}H_{11}$ in CH_2Cl_2, this being discussed in more detail in **Section 2.2.3**. The ease of cleavage of the metal-carbon bond has meant that the chemistry of these compounds has not been thoroughly investigated.

In 1970 Mitchell and Stone[80] synthesised class 3 σ-bonded gold carbaboranes of "unusual stability" using the reaction scheme outlined in **Figure 2.1**. This atypical stability was exemplified by the complex 1-Me-2-{PPh_3Au}-1,2-*closo*-$C_2B_{10}H_{10}$ not reacting with trifluoroacetic acid in benzene solution whereas PPh_3AuMe reacts with the CF_3COOH at room temperature to give $PPh_3AuOOCCF_3$. The latter reaction involves cleavage of the gold-methyl carbon σ-bond intimating that the gold-cage

carbon bond is stronger than the gold-methyl carbon bond and is therefore remarkably stable. No characterisation of the gold-carbaborane species was offered but it was suggested that the stability of the complexes could be attributed to "the...electron withdrawing influence of the car(ba)borane group." The corollary to this, that the $\{PPh_3Au\}^+$ fragment bonded to the carbaborane is acting as an electron donor, is contrary to current ideas about its bonding capability[64] as outlined in **Section 1.5.2.**

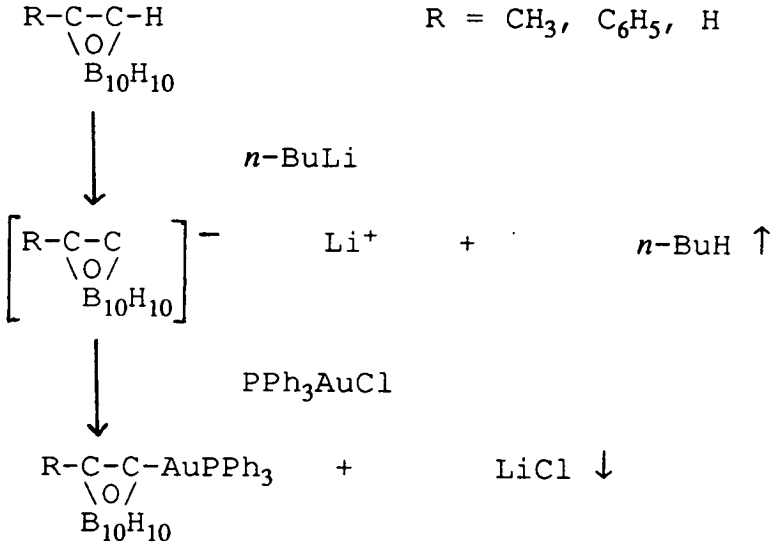

Figure 2.1 Synthesis of σ-bonded gold carbaboranes.

This chapter reports the synthesis and characterisation of a series of class 3 phosphine and arsine gold-carbaborane complexes by extension of the previous work in this area[80] **(Section 2.2).**

Discussion of the results of the spectroscopic, crystallographic and theoretical studies undertaken **(Section 2.3)** leads to the conclusion that the *closo*-carbaborane ligand is, in fact, an effective σ-electron ***donor*** in marked contrast to its previous ligand function description **(Section 2.4).**

2.2 Synthesis and Characterisation of σ-Bonded Gold(I) Carbaboranes

2.2.1 Synthesis of Compounds **3**

1-Ph-2-{PPh_3Au}-1,2-*closo*-$C_2B_{10}H_{10}$, (**3a**) which is one of the compounds prepared, but not characterised, by Mitchell and Stone[80], 1-Ph-2-{$P(o\text{-tol})_3Au$}-1,2-*closo*-$C_2B_{10}H_{10}$ (**3b**) and 1-Ph-2-{PCy_3Au}-1,2-*closo*-$C_2B_{10}H_{10}$ (**3c**) were each produced when equimolar amounts of the appropriate phosphine gold(I) chloride[59, 81] and Li[1-Ph-*closo*-$C_2B_{10}H_{10}$][82] were reacted at room temperature in diethyl ether. For each complex, the colourless product was recovered from the pale orange solution (the orange colouration is probably due to a minor Au(III) co-product) by filtering off the LiCl, removing the solvent *in vacuo* and crystallising by slow diffusion (at -30°C) of *n*-hexane into a dichloromethane solution of the crude compound. In this way colourless crystalline compounds were obtained in reasonable yields.

Similarily, 1-Ph-2-{$AsPh_3Au$}-1,2-*closo*-$C_2B_{10}H_{10}$ (**3e**) was synthesised by reacting equimolar amounts of $AsPh_3AuCl$ and the lithium salt of the 1-phenylcarbaborane anion at room temperature in Et_2O. Crystallisation from CH_2Cl_2/*n*-hexane (1:4) at -30°C resulted in a moderate yield of pure crystalline compound.

Compounds **3** were fully characterised by microanalysis and infra-red and NMR spectroscopies. Microanalyses were consistent with the proposed formulation for each compound. IR spectra exhibited the expected strong, broad band between 2500-2600 cm^{-1} due to B-H stretches.

For **3a**, **3b** and **3c** a single resonance was observed in each of the $^{31}P\{^1H\}$ NMR

spectra as expected (**Table 2.1**). All the $^{11}B\{^1H\}$ NMR spectra showed two peaks of integral 1 at highest frequency due to the only unique boron atoms B(9) and B(12) (see **Section 1.3**) but, at the field strength used (64.21 MHz), the spectra do not fully distinguish between the four pairs of low frequency symmetry equivalent boron atoms [B(4)/B(5), B(3)/B(6), B(8)/B(10) and B(7)/B(11) - see **Section 1.3**]. Consequently only a further two peaks, both of integral 4, were observed (**Table 2.2**) with each peak a double coincidence. The ^{11}B NMR spectra confirmed that all signals have doublet coupling with $^1J_{B\text{-}H}$, the boron-proton coupling constant, in the range 139-176 Hz indicating that the expected proton is bound to each boron atom. As an example, the $^{11}B\{^1H\}$ and the ^{11}B NMR spectra for **3e** are displayed in **Figure 2.2**.

	$^{31}P\{^1H\}$ (δ/ppm)	
PR_3	compounds **3**	compounds **4**
(a) PPh_3	38.6	38.6
(b) $P(o\text{-}tol)_3$	16.6	16.6
(c) PCy_3	55.2	55.6
(d) PEt_3	----	37.2

Table 2.1 $^{31}P\{^1H\}$ NMR Data for Compounds **3** and **4** (36.46 MHz).

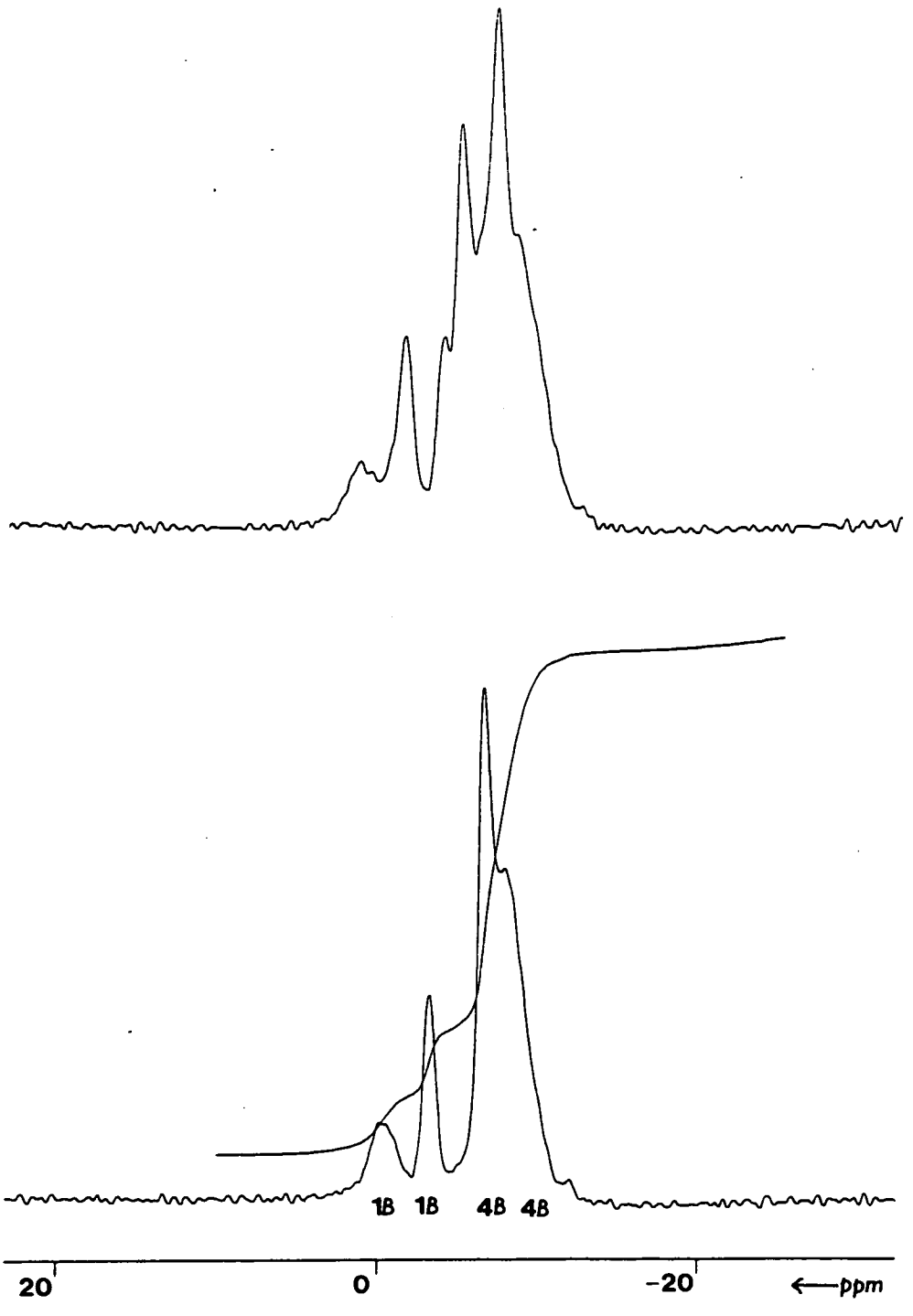

Figure 2.2 $^{11}B\{^1H\}$ and ^{11}B NMR Spectra of **3e** (64.21 MHz).

	$^{11}B\{^1H\}$ (δ/ppm)			
	3a	**3b**	**3c**	**3e**
1B	-0.42	-0.63	-0.60	-0.27
1B	-3.45	-3.24	-3.54	-3.43
4B	-6.99	-6.92	-6.98	-6.95
4B	-8.34	-8.43	-8.45	-8.55

Table 2.2 $^{11}B\{^1H\}$ NMR data for compounds **3** (64.21 MHz).

As the $^{11}B\{^1H\}$, ^{11}B and ^1H NMR spectra of the parent carbaborane, **2**, have not been reported in the literature, these spectra were duly obtained (in $CDCl_3$). The $^{11}B\{^1H\}$ spectrum (**Figure 2.3**) showed five peaks of relative integral 1:1:2:4:2 (high to low frequency: δ -1.30, -3.59, -8.18, -10.17 and -12.01 ppm) consistent with the symmetry of the molecule: There are two symmetry-unique boron atoms (two peaks of integral 1) and four pairs of symmetry related boron atoms (two peaks of integral 2 and a double coincidence giving one peak of integral 4). The ^{11}B NMR spectrum confirmed the expected doublet coupling to the single proton bound to each boron atom ($^1J_{B\text{-}H}$ = 121-149 Hz). Comparison of these boron-11 NMR spectra with those of compounds **3** are made in **Section 2.3.2.** The ^1H NMR spectrum (**Figure 2.4**) displayed resonances due to the phenyl substituent protons (multiplet: δ 7.58-7.33 ppm) and the cage carbon proton (broad: δ 3.97 ppm) in the expected ratio (5:1).

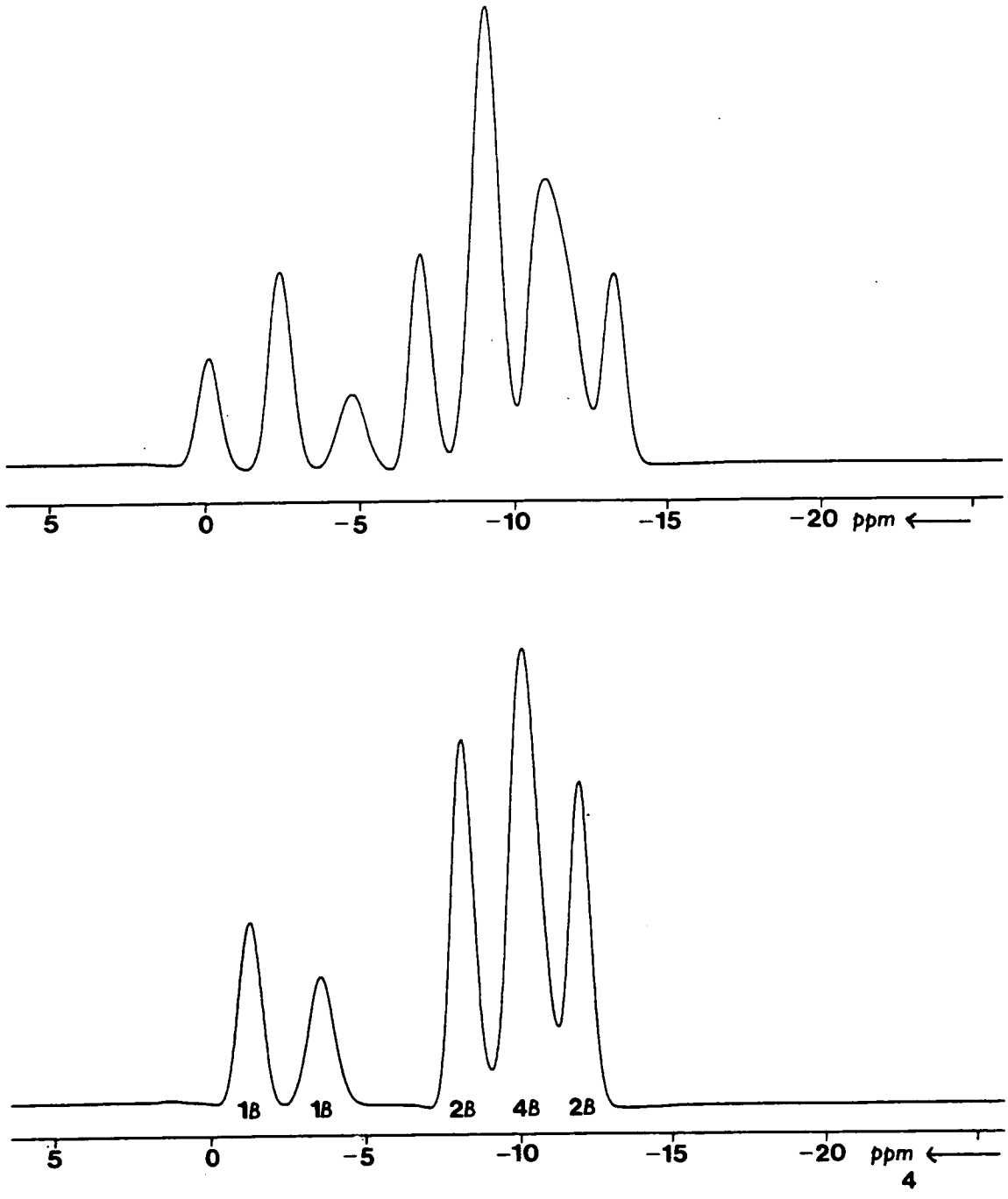

Figure 2.3 $^{11}B\{^{1}H\}$ and ^{11}B NMR Spectra of **2** (64.21 MHz).

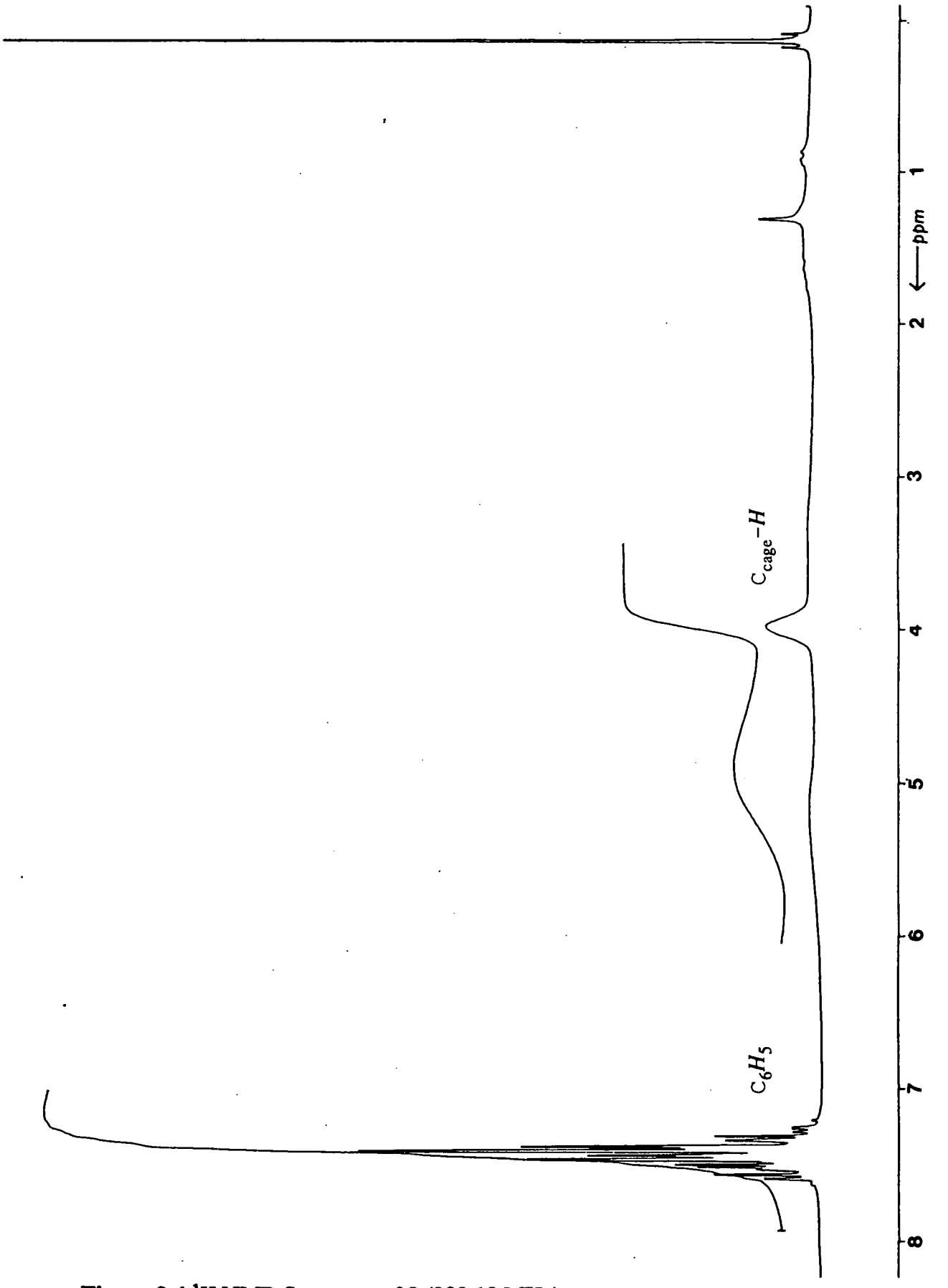

Figure 2.4 ^{1}H NMR Spectrum of **2** (200.13 MHz).

^{1}H NMR spectra of compounds **3** showed resonances due to the phenyl group substituent on the carbaborane and the aryl/alkyl groups of the phosphine in the expected ratios (**Table 2.3**). The spectra also confirmed the absence of the broad peak at δ 3.97 ppm due to the C*H*(2) of the parent carbaborane, **2**. This verifies that the acidic proton has been removed (replaced by the isolobal[65] gold (I) fragment with the gold atom bound to the cage carbon atom [C(2)]). A more detailed discussion of the NMR spectra is given in **Section 2.3.2.**

	^{1}H (δ/ppm)
3*a*	7.86 - 7.10 (m, C_6H_5)
3*b*	7.72 - 6.62 (m, 17H: aryl) 2.35 (s, 9H, $C_6H_4CH_3$)
3*c*	7.81 - 7.15 (m, 5H, C_6H_5) 1.84 - 1.15 (m, 33H, C_6H_{11})
3*e*	7.90 - 7.12 (m, C_6H_5)

Table 2.3 ^{1}H NMR Data for Compounds **3** (200.13 MHz).

2.2.2 Synthesis of Compounds 4

1-CH_3OCH_2-2-{PPh_3Au}-1,2-*closo*-$C_2B_{10}H_{10}$ (**4a**), 1-CH_3OCH_2-2-{$P(o\text{-tol})_3$ Au}-1,2-*closo*-$C_2B_{10}H_{10}$ (**4b**) and 1-CH_3OCH_2-2-{PCy_3Au}-1,2-*closo*-$C_2B_{10}H_{10}$ (**4c**) were formed by reacting equimolar amounts of the appropriate phosphine gold (I) chloride and Li[1-CH_3OCH_2-1,2-*closo*-$C_2B_{10}H_{10}$] at room temperature in diethyl ether. The crude pale orange (due to a minor Au^{III} co-product) solid obtained by removing the Et_2O from the filtered solution was crystallised by slow diffusion of *n*-hexane into a dichloromethane solution at -30°C. This yielded a moderate amount of colourless crystals in each case.

1-CH_3OCH_2-2-{$AsPh_3Au$}-1,2-*closo*-$C_2B_{10}H_{10}$ (**4e**) was prepared using the same method by reacting $AsPh_3AuCl$ with the lithium salt of ether carbaborane, crystallisation yielding a colourless product. Also, 1-CH_3OCH_2-2-{PEt_3Au}-1,2-*closo*-$C_2B_{10}H_{10}$ (**4d**) was synthesised in a similar way except that purification of the crude product by TLC with CH_2Cl_2 as the eluant was required before crystallisation. This was necessary because a brown, as yet unidentified, species contaminated the product if crystallisation was attempted without prior chromatography.

Compounds **4** were fully characterised by microanalysis and infra-red and NMR spectroscopies. Microanalyses were consistent with the proposed formulation for each compound. Infra-red spectra showed the expected broad, strong band between 2500 and 2600 cm^{-1} indicative of B-H stretches. Also, in each spectrum, single sharp peaks were observed in the regions 1460-1430 cm^{-1}, 1380-1410 cm^{-1} and 1100-1150 cm^{-1} due to the ether substituent[20] on the carbaborane group.

For **4a**, **4b**, **4c** and **4d** the $^{31}P\{^1H\}$ NMR spectrum exhibited the expected single resonance (**Table 2.1**, p43).

Alternatively, **4a** can be synthesised by stirring **4e** with one equivalent of triphenylphosphine in CH_2Cl_2 for 30 minutes at room temperature and extracting the product into Et_2O, the displaced triphenylarsine being recovered from the dichloromethane solution. The $^{31}P\{^1H\}$ NMR shift of the solid recovered from the Et_2O was the same as that for **4a** obtained by the direct route, indicating replacement of the arsine by the phosphine, as expected.

	$^{11}B\{^1H\}$ (δ/ppm)				
	4a	**4b**	**4c**	**4d**	**4e**
1B	-0.97	-1.49	-1.36	-1.48	-1.34
1B	-3.97	-3.95	-4.14	-4.09	-4.01
2B	-7.27	-7.35	-7.28	-7.20	-7.28
6B	-9.27	-9.68	-9.71	-9.73	-8.78

Table 2.4 $^{11}B\{^1H\}$ NMR Data for Compounds **4** (64.21 MHz).

All the $^{11}B\{^1H\}$ NMR spectra displayed two peaks of integral 1 at highest frequency which, again, must be due to the symmetry unique atoms B(9) and B(12). As with compounds **3**, the field strength used (64.21 MHz) does not distinguish fully between the four pairs of low frequency symmetry equivalent boron atoms. Thus, compounds **4** also show two other peaks, but this time with a triple coincidence at lowest frequency. Therefore each spectrum has four peaks of relative integral 1:1:2:6 (**Table 2.4**). The ^{11}B NMR spectra showed the expected boron-proton coupling for each boron atom with $^1J_{B\text{-}H}$ between 144 and 200 Hz. In order to assign the resonances in the $^{11}B\{^1H\}$ NMR spectrum of **4a** to specific boron atoms, the ^{11}B-^{11}B

COSY NMR spectrum of **4a** was obtained at 192.63 MHz. The assignment of the spectrum is discussed in detail in **Section 2.3.2.**

The ^{1}H NMR spectra of compounds **4** revealed the resonances due to the CH_3OCH_2 substituent of the carbaborane group, the signal due to C*H*$_3$ at lower frequency than that due to C*H*$_2$, and the aryl/alkyl groups of the phosphine in the expected ratios (**Table 2.5**). The spectra also confirmed the disappearance of the broad peak at δ 4.00 ppm[20] due to C*H*(2) of the parent carbaborane, **1**, denoting replacement of the proton with a gold(I) fragment. A more detailed discussion of all the NMR data is provided in **Section 2.3.2.**

	^{1}H (δ/ppm)		
	OC*H*$_3$	OC*H*$_2$	PR$_3$
4a	3.89	3.27	7.56-7.32 (m, 15H, C$_6$*H*$_5$)
4b	3.78	3.12	7.77-6.73 (m, 12H, C$_6$*H*$_4$Me) 2.67 (s, 9H, C$_6$H$_4$C*H*$_3$)
4c	3.82	3.33	2.14-1.21 (m, 33H, C$_6$*H*$_{11}$)
4d	3.82	3.32	1.73 (t, 9H, CH$_2$C*H*$_3$) 1.22 (q, 6H, C*H*$_2$CH$_3$)
4e	3.93	3.31	7.56-7.46 (m, 15H, C$_6$*H*$_5$)

Table 2.5 ^{1}H NMR Data for Compounds **4** (200.13 MHz).

2.2.3 Properties of 3 and 4

Compounds **3** and **4** were found to be readily soluble in Et_2O, THF, $CHCl_3$ and CH_2Cl_2. These solutions of the compounds were found to be indefinitely stable in air which, beyond Stone's observations[80] (see **Section 2.1**), is the first indication that these compounds are more stable than expected. This conclusion arises from the comparison of the properties of **3** and **4** with a known σ-bonded transition metal carbaborane, 1-Ph-2-{$CpFe(CO)_2$}-1,2-*closo*-$C_2B_{10}H_{10}$[48] (**Figure 1.21**, p28). This iron(II) complex readily decomposes in chlorinated solvents such as CH_2Cl_2 by cleavage of the iron-cage carbon σ-bond resulting in the carbonyl bridged iron dimer, $[CpFe(CO)_2]_2$ and the reprotonated parent carbaborane, **2**. The reprotonation can occur because chlorinated solvents, in particular $CHCl_3$ and CH_2Cl_2, contain small amounts of HCl (a decomposition product) and it is HCl that attacks the relatively weak metal-carbon bond in the iron carbaborane compound. Although not fully investigated, this could account for the apparent non-reaction encountered when certain Rh^I, Pt^{II} and Mn^I reactions with Li[1-CH_3OCH_2-1,2-*closo*-$C_2B_{10}H_{10}$] were attempted. These reactions were analogous to ones reported in the literature (Rh^I [50], Pt^{II} [78], Mn^I [48]) except that a 'purification' step involved the use of CH_2Cl_2. However, the gold-carbon bond in compounds **3** and **4** appears to be stable to HCl attack signifying increased metal-cage carbon bond stability over those compounds previously prepared.

The stability of these complexes can be further demonstrated by considering a standard carbaborane reaction: Deboronation (removal of a $\{BH\}^{2+}$ vertex) by refluxing with six equivalents of KOH in ethanol[83] (**Figure 2.5**). Under these conditions the iron(II) complex rapidly degrades to give the dimer, $[CpFe(CO)_2]_2$, which is recovered from the solvent and identified by IR and ^1H NMR spectroscopies. The carbaborane fragment is recovered as the dipotassium salt of the

deboronated species of the parent *closo*-carbaborane (**2**), [7-Ph-7,8-*nido*-$C_2B_9H_{10}$]$^{2-}$. In contrast, when **3a** or **4a** were refluxed in ethanol with six equivalents of KOH, the gold-carbon bond remains intact. Moreover, after refluxing for 3 hours the complexes were recovered unaltered: Remarkably, no deboronation had been achieved on this time scale leading to the conclusion that the complexes are far more stable than expected.

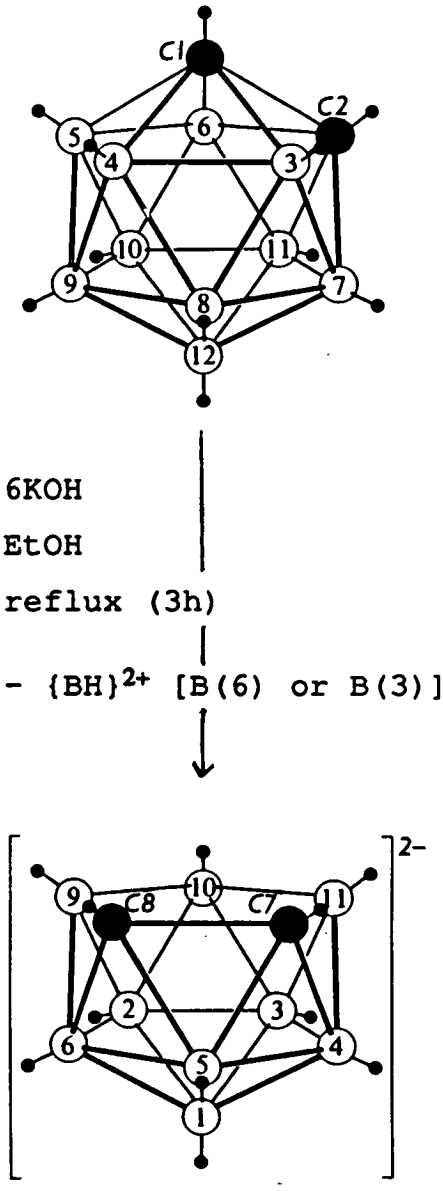

Figure 2.5 Deboronation of Icosahedral *closo*-Carbaboranes.

2.2.4 $AsPh_3AuMe$ (5)

Compound **5**, $AsPh_3AuMe$, was synthesised using a cosmopolitan of literature methods[84, 85, 86]. The reaction involved the methylation of $AsPh_3AuCl$ by MeLi, purification yielding an off-white solid which was found to decompose slowly in solution at room temperature. Crystallisation of the solid from CH_2Cl_2/*n*-hexane (1:4) produced colourless crystals of X-ray diffraction quality.

Microanalysis of the crystals was consistent with the proposed formulation, $C_{19}H_{18}AuAs$. The ^1H NMR spectrum of **5** contained a singlet at δ 0.63 ppm (CH_3) and a multiplet at δ 7.46-7.38 ppm (C_6H_5) in the expected ratio (1:5).

Stirring **5** with one equivalent of triphenylphosphine in CH_2Cl_2 at 0°C, removing the solvent after 1 hour and then recording the $^{31}P\{^1H\}$ NMR spectrum in $CDCl_3$ revealed a singlet at δ 47.4 ppm only. This phosphorus chemical shift corresponds to PPh_3AuMe[86], confirming the complete replacement of the arsine ligand by the phosphine group and further establishing the existence of the arsine complex. An X-ray diffraction study was performed on a single crystal of **5**, details of which are given in **Section 2.3.3.**

2.3 Structural Studies on Compounds 3 and 4

2.3.1 Introduction

In order to understand and clarify the reported[80] (and observed - see **Section 2.2.3**) relative stability of the gold-cage carbon σ-bond, structural studies were undertaken on compounds **3** and **4**. These involved a detailed comparison of their NMR spectra with those of the corresponding parent carbaboranes, **2** and **1** respectively ($^{11}B\{^1H\}/^{11}B$ and ^1H) or with the corresponding phosphine gold(I) chloride and phosphine gold(I) methyl compounds ($^{31}P\{^1H\}$). These comparisons are discussed in **Section 2.3.2.**

X-ray crystallographic studies of a single crystal of **4e** and then of **5** were performed and the solid state molecular structures obtained were compared, the length of the gold-carbon bond being of most interest. **(Section 2.3.3).**

Finally, extended Hückel molecular orbital (EHMO) calculations on model compounds [2-{AsH_3Au}-1,2-*closo*-$C_2B_{10}H_{11}$ **(I)**, AsH_3AuCH_3 **(II)**, [1,2-*closo*-$C_2B_{10}H_{11}]^-$ **(III)** and $[CH_3]^-$ **(IV)**] were conducted in order to quantify the conclusions deduced from the results of the NMR and crystallographic studies **(Section 2.3.4).**

2.3.2 NMR Studies

When comparing the phosphorus resonances of **4a** and **4b** to those obtained for compounds **3a** and **3b** (**Table 2.1**, p43) it can be seen that there is no apparent difference in the frequency at which they occur. This suggests that changing the substituent on C(1) of the carbaborane has no real effect on the environment of the phosphorus atom bound, through Au, to C(2). This is not unexpected as the phosphorus atom is four bonds away from the ether or phenyl substituent. In fact, the only measurable difference is in the phosphorus NMR shifts of **3c** and **4c** (Δ = 15 Hz; 0.41 ppm).

		$^{31}P\{^{1}H\}$ (δ/ppm)		
PR_3	X =	carb*	Cl	CH_3
PPh_3		38.6	33.5	47.4
$P(o\text{-}tol)_3$		16.6	8.62	37.4
PCy_3		55.6 (.2)#	54.3	60.0
PEt_3		37.2	32.0	45.3

* carb = 1-R′-1,2-*closo*-$C_2B_{10}H_{11}$ (R′ = CH_3OCH_2 & #C_6H_5)

Table 2.6 $^{31}P\{^{1}H\}$ NMR Data for PR_3AuX (36.46 MHz).

However, it is NMR spectra that give the first indication that the carbaborane is probably not acting as an electron acceptor ligand. By comparing the observed

$^{31}P\{^{1}H\}$ NMR resonances for **3a-3c** and **4a-4d**, where the carbaborane is *trans* to phosphine, with similar species, PR_3AuCl and PR_3AuMe with, respectively, the chloride and methyl carbanion *trans* to phosphine (**Table 2.6**) it can be seen that the chemical shift of the carbaborane species is between 1 and 8 ppm to higher frequency than that of the appropriate chloride species, and between 6 and 28 ppm to lower frequency than that of the appropriate methyl species. Using a specific example, PPh_3AuX (**Figure 2.6**), when X = Me the phosphorus resonance is at δ 47.3 ppm; when X = carbaborane (i.e. **3a** or **4a**) the resonance is at δ 38.6 ppm ; and when X = Cl the resonance is at δ 33.5 ppm. Thus, when phosphine is *trans* to carbaborane the $^{31}P\{^{1}H\}$ NMR resonance is between that when phosphine is *trans* to a good σ-donor ligand (Me) and that when phosphine is *trans* to a good σ- and π- (and overall better) donor ligand (Cl). This could mean that the carbaborane has *donor* properties somewhere between methyl and chloride.

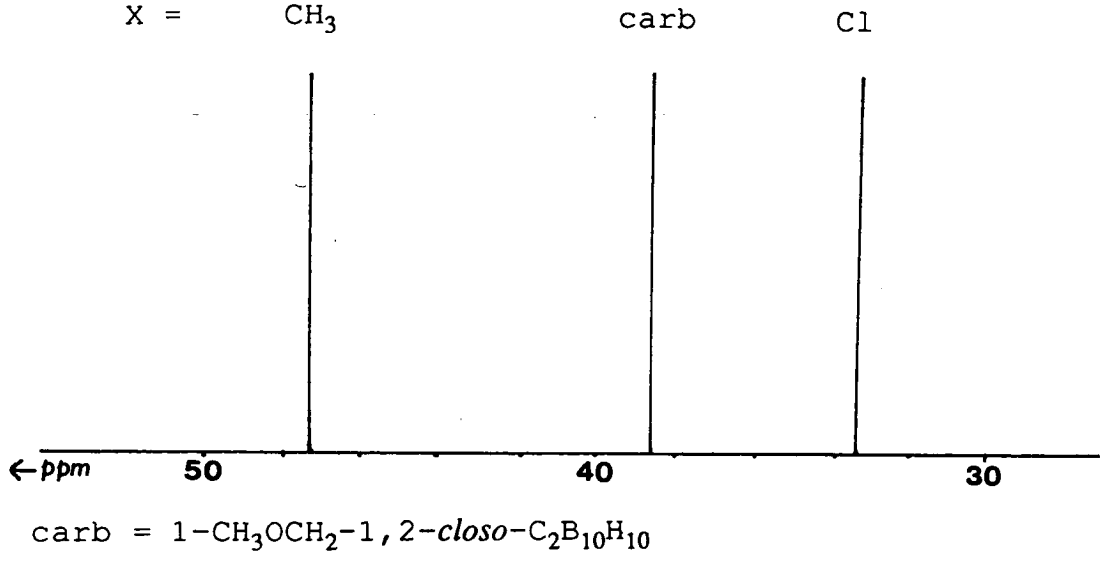

Figure 2.6 $^{31}P\{^{1}H\}$ NMR Spectra of PPh_3AuX (36.46 MHz).

Greater donation of electrons by the ligand X to the metal centre means less donation is required by the phosphine ligand. The result is greater electron density associated with the phosphorus atom which has a shielding effect: The better the donor the lower the phosphorus resonance. This is accordant with what is observed with PR_3AuCl and PR_3AuMe: Chloride is a better donor than methyl and so the phosphorus resonance is at lower frequency indicative of a greater shielding effect because of increased electron density around the phosphorus atom. Therefore, the $^{31}P\{^1H\}$ NMR spectra of the carbaboranes imply that, as a ligand, carbaborane is a better electron donor than methyl.

The emerging donor properties of the carbaborane are further confirmed by analysis of the $^{11}B\{^1H\}$ NMR spectra (acquired at 64.21 MHz). For example, if the spectrum of **4a** is compared to that of **1** it is found that, in $CDCl_3$, the boron resonances are in the range δ -0.97 to -9.27 ppm (a spectrum width of 8.30 ppm) and δ -2.47 to -12.45 ppm (a width of 9.98 ppm) respectively. It is therefore clear that when H on C(2) is replaced by a $\{PR_3Au\}$ fragment, $\{PPh_3Au\}$ in the case of **4a**, the boron resonances overall move to higher frequency and the range within which the peaks are observed (the spectrum width) is narrowed. This is consistent with the proposal that carbaborane is acting as a donor to the metal fragment, since it indicates that the corollary is true (*i.e.* that $\{PR_3Au\}$ is more electron withdrawing with respect to the cage than H): A shift to higher frequency means that the boron environment is becoming less shielded - electron density around the boron atoms is decreasing. Donation to / withdrawal by the metal would result in an overall loss of electron density within the cage, the boron atoms nearest the point of substitution, C(2), being most affected. This can be confirmed by analysing the shift in resonance from that in **1** to that in **4a** for each boron atom. This requires the assignment of the $^{11}B\{^1H\}$ NMR spectrum of **4a** from its ^{11}B-^{11}B COSY NMR spectrum (acquired at 192.63 MHz): The $^{11}B\{^1H\}$ spectrum of **4a** was fully assigned by analysis of the resonance

correlations in the COSY NMR spectrum and by analogy with the assigned spectrum of **1** (acquired at 192.63 MHz; see **Figure 1.10**, p16).

The acquirement of the $^{11}B\{^1H\}/^{11}B$ NMR and ^{11}B-^{11}B COSY NMR spectra for **4a** at a higher field strength (192.63 MHz) resulted in improved resolution: The $^{11}B\{^1H\}$ NMR spectrum now showed five peaks of relative integral 1:1:2:2:4, the broad peak of integral 6 in the corresponding spectrum acquired at 64.21 MHz field strength becoming two peaks of integral 2 and 4 (a double coincidence) at 192.63 MHz. The $^{11}B\{^1H\}$ and ^{11}B NMR spectra obtained for **4a** at 192.63 MHz are presented in **Figure 2.7**. The ^{11}B-^{11}B COSY NMR spectrum of **4a** is shown in the upper part of **Figure 2.8**, the assignment in the lower with resonances numbered *1* to *5* (high to low frequency).

The assignment was accomplished as follows: In the ^{11}B-^{11}B COSY NMR spectrum of **4a**, the two highest frequency resonances of integral 1 (resonances *1* and *2* in **Figure 2.8**) must be due to the only symmetry unique boron atoms, B(9) and B(12) [or B(12) and B(9)]. The only boron atom pair connected to both B(9) and B(12) is B(8)/B(10) and since resonance *3* shows correlation to both resonances *1* and *2*, this resonance (at δ -7.27 ppm) must be due to B(8)/B(10). Similarily, the only boron atom pair not connected to B(9) and B(12) is B(3)/B(6). As resonance *4* correlates to resonance *2*, by a process of elimination, one of the atom pairs giving rise to the resonance of integral 4 at lowest frequency (δ -9.73 ppm) must be B(3)/B(6). Unfortunately the other resonances cannot be assigned from the COSY NMR spectrum of **4a** alone. However, if compared to the (assigned) $^{11}B\{^1H\}$ NMR spectrum of **1** (**Figure 1.10**, p16), resonances *1* and *2* may be assigned: Substitution at C(2) with an (assumedly) electron withdrawing group ($\{PPh_3Au\}$) will result in a decrease in electron density at C(2) and therefore a complementary increase in electron density at B(9) as a consequence of the antipodal effect[17]: The antipodal effect is an observed anomalous increase in electron density at a cage atom when the

atom directly opposite (*i.e.* antipodal) experiences a marked decrease in electron density. Therefore, resonance *2* is due to B(9) [which is antipodal to C(2)] because, on comparison with the NMR spectrum of **1**, this resonance has shifted to lower frequency (to δ -3.99 ppm), as expected. Thus, resonance *1* (at δ -1.18 ppm) is attributable to B(12). As resonance *4* (at δ -8.62 ppm) correlates to resonance *2* [B(9)], this must be due to B(4)/B(5). Finally, the resonance of integral 4 at lowest frequency, resonance *5*, correlates to resonance *1* [B(12)] and is therefore attributable to B(7)/B(11) [aswell as B(3)/B(6)]. All other correlations observed are consistent with this assignment.

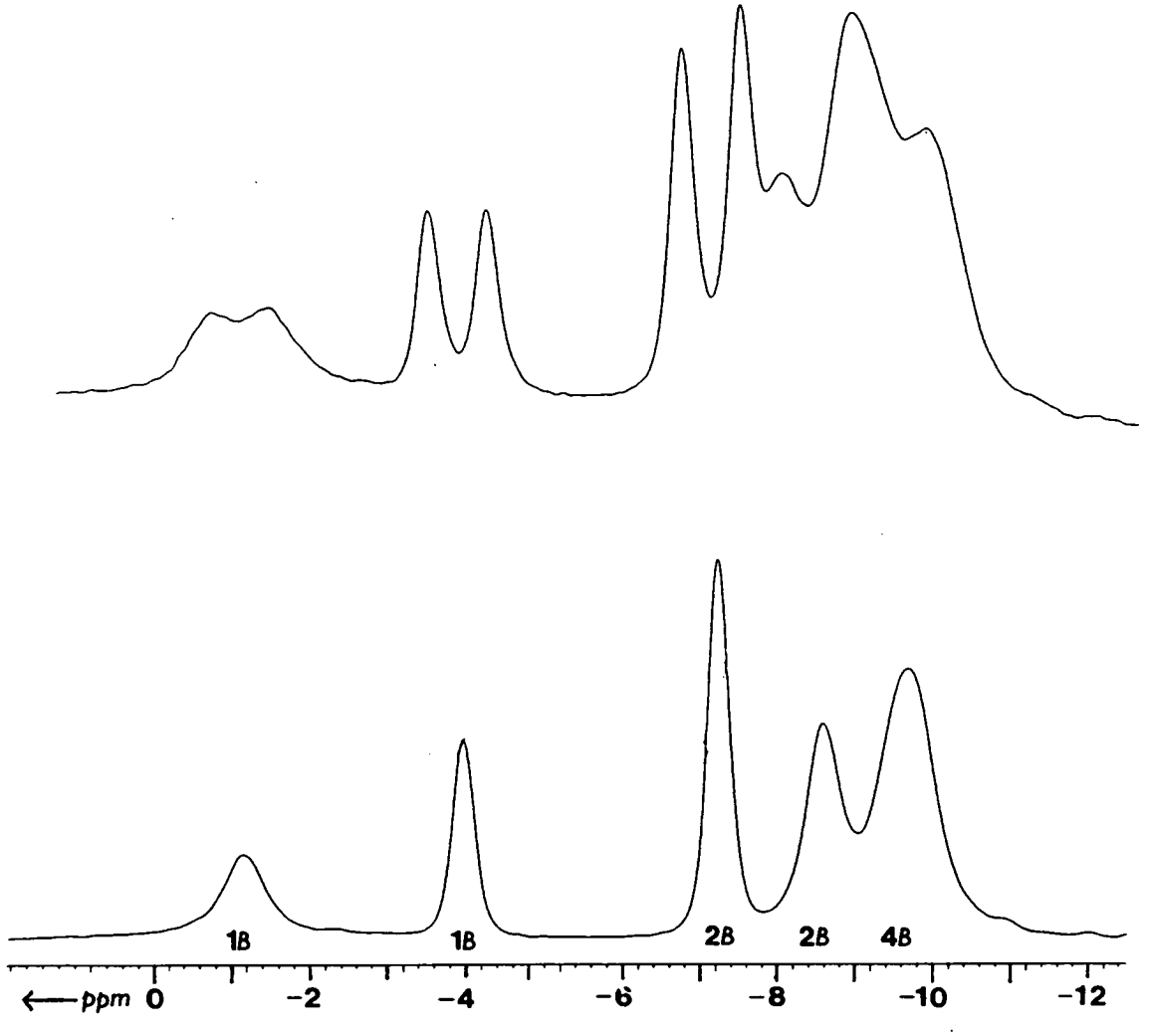

Figure 2.7 $^{11}B\{^{1}H\}$ and ^{11}B NMR Spectra of **4a** (192.63 MHz).

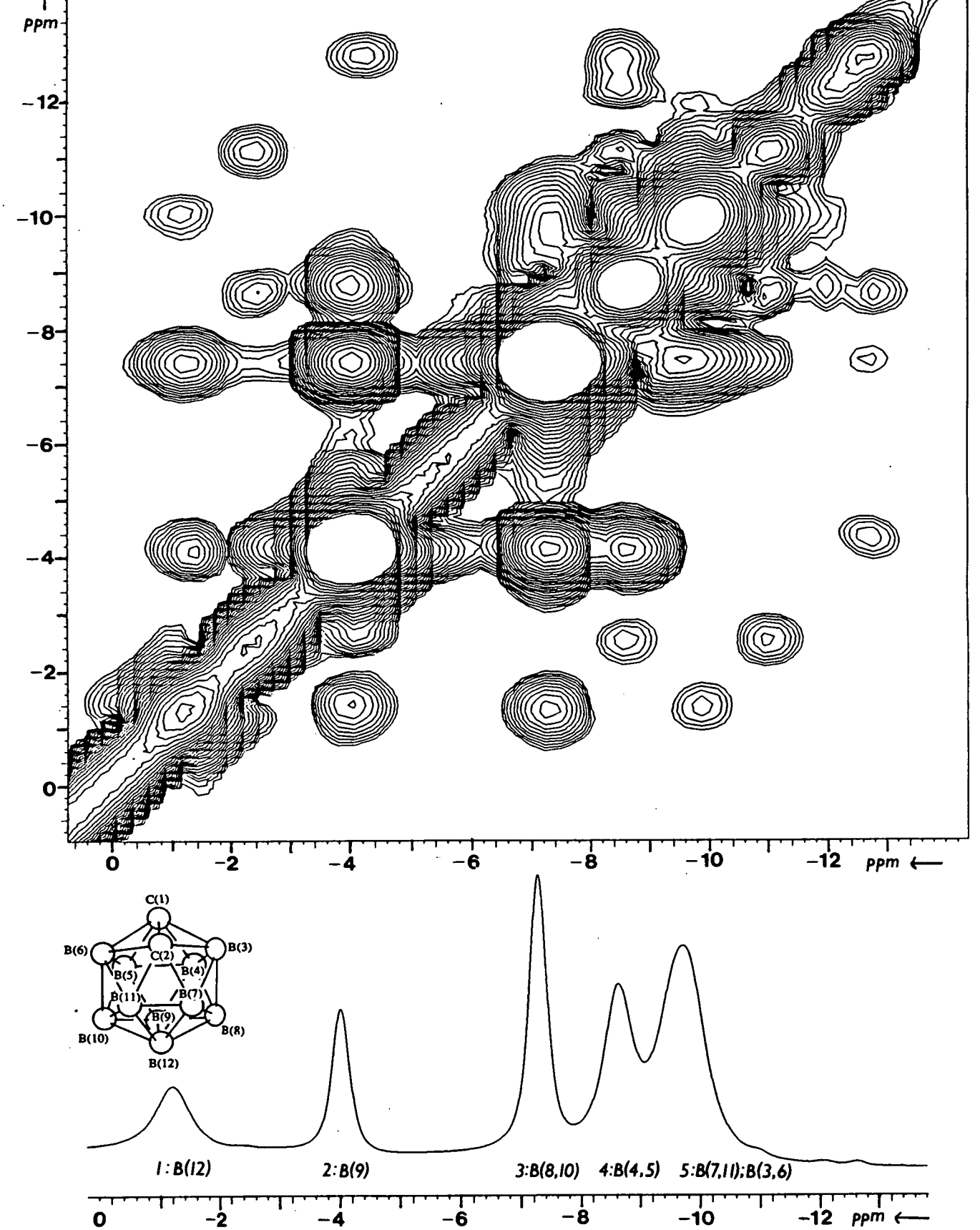

Figure 2.8 ^{11}B-^{11}B COSY NMR Spectrum of **4a** (192.63 MHz).

For the comparison with the $^{11}B\{^1H\}$ NMR spectrum of **1**, the spectra of **1** and **4a** acquired at 192.63 MHz are analysed. However, for the general comparison of the $^{11}B\{^1H\}$ NMR spectra of **1** to those of compounds **4** (**Table 2.7**; *vide infra*), the spectra acquired at 64.21 MHz are compared, since only the spectra of **1** and **4a** have been obtained at the higher field strength.

Substitution of the H atom on C(2) by a $\{PR_3Au\}$ fragment will affect B(7)/B(11) and B(3)/B(6) the most as they are directly connected to C(2). Removal of electron density from these boron atoms would therefore be the greatest, leading to the largest shifts to higher frequency. This is observed with B(3)/B(6) and B(7)/B(11) generating the resonance of integral 4 at δ -9.73 ppm with shifts of 2.95 and 2.41 ppm to higher frequency, as compared to the corresponding resonances in the $^{11}B\{^1H\}$ NMR spectrum of **1**, respectively. B(8)/B(10) and B(4)/B(5) would also be affected by substitution on C(2), but not by as much as B(7)/B(11) and B(3)/B(6), being one connectivity further from the atom at which substitution occurs [C(2)]. A smaller shift to higher frequency (1.29 ppm) is therefore observed for the resonance due to B(8)/B(10), this boron atom pair producing the resonance at δ -7.27 ppm. The resonance due to B(4)/B(5) also shifts to higher frequency, but by more than expected with a shift of 2.42 ppm yielding the resonance at δ -8.62 ppm. Similarily, the resonance due to B(12) shifts to higher frequency, the magnitude of the shift also unexpectedly large, to give the resonance at δ -1.18 ppm which represents a shift of 3.12 ppm.

However, the resonance due to B(9) anomalously shifts to lower frequency (by 1.51 ppm) as compared to the corresponding resonance in the spectrum of **1**, a shift which may be accounted for by the antipodal effect: As B(9) is antipodal to C(2), and assuming the metal fragment is acting as an electron withdrawer, an anomalous increase in electron density (and therefore resonance shift to lower frequency) would be expected for B(9), and is observed. Also, B(4)/B(5), B(8)/B(10) and B(12) are all

connected to B(9) and so an anomalous increase in electron density at B(9) could presumably cause an unexpectedly larger decrease of electron density at these other atoms. Thus, one of the factors contributing to the unusually larger shifts to higher frequency of the resonances due to B(4)/B(5) and B(12) is probably the redistribution of electron density as a consequence of the antipodal effect experienced by B(9). Interestingly, although B(4)/B(5) and B(8)/B(10) are antipodal to B(11)/B(7) and B(6)/B(3) respectively, where a large shift to higher frequency is observed in the resonances due to the latter atoms, an anomalous shift is not observed in the resonances due to the former atoms. Presumably, the effect of the $\{PPh_3Au\}$ fragment on the electron density distribution in the cage is greater than the antipodal effect on these atoms.

Therefore, overall, there is an average shift to higher frequency of 1.98 ppm (192.63 MHz) or 2.03 ppm (64.21 MHz) intimating that there is a net loss of electron density from the cage. Thus, both the $^{31}P\{^1H\}$ and $^{11}B\{^1H\}$ NMR data suggest that carbaborane is acting as an electron donor to gold: The $^{31}P\{^1H\}$ NMR data imply that carbaborane is a better donor than methyl; the $^{11}B\{^1H\}$ NMR data infer that $\{PR_3Au\}$ is a better withdrawing moiety with respect to the cage than H. If methyl and H are placed at the same point of reference on a scale of donating / withdrawing ability (a valid assumption since the electronegativities of H and C are similar), then $\{PR_3Au\}$ would be relatively electron withdrawing and carbaborane relatively electron donating with respect to the reference point (H and Me). This therefore indicates that, although $^{31}P\{^1H\}$ NMR data imply one aspect of the metal-ligand relationship (carbaborane donation) and the $^{11}B\{^1H\}$ NMR data another ($\{PR_3Au\}$ withdrawl), it may be assumed the corollary to each is also true. Consequently, the (independent) deductions made from the $^{31}P\{^1H\}$ and $^{11}B\{^1H\}$ NMR data are consistent with each other.

The trends in the $^{11}B\{^1H\}$ NMR spectra are also observed with the other compounds **4**. As this comparison required analysis of $^{11}B\{^1H\}$ NMR spectra acquired at a field strength of 64.21 MHz and assignment was accomplished using (better resolved) spectra acquired at 192.63 MHz, the assignment of the $^{11}B\{^1H\}$ NMR spectra of **1** and **4a** at 64.21 MHz had to be deduced from the spectra acquired at 192.63 MHz. **Figure 2.9** outlines the assignment of the $^{11}B\{^1H\}$ NMR spectra of **1** and **4a** acquired at 64.21 MHz. **Figure 2.10** outlines the comparison of the two spectra and, consequently, illustrates the overall general shift of the resonances in **4a** to higher frequency with respect to those in **1**. Since compounds **4** (and, indeed, compounds **3**) are all related, the assignment of the $^{11}B\{^1H\}$ NMR spectra can be deduced for compounds **4** (and tentatively for compounds **3**) from the assignment of the spectrum of **4a**. **Table 2.7** outlines the spectrum width narrowing and the overall average shift to higher frequency as compared to the $^{11}B\{^1H\}$ NMR spectrum (64.21 MHz) of **1**. Similarily for compounds **3**, using the $^{11}B\{^1H\}$ NMR spectrum (64.21 MHz) of **3e** as an example and comparing it to that of **2** (64.21 MHz), it can be seen that again there is spectrum width narrowing and an apparent overall shift to higher frequency (**Figure 2.11**).

The ^1H NMR data confirm the number of protons in each species in the correct ratio. The shift in the resonances due to the protons of the substituent on C(1) of the carbaborane is minimal when comparing compounds **3** to compound **2** and compounds **4** to compound **1**, implying that the organic substituents are not drastically affected by substitution on C(2). This is congruous with the observed $^{31}P\{^1H\}$ NMR data where the phosphorus environment is not dramatically affected by substitution on C(1) (*vide retro*).

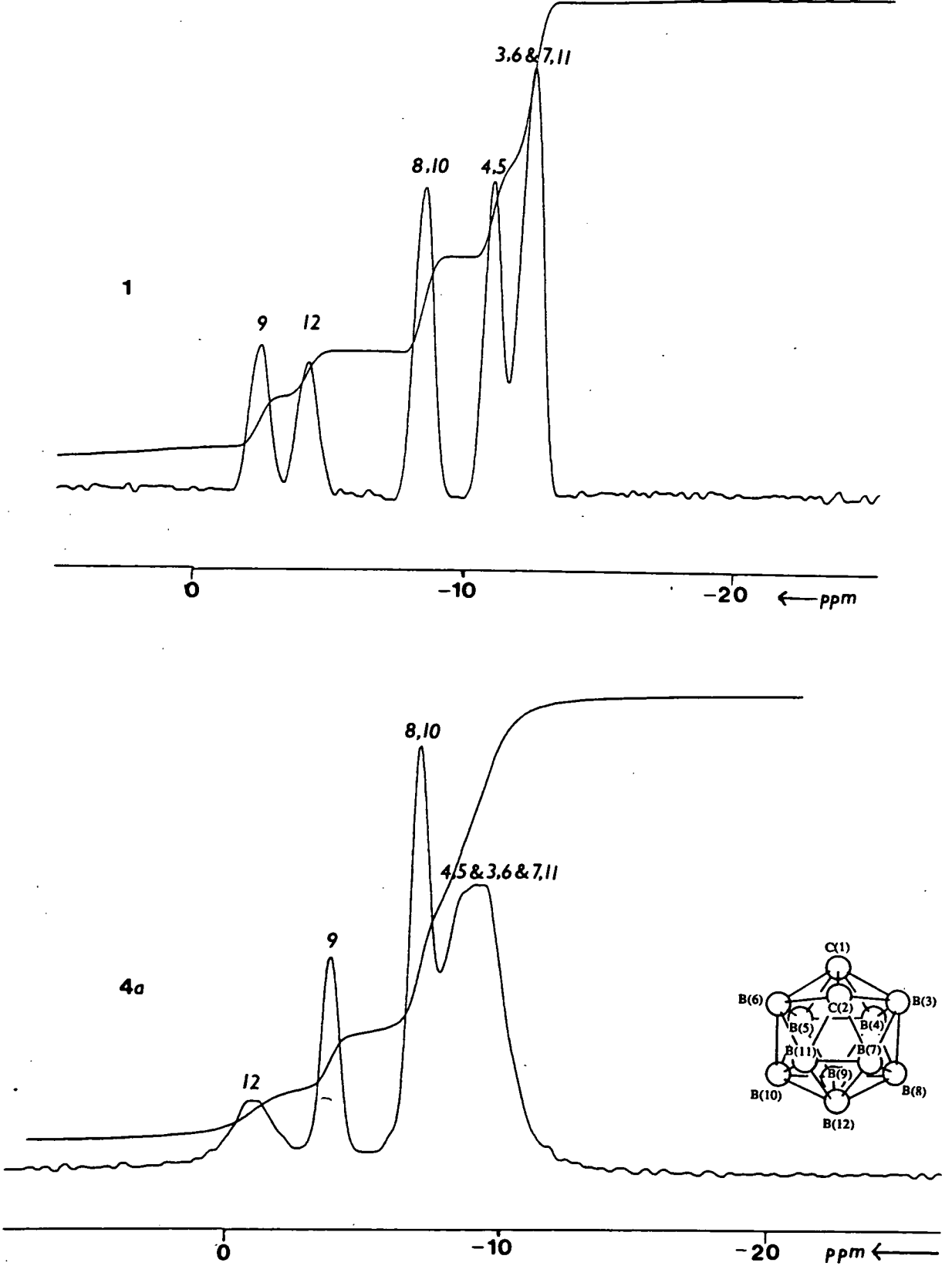

Figure 2.9 Assignment of $^{11}B\{^{1}H\}$ NMR spectra of **1** and **4a** acquired at 64.21 MHz.

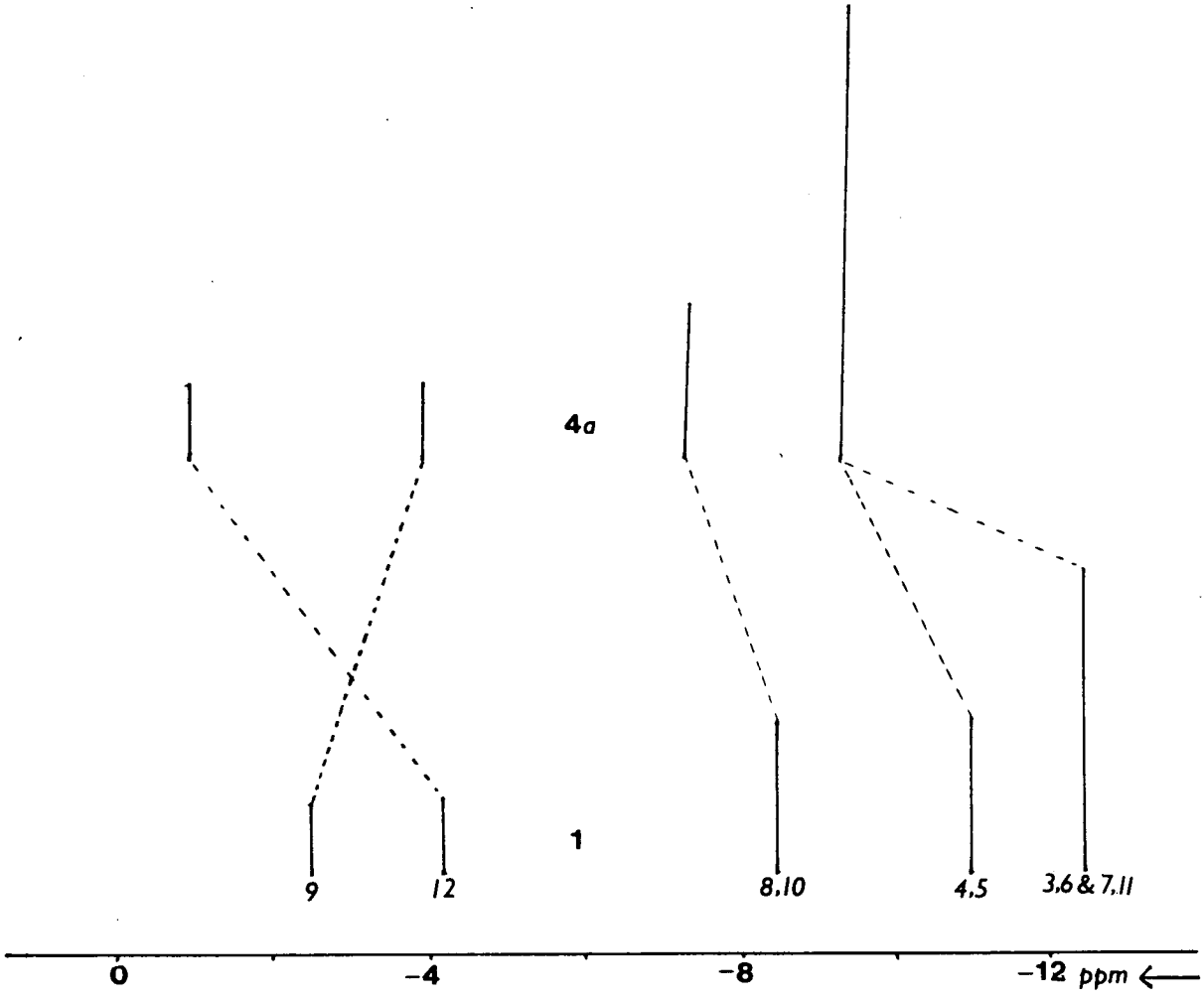

Figure 2.10 Comparison of $^{11}B\{^1H\}$ NMR Spectra of **1** and **4a** (64.21 MHz).

	average shift/ppm	spectral width/ppm
1	----	9.98
4a	+2.03	8.30
4b	+1.72	8.19
4c	+1.71	8.35
4d	+1.70	8.25
4e	+2.10	7.44

Table 2.7 Average Shift of $^{11}B\{^1H\}$ NMR Resonances from **1** to Compounds **4** (64.21 MHz).

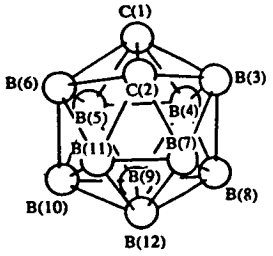

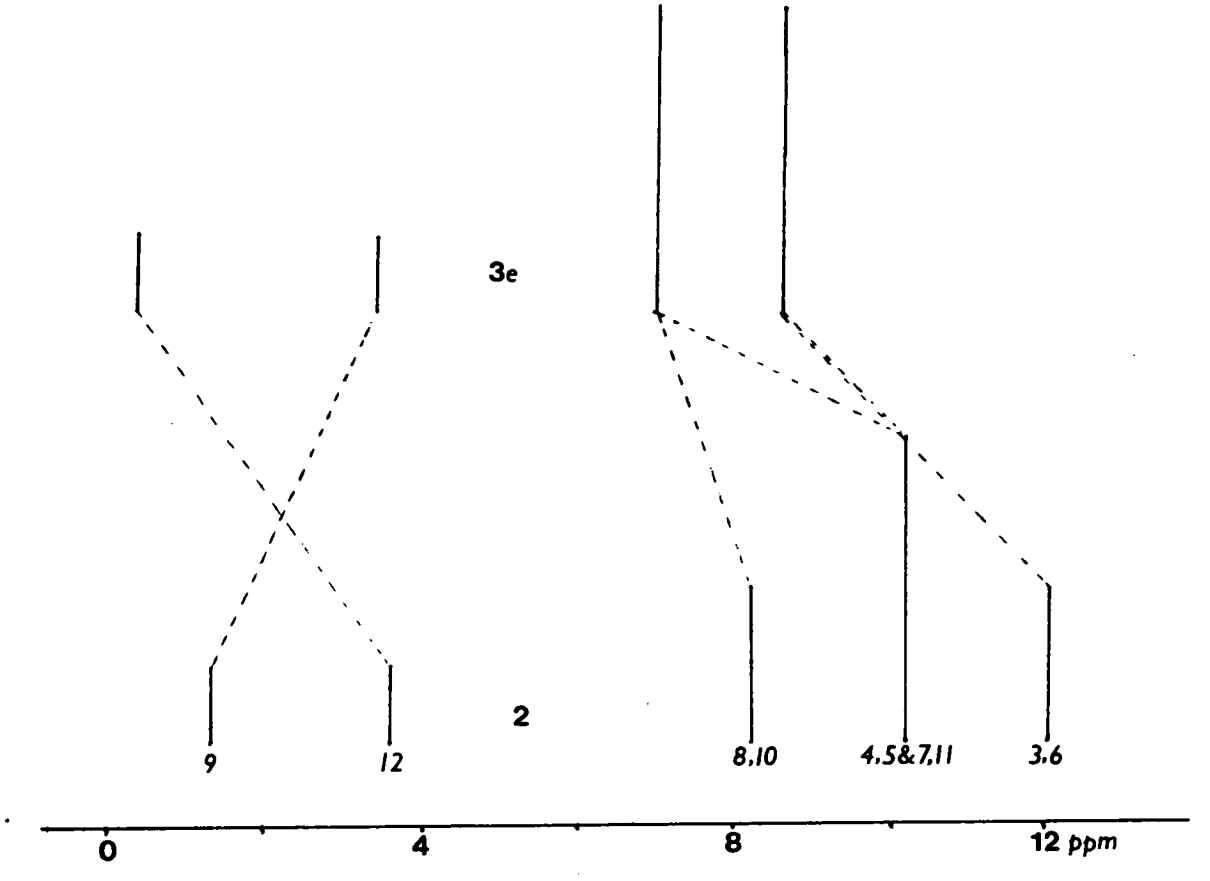

Figure 2.11 Comparison of $^{11}B\{^1H\}$ NMR Spectra of **2** and **3e** (64.21 MHz).

2.3.3 Crystallographic Studies

In order to quantify molecular dimensions a crystallographic study on one of the complexes needed to be performed. Both **4a** and **4e** afforded high quality crystals from the CH_2Cl_2/*n*-hexane crystallisation step. Both were shown to be isomorphous by unit cell determinations (**Table 2.8**). However, crystals of **4a** became opaque after about 20 hours at room temperature probably through loss of loosely bound solvent in the crystal, resulting in intensity loss when collecting data. Thus, intensity data were collected from a single crystal of **4e** at low temperature. **Table 2.9** lists atomic positions and equivalent isotropic thermal parameters for all non-hydrogen atoms and **Table 2.10** details selected bond distances and interbond angles. Anisotropic thermal parameters and hydrogen atom positions are given in **Appendix B. Figure 2.12** shows a perspective view of a single molecule of **4e** and demonstrates the numbering scheme adopted. **4e** cocrystallises with one molecule of CH_2Cl_2 solvate but this is disordered in the lattice and consequently is poorly defined.

	4a	**4e**
crystal system	triclinic	triclinic
a/Å	9.7109(71)	9.6664(22)
b/Å	12.6400(71)	12.7060(80)
c/Å	12.813(22)	12.7870(40)
$\alpha/^\circ$	94.53(9)	93.78(4)
$\beta/^\circ$	97.03(10)	97.28(2)
$\gamma/^\circ$	103.22(6)	102.32(2)
V/Å^3	1510.27(30)	1514.8(12)

Table 2.8 Unit Cell Data of Single Crystals of **4a** and **4e**.

	x	y	z	Ueq
Au	0.17560(3)	0.48470(2)	0.26374(2)	0.0398(2)
As	0.00550(9)	0.33080(6)	0.17702(6)	0.0385(4)
C(11)	0.0461(9)	0.2846(6)	0.0385(6)	0.041(4)
C(12)	0.1316(10)	0.3605(8)	-0.0130(8)	0.055(5)
C(13)	0.1684(10)	0.3294(10)	-0.1087(8)	0.065(6)
C(14)	0.1256(11)	0.2250(9)	-0.1521(8)	0.069(7)
C(15)	0.0351(14)	0.1484(9)	-0.0993(8)	0.071(7)
C(16)	-0.0024(11)	0.1810(8)	-0.0047(8)	0.059(6)
C(21)	-0.0113(9)	0.2033(6)	0.2518(6)	0.039(4)
C(22)	0.1115(11)	0.1785(7)	0.2984(9)	0.062(6)
C(23)	0.1053(13)	0.0872(8)	0.3500(9)	0.076(8)
C(24)	-0.0281(14)	0.0208(8)	0.3588(8)	0.067(7)
C(25)	-0.1474(12)	0.0452(7)	0.3122(8)	0.063(6)
C(26)	-0.1404(10)	0.1367(7)	0.2595(8)	0.054(5)
C(31)	-0.1877(10)	0.3523(6)	0.1540(6)	0.045(5)
C(32)	-0.2460(12)	0.3781(8)	0.2437(7)	0.067(6)
C(33)	-0.3845(12)	0.3975(9)	0.2299(7)	0.073(7)
C(34)	-0.4627(13)	0.3891(9)	0.1300(8)	0.072(7)
C(35)	-0.4044(12)	0.3613(9)	0.0470(8)	0.069(7)
C(36)	-0.2651(10)	0.3436(8)	0.0561(6)	0.055(5)
C(101)	0.1062(10)	0.7069(8)	0.3936(10)	0.060(6)
O	0.0635(7)	0.6378(6)	0.4696(6)	0.070(5)
C(102)	-0.0811(11)	0.6231(9)	0.4756(9)	0.072(7)
C(1)	0.2632(8)	0.7214(6)	0.3892(6)	0.037(4)
C(2)	0.3207(9)	0.6207(5)	0.3312(6)	0.036(4)
B(3)	0.3576(9)	0.6467(7)	0.4665(7)	0.035(4)
B(6)	0.3177(10)	0.7371(7)	0.2689(7)	0.040(5)
B(7)	0.4868(10)	0.6210(7)	0.3923(8)	0.042(5)
B(8)	0.5326(11)	0.7273(9)	0.4964(8)	0.050(6)
B(12)	0.5973(11)	0.7452(9)	0.3726(9)	0.054(6)
B(11)	0.4668(10)	0.6751(7)	0.2729(7)	0.042(5)
B(5)	0.3609(11)	0.8439(7)	0.3688(9)	0.052(6)
B(9)	0.5350(12)	0.8487(9)	0.4380(10)	0.058(7)
B(10)	0.4941(11)	0.8164(8)	0.2952(8)	0.048(6)
B(4)	0.3859(12)	0.7905(8)	0.4918(8)	0.048(6)
Cl(1)	-0.566(3)	0.0963(18)	0.2004(19)	
Cl(2)	-0.674(6)	0.054(4)	0.034(5)	
Cl(3)	-0.610(8)	0.000(6)	0.056(8)	
Cl(4)	-0.531(10)	-0.034(5)	-0.057(7)	
CX(1)	-0.816(13)	-0.042(8)	0.164(9)	
CX(2)	-0.884(18)	0.168(13)	-0.033(15)	

Table 2.9 Coordinates of Refined Atoms and Equivalent Isotropic Thermal Parameters ($Å^2$) for **4e**.

Au	- As	2.3740(8)	C(1)	- B(6)	1.698(12)
Au	- C(2)	2.039(8)	C(1)	- B(5)	1.695(13)
As	-C(11)	1.943(8)	C(1)	- B(4)	1.705(13)
As	-C(21)	1.922(8)	C(2)	- B(3)	1.717(11)
As	-C(31)	1.933(8)	C(2)	- B(6)	1.730(12)
C(11)	-C(12)	1.389(13)	C(2)	- B(7)	1.693(12)
C(11)	-C(16)	1.354(13)	C(2)	-B(11)	1.716(12)
C(12)	-C(13)	1.373(14)	B(3)	- B(7)	1.732(13)
C(13)	-C(14)	1.360(15)	B(3)	- B(8)	1.760(14)
C(14)	-C(15)	1.429(16)	B(3)	- B(4)	1.789(13)
C(15)	-C(16)	1.369(15)	B(6)	-B(11)	1.781(13)
C(21)	-C(22)	1.367(13)	B(6)	- B(5)	1.744(14)
C(21)	-C(26)	1.369(12)	B(6)	-B(10)	1.764(14)
C(22)	-C(23)	1.366(16)	B(7)	- B(8)	1.776(14)
C(23)	-C(24)	1.405(16)	B(7)	-B(12)	1.760(15)
C(24)	-C(25)	1.336(15)	B(7)	-B(11)	1.720(13)
C(25)	-C(26)	1.375(14)	B(8)	-B(12)	1.785(15)
C(31)	-C(32)	1.391(13)	B(8)	- B(9)	1.755(16)
C(31)	-C(36)	1.359(12)	B(8)	- B(4)	1.769(15)
C(32)	-C(33)	1.404(15)	B(12)	-B(11)	1.724(14)
C(33)	-C(34)	1.385(16)	B(12)	- B(9)	1.764(16)
C(34)	-C(35)	1.325(16)	B(12)	-B(10)	1.745(15)
C(35)	-C(36)	1.404(14)	B(11)	-B(10)	1.757(14)
C(101)	- O	1.394(13)	B(5)	- B(9)	1.786(16)
C(101)	- C(1)	1.498(13)	B(5)	-B(10)	1.766(15)
O	-C(102)	1.384(14)	B(5)	- B(4)	1.762(15)
C(1)	- C(2)	1.667(11)	B(9)	-B(10)	1.820(16)
C(1)	- B(3)	1.725(11)	B(9)	- B(4)	1.721(16)

As	- Au - C(2)	177.05(21)	B(7)	- C(2) -B(11)	60.6(5)
Au	- As -C(11)	113.51(24)	C(1)	- B(3) - C(2)	58.0(4)
Au	- As -C(21)	114.87(23)	C(1)	- B(3) - B(4)	58.0(5)
Au	- As -C(31)	113.61(25)	C(2)	- B(3) - B(7)	58.8(5)
C(11)	- As -C(21)	104.4(3)	B(7)	- B(3) - B(8)	61.1(5)
C(11)	- As -C(31)	105.6(3)	B(8)	- B(3) - B(4)	59.8(6)
C(21)	- As -C(31)	103.8(3)	C(1)	- B(6) - C(2)	58.2(5)
As	-C(11) -C(12)	117.7(6)	C(1)	- B(6) - B(5)	59.0(5)
As	-C(11) -C(16)	121.3(7)	C(2)	- B(6) -B(11)	58.5(5)
C(12)	-C(11) -C(16)	121.0(8)	B(11)	- B(6) -B(10)	59.4(5)
C(11)	-C(12) -C(13)	119.3(9)	B(5)	- B(6) -B(10)	60.5(6)
C(12)	-C(13) -C(14)	121.0(10)	C(2)	- B(7) - B(3)	60.2(5)
C(13)	-C(14) -C(15)	119.0(10)	C(2)	- B(7) -B(11)	60.4(5)
C(14)	-C(15) -C(16)	119.3(10)	B(3)	- B(7) - B(8)	60.2(5)

Table 2.10 Selected Interatomic Distances (Å) and Interbond Angles (°) in **4e**.

C(11)	-C(16)	-C(15)	120.4(10)	B(8)	- B(7)	-B(12)	60.7(6)
As	-C(21)	-C(22)	118.1(6)	B(12)	- B(7)	-B(11)	59.4(6)
As	-C(21)	-C(26)	122.8(6)	B(3)	- B(8)	- B(7)	58.6(5)
C(22)	-C(21)	-C(26)	119.1(8)	B(3)	- B(8)	- B(4)	60.9(6)
C(21)	-C(22)	-C(23)	120.3(9)	B(7)	- B(8)	-B(12)	59.2(6)
C(22)	-C(23)	-C(24)	119.8(10)	B(12)	- B(8)	- B(9)	59.8(6)
C(23)	-C(24)	-C(25)	119.4(10)	B(9)	- B(8)	- B(4)	58.5(6)
C(24)	-C(25)	-C(26)	120.4(10)	B(7)	-B(12)	- B(8)	60.1(6)
C(21)	-C(26)	-C(25)	120.9(9)	B(7)	-B(12)	-B(11)	59.2(6)
As	-C(31)	-C(32)	116.6(7)	B(8)	-B(12)	- B(9)	59.3(6)
As	-C(31)	-C(36)	123.0(7)	B(11)	-B(12)	-B(10)	60.8(6)
C(32)	-C(31)	-C(36)	120.4(8)	B(9)	-B(12)	-B(10)	62.5(6)
C(31)	-C(32)	-C(33)	118.2(9)	C(2)	-B(11)	- B(6)	59.2(5)
C(32)	-C(33)	-C(34)	121.2(10)	C(2)	-B(11)	- B(7)	59.0(5)
C(33)	-C(34)	-C(35)	118.5(11)	B(6)	-B(11)	-B(10)	59.8(5)
C(34)	-C(35)	-C(36)	122.6(10)	B(7)	-B(11)	-B(12)	61.5(6)
C(31)	-C(36)	-C(35)	119.0(9)	B(12)	-B(11)	-B(10)	60.2(6)
O	-C(101)	- C(1)	110.9(8)	C(1)	- B(5)	- B(6)	59.2(5)
C(101)	- O	-C(102)	112.2(8)	C(1)	- B(5)	- B(4)	59.1(5)
C(101)	- C(1)	- C(2)	118.6(7)	B(6)	- B(5)	-B(10)	60.3(6)
C(101)	- C(1)	- B(3)	118.4(7)	B(9)	- B(5)	-B(10)	61.6(6)
C(101)	- C(1)	- B(6)	117.1(7)	B(9)	- B(5)	- B(4)	58.0(6)
C(101)	- C(1)	- B(5)	119.7(7)	B(8)	- B(9)	-B(12)	61.0(6)
C(101)	- C(1)	- B(4)	120.6(7)	B(8)	- B(9)	- B(4)	61.2(6)
B(3)	- C(1)	- C(2)	60.8(5)	B(12)	- B(9)	-B(10)	58.3(6)
B(3)	- C(1)	- B(4)	62.9(5)	B(5)	- B(9)	-B(10)	58.7(6)
B(6)	- C(1)	- C(2)	61.9(5)	B(5)	- B(9)	- B(4)	60.3(6)
B(6)	- C(1)	- B(5)	61.9(5)	B(6)	-B(10)	-B(11)	60.8(5)
B(5)	- C(1)	- B(4)	62.4(6)	B(6)	-B(10)	- B(5)	59.2(6)
Au	- C(2)	- C(1)	119.3(5)	B(12)	-B(10)	-B(11)	59.0(6)
Au	- C(2)	- B(3)	120.4(5)	B(12)	-B(10)	- B(9)	59.3(6)
Au	- C(2)	- B(6)	116.0(5)	B(5)	-B(10)	- B(9)	59.7(6)
Au	- C(2)	- B(7)	124.1(5)	C(1)	- B(4)	- B(3)	59.1(5)
Au	- C(2)	-B(11)	121.5(5)	C(1)	- B(4)	- B(5)	58.5(5)
B(3)	- C(2)	- C(1)	61.3(5)	B(3)	- B(4)	- B(8)	59.3(5)
B(3)	- C(2)	- B(7)	61.1(5)	B(8)	- B(4)	- B(9)	60.4(6)
B(6)	- C(2)	- C(1)	59.9(5)	B(5)	- B(4)	- B(9)	61.7(6)
B(6)	- C(2)	-B(11)	62.3(5)				

Table 2.10 Selected Interbond Angles (°) in **4e** (continued).

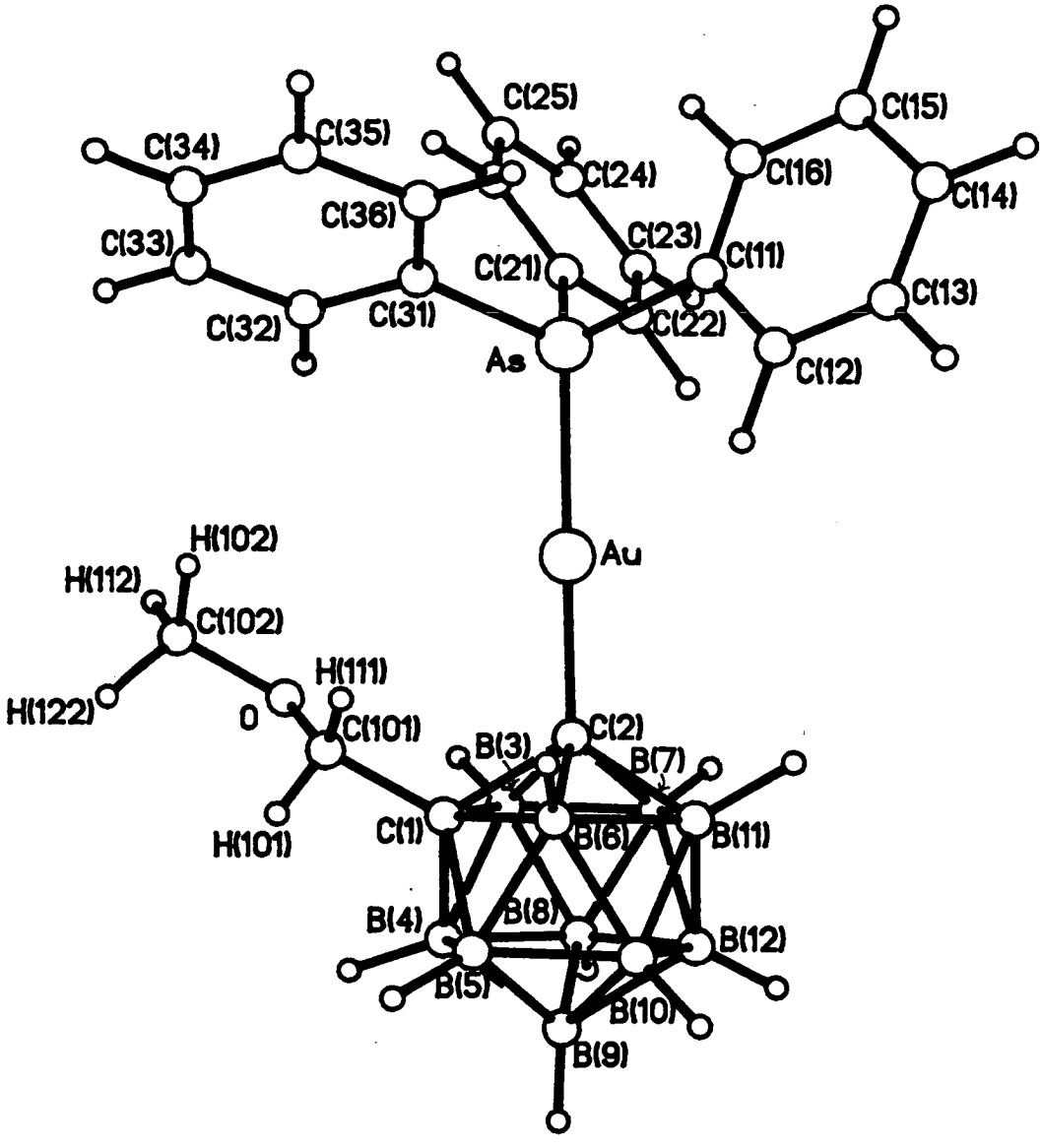

Figure 2.12 Perspective View of **4e** (cage H atoms carry the same number as the B atoms to which they are bound).

In **4e** the {1,2-*closo*-C_2B_{10}} cage has the expected icosahedral geometry and the C(1)-C(2) distance is 1.667(11) Å. This is longer than in the parent carbaborane, **1**, which has a C(1)-C(2) distance of 1.636(9) Å[20], but not significantly so. With twist angles of 24°, 43° and 60° about the As-C(11), As-C(21) and As-C(31) bonds respectively, where a 0° twist is equivalent to an eclipsed Au-As-C-C arrangement, the phenyl rings of the arsine group adopt a propellar-like configuration. The orientation of the ether substituent is defined by the C(2)-C(1)-C(101)-O torsion angle of 74.9(8)° and the C(1)-C(101)-O-C(102) torsion angle of 179.8(8)°. Therefore the ether substituent is *trans* staggered and results in a closest interligand contact of 2.659(15) Å between H(32) and H(112). The O-Au distance of 3.582(7) Å is greater than the sum of their respective van der Waals' radii[87] and is therefore too long for there to be any interaction. In a similar species previously characterised, 1-$C_2H_5OCH_2$-2-{MeHg}-1,2-*closo*-$C_2B_{10}H_{10}$[55] (**Figure 1.23b**, p30), which is isoelectronic with **4e**, the C(2)-C(1)-C-O torsion is almost 0° and the Hg-O distance is 2.747(4) Å, both of which suggest that there is some secondary bonding between the metal and the ether substituent oxygen atom. Bonding can occur by donation of the oxygen lone pair of electrons into the (empty) $6p_x/6p_y$ orbitals on the metal (Hg and Au). This certainly happens with Hg but not with Au. Moreover, any Au-O interaction would presumably show a deviation from linearity of the As-Au-C(2) sequence, Au^I complexes being typically two coordinate and linear, although occassionally three coordinate and trigonal (and four coordinate and tetrahedral). With an As-Au-C(2) bond angle of 177.05(21)° there is clearly no significant deviation from linearity.

The Au-As bond length is 2.3740(8) Å and the Au-C(2) length is 2.039(8) Å. The only reported[88] molecular structure of a σ-gold carbaborane compound is that of 1-{PPh_3Au}-1,2-*closo*-$C_2B_{10}H_{11}$ (**Figure 2.13**) which was synthesised by reaction between 1,2-*closo*-$C_2B_{10}H_{12}$ and $[O(AuPPh_3)_3]BF_4$. In this compound, the Au-P

bond length is 2.272(2) Å which is shorter than the As-Au distance in **4e**, as expected. The Au-C bond length is 2.039(8) Å and is therefore identical to that observed in **4e** (including the estimated standard deviation!). The congruity of the Au-C bond lengths intimates that the As-Au and P-Au bonds are the same strength. [Indeed, the difference in As-C and P-C bond lengths (Δ = 0.1 Å) is equivalent to the difference in the covalent radii of As and P]. Therefore, there must be no appreciable metal-to-phosphine/arsine back-bonding since this would result in a shorter P-Au (versus As-Au) bond as a consequence of the 3*d* orbitals of P being more accessible for back-bonding than the 4*d* orbitals of As.

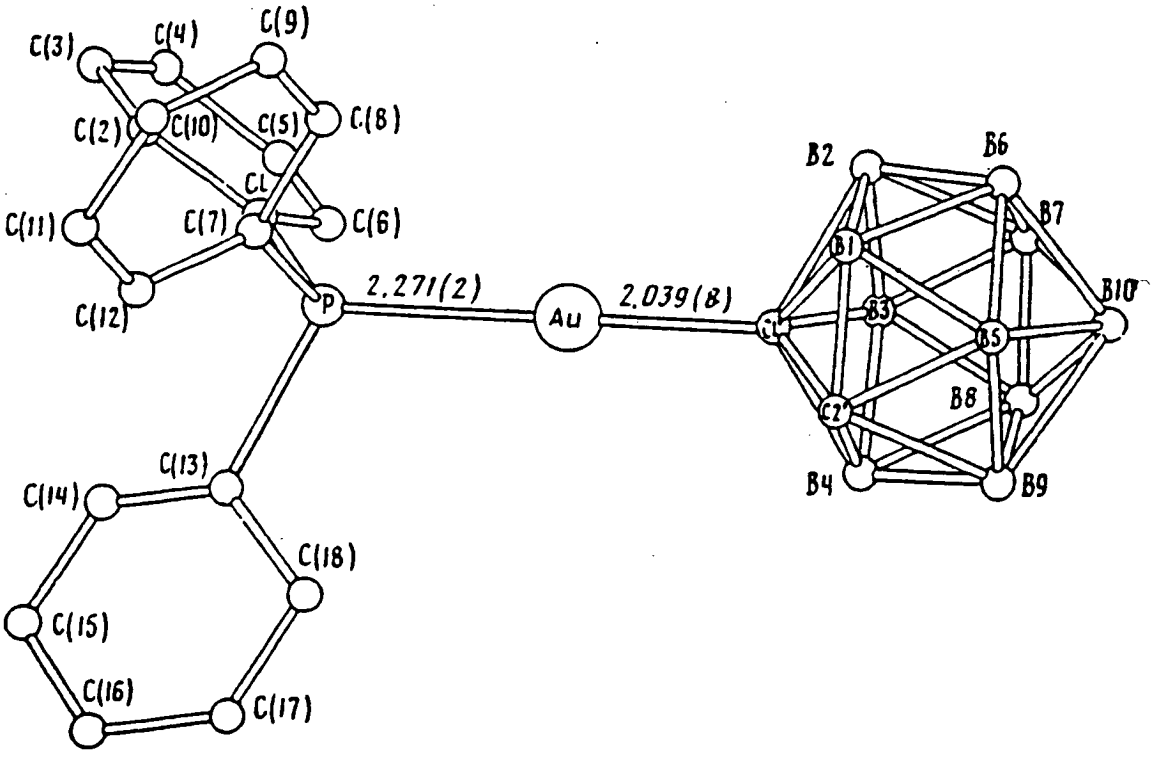

Figure 2.13 Molecular Structure of 1-{PPh_3Au}-1,2-*closo*-$C_2B_{10}H_{11}$[88].

Despite the consistency observed in the molecular structures of the σ-gold carbaborane compounds, the question that needed to be answered was whether the stability of these compounds was due to stronger, and therefore presumably shorter, gold-carbon bonds. Organometallic gold(I) species, in particular phosphine gold(I) methyl complexes, are well known and characterised, and so comparison of the gold-carbaborane bond length with a typical gold-methyl bond length would give an indication of their relative bond strengths. A single Au-C bond *trans* to triphenylarsine could be expected to be about 2.1 Å by comparison of the Au-CH_3 and Au-Br bond lengths [2.124(28) and 2.407(2) Å] in PPh_3AuMe[89] and PPh_3AuBr[90] respectively (Δ = 0.28 Å) and subtraction of this difference from the Au-Br bond length of 2.377(6) Å in $AsPh_3AuBr$[91]. This would lead to the prediction that the Au-CH_3 bond length in $AsPh_3AuMe$ is 2.097 Å and on this assumption the bond length in **4e** appears to be unusually short.

The above crude comparison is of fundamental importance to the understanding of the stability of the gold carbaboranes. Therefore, before further consideration can be given to the above result, it is obviously important to accurately determine the length of a typical gold-carbon bond *trans* to triphenylarsine.

Consequently $AsPh_3AuMe$ (**5**) was synthesised (**Section 2.2.4**) and its molecular structure determined. Intensity data were collected from a single crystal of **5** at room temperature. **Table 2.11** details atomic positions and equivalent isotropic thermal parameters for all non-hydrogen atoms and **Table 2.12** lists selected interatomic distances and interbond angles. **Appendix B** contains lists of anisotropic thermal parameters and hydrogen atom positions. **Figure 2.14** shows a perspective view of a single molecule of **5**. Again the phenyl rings adopt a propellar-like twist with angles of 32°, 57° and 37° about the As-C(11), As-C(21) and As-C(31) bonds respectively. The As-Au-C sequence is again essentially linear with an angle of 178.60(24)°. Comparing the molecular structures of **5** and **4e**, the Au-As distance in **5**, 2.3800(11)

Å, is within 0.0060(14) Å of that in **4e**, but the Au-C_{methyl} distance, 2.124(9) Å, is 0.085(12) Å longer than the Au-$C_{carbaborane}$ distance, supporting the proposal that the gold-carbon σ-bond in **4e** is anomalously short.

The crystallographic studies give no indication of the function of the carbaborane ligand. Loss of electron density from the cage could result in connectivity lengthening (compared to the parent carbaborane [**1**]) in the bonds between C(2) and the carbon and boron atoms to which it is directly connected: C(1), B(3), B(6), B(7) and B(11). Certainly, studies of the molecular structures of several diborane and dicarbaborane species[92, 93] in which the boron-boron bond between the two (carba)boranes is short and strong due to electron density being donated from the respective cages have shown lengthening [compared to the parent (carba)borane] of the boron-boron (carbon-boron) connectivities between the substituted boron atom and those boron atoms bonded directly to it. Since these studies have all involved symmetrical molecules with small cage sizes (5-8 atoms) where the substituent is another (carba)borane, the observations may not hold for a comparison between the larger (12 cage atoms) and less symmetrical **1** and **4e**. Unfortunately this appears to be so as, while the C(2)-C(1), C(2)-B(6) and C(2)-B(11) connectivities are longer in **4e** than in **1**, the C(2)-B(3) connectivity is about the same and the C(2)-B(7) connectivity is in fact shorter in **4e** than in **1**. Hence, no firm conclusions about the carbaborane ligand function can be drawn from these comparisons.

	x	y	z	Ueq
Au(1)	0.31219(5)	0.04654(3)	0.10622(2)	0.0493(2)
As(1)	0.40587(11)	0.22500(8)	0.06482(6)	0.0459(6)
C(11)	0.3325(11)	0.2634(8)	-0.0452(6)	0.050(6)
C(12)	0.4180(12)	0.3267(9)	-0.0872(6)	0.056(7)
C(13)	0.3575(12)	0.3616(9)	-0.1638(6)	0.059(7)
C(14)	0.2093(14)	0.3351(9)	-0.2009(6)	0.067(8)
C(15)	0.1214(12)	0.2688(11)	-0.1617(7)	0.069(8)
C(16)	0.1828(10)	0.2313(9)	-0.0835(6)	0.055(7)
C(21)	0.3455(10)	0.3624(8)	0.1166(6)	0.048(6)
C(22)	0.2629(13)	0.4520(9)	0.0727(7)	0.063(7)
C(23)	0.2158(14)	0.5438(10)	0.1172(9)	0.077(9)
C(24)	0.2560(15)	0.5435(12)	0.1972(9)	0.077(9)
C(25)	0.3360(14)	0.4577(12)	0.2383(7)	0.074(8)
C(26)	0.3850(12)	0.3654(10)	0.1986(7)	0.063(7)
C(31)	0.6260(10)	0.2347(9)	0.0857(6)	0.049(6)
C(32)	0.7063(12)	0.1340(11)	0.0755(7)	0.068(8)
C(33)	0.8640(14)	0.1409(13)	0.0857(8)	0.083(9)
C(34)	0.9416(14)	0.2434(14)	0.1102(8)	0.088(10)
C(35)	0.8605(13)	0.3418(13)	0.1198(8)	0.081(9)
C(36)	0.7039(12)	0.3381(10)	0.1085(7)	0.072(8)
C(1)	0.2266(10)	-0.1104(7)	0.1452(5)	0.042(5)

Table 2.11 Coordinates of Refined Atoms and Equivalent Isotropic Thermal Parameters ($Å^2$) for **5**.

Au(1)	-As(1)	2.3800(11)	C(21)	-C(26)	1.382(15)
Au(1)	- C(1)	2.124(9)	C(22)	-C(23)	1.426(17)
As(1)	-C(11)	1.913(10)	C(23)	-C(24)	1.349(19)
As(1)	-C(21)	1.949(10)	C(24)	-C(25)	1.314(19)
As(1)	-C(31)	1.929(10)	C(25)	-C(26)	1.389(17)
C(11)	-C(12)	1.389(14)	C(31)	-C(32)	1.390(15)
C(11)	-C(16)	1.396(14)	C(31)	-C(36)	1.376(15)
C(12)	-C(13)	1.368(15)	C(32)	-C(33)	1.390(18)
C(13)	-C(14)	1.364(16)	C(33)	-C(34)	1.372(20)
C(14)	-C(15)	1.392(17)	C(34)	-C(35)	1.370(20)
C(15)	-C(16)	1.402(16)	C(35)	-C(36)	1.376(18)
C(21)	-C(22)	1.376(15)			

As(1)	-Au(1)	- C(1)	178.60(24)	As(1)	-C(21)	-C(26)	117.9(8)
Au(1)	-As(1)	-C(11)	116.0(3)	C(22)	-C(21)	-C(26)	121.2(10)
Au(1)	-As(1)	-C(21)	112.5(3)	C(21)	-C(22)	-C(23)	115.8(10)
Au(1)	-As(1)	-C(31)	114.7(3)	C(22)	-C(23)	-C(24)	121.3(12)
C(11)	-As(1)	-C(21)	102.3(4)	C(23)	-C(24)	-C(25)	122.2(13)
C(11)	-As(1)	-C(31)	104.8(4)	C(24)	-C(25)	-C(26)	119.4(12)
C(21)	-As(1)	-C(31)	105.1(4)	C(21)	-C(26)	-C(25)	120.1(10)
As(1)	-C(11)	-C(12)	123.2(8)	As(1)	-C(31)	-C(32)	118.2(8)
As(1)	-C(11)	-C(16)	117.9(7)	As(1)	-C(31)	-C(36)	122.0(8)
C(12)	-C(11)	-C(16)	118.9(9)	C(32)	-C(31)	-C(36)	119.8(10)
C(11)	-C(12)	-C(13)	121.7(10)	C(31)	-C(32)	-C(33)	119.1(11)
C(12)	-C(13)	-C(14)	120.1(10)	C(32)	-C(33)	-C(34)	120.9(13)
C(13)	-C(14)	-C(15)	119.9(11)	C(33)	-C(34)	-C(35)	119.1(13)
C(14)	-C(15)	-C(16)	120.5(11)	C(34)	-C(35)	-C(36)	121.1(12)
C(11)	-C(16)	-C(15)	118.9(10)	C(31)	-C(36)	-C(35)	119.9(11)
As(1)	-C(21)	-C(22)	120.9(8)				

Table 2.12 Selected Interatomic Distances (Å) and Interbond Angles (°) for **5**.

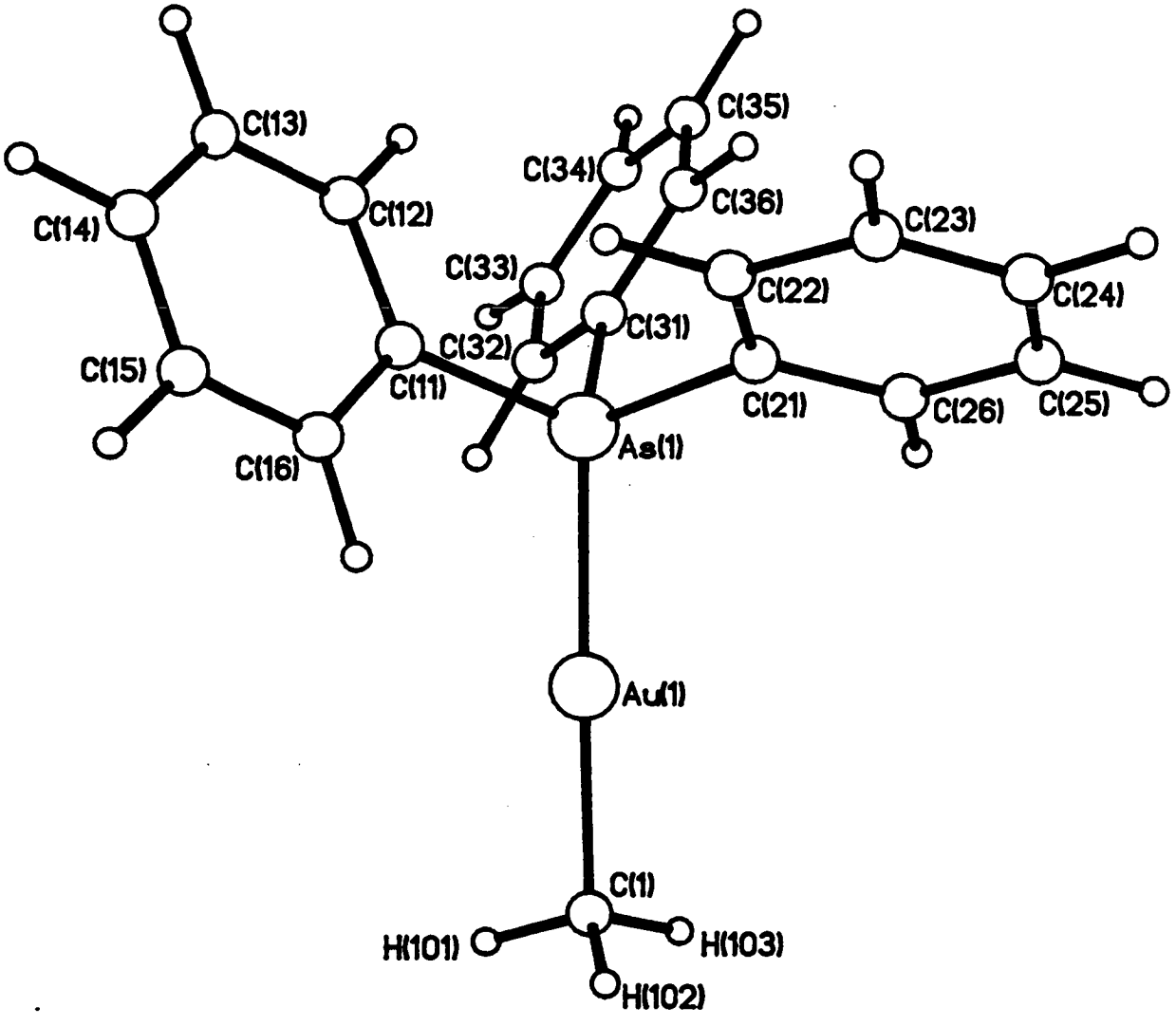

Figure 2.14 Perspective View of **5**.

2.3.4 Molecular Orbital Calculations

By taking the NMR and crystallographic studies together it would appear that the stability of the σ-bonded carbaborane compounds is due to the shorter than expected gold-carbon σ-bond which, in turn, may be a result of the donating properties of the carbaborane ligand. In order to understand the origin of this unexpected bond shortening and to confirm the mounting evidence that the carbaborane is an electron donor, extended Hückel molecular orbital (EHMO) calculations (see **Section 5.3**) have been performed on the model compounds 2-{AsH_3Au}-1,2-*closo*-$C_2B_{10}H_{11}$, **I**, and AsH_3AuCH_3, **II**, (**Figure 2.15**). The pertinent results are presented in **Table 2.13**.

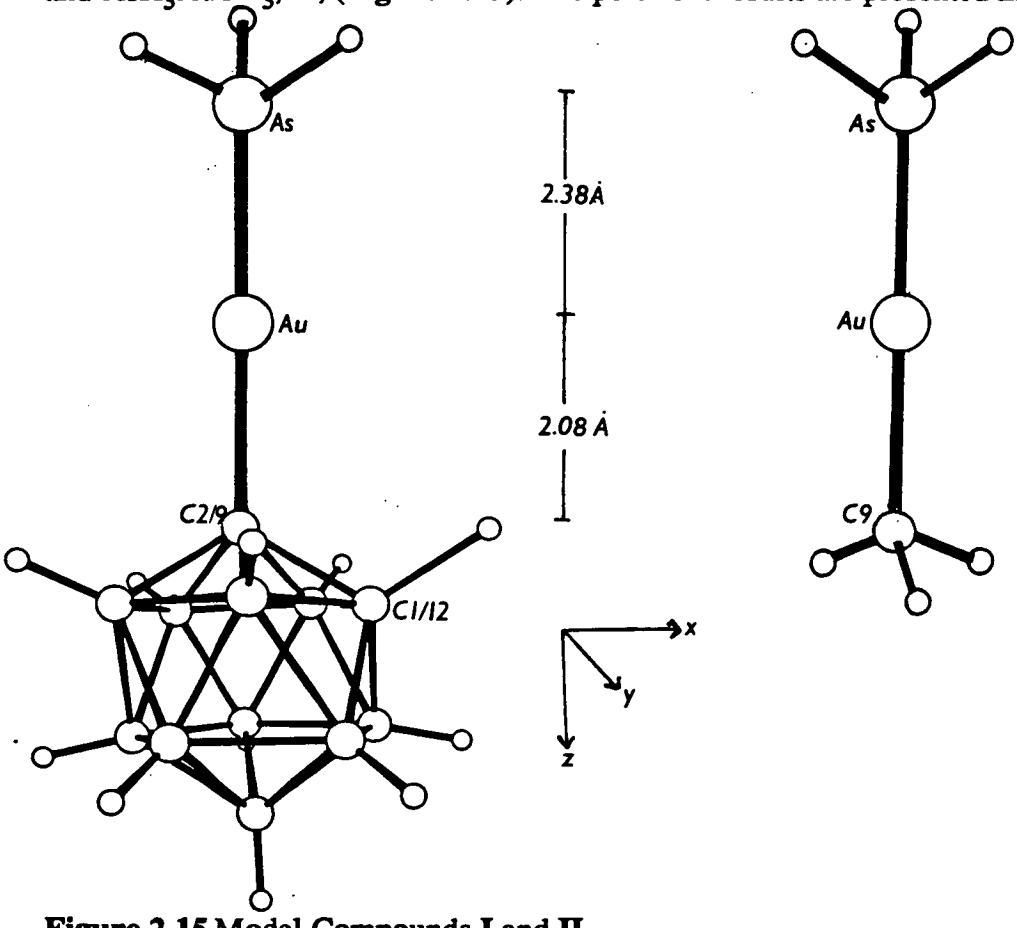

Figure 2.15 Model Compounds **I** and **II**.

Comparison of the reduced overlap population matrix (ROPM) elements confirms that the Au-As bond strength in **I** and **II** is essentially the same, but shows that the

shorter Au-C bond length in the carbaborane is due to an increase in bond strength. In **I** the gold atom carries a negative charge of -0.0173 electrons, a total of 0.0182 electrons greater than the charge on the gold atom in **II**. This is distinctly symptomatic of an increase in electron density around the gold atom and must originate from the carbaborane ligand. Analysis of the individual atomic orbital occupations show that this increased charge lies predominantly in the $6p_z$ and $6s$ orbitals of gold, with a small, insignificant, increase in the orbital occupation of the $6p_x$ and $6p_y$ orbitals. These results show that the carbaborane ligand is a better σ-donor than the methyl ligand.

	II	**I**	**Δ (I-II)**
ROPM elements			
Au-As	0.6296	0.6310	0.0014
Au-C	0.5323	0.5797	0.0474
Net atomic charge/e			
Au	0.0009	-0.0173	-0.0182
Gold AOO/e			
$6s$	0.8127	0.8197	0.0070
$6p_x$	0.0015	0.0065	0.0050
$6p_y$	0.0015	0.0040	0.0025
$6p_z$	0.3488	0.3638	0.0150
$5d_{x^2-y^2}$	1.9999	1.9998	-0.0001
$5d_{z^2}$	1.8619	1.8607	-0.0012
$5d_{xy}$	1.9999	1.9998	-0.0001
$5d_{xz}$	1.9865	1.9828	-0.0037
$5d_{yz}$	1.9865	1.9802	-0.0063

Table 2.13 Summary of Pertinent Results from Calculations on **I** and **II**.

Further calculations on the respective carbanions [1,2-*closo*-$C_2B_{10}H_{11}]^-$ (**III**), derived from **I** by removal of the $\{AsH_3Au\}^+$ fragment, and $[CH_3]^-$ (**IV**) were performed and confirmed that the results obtained from the first calculation were reasonable: The HOMO of the carbaborane ligand lies at -10.68 eV, almost 1 eV higher than that of the methyl ligand (-11.75 eV). The HOMO of $[CH_3]^-$ is (as expected) a carbon $2s$-$2p_z$ hybrid orbital directed towards the fourth tetrahedral position, with the HOMO *ca.* 95% localised on the carbon atom. In **III** the HOMO is again an sp_z hybrid and is outpointing from the *closo* icosahedron. However, although localised mainly on C(2) [30%], the HOMO has substantial boron character with 60% divided more or less equally among 7 boron atoms. It is the boron character that increases the energy of the HOMO: Boron is more electropositive than carbon and so its valence atomic orbitals lie at higher energy. Thus, the carbaborane ligand is a better donor than methyl because its HOMO lies at higher energy due to its significant boron character.

2.4 Conclusions

The σ-bonded carbaboranes, compounds **3** and **4**, were successfully synthesised and fully characterised by microanalysis and IR and NMR spectroscopies. The IR spectra all showed the characteristic B-H peak between 2500 and 2600 cm^{-1} and compounds **4** also showed stretches between 1400 and 1100 cm^{-1} due to the ether substituent. The $^{31}P\{^1H\}$ NMR spectra, where appropriate, exhibited the expected singlet resonance at higher and lower frequency than the corresponding chloride and methyl respectively, intimating that the carbaborane ligand is a better donor than methyl but not as good as chloride.

The $^{11}B\{^1H\}$ NMR spectrum of **4a** has been assigned by an ^{11}B-^{11}B COSY NMR experiment and the changes in the spectrum, as compared to the assigned spectrum of **1**, noted: There is an overall shift of the boron resonances to higher frequency in accordance with electron density being donated from carbaborane to gold. This trend is observed (somewhat speculatively as not all the NMR spectra have been assigned by COSY experiments) for all of compounds **3** and **4**, as would be expected.

The σ-gold carbaborane compounds have been shown to exhibit increased stability with respect to the metal-carbon σ-bond compared, firstly, to corresponding σ-gold alkyl compounds and, secondly, to other σ-transition metal carbaborane compounds previously prepared: The former was first recognised by Stone[80] who observed that trifluoroacetic acid did not react with σ-gold carbaborane compounds while synonymous σ-methyl complexes reacted readily at room temperature; the latter was confirmed by the fact that compounds **3** and **4** have been found to be indefinitely stable in air and in solution and are stable to cage degradation. This was shown to be in contrast to 1-Ph-2-{$CpFe(CO)_2$}-1,2-*closo*-$C_2B_{10}H_{10}$ in which the iron-cage carbon σ-bond is readily cleaved on dissolution in CH_2Cl_2 and on attempted cage

degradation.

The molecular structures of one of compounds **4**, **4e**, and a comparable, typical organometallic gold(I) complex, **5**, have been determined. Both showed the expected geometry with the gold atom two coordinate and linear, the gold being σ-bonded to carbon. Comparison of the two revealed an equal gold-arsenic bond but a shorter gold-carbon bond in the carbaborane compound. The molecular dimensions of **4e** were found to be comparable to those in the only molecular structure of a σ-gold carbaborane compound determined (that of 1-{PPh_3Au}-1,2-*closo*-$C_2B_{10}H_{11}$[88]) and, consequently, these conclusions are consistent with that alternative structural study.

The EHMO calculations finally confirmed that the stability of the gold-carbon bond in the phosphine and arsine carbaborane compounds **3** and **4** is primarily due to carbaborane acting as an efficient σ-donor ligand, consistent with all the trends observed in the NMR spectra, in contrast to the previous[43, 80] (and current[79]) descriptions of its ligand function *viz* an electron withdrawing ligand.

The previously synthesised class 3 carbametallaboranes have relied on the assumption that carbaborane is an electron withdrawing ligand and so requires a metal with a high d^n configuration in a low oxidation state and, consequently, work has concentrated on the late transition metals. Gold(I) is an unusual case in that although it has a high d^n configuration these *d* orbitals are so low lying in energy that they can essentially be considered as core (**Section 1.5.2**). The fact that the carbaborane ligand is, in reality, an electron donor suggests that stable class 3 carbametallaboranes could be formed with high oxidation state low d^n configuration metal centres, *i.e.* early transition metals. Certainly the chemistry of alkyl metal complexes with early transition metals is well established[94] and as the carbaborane and methyl ligands have similar donor properties this could be used as a guide for the future development of this area of carbametallaborane chemistry.

CHAPTER 3
σ-BONDED TITANIUM CARBABORANES

3.1 Introduction

The emphasis of past research into σ-bonded transition metal carbaborane compounds has been such that only compounds in which the metal centre is in a low oxidation state and has a high d^n configuration have been synthesised. Presumably, the direction of the research has been influenced by the assumption that the *closo*-carbaborane acts as an electron withdrawing ligand. However, one of the conclusions arising from the study of (class 3) σ-bonded gold carbaborane compounds (**Chapter 2**), that the *closo*-carbaborane acts as an efficient electron donor, intimates that stable σ-bonded metal carbaborane compounds could be produced when the metal centre is in a high oxidation state with a low d^n configuration. This conclusion stimulated research into σ-carbametallaborane compounds containing early transition metals.

Although not necessarily a 'rule of thumb' the prediction can be made that, if the transition metal alkyl complex is known then the *closo*-carbaborane (a better σ-donor) compound may be synthesised. Furthermore, because of their enhanced donor properties over alkyl ligands, the carbaborane compounds should generally be more stable than their alkyl analogues with respect to the M-C σ-bond. The chemistry of early transition metal alkyl complexes, in particular involving metals in the titanium and vanadium triads, has been well established[94]. As organometallic titanium(IV) complexes are used in industry as catalysts (for example, Ziegler-Natta catalysts are commonly a combination of titanium(IV) and Group 1, 2 or 13 organometallic complexes and are used in the polymerisation of alkenes) the chemistry of such complexes has been extensively researched[94]. The important steps

involved in alkene polymerisation using titanium based catalysts are highlighted in **Figure 3.1.** The termination step resulting from cleavage of the Ti-C σ-bond, involves β-elimination, a process which is prevalent throughout organometallic titanium(IV) chemistry. In fact, the ease of β-elimination is an important factor in determining the stability of titanium(IV) organometallic complexes: The majority of complexes in which β-elimination can occur are thermally unstable (*vide infra*).

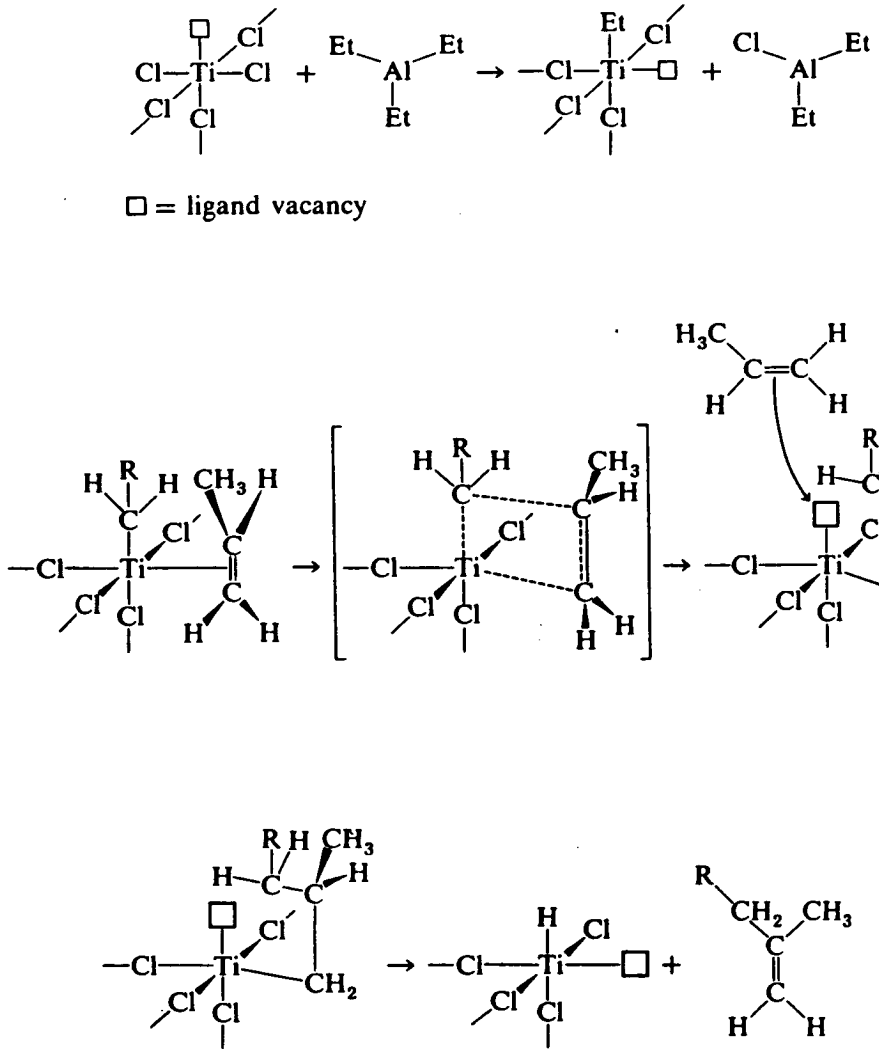

Figure 3.1 Alkene Polymerisation using Ziegler-Natta Catalysts.

The titanium(IV) metal centre is a small highly charged cation with a d^0

configuration and therefore has the potential to exhibit a variety of coordination numbers. This is reflected in the several examples of titanium(IV) alkyl complexes which are known as 4-, 6- and 8-coordinate species, the overall stability increasing with increasing coordination number.

Four coordinate complexes of the type $TiCl_3R$ (R = alkyl or aryl) are thermally unstable low melting solids, decomposing at room temperature (readily for higher alkyls than ethyl) to $TiCl_2$. However, these compounds have been widely studied because of their relationship to Ziegler-Natta catalysis. The most thermally stable of the compounds is the deeply coloured $TiCl_3Me$ which is readily synthesied by a variety of methods[95] and is stable at room temperature in its pure form (impurities may catalyse decomposition[94]) for many hours. Complexes in which R is alkyl greater than ethyl, for example propyl, have only been isolated as six coordinate adducts with Lewis bases such as pyridine or 2,2'-bipyridyl. Adduct formation appears to stabilise these complexes by blocking the sites at the metal centre which would have been used in decomposition reactions. Consequently, when the titanium(IV) metal centre becomes more coordinatively saturated, more stable complexes should be formed. This increase in stability is observed with 6- and 8-coordinate titanium(IV) alkyls exhibiting increased thermal stability over their 4-coordinate counterparts.

The 6-coordinate $CpTiR_3$ ($Cp = \eta^5\text{-}C_5H_5$) and $CpTiCl_2R$ are yellow liquids or low melting solids which are generally thermally unstable and air sensitive, but seemingly less so than $TiCl_3R$ species. Whereas $TiCl_3Me$ exhibits greater themal stability than $TiClMe_3$[96] (the latter has not been isolated), $CpTiCl_2Me$ is less thermally stable than $CpTiMe_3$, the former having only been isolated in solution[97] while the latter has been recovered as a low melting crystalline solid. The chemistry of $CpTiMe_3$ demonstrates the catalytic nature of organometallic titanium complexes, with insertion into the Ti-C σ-bond occurring readily (**Figure 3.2**).

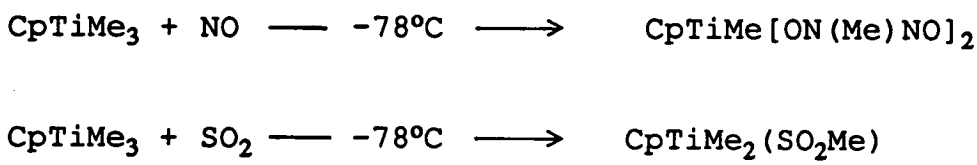

Figure 3.2 Ti-C Bond Insertion in $CpTiMe_3$.

The chemistry of 8-coordinate Cp_2TiR_2 alkyl complexes is significantly more developed, this being a consequence of their relative ease of preparation and good thermal, air and moisture stability. The orange-yellow Cp_2TiMe_2 has been prepared in good yield and high purity by reaction of Cp_2TiCl_2 and LiMe[98]. It is interesting to note that: Firstly, $Cp_2Ti(CH_2SiCH_3)_2$ has enhanced thermal stability which may be attributed to the presence of relatively bulky ligands and the absence of β-hydrogen atoms; the 1,2-*closo*-carbaborane ligand is also a bulky ligand and does not contain either α- or β-hydrogen atoms, suggesting that thermally stable titanium σ-carbaborane complexes could be expected: Secondly, Cp_2TiCl_2 exhibits anti-tumour activity[99], something which may be of future interest in BNCT (**Section 1.6**) with respect to the Cp^- / [*nido*-$C_2B_9H_{11}]^{2-}$ analogy.

The only titanium complex containing a *closo*-carbaborane ligand thus far reported is the biscyclopentadienyl-bismethylenecarbaborane titanium complex illustrated in **Figure 3.3** in which the Ti^{IV} is bonded to the carbaborane *via* a CH_2 group[49]. Although containing a Ti-C σ-bond, the metal centre in this complex is not directly bonded to the carbaborane and it is the reactivity of the substituent group on the carbaborane and, not the *closo*-carbaborane ligand itself which is relevant.

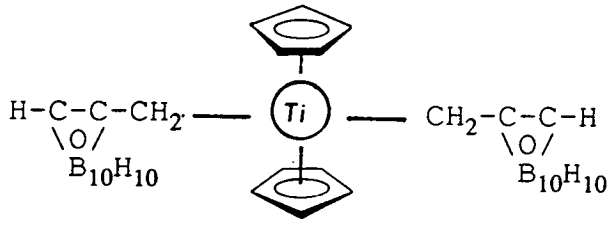

Figure 3.3 Proposed Structure of $Cp_2Ti(CH_2\text{-}C_2B_{10}H_{11})_2$.

This chapter reports the synthesis and characterisation of class 3 titanium(IV) carbaborane complexes (**Section 3.2**) followed by a full discussion of the results of spectroscopic and crystallographic analysis of the complexes synthesised (**Section 3.3**).

Unsuccessful attempts to synthesise titanium(IV) and gold(I) σ-carbaborane compounds using THF as the reaction solvent (instead of Et_2O) lead to a consideration of the role of the lithium carbaborane intermediate in the formation of σ-carbametallaborane compounds (**Section 3.4**).

The chapter finishes with a discussion of the conclusions derived from the research described therein (**Section 3.5**).

3.2 Synthesis and Characterisation of σ-Bonded Titanium(IV) Carbaboranes

3.2.1 Synthesis of 1-CH_3OCH_2-2-{$TiCl_3$}-1,2-*closo*-$C_2B_{10}H_{10}$ (6)

Compound **6** was produced when equimolar amounts of $TiCl_4$ and Li[1-CH_3OCH_2-1,2-*closo*-$C_2B_{10}H_{10}$] were slowly warmed from frozen (-196°) in diethyl ether. The yellow/green solid recovered from the Et_2O solution was found to be mildly air and moisture sensitive with solutions even more so, these, on standing in air, changing in colour from green to orange in under 30 minutes. However, the solid and solutions are indefinately stable at room temperature in an atmosphere of dry oxygen-free nitrogen and so have the expected enhanced thermal stability (see **Section 3.1**).

Characterisation was effected by microanalysis and infra-red and NMR spectroscopies. Microanalysis was consistent with the proposed formulation of $C_7H_{15}B_{10}Cl_3OTi$. The IR spectrum showed the expected broad band at 2590 cm^{-1} indicative of B-H stretches. Also present were peaks at 1445, 1377 and 1114 cm^{-1} due to the various vibrational modes of the CH_3OCH_2 substituent on the carbaborane.

NMR spectra were not recorded in the complete absence of air and so some decompositon was observed, and resonances due to decomposition products were present in the spectra (but are not referred to in the following text). The ^1H NMR spectrum exhibited two peaks due to the product **6** (OCH_2 and the OCH_3 of the carbaborane substituent at δ 4.48 and 4.08 ppm respectively) in the expected ratio. The broad peak found at δ 4.00 ppm in the ^1H NMR spectrum of **2** was notable by its absence here indicating the removal of hydrogen bound to C(2). The $^{11}B\{^1H\}$ NMR spectrum showed six peaks of relative integral 1:1:2:2:2:2 from high to low frequency at δ -1.98, -3.47, -5.03, -8.88, -10.67 and -12.24 ppm respectively. The peaks of

integral 1 are due to the symmetry unique boron atoms, B(9) and B(12), and the remaining four peaks of integral 2 are due to the remaining four symmetry pairs of boron atoms [B(3)/B(6), B(4)/B(5), B(8)/B(10) and B(7)/B(11)]. The ^{11}B NMR spectrum indicates that each boron atom has the expected bound hydrogen atom with $^{1}J_{B\text{-}H}$ in the range 142-190 Hz.

The air and moisture sensitivity of this titanium(IV) carbaborane complex is not unusual in 4-coordinate titianium(IV) chemistry (**Section 3.1**) though the steric bulk of the carbaborane and the absence of β-hydrogen atoms has resulted in increased thermal stability. It has been observed that the stability of 4-coordinate complexes can be enhanced by adduct formation producing a more saturated 6-coordinate species, the adduct seemingly blocking sites at the metal centre that are utilised in the decomposition reactions.

3.2.2 Synthesis of 1-CH_3OCH_2-2-{(bipy)$TiCl_3$}-1,2-*closo*-$C_2B_{10}H_{10}$ (7)

By adding a 1.5 excess of 2,2'-bipyridyl in diethyl ether to an ethereal solution of compound **6**, crude compound **7** was precipitated out. The pale pink solid was purified by stirring with *n*-hexane, this procedure removing the contaminating excess of 2,2'-bipyridyl. The solid was found to be extremely insoluble in most solvents and partially soluble only in methanol. Attempts to crystallise compound **7** from warm methanol proved fruitless. The compound demonstrated the expected increased stability over compound **6**, being stable in air for several days and insensitive to moisture.

Compound **7** was identified as 1-CH_3OCH_2-2-{(bipy)$TiCl_3$}-1,2-*closo*-$C_2B_{10}H_{10}$ from microanaysis and infra-red spectroscopy data: Microanalysis was consistent with the expected formulation of $C_{14}H_{23}N_2B_{10}Cl_3OTi$; the IR spectrum revealed peaks at 2591 cm^{-1} (B-H stretches) and 1442, 1394 and 1135 cm^{-1} (CH_3OCH_2 vibrations). Because of the insolubility of the solid, solution NMR spectroscopic data were not obtained and, as a result, further characterisation could not be achieved.

3.2.3 Synthesis of 1-CH_3OCH_2-2-{$CpTiCl_2$}-1,2-*closo*-$C_2B_{10}H_{10}$ (8)

Compound **8** was synthesised by the 1:1 stoichiometric reaction of 6-coordinate $CpTiCl_3$ and the lithium salt of the ether carbaborane in diethyl ether. The partially soluble orange product was recovered by reducing the volume of the ether before filtering and redissolving the solid in CH_2Cl_2. Purification was achieved by crystallisation from CH_2Cl_2/*n*-hexane (1:4), small orange platelets of **8** being recovered. The crystals were found to be stable in air at room temperature and of suitable quality for an X-ray diffraction study.

The good air, moisture and thermal stability of compound **8** allowed full characterisation to be undertaken. Microanalysis of the crystals was consistent with the proposed formulation of $C_{12}H_{20}B_{10}Cl_2OTi$. The IR spectrum showed peaks due to the B-H and the various CH_3OCH_2 vibrations at 2585 and 1483, 1407 and 1119 cm^{-1} respectively.

The ^1H NMR spectrum (**Figure 3.4**) showed single peaks at δ 6.92, 4.23 and 3.71 ppm due to the C_5H_5, OCH_2 and OCH_3 respectively in the correct ratio (5:2:3). The absence of the broad peak due to the hydrogen atom bound to C(2) in the parent carbaborane (**1**), indicating its expected removal, was also noted. Six peaks of relative integral 1:1:2:2:2:2 (high to low frequency) were observed in the $^{11}B\{^1H\}$ NMR spectrum (**Figure 3.5**), the two high frequency peaks (at δ -2.41 and -3.53 ppm) due to the only two symmetry unique boron atoms and the four peaks of integral 2 (at δ -5.19, -8.52, -10.82 and -12.41 ppm) due to the four pairs of equivalent boron atoms. The ^{11}B NMR spectrum displayed the expected boron-hydrogen coupling with $^1J_{B\text{-}H}$ in the range 133-198 Hz. An X-ray diffraction study using a single crystal of compound **8** provided structural data for a single molecule in the solid state, this being discussed in more detail in **Section 3.3.2.**

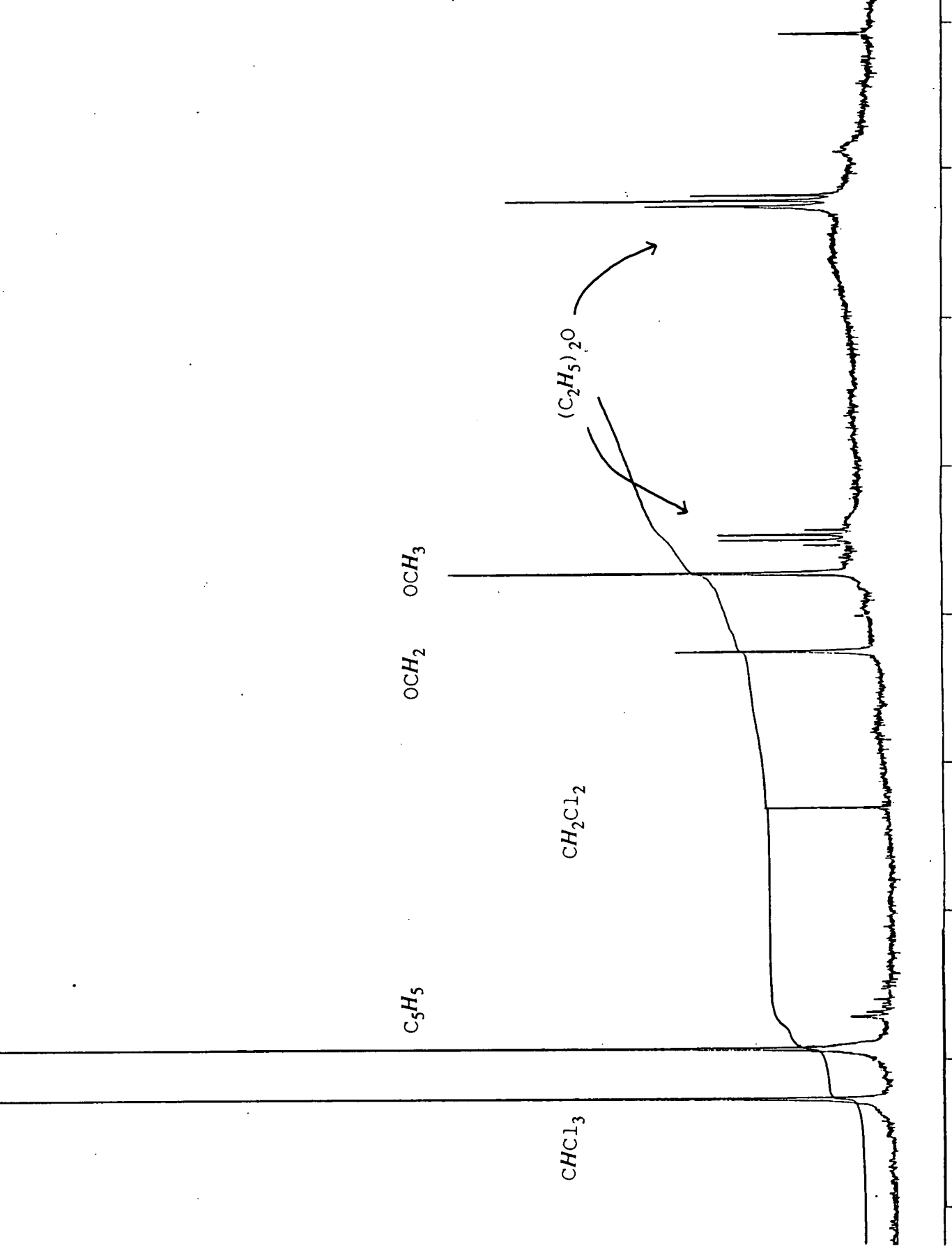

Figure 3.4 ^{1}H NMR Spectrum of **8** (200.13 MHz).

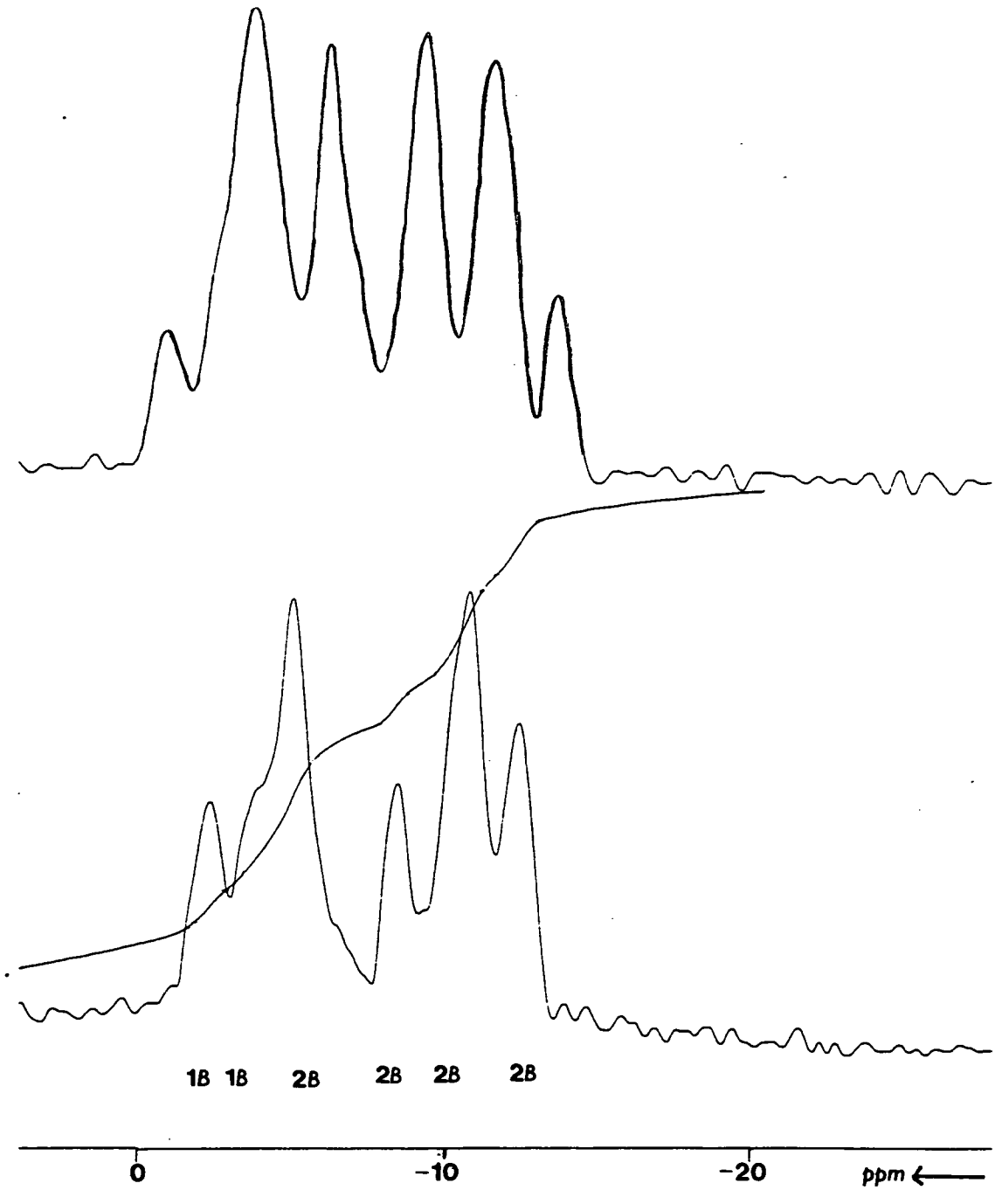

Figure 3.5 $^{11}B\{^{1}H\}/^{11}B$ NMR Spectra of **8** (64.21 MHz).

3.2.4 Reactions of Cp_2TiCl_2 with Li[1-CH_3OCH_2-1,2-*closo*-$C_2B_{10}H_{10}$]

When equimolar amounts of red Cp_2TiCl_2 and Li[1-CH_3OCH_2-1,2-*closo*-$C_2B_{10}H_{10}$] were stirred for 4 hours in Et_2O (or for 1 hour in benzene) at room temperature, a copious amount of an orange solid was produced. The solid was isolated by filtration followed by crystallisation from CH_2Cl_2/*n*-hexane (1:4) which afforded small orange-red crystals. The crystals exhibited good thermal, air and moisture sensitivity. Analysis of the crystals by infra-red spectroscopy revealed a non-boron containing species. The solid was identified as Cp_2TiCl (**9**) by ^1H NMR spectroscopy and elemental analysis: The ^1H NMR spectrum showed two resonances at δ 6.30 and 5.25 ppm in a 5:1 integral ratio corresponding to C_5H_5 and CH_2Cl_2 respectively. Microanalysis results (of the crystals) were consistent with the formulation $C_{10}H_{10}ClTi.CH_2Cl_2$, confirming that the product cocrystallises with one molecule of CH_2Cl_2.

Analysis of the filtrate by ^1H NMR spectroscopy revealed a mixture of a small amount of **9** [singlet at δ 6.30 ppm (C_5H_5)] and the parent carbaborane (**1**) [three singlets in the ratio 1:2:3 at δ 3.97 ppm (C_{cage}-*H*), δ 3.79 ppm (OCH_2) and δ 3.36 ppm (OCH_3) respectively].

Stirring two equivalents of Li[1-CH_3OCH_2-1,2-*closo*-$C_2B_{10}H_{10}$] with Cp_2TiCl_2 in a 1:1 diethyl ether/benzene solvent mixture for 24 hours at room temperature produced the orange solid of **9** and an extremely air-sensitive green solution. The solid and solution were separated by filtration under an atmosphere of dry, oxygen-free nitrogen and on removal of the volatiles *in vacuo* a green oil was revealed. However, after about *ca.* 1h at ambient temperature in an anaerobic atmosphere the green oil had decomposed to an orange oil. Analysis of this oil by ^1H NMR spectroscopy revealed a mixture of compounds **9** and **1**, and other unidentified Cp-containing species.

It has been reported[100] that reaction of Cp_2TiCl_2 with two equivalents of $Li[CH_2SiMe_3]$ afforded the bisalkyl compound, $Cp_2Ti(CH_2SiMe_3)_2$. However, reaction of Cp_2TiCl_2 with two equivalents of the more sterically demanding $Li[CH(SiMe_3)_2]$ yielded the titanocene(III) monoalkyl compound, $Cp_2Ti\{CH(SiMe_3)_2\}$[101]. The proposed mechanism for this (**Figure 3.6**) indicates a two stage reaction: The first equivalent of alkyl lithium produces $Cp_2Ti(Cl)CH(SiMe_3)_2$ which, because of the steric bulk of the alkyl group, decomposes by Ti-C homolysis to produce Cp_2TiCl or $[Cp_2TiCl]_2$ (thermochemical evidence for tetra-alkyl titanium species intimates that the mean titanium-carbon bond strength can be significantly weakened by increased steric effects of the alkyl[102]). This titanium(III) species then reacts with the second equivalent of alkyl lithium yielding the dark green titanium(III) monoalkyl compound, $Cp_2Ti\{CH(SiMe_3)_2\}$. Thus, reaction of titanocene dichloride with one equivalent of $Li[CH(SiMe_3)_2]$ means that the reaction stops at the first stage and only Cp_2TiCl or $[Cp_2TiCl]_2$ is isolated.

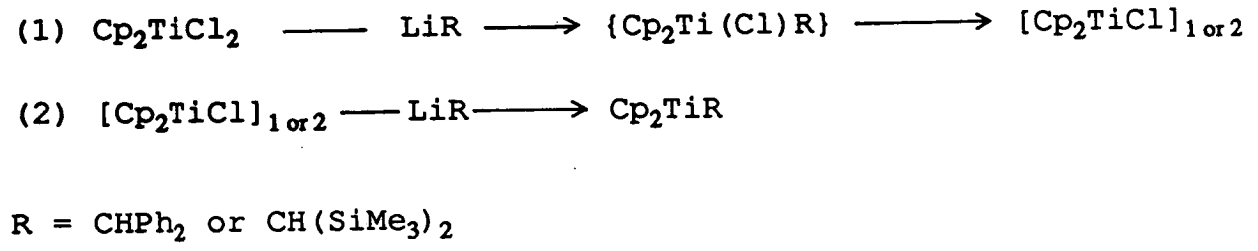

Figure 3.6 Mechanism For Reaction of Cp_2TiCl_2 with Sterically Hindered Lithium Alkyls.

The three-dimensional bulky nature of the icosahedral carbaborane means that it is likely to be as least as sterically demanding as $\{CH(SiMe_3)_2\}$ and, consequently, similar results from the reactions of one and two equivalents of lithium carbaborane with titanocene dichloride might have been predicted. Indeed, the 1:1 reaction

produced an orange solid identified as Cp_2TiCl and therefore the reaction appears to proceed as in the first stage of the mechanism of **Figure 3.6.** Furthermore, the 1:2 reaction produces a transient dark green product which could speculatively be assigned as the titanocene(III) mono-carbaborane compound, 1-CH_3OCH_2-2-{Cp_2Ti}-1,2-*closo*- $C_2B_{10}H_{10}$, since corresponding alkyl compounds are this dark green colour. However, whereas the sterically hindered bis(trimethylsilyl)methyl compounds show relatively good thermal stability as a consequence of the absence of β-hydrogens, this transient species appears to show poor thermal stability and, as of yet, has not been isolated. The reason for the poor thermal stability is not clear as metal alkyls usually decompose by a β-elimination mechanism (although α-elimination and homolysis of M-C are also known) but carbaborane has no α- or β-hydrogen atoms. It is possible that the competing steric demands of directly bonded carbaborane and two Cp rings about the titanium centre result in the facile loss of the carbaborane ligand by homolysis. As no spectroscopic or analytical data has been obtained for this titanocene mono-carbaborane compound, its formation remains speculative.

It is of note that the synthesis of $Cp_2Ti(CH_2\text{-}C_2B_{10}H_{10})_2$[49] (**Figure 3.3**) has indicated that inserting a methylene spacer between the titanium centre and carbaborane alleviates the steric problems and two carbaborane moieties can bond to the titanium(IV) centre.

In conclusion, reaction of titanocene dichloride with lithium carbaborane seemingly proceeds according to the mechansim proposed by Atwood *et al*[101] (**Figure 3.6**) but the carbaborane species is (presumably thermally) less stable than the reported alkyl compounds. Subsequent work in this area should include repetition of the reaction at much lower temperature and possibly isolation the titanium(III) carbaborane species.

3.3 Structural Studies

3.3.1 Crystallographic Study on **8**

Crystallisation of compound **8** by slow diffusion of *n*-hexane into a dichloromethane solution at -30° afforded small orange platelets which were found to be of suitable quality for an X-ray diffraction study. Intensity data were therefore collected from a single crystal of **8** at ambient temperature. **Table 3.1** lists atomic positions and equivalent isotropic thermal parameters for all non-hydrogen atoms and **Table 3.2** details selected bond distances and interbond angles. Anisotropic thermal parameters and hydrogen atom coordinates are given in **Appendix B. Figure 3.7** shows a perspective view of a single molecule of **8**.

	x	y	z	Ueq
Ti	0.2276(3)	0.23370(22)	0.49527(21)	0.0333(20)
Cl(1)	0.2883(4)	0.1700(4)	0.3652(3)	0.058(4)
Cl(2)	0.0959(4)	0.3589(4)	0.3922(3)	0.056(4)
C(11)	0.2008(11)	0.0523(8)	0.5234(9)	0.043(5)
C(12)	0.0747(11)	0.0900(8)	0.4547(9)	0.045(5)
C(13)	0.0168(11)	0.1645(8)	0.5051(9)	0.064(6)
C(14)	0.1071(11)	0.1727(8)	0.6049(9)	0.049(5)
C(15)	0.2208(11)	0.1034(8)	0.6163(9)	0.046(5)
C(101)	0.3849(14)	0.4253(12)	0.6377(11)	0.035(4)
O	0.2568(10)	0.3645(8)	0.6038(7)	0.040(3)
C(102)	0.1441(14)	0.4306(12)	0.6118(11)	0.039(5)
C(1)	0.5008(15)	0.3510(12)	0.6447(10)	0.034(4)
C(2)	0.4550(13)	0.2354(12)	0.5827(9)	0.026(4)
B(3)	0.5369(17)	0.3313(15)	0.5324(13)	0.028(5)
B(4)	0.6541(20)	0.3990(16)	0.6383(15)	0.041(6)
B(5)	0.6404(17)	0.3399(15)	0.7484(12)	0.032(5)
B(6)	0.5115(17)	0.2371(14)	0.7130(12)	0.028(5)
B(7)	0.7813(18)	0.3055(15)	0.7078(14)	0.040(6)
B(8)	0.6898(19)	0.2058(14)	0.7507(13)	0.037(6)
B(9)	0.5702(18)	0.1416(14)	0.6461(13)	0.034(5)
B(10)	0.5903(18)	0.2017(14)	0.5385(13)	0.027(5)
B(11)	0.7182(19)	0.2993(15)	0.5722(14)	0.037(6)
B(12)	0.7384(20)	0.1820(16)	0.6434(16)	0.044(6)

Table 3.1 Atomic Positions and Equivalent Isotropic Thermal Parameters ($Å^2$) for All Non-hydrogen Atoms in **8**.

Ti -Cl(1)	2.266(5)	C(2) - B(9)	1.711(23)
Ti -Cl(2)	2.281(5)	C(2) -B(10)	1.732(23)
Ti -C(11)	2.374(11)	B(3) - B(4)	1.80(3)
Ti -C(12)	2.347(11)	B(3) -B(10)	1.73(3)
Ti -C(13)	2.356(11)	B(3) -B(11)	1.79(3)
Ti -C(14)	2.388(11)	B(4) - B(5)	1.77(3)
Ti -C(15)	2.399(11)	B(4) - B(7)	1.80(3)
Ti - O	2.219(10)	B(4) -B(11)	1.81(3)
Ti - C(2)	2.241(14)	B(5) - B(6)	1.804(25)
B(5) - B(7)	1.75(3)	B(5) - B(8)	1.78(3)
B(6) - B(8)	1.76(3)	B(6) - B(9)	1.76(3)
B(7) - B(8)	1.79(3)	C(101)- O	1.455(18)
B(7) -B(11)	1.82(3)	C(101)- C(1)	1.487(21)
B(7) -B(12)	1.80(3)	O -C(102)	1.452(18)
B(8) - B(9)	1.78(3)	C(1) - C(2)	1.699(21)
B(8) -B(12)	1.76(3)	C(1) - B(3)	1.756(24)
B(9) -B(10)	1.77(3)	C(1) - B(4)	1.70(3)
B(9) -B(12)	1.79(3)	C(1) - B(5)	1.687(23)
B(10) -B(11)	1.75(3)	C(1) - B(6)	1.726(23)
B(10) -B(12)	1.76(3)	C(2) - B(3)	1.749(23)
B(11) -B(12)	1.78(3)	C(2) - B(6)	1.745(22)

Cl(1) - Ti -Cl(2)	89.27(19)	Ti -C(15) -C(11)	71.7(6)
Cl(1) - Ti -C(11)	82.1(3)	Ti -C(15) -C(14)	72.3(6)
Cl(1) - Ti -C(12)	81.5(3)	(11) -C(15) -C(14)	108.0(10)
Cl(1) - Ti -C(13)	113.5(3)	O -C(101)- C(1)	106.6(12)
Cl(1) - Ti -C(14)	137.5(3)	Ti - O -C(101)	122.4(8)
Cl(1) - Ti -C(15)	114.0(3)	Ti - O -C(102)	123.7(8)
Cl(1) - Ti - O	144.9(3)	(101)- O -C(102)	107.9(11)
Cl(1) - Ti - C(2)	87.3(4)	(101)- C(1) - C(2)	115.9(12)
Cl(2) - Ti -C(11)	135.4(3)	(101)- C(1) - B(3)	114.7(12)
Cl(2) - Ti -C(12)	100.5(3)	(101)- C(1) - B(4)	118.9(13)
Cl(2) - Ti -C(13)	86.6(3)	(101)- C(1) - B(5)	122.4(13)
Cl(2) - Ti -C(14)	109.0(3)	(101)- C(1) - B(6)	118.7(12)
Cl(2) - Ti -C(15)	142.6(3)	C(2) - C(1) - B(3)	60.8(9)
Cl(2) - Ti - O	80.7(3)	C(2) - C(1) - B(6)	61.3(9)
Cl(2) - Ti - C(2)	129.4(4)	B(3) - C(1) - B(4)	63.0(11)
C(11) - Ti -C(12)	35.0(4)	B(4) - C(1) - B(5)	63.1(11)
C(11) - Ti -C(13)	58.1(4)	B(5) - C(1) - B(6)	63.8(10)
C(11) - Ti -C(14)	57.7(4)	Ti - C(2) - C(1)	110.9(9)
C(11) - Ti -C(15)	34.6(4)	Ti - C(2) - B(3)	108.7(9)
C(11) - Ti - O	127.7(4)	Ti - C(2) - B(6)	121.0(9)
C(11) - Ti - C(2)	94.0(5)	Ti - C(2) - B(9)	133.8(10)
C(12) - Ti -C(13)	35.1(4)	Ti - C(2) -B(10)	126.3(9)
C(12) - Ti -C(14)	58.0(4)	C(1) - C(2) - B(3)	61.2(9)
C(12) - Ti -C(15)	57.9(4)	C(1) - C(2) - B(6)	60.1(9)

Table 3.2 Selected Interatomic Bond Distances (Å) and Angles (°) in **8**.

C(12) - Ti - O	133.3(4)	B(3) - C(2) -B(10)	59.6(10)
C(12) - Ti - C(2)	128.7(5)	B(6) - C(2) - B(9)	61.1(10)
C(13) - Ti -C(14)	34.8(4)	B(9) - C(2) -B(10)	61.9(10)
C(13) - Ti -C(15)	57.8(4)	C(1) - B(3) - C(2)	58.0(9)
C(13) - Ti - O	99.4(4)	C(1) - B(3) - B(4)	57.0(10)
C(13) - Ti - C(2)	139.8(5)	C(2) - B(3) -B(10)	59.7(10)
C(14) - Ti -C(15)	34.5(4)	B(4) - B(3) -B(11)	60.6(11)
C(14) - Ti - O	77.2(4)	(10) - B(3) -B(11)	59.6(10)
C(14) - Ti - C(2)	107.1(5)	C(1) - B(4) - B(3)	60.1(10)
C(15) - Ti - O	93.1(4)	C(1) - B(4) - B(5)	58.1(10)
C(15) - Ti - C(2)	82.6(4)	B(3) - B(4) -B(11)	59.2(11)
O - Ti - C(2)	74.0(4)	B(5) - B(4) - B(7)	58.8(11)
Ti -C(11) -C(12)	71.5(6)	B(7) - B(4) -B(11)	60.4(11)
Ti -C(11) -C(15)	73.7(6)	C(1) - B(5) - B(4)	58.7(10)
C(1) - B(5) - B(6)	59.1(9)	Ti -C(12) -C(11)	73.5(6)
B(4) - B(5) - B(7)	61.3(11)	Ti -C(12) -C(13)	72.8(6)
B(6) - B(5) - B(8)	58.8(10)	B(7) - B(5) - B(8)	60.8(10)
Ti -C(13) -C(12)	72.1(6)	C(1) - B(6) - C(2)	58.6(9)
Ti -C(13) -C(14)	73.8(6)	C(1) - B(6) - B(5)	57.0(9)

C(2) - B(6) - B(9)	58.5(9)	Ti -C(14) -C(13)	71.3(6)
B(5) - B(6) - B(8)	59.8(10)	Ti -C(14) -C(15)	73.2(6)
B(8) - B(6) - B(9)	61.0(10)	B(4) - B(7) - B(5)	59.8(11)
B(4) - B(7) -B(11)	60.2(11)	C(2) -B(10) - B(9)	58.4(9)
B(5) - B(7) - B(8)	60.2(10)	B(3) -B(10) -B(11)	61.9(11)
B(8) - B(7) -B(12)	58.9(11)	B(9) -B(10) -B(12)	61.1(11)
B(11) - B(7) B(12)	58.8(11)	(11) -B(10) -B(12)	60.8(11)
B(5) - B(8) - B(6)	61.4(10)	B(3) -B(11) - B(4)	60.1(11)
B(5) - B(8) - B(7)	59.0(10)	B(3) -B(11) -B(10)	58.5(10)
B(6) - B(8) - B(9)	59.5(10)	B(4) -B(11) - B(7)	59.4(11)
B(7) - B(8) -B(12)	60.9(11)	B(7) -B(11) -B(12)	60.0(11)
B(9) - B(8) -B(12)	60.7(11)	(10) -B(11) -B(12)	59.9(11)
C(2) - B(9) - B(6)	60.4(9)	B(7) -B(12) - B(8)	60.2(11)
C(2) - B(9) -B(10)	59.6(10)	B(7) -B(12) -B(11)	61.2(11)
B(6) - B(9) - B(8)	59.6(10)	B(8) -B(12) - B(9)	60.2(11)
B(8) - B(9) -B(12)	59.1(11)	B(9) -B(12) -B(10)	59.8(11)
B(10) - B(9) -B(12)	59.1(11)	(10) -B(12) -B(11)	59.3(11)
C(2) -B(10) - B(3)	60.7(10)		

Table 3.2 Selected Interatomic Bond Distances (Å) and Angles (°) in **8** (continued).

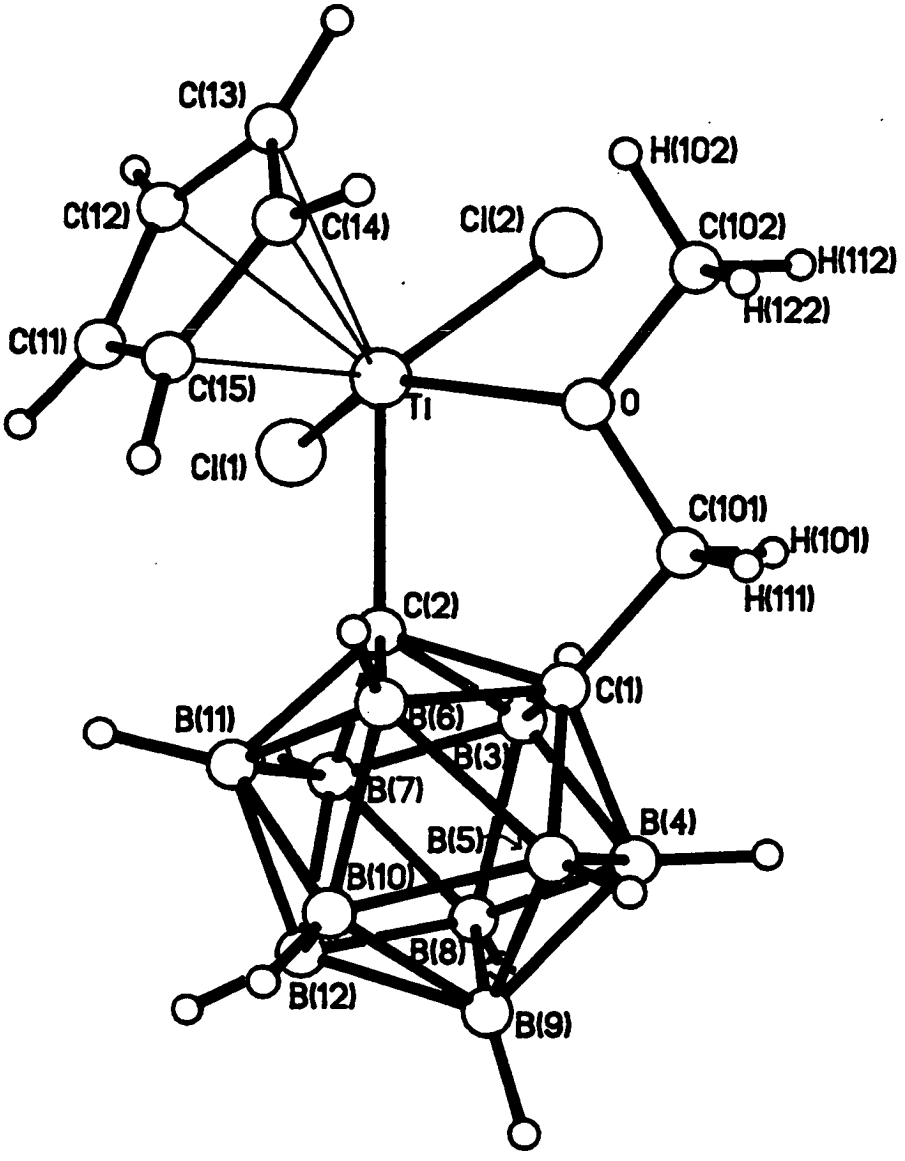

Figure 3.7 Perspective View of **8** (cage H atoms carry the same number as the B atoms to which they are bound).

In the solid state, compound **8** contains a Ti^{IV} centre which is formally 7-coordinate, the oxygen atom of the carbaborane ether substituent forming a single σ-bond of length 2.219(10) Å to the metal. This is not unexpected as, firstly, it is a hard metal-hard donor interaction and, secondly, the titanium centre has vacant sites for coordination. The formation of the Ti-O bond produces a 5-membered ring incorporating Ti, C(2), C(1), C(101) and O atoms. This 5-membered ring is not planar (**Table 3.3**) but is best referred to as approximately of envelope conformation about a vector from Ti to C(101), as amply illustrated in **Figure 3.8.**

atom	x	y	z
C(2)	-0.4987	-1.3740	0.1136
Ti	-1.9365	0.3234	-0.1543
O	0.0938	1.2529	0.2391
C(101)	1.2888	0.6325	0.1767
C(1)	1.1067	-0.8348	-0.0217

Table 3.3 Atom Coordinates (orthorgonal Å) Referred to the Best (Least-Squares) Plane Through the 5-membered ring in **8.** (z is the approximate displacement from the least-squares plane).

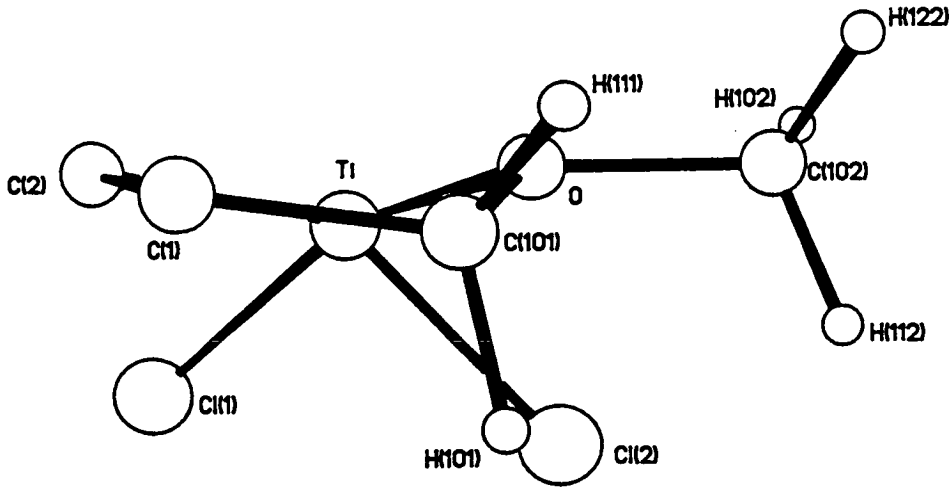

Figure 3.8 Side View of the 5-membered ring in **8**.

The formation of the intramolecular 5-membered ring results in several changes in the orientation (bond lengths and angles) of the metal fragment and ether substituents with respect to related species, for example, as compared to compound **4e** in which there is no metal-oxygen interaction. The most energetically favoured position (greatest orbital overlap) would be when the Ti-C(2)-B(9) angle is 180° because the molecular orbital outpointing from C(2) (*exo* to the cage) lies along the C(2)-B(9) vector (**Figure 3.9**). Therefore, in **8**, the observed Ti-C(2)-B(9) angle of 133.8(10)° is a significant deviation from its expected value. This contraction of the Ti-C(2)-B(9) angle intimates a weaker overlap between Ti and C(2) and so the bond is probably longer than otherwise. Indeed, assuming maximum orbital overlap between Ti and C(2), the Ti-C(2) bond length could be expected to be 2.01 Å. This prediction is made by estimating the covalent radii of Ti and C(2) (1.284 Å and 0.747 Å respectively):

The former is evaluated by assuming a covalent radius of 0.99 Å for Cl[87] and subtracting this from the average determined Ti-Cl bond length (2.274 Å) in **8**; and the latter is calculated by determining the covalent radius of Au by subtracting that for Cl from the Au-Cl bond length in PPh_3AuCl[103] (2.279 Å) and then using the Au radius to determine the C(2) covalent radius in the gold carbaborane compound, **4e** [Au-C(2) = 2.039(8) Å: **Section 2.3.3**].

The Ti-C(2) σ-bond would consequently be expected to be much shorter than is observed experimentally in **8**, even allowing for the fact that Au-C(2) in **4e** is slightly shortened by bond strengthening. The lengthening appears to be due to a poorer (and therefore less energetically favourable) orbital overlap between Ti and C(2), this a consequence of the Ti and O atoms being pulled towards each other to form the 5-membered ring. The conclusion from this is that the energy loss by reducing the Ti-C(2) orbital overlap is more than compensated by the energy gain in the formation of the Ti-O bond and the 5-membered ring.

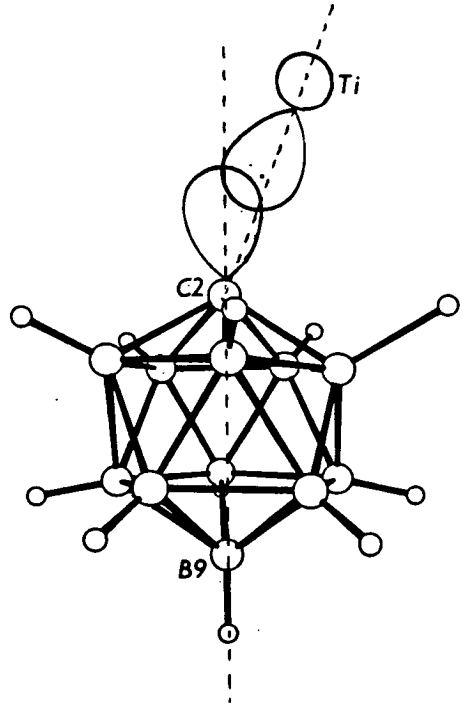

Figure 3.9 Ti-C(2) Molecular Orbital Overlap in **8**.

The effect the Ti-O bond formation has upon the ether substituent can be assessed by comparison with related species. **Table 3.4** details bond lengths and angles relevant to the ether substituent in 1-CH_3OCH_2-1,2-*closo*-$C_2B_{10}H_{11}$[20] (**1**), 1-CH_3OCH_2-2-{$As.Ph_3Au$}-1,2-*closo*-$C_2B_{10}H_{10}$ (**4e**), 1-$CH_3CH_2OCH_2$-2-{CH_3Hg}-1,2-*closo*-$C_2B_{10}H_{10}$[55] (**10**) and **8**, allowing comparison of species where there is no metal-oxygen interaction (**1** [no metal!] and **4e**), secondary metal-oxygen interaction (**10**) and a full metal-oxygen bond (**8**). The C(1)-C(2) connectivity in **8** is 1.699(21) Å, significantly longer than in the parent carbaborane (**1**), 1.636(9) Å. The C(1)-C(101) bond length of 1.487(21) Å in **8** is shorter and C(101)-O and C(102)-O bonds [1.455(18) Å and 1.451(18) Å respectively] are both longer than the corresponding bonds in the parent carbaborane. For each of these bond distances there is an observed progression as metal-oxygen interaction increases: The C(1)-C(2), C(101)-O and C(102)-O bond distances lengthen and the C(1)-C(101) bonds shortens from the parent carbaborane and then, as metal-oxygen interaction increases, from the gold to the mercury and titanium carbaboranes. [Note: except for C(1)-C(101) in **10** which is longer than in **4e** (or *vice-versa* since which one is anomalous is not clear) and C(102)-O in **4e** in which the bond is shorter than in the parent carbaborane]. Assumedly, the observed changes in bond lengths and angles are a consequence of the constraining effect of the intramolecular 5-membered ring.

Analysis of C(1)-C(101)-O and C(101)-O-C(102) bond angles reveals that they are more acute in **8** [106.6(12) and 107.9(11)° respectively] than in **1**, **4e** and **10** (*ca.* 110 and 113° respectively). Again this appears to be a result of the formation of the strong Ti-O bond, the O and Ti atoms being pulled towards each other (see above). It is also worth noting that the bond angles around the oxygen atom in **8** of 122.4(8), 123.7(8) and 107.9(11) (C(101)-O-Ti, C(102)-O-Ti and C(101)-O-C(102) respectively) suggest pseudo sp^2 hybridisation.

	1	4e	10	8
M-O/Å	----	3.582(7)	2.747(7)	2.219(10)
C(1)-C(2)/Å	1.636(9)	1.667(11)	1.669(8)	1.699(21)
C(1)-C(101)/Å	1.536(10)	1.498(13)	1.526(8)	1.487(21)
C(101)-O/Å	1.343(10)	1.394(13)	1.406(8)	1.455(18)
O-C(102)/Å	1.410(10)	1.384(14)	1.442(8)	1.451(18)
C(1)-C(101)-O/°	110.9(6)	110.9(8)	110.2(5)	106.6(12)
C(101)-O-C(102)/°	113.2(6)	112.2(8)	112.2(5)	107.9(10)
M-C(2)-B(9)/°	----	175.8(4)	177.3(3)	133.9(10)

Table 3.4 Ether Substituent Interatomic Bond Lengths and Angles in Various Carbaboranes.

It is also interesting to note that the M-C(2)-B(9) angle in **4e** and **10** is close to 180° [175.8(4) and 177.3(3)° respectively], as expected, since this represents maximum M-C(2) overlap and is consequently the most energetically favoured position. As discussed previously, the Ti-C(2)-B(9) angle is substantially less than 180° [133.8(10)°], as a result of the strong Ti-O bond formation pulling the two atoms together.

In **8** the torsion angle C(2)-C(1)-C(101)-O of 17.2(16)° approaches the expected eclipsed arrangement (0°C) but the deviation from fully eclipsed confirms the

non-planarity of the 5-membered ring. The C(1)-C(101)-O-C(102) torsion angle is 170.8(11)° defining the expected *trans* staggered arrangement about C(1)-C(101).

Moreover, the methylene hydrogen atoms and two of the methyl hydrogen atoms of the ether group in the solid state appear to be eclipsed, though in solution there is clearly free rotation about the C(102)-O bond, this emphasised by the observation of a singlet in the ^{1}H NMR spectrum. However, in the solid state the methylene hydrogen atoms are inequivalent and therefore, in the ^{1}H NMR spectrum, an AB pattern would be expected. As only a singlet is observed, there must, in solution, be inversion at titanium imposing time-averaged mirror symmetry on the (asymmetric) molecule (*vide infra*).

In the refinement of the molecular structure, the Cp ring was idealised so that the carbon atoms formed a regular pentagon with C-C = 1.420 Å and internal C-C-C angles were 108.0°. The ring adopts a slightly tilted position (of 2° from the position in which all C atoms are equidistant from Ti) such that the carbon atoms most *cis* to the chlorine atoms [C(12) and C(13)] are 0.03-0.05 Å closer to the Ti centre than the carbon atoms most *trans* to the chlorine atoms [C(14) and C(15)].

Figure 3.10 shows a perspective view of a single molecule of **8** with all atoms except those directly bonded to the Ti centre [Cl(1), Cl(2), O, C(2) and Cp] having been removed. The figure clearly illustrates that the geometry of the molecule is a 'piano stool' with Cl(1), Cl(2), C(2) and O forming a square base pyramid with Ti at the apex [Cl(1)-Ti-Cl(2) = 89.3(2)°, Cl(2)-Ti-O = 80.7(3)°, C(2)-Ti-O = 74.0(5)° and C(2)-Ti-Cl(1) = 87.3(4)°] and the Cp ring occupying three coordination sites of the Ti centre resulting in the metal centre being overall 7-coordinate.

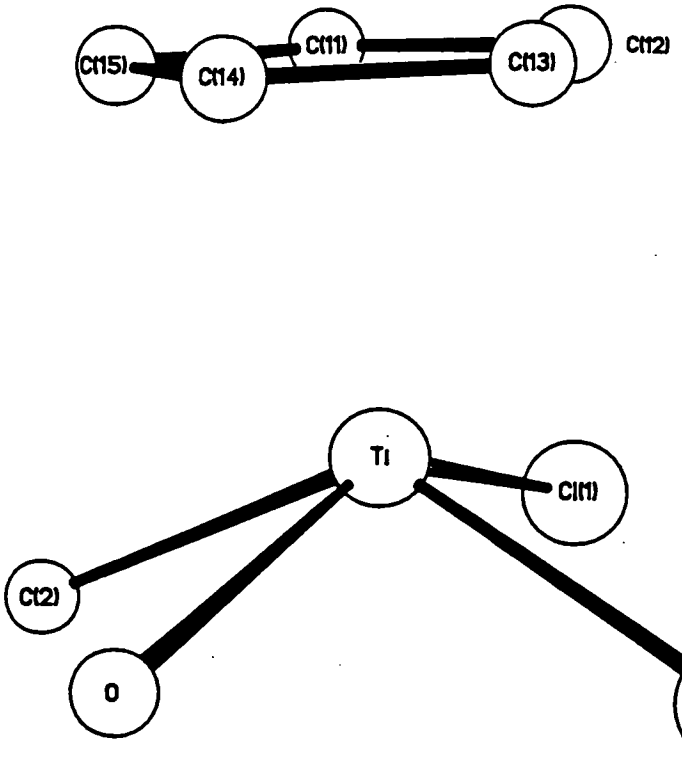

Figure 3.10 Perspective View of **8** With Only Atoms Bonded to Metal Included.

3.3.2 NMR Studies

It was observed that introduction of a phosphine gold(I) fragment onto C(2) of the parent carbaboranes **1** and **2** to give class 3 gold carbaborane compounds (**3** and **4**) resulted in overall electron density removal from the cage (see **Section 2.3.2**). The removal of electron density from the cage is reflected in the $^{11}B\{^1H\}$ NMR spectra of compounds **3** and **4**, with an overall shift of the boron resonances to higher frequency and spectrum width narrowing compared to the appropriate parent carbaborane. Comparison of the $^{11}B\{^1H\}$ NMR spectra of compounds **6** and **8** with that of 1-CH_3OCH_2-1,2-*closo*-$C_2B_{10}H_{11}$, **1**, (**Table 3.5**) reveals that narrowing of the spectrum width is not observed, the spectrum widths for **6** and **8** being 10.26 and 10.00 ppm respectively as compared to 9.98 ppm for **1**. However, the boron resonances do appear to shift (overall) to higher frequency, if only slightly: the three boron resonances (of relative integral 2:4:2) between δ -8.47 and -12.45 ppm in **1** become four resonances (of relative integral 2:2:2:2) between δ -5.03 and -12.24 ppm and δ -5.19 and -12.41 ppm in **6** and **8** respectively; the two resonances of integral 1, due to B(9) and B(12), at δ -2.47 and -4.23 ppm in **1** move to δ -1.98 and -3.47 ppm in **6** and δ -2.41 and -3.53 ppm in **8**, again indicating a small general shift to higher frequency.

A more distinctive shift of the boron resonances to higher frequency, as observed with the gold carbaborane compounds, might have been anticipated. It therefore appears that the Ti^{IV} centre does not have the expected electron withdrawing effect upon the cage, and this may, in part, be due to the formation of the intramolecular Ti-O bond: The solid state molecular structure of **8** conveyed that the Ti-C(2) bond is longer than might be expected because of poor Ti-C(2) overlap, titanium being pulled out of its optimum [*vis à vis* C(2)] position by bonding to the oxygen atom of the ether substituent. Consequently, titanium interaction with the carbaborane cage is not

at a maximum and so its overall electron withdrawing effect on the carbaborane is smaller. Moreover, since the titanium centre is 7-coordinate as a result of the intramolecular Ti-O bond, it clearly acquires electron density from the oxygen atom and that required from the cage is likely to be less than if no intramolecular metal-oxygen interaction were present.

	$^{11}B\{^1H\}$ (δ/ppm)		
	1	**6**	**8**
1B	- 2.47	- 1.98	- 2.41
1B	- 4.23	- 3.47	- 3.53
2B	- 8.47	- 5.03	- 5.19
2B	-10.97	- 8.88	- 8.52
2B	-12.45	-10.67	-10.82
2B	-12.45	-12.24	-12.41

Table 3.5 Comparison of $^{11}B\{^1H\}$ NMR Spectra of **1**, **6** and **8** (64.21 MHz).

The similarity between the boron-11 NMR spectra of **6** and **8** suggest that there is also an intramolecular Ti-O interaction in **6** similar to that observed in **8** and, indeed, it would be most unlikely that Ti-O bonding would not occur given the coordinative unsaturation at the metal. Presumably, if there were no metal-oxygen interaction, the $^{11}B\{^1H\}$ NMR spectrum of **6** would be different with boron resonances moving distinctively to higher frequency due to the increased electron withdrawl towards the titanium centre. Furthermore, the ^1H NMR spectra of **6** and **8** with respect to the relative shift of the ether substituent proton resonances are similar: Comparison of the ^1H NMR spectra of **6** and **8** with that of **1** show that the OCH_2 and OCH_3 resonances (at δ 4.48 and 4.08 ppm respectively in **6** and δ 4.23 and 3.71 ppm respectively in **8**) in both are shifted significantly to higher frequency (0.69 and 0.72 ppm in **6** and 0.44 and 0.35 ppm in **8**) than the corresponding resonances in **1**. This is in contrast to the

observed resonance shifts in the gold carbaborane compounds in which the OCH_2 resonances shifted *ca.* 0.1ppm to higher frequency and the OCH_3 resonances shifted slightly to lower frequency. The resonance shifts in **8** can be attributed to the effect of O bonding to Ti upon the ether substituent as a whole: The shift to higher frequency is indicative of a decrease in electron density, the oxygen atom drawing electron density from the methylene and methyl groups as a result of its electron donation (hard donor [O] to hard acceptor [Ti]) to the metal centre.

In summary, the similar resonance shift in both the $^{11}B\{^1H\}$ and ^1H NMR spectra compared to **1** of **6** as of **8** therefore strongly suggests that **6** must have a similar structure to **8** with respect to metal-oxygen intramolecular bonding. **Figure 3.11** illustrates the proposed structure of **6**. In this, titanium is 5-coordinate and because of the steric constraints of the ('bidentate') carbaborane ligand and the intramolecular 5-membered ring, the shape of the molecule is probably based on a square based pyramid with two chlorine atoms and C(2) and O of the ether carbaborane ligand occupying the basal positions, and the third chlorine atom at the apex (**Figure 3.12**). It is interesting to note that the methylene group of the ether substituent whose movement is constrained as part of the 5-membered ring, gives a singlet resonance in the ^1H NMR spectra of both **6** and **8**: An AB pattern, due to the two inequivalent methylene protons coupling to each other, would be predicted. For the methylene hydrogen atoms to become equivalent there must be inversion at the titanium centre (not unexpected for 5- and 7-coordinate species) imposing time-averaged mirror symmetry on the (asymmetric) compounds. Indeed, the $^{11}B\{^1H\}$ NMR spectra intimate a symmetrical structure in solution (resonances of relative integral 1:1:2:2:2:2, the four resonances of integral 2 attributable to the four pairs of symmetry related boron atoms) whilst in the solid state the structures are clearly asymmetric.

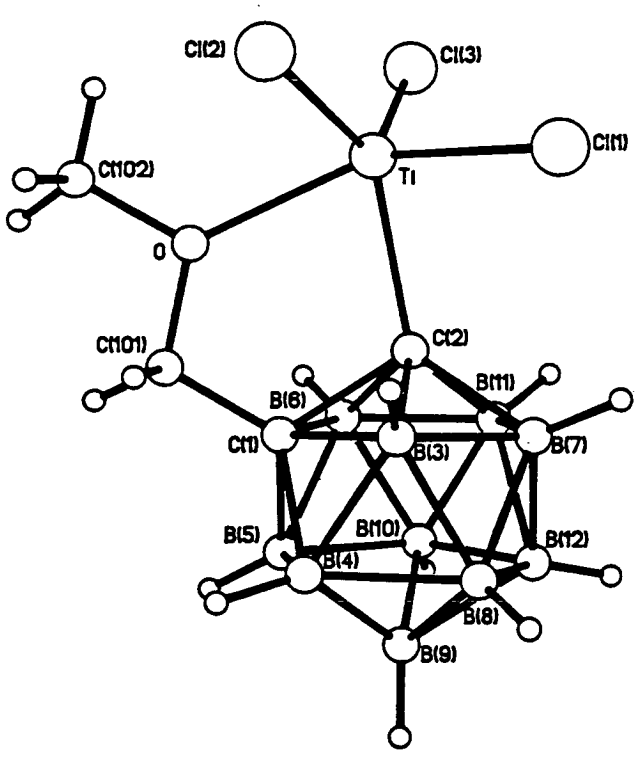

Figure 3.11 Proposed Structure of **6**.

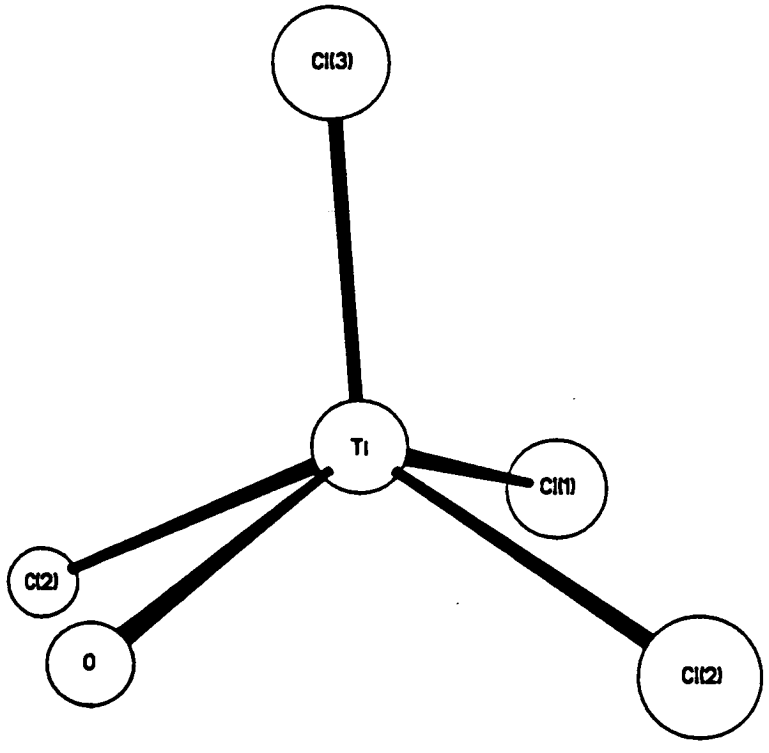

Figure 3.12 Proposed Metal Coordination Sphere of **6**.

3.4 Chemical Studies

3.4.1 Introduction

This section highlights chemical studies arising from the synthesis of the σ-bonded titanium carbaboranes. A brief study of the chemistry of compounds **6** and **8** are described in **Section 3.4.2.**

Over the period of the research described in this thesis it was observed that when successful syntheses (using Et_2O as the reaction solvent) were repeated in THF, no reaction occurred. **Section 3.4.3** speculates on possible reasons for these non-reactions.

3.4.2 Chemistry of Titanium Carbaboranes

In comparison to the thermally unstable compounds $TiCl_3R$ (R = alkyl or aryl), compound **6** exhibits good thermal stability and is indefinately stable in the solid state and in solution at room temperature in an anaerobic atmosphere: The compound is, however, air-sensitive, decomposing to an unidentified orange species, but is stabilised by adduct formation yielding compound **7** as described in **Section 3.2.2.** Compound **7** demonstrates good thermal, air and moisture stability but has the drawback of being insoluble in most solvents and partially soluble in only methanol.

When compound **8** was dissolved in THF, a colour change from orange to yellow was observed. On removal of THF *in vacuo* the solid recovered was found to be the same colour as the solution. Initially, it was thought that THF had coordinated (through oxygen) to the titanium centre resulting in cleavage of the intramolecular Ti-O bond. The retention of colour on removal of the solvent was thought to indicate that bound THF was also present in the solid state. However, analysis of the yellow solid by $^{11}B\{^1H\}$ and ^1H NMR spectroscopies revealed that it consisted of a mixture

of parent carbaborane (**1**) and a non-boron containing titanium species. Crystals of the titanium compound were produced by slow diffusion of *n*-hexane into a dichloromethane solution at -30°C. An X-ray study (unit cell dimensions and space group determination: **Table 3.6**) identified the compound as the oxo-tetramer, $\{CpTiClO\}_4$ (**Figure 3.13**[104]), which is usually produced by hydrolysis of $CpTiCl_3$[105]. As the only oxygen source (all solvents were dry and oxygen free, this ensured by thorough solvent degassing techniques - see **Section 5.2.1**), THF must somehow be involved in the decomposition of **8** and the generation of the oxo-titanium tetramer.

	observed	literature
crystal system	orthorhombic	orthorhombic
space group	$Cmc2_1$	$Cmc2_1$
a/Å	15.326(9)	15.320(5)
b/Å	11.728(11)	11.715(5)
c/Å	14.557(9)	14.515(5)
V/Å^3	2616.5	2605.1

Table 3.5 Crystal Data for $\{CpTiClO\}_4$.

A possible (but speculative) mechanism for the decomposition of **8** could be initiated by THF binding through oxygen to the metal centre which results in cleavage of the intramolecular Ti-O bond. This would probably result in an increasingly sterically congested metal centre leading to M-C homolysis, assumedly producing the carbaborane anion and a $\{CpTiCl_2THF\}$ fragment which may be a precursor for the oxo-titanium tetramer. It is unclear how the tetramer may be formed from this fragment as it would involve the break up of THF, a process which would have great thermodynamic demands. What is clear, however, is that addition of THF to **8** gives $\{CpTiClO\}_4$ rapidly and in essentially quantitative yields.

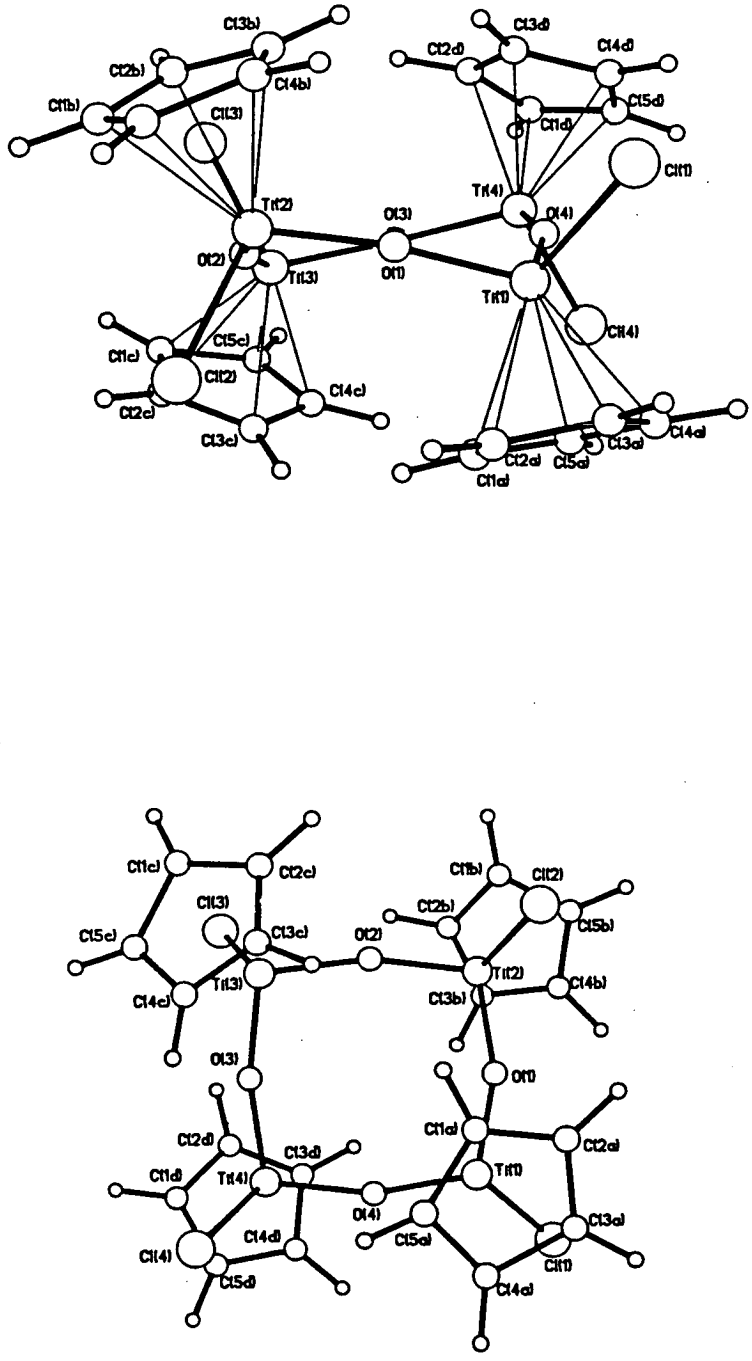

Figure 3.13 Perspective and Plan Views of $\{CpTiClO\}_4$[104].

3.4.3 The Reactivity of Lithium Carbaborane in THF

THF has been used as an oxygen bound ligand to metal centres in very many coordination compounds, for example, $[VCl(NO)(THF)_4]^+$ [106] and $UO_2(NO_3)_2(THF)_2$[107]. Oxygen, as a hard donor, prefers to coordinate to hard acceptors such as the small highly charged titanium(IV) centre and so THF coordination to titanium(IV) is favourable. In order to discourage the creation of the Ti-O intramolecular bond in **8**, the reaction between $CpTiCl_3$ and Li[1-CH_3OCH_2-1,2-*closo*-$C_2B_{10}H_{10}$] was attempted using THF as the solvent instead of Et_2O. It was anticipated that THF solvation of the titanium centre would obviate formation of the intramolecular Ti-O bond. However, no obvious reaction was observed, and after stirring the reactants together in THF for 4 hours, both lithium carbaborane and $CpTiCl_3$ were recovered intact. It is interesting to note that although a small amount of the oxo-titanium tetramer was isolated, it was not produced in quantitative yields as when compound **8** was dissolved in THF, indubitably indicating that reaction followed by decomposition had not occurred.

The non-reaction of $CpTiCl_3$ and Li[1-CH_3OCH_2-1,2-*closo*-$C_2B_{10}H_{10}$] in THF, compared to the ready reaction in Et_2O producing **8** in good yield, encouraged consideration of the role of the lithium carbaborane intermediate in synthesis of σ-bonded transition metal species.

Repetition of the reaction between PPh_3AuCl and Li[1-CH_3OCH_2-1,2-*closo*-$C_2B_{10}H_{10}$], which in Et_2O gives 38% yield of 1-CH_3OCH_2-2-{PPh_3Au}-1,2-*closo*-$C_2B_{10}H_{10}$ (**4a** - see **Section 5.2.5**), in THF results in no reaction taking place. Similarily, other reactions which occur readily in Et_2O do not take place in THF: For example, no reaction occurs when either Li[1-CH_3OCH_2-1,2-*closo*-$C_2B_{10}H_{10}$] or Li[1-Ph-1,2-*closo*-$C_2B_{10}H_{10}$] is added to PCy_3AuCl in THF in comparison to the rapid reaction observed when the reaction solvent is Et_2O. In each case PR_3AuCl and

either lithium carbaborane or (surprisingly) parent carbaborane are recovered. The non-reaction of established syntheses in THF could be explained in three ways:

(1) The presence of H_2O in THF would either consume the lithiating reagent or react with the lithium carbaborane, regenerating the parent carbaborane and so quenching the reaction. THF and water are certainly miscible and as received the solvent routinely contains 100 ppm of H_2O. However, the quantity of H_2O in THF as used should be negligible: THF is predried over sodium wire and then dried further by distillation over sodium wire/benzophenone prior to use. Any water remaining after this procedure would be unlikely to be present in sufficient quantity to quench the whole reaction. The freeze-pump-thaw method of degassing the solvent involves cooling to -196°C under an atmosphere of dry oxygen-free nitrogen. In theory, this could cause condensation of water into the solvent if present in the closed system of the Schlenk line, but the standard 'muck trap' previously cooled to -196°C should condense any water in the system prior to the degassing. Besides, degassing by saturating THF with nitrogen gas does not alter the outcome of the (non-) reactions.

The ^1H NMR spectrum of distilled THF, degassed by the freeze-pump-thaw method, was recorded as a $CDCl_3$ solution and showed peaks at δ 3.82-3.66 ppm (multiplet, OCH_2) and δ 1.98-1.77 ppm (multiplet, CH_2) due to THF but no broad peak between 3 and 5 ppm which would have indicated the presence of H_2O. Thus, although possible, quenching of the reaction by H_2O is improbable because the scrupulous drying of the solvents removes all measurable traces of H_2O from them.

(2) Similarily, the presence of H^+ in THF would either consume the lithiating reagent or reprotonate the lithium carbaborane resulting in the quenching of the reaction. The source of H^+ could be THF: In a recent study[108] it was found that when the macrocyclic compound Ru[*cyclo*-$(SCH_2CH_2)_3$]Cl_2 (Ru(9S3)Cl_2) was stirred with PPh_3Cl_2 and Tl[PF_6] in CH_3NO_2 and THF, a small amount of the product

$[Ru(9S3)(PPh_3Cl_2)(C_4H_4O)][PF_6]$, surprisingly containing a furan ligand, was obtained. It is not clear what the mechanism for this reaction is but, as THF and furan are obviously related, it would be an intelligible assumption that THF is the source of furan.

Further studies[109] of this particular reaction have shown that furan is not present as a contaminant in commercial THF (or, for that matter, in any of the other reactants) and that the generation of furan from THF would result in H^+ and/or H_2 gas being produced. However, as the mechanism of the furan production is currently unknown (making production of H^+ from THF uncertain) and because there is no evidence in any of the ^1H NMR spectra of the attempted reactions that furan is present, this seems to be a dubious cause for the non-reaction. Moreover, if furan was present, it is probable that it would be in such small amounts as not to affect the reaction significantly.

(3) The most probable explanation for the non-reactions in THF is the inability of the lithium carbaborane in THF to react. The lithium carbaborane is a very reactive species in Et_2O and, if isolated from solvent and exposed to the air, it rapidly absorbs moisture from the atmosphere and becomes a pool of liquid. This sensitivity in air/moisture can be attributed to Li^+ preference for a solvation sphere: Li^+ is a small (mono) charged cation and being a hard centre (acceptor) has a strong affinity for hard donors, in particular oxygen and nitrogen.

Ether coordination to the metal centre is unlikely when lithium carbaborane is prepared in diethyl ether because Et_2O is a volatile solvent and the molecules have a high degree of freedom. As this means that it would be readily lost, Et_2O a poor ligand in coordination chemistry and, consequently, ether coordination has not been widely observed. Furthermore, ionic compounds such as lithium carbaborane have low solubility in a weakly polar solvent such as diethyl ether. THF is a less volatile,

more polar solvent and being cyclic has fewer degrees of freedom and is therefore an overall better donor ligand than diethyl ether. The polar nature of THF results in increased solubility of ionic compounds and so solvation of receptive cations is easier.

The preference for the lithium cation to be solvated has been demonstrated in carbaborane chemistry *via* study of the molecular structures of, firstly, the lithium salt of the mono-carbon substituted 1,2-*closo*-carbaborane as its pentamethyl-diethylenetriamine adduct[45] (**Figure 1.19** p26) and, secondly, the unusual {*nido*-C_2B_9} lithium species illustrated in **Figure 3.14**[21]. In the latter species, the lithium atom is bound to the oxygen atoms of two THF solvent molecules and the two oxygen atoms of the carbaborane ether substituents highlighting the preference of Li^+ to be solvated by hard donor ligands.

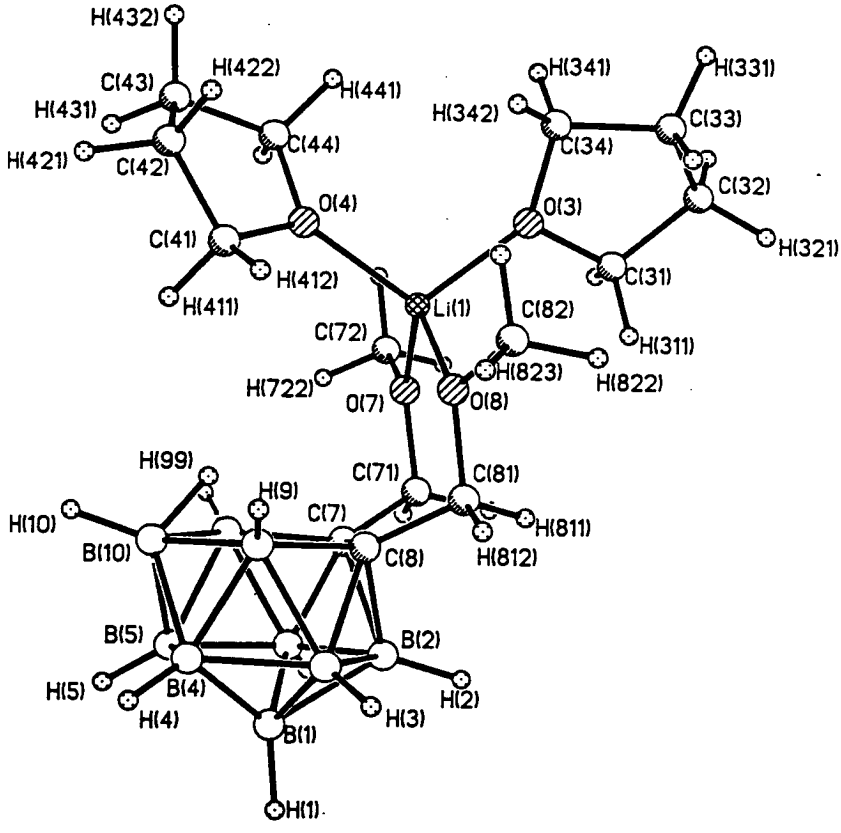

Figure 3.14 Molecular Structure of $(THF)_2Li\{7,8\text{-}(CH_3OCH_2)_2\text{-}7,8\text{-}nido\text{-}C_2B_9H_9\}$.

Therefore, it is highly probable that, in THF, the lithium cation in the carbaborane salt is solvated by several THF ligands bound strongly to Li^+ and holding it tight to the carbaborane rendering it unreactive. THF coordination must therefore have a thermodynamic and/or kinetic stability over the formation of LiCl, the usual driving force of these reactions. Unfortunately, attempts to crystallise the lithium carbaborane compound as its THF adduct have been unsuccessful.

The occasional detection of the parent carbaborane can be attributed to the method of analysis of the reactants: The removal of THF followed by addition of $CDCl_3$ which often contains small amounts of HCl (a decomposition product) and/or (sometimes) H_2O may cause reprotonation of the carbaborane anion.

In conclusion, these reactions, which take place readily in Et_2O, do not occur when the solvent is THF because lithium carbaborane rendered inactive due, apparently, to thermodynamically and/or kinetically favourable THF solvation.

3.5 Conclusions

As predicted from the conclusions derived from the previous chapter, σ-bonded titanium carbaborane compounds were successfully synthesised from reaction between lithium carbaborane and the appropriate titanium(IV) chloride ($TiCl_4$ or $CpTiCl_3$). Characterisation was effectively accomplished by microanalysis and IR and NMR spectroscopies. The absence of β-hydrogen atoms in these compounds has resulted in increased thermal stability over their alkyl analogues. However, 1-CH_3OCH_2-2-{$TiCl_3$}-1,2-*closo*-$C_2B_{10}H_{10}$ (**6**) was found to be air and moisture sensitive (which is not unusual in Ti^{IV} chemistry), although the sensitivity was alleviated by coordination of 2,2'-bipyridyl to the titanium centre (producing compound **7**).

The molecular structure of 1-CH_3OCH_2-2-{$CpTiCl_3$}-1,2-*closo*-$C_2B_{10}H_{10}$ (**8**) not only demonstrated the expected Ti-C σ-bond, but also revealed intramolecular coordination of the ether substituent oxygen atom to the titanium atom, thereby illustrating the preference of titanium(IV) for a high coordination number. The Ti-O coordination produced a non-planar (intramolecular) 5-membered ring, the formation of which resulted in measurable molecular distortions: The titanium atom is pulled out of its optimum position with respect to the cage by the coordination to oxygen and, consequently, the titanium-cage carbon orbital overlap is reduced, resulting in a longer Ti-C bond than expected; some lengthening and shortening of the bonds within the 5-membered ring with respect to related (non-coordinated) species is observed and this presumably occurs to accommodate the ring formation. It can therefore be concluded that the energy loss as a consequence of these distortions is more than compensated for by the energy gain in the formation of the ring.

The intramolecular coordination is reflected in the $^{11}B\{^1H\}$ NMR spectrum of **8**:

The shifts in the boron resonances with respect to the corresponding resonances in the spectrum of **1** are not as large as expected, implying a weaker than expected influence of the titanium centre on the carbaborane ligand. This is consistent with the observations made from the molecular structure in which the Ti-C_{cage} overlap is reduced by oxygen coordination, probably reducing the electron withdrawing influence of the titanium atom with respect to the cage. Comparison of the $^{11}B\{^1H\}$ and ^1H NMR spectra of **6** and **8** allowed proposition of the structure of **6**, the most notable aspect being that intramolecular coordination is also predicted: In both the ^1H NMR spectra of **6** and **8**, the OCH_2 and OCH_3 resonances showed significant shifts to higher frequency compared to **1**, suggesting loss of electron density from the ether group; the $^{11}B\{^1H\}$ NMR spectrum of **6** was similar to that of **8** in that both exhibited similar shifts in resonances with respect to in the spectrum of **1**, the shifts for both not as large as expected. Since these observations are consistent with the observed intramolecular Ti-O bond formation in **8**, it appears that this is also the case in **6**.

Reaction of Cp_2TiCl_2 with one and two equivalents of lithium carbaborane produced, respectively, Cp_2TiCl (**9**) and a transient (apparently thermally unstable) green species tentatively assigned as 1-CH_3OCH_2-{Cp_2Ti}-1,2-*closo*-$C_2B_{10}H_{10}$. Both products are comparable to those obtained from the reaction between titanocene dichloride and one or two equivalents of the sterically demanding $Li[CH(SiMe_3)_2]$. The formulation of the latter compound was deduced only by comparison with the results of this reaction. Therefore, without conclusive spectroscopic data, the formation of the latter compound is purely speculative.

Finally, the investigation of the non-reaction of lithium carbaborane with gold and titanium chlorides in THF, where reactions occur readily in Et_2O, concluded that both solvents probably solvate the lithium cation through oxygen donation. However, as THF is less volatile and is a better donor than Et_2O, it presumably binds more tightly to the lithium cation (which prefers a solvation sphere), so much so that it effectively

renders Li^+ unreactive. Since the driving force of the reactions to synthesise σ-bonded carbametallaboranes is usually the formation of lithium chloride, THF solvation would result in no reaction occurring, as observed.

Overall, the successful synthesis of the thermally stable 5- and 7-coordinate σ-bonded $\{TiCl_3\}$ and $\{CpTiCl_2\}$ carbaborane compounds intimates that some future work in this area should include the synthesis of 4- and 6-coordinate $\{TiCl_3\}$ and $\{CpTiCl_2\}$ carbaboranes and the synthesis of related group 4, group 5, lanthanide and actinide compounds.

CHAPTER 4
PHOSPHINE CARBABORANE COMPOUNDS

4.1 Introduction

In mono-substituted icosahedral 1,2-*closo*-carbaboranes, the hydrogen atom bound to C(2) is readily abstracted by alkyl lithium reagents to form the (mono) lithium salt of the *closo*-carbaborane anion (**Section 1.3.2**). Mono-lithium carbaborane has been used to synthesise (class 3) σ-bonded carbametallaborane complexes such as those described in **Chapters 2** and **3** by reaction with the appropriate metal chloride.

However, lithium carbaborane has also been used as a precursor in the synthesis of numerous other (carbon) substituted carbaborane derivatives, in some reactions not necessarily using a chlorinated starting material[13]: **Figure 4.1** outlines the synthesis of some carbaborane derivatives from mono- and di-lithium carbaborane. The use of lithium carbaborane provides an alternative synthetic route to the reaction of *arachno*-bisligand decaborane(12) with a substituted alkyne in the production of derivatised carbaboranes (**Figure 1.6, p11**).

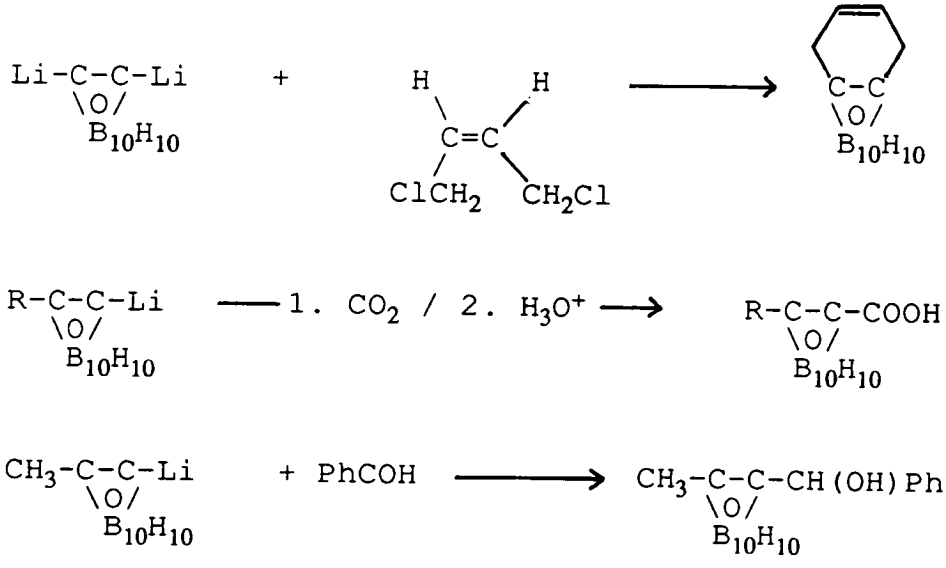

Figure 4.1 Syntheses of Derivatised Carbaboranes from Lithium Carbaboranes.

Similarly, reactions of chlorophosphines with lithium carbaboranes have produced phosphine carbaborane compounds[110] as illustrated in **Figure 4.2.** Despite the varied chemistry displayed by analogous tertiary aryl and alkyl phosphines, little organometallic chemistry has been studied using phosphine carbaborane compounds as ligands: **Figure 4.3** details Ni^{II} [111] and Fe^{0} [112] derivatives that have been reported and **Figure 4.4** illustrates the recent molecular structure of a phosphine carbaborane gold(I) complex[61].

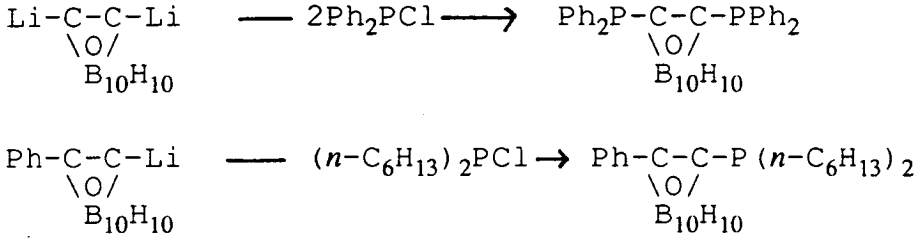

Figure 4.2 Synthesis of Phosphine Carbaboranes.

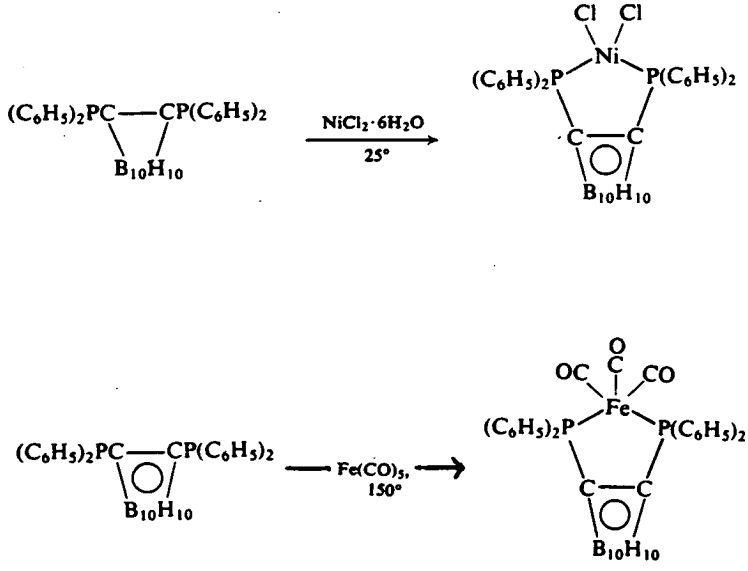

Figure 4.3 Synthesis of Metal Complexes of Phosphine Carbaboranes.

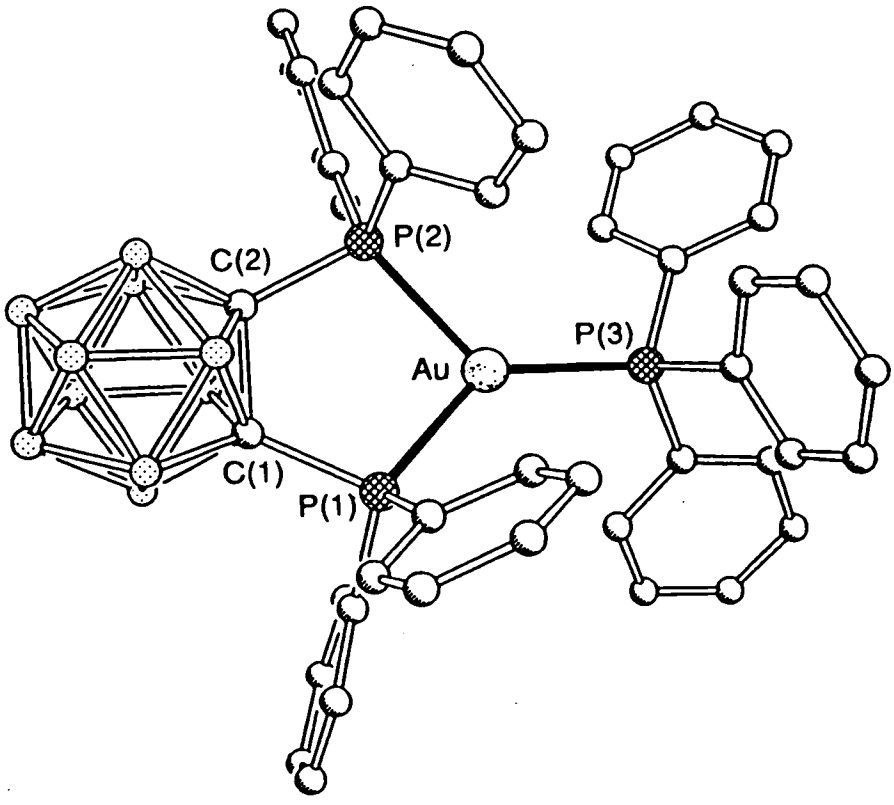

Figure 4.4 Structure of $[1,2\text{-}(PPh_2)_2\{\mu\text{-}PPh_3Au\}\text{-}1,2\text{-}closo\text{-}C_2B_{10}H_{10}]^+$.

A variety of phosphine carbaborane gold(I) complexes has recently been reported[61]. This research has involved the (bidentate) bisphosphine derivative of *ortho*-carbaborane, produced from the reaction of PPh_2Cl with $Li_2[1,2\text{-}closo\text{-}C_2B_{10}H_{10}]$, as a bridging phosphine to gold.

Reaction of mono-(carbon) substituted lithium carbaborane with PPh_2Cl would produce the simpler (mono-dentate) phosphine, $1\text{-}R\text{-}2\text{-}PPh_2\text{-}1,2\text{-}closo\text{-}C_2B_{10}H_{10}$. This type of phosphine would be analogous to tertiary aryl phosphines and so might be expected to exhibit similar chemistry. Therefore, by using such a phosphine carbaborane to synthesise phosphine carbaborane gold(I) chloride (analogous to PR_3AuCl), some novel phosphine carbaborane gold(I) compounds could be synthesised. Because of the smaller steric demands of ether versus phenyl, and since phenyl carbaborane phosphines had been synthesised previously[113], the ether carbaborane (**1**) was chosen as the basic framework for phosphine carbaborane

gold(I) compounds.

Section 4.2 describes the synthesis and characterisation of phosphine ether carbaborane and, from this, the formation of gold(I) chloride and subsequently gold(I) methyl compounds. **Section 4.3** outlines the synthesis and characterisation of a novel biscarbaborane compound analogous to the tertiary phosphine gold(I) compounds described in **Chapter 2. Section 4.4** discusses the synthesis and characterisation of a novel carbaborane-borane compound analogous to tertiary phosphine gold(I) boranes synthesised previously[24]. **Section 4.5** describes research related to BNCT in which phosphine carbaboranes may be useful as precursors to BNCT reagents. Finally, the conclusions from this chapter and the overall conclusions from the thesis are outlined in **Section 4.6** and **Section 4.7** respectively.

4.2 Simple Phosphine Carbaborane Compounds

4.2.1 Synthesis and Characterisation of 1-CH_3OCH_2-2-PPh_2-1,2-*closo*-$C_2B_{10}H_{10}$ (**11**)

1-CH_3OCH_2-2-PPh_2-1,2-*closo*-$C_2B_{10}H_{10}$, compound **11**, was synthesised in a similar manner to that described previously[113] for 1-Ph-2-P(*n*-$C_6H_{13})_2$-1,2-*closo*-$C_2B_{10}H_{10}$: Refluxing stoichiometric amounts of PPh_2Cl and Li[1-CH_3OCH_2-1,2-*closo*-$C_2B_{10}H_{10}$] in benzene afforded, after work-up, a good yield of compound **11**. By dissolving **11** in a minimum of warm (*ca.* 45°C) ethanol and then cooling to -30°C, colourless crystals of **11** were produced. Compound **11** in the solid state or as CH_2Cl_2, THF or EtOH solutions was found to be stable in air at room temperature. Characterisation was effected by microanalysis and by infra-red and $^{31}P\{^1H\}$, $^{11}B\{^1H\}/^{11}B$ and ^1H NMR spectroscopies. Microanalysis of crystals of **11** was accordant with the proposed formulation of $C_{16}H_{25}B_{10}OP$. The infra-red spectrum displayed peaks at 2582 cm^{-1} (broad) and at 1458, 1383 and 1115 cm^{-1} (sharp) consistent with B-H and CH_3OCH_2 vibrations respectively.

The $^{31}P\{^1H\}$ NMR spectrum exhibited the expected sharp singlet resonance, at δ 12.5 ppm. Three peaks of relative integral 1:1:8 were observed in the $^{11}B\{^1H\}$ NMR spectrum of **11**, the broad peak of integral 8 a quadruple coincidence (at the field strength used [64.21 MHz]) of the four symmetry related pairs of boron atoms [B(3)/B(6), B(4)/B(5), B(7)/B(11), B(8)/B(10)]. Each peak showed the expected doublet due to coupling of each boron atom to its bound hydrogen atom in the ^{11}B NMR spectrum ($^1J_{B\text{-}H}$ = 141-164 Hz). The ^1H NMR spectrum revealed resonances due to the various substituent protons (C_6H_5, OCH_2, OCH_3) in the correct integral ratio (10:2:3). The absence of the broad peak at δ 4.00 ppm in the ^1H NMR spectrum, due, in the parent carbaborane (**1**), to the hydrogen atom bound to C(2), was also noted. All NMR data are discussed in more detail in **Section 4.2.5**.

4.2.2 Synthesis and Charcterisation of 1-CH_3OCH_2-2-{PPh_2AuCl}-1,2-*closo*-$C_2B_{10}H_{10}$ (**12**)

The synthesis of compound **12** was attempted using two synthetic methods described for the general synthesis of phosphine gold(I) complexes: PR_3AuCl has been successfully synthesised in high yield either by reacting two equivalents of PR_3 with $HAuCl_4.3H_2O$[59] or by reacting stoichiometric amounts of PR_3 and thtAuCl[61] (tht = *cy*-C_4H_8S). The former synthetic route is more expensive in terms of phosphine reagent since two equivalents of phosphine are required for every one equivalent of gold. Consequently, in order to obtain a better yield of phosphine carbaborane gold(I) chloride with respect to the phosphine reagent, the latter route would be preferable.

Stirring two equivalents of 1-CH_3OCH_2-2-PPh_2-1,2-*closo*-$C_2B_{10}H_{10}$, **11**, with $HAuCl_4.3H_2O$ in ethanol at room temperature resulted in eventual reduction from gold(III) to gold(0) (black deposits of colloidal gold) and not to gold(I) as required. As no amount of **12** was recovered from the reaction mixture, this was obviously not a suitable synthetic route to **12**.

However, compound **12** was successfully synthesised in good yield by stirring stoichiometric amounts of thtAuCl and **11** in dichloromethane at room temperature, although some decompositon to gold(0) also occurred. The product was recovered (after filtration) by precipitating it out of solution with *n*-hexane and was isolated in good yield and purity. Crystallisation from CH_2Cl_2/*n*-hexane (1:4) at -30°C yielded high quality colourless crystals of 1-CH_3OCH_2-2-{PPh_2AuCl}-1,2-*closo*-$C_2B_{10}H_{10}$ (**12**), suitable for an X-ray diffraction study (**Section 4.2.4**).

In the solid state, **12** is stable in air but was found to be mildly light sensitive, turning grey on prolonged exposure. Further, as di- and trichloromethane solutions in particular, 12 decomposed slowly (over *ca.* 24h) on exposure to the atmosphere

and/or light with black colloidal material, presumably gold(0), being produced.

Characterisation was accomplished in the usual manner by microanalysis and spectroscopic (IR and multinuclear NMR) analysis. Microanalyses of both the bulk solid and the colourless crystals were consistent with the proposed formulation of $C_{16}H_{25}AuB_{10}ClOP$. The infra-red spectrum contained all the expected peaks due to B-H and CH_3OCH_2 vibrations with ν_{max} at 2572 and 1435, 1384, 1110 cm^{-1} respectively.

As anticipated, a single sharp peak was observed in the $^{31}P\{^1H\}$ NMR spectrum, at δ 54.6 ppm. As with **11**, the $^{11}B\{^1H\}$ NMR spectrum (**Figure 4.5**) contained three peaks of relative integral 1:1:8, the lowest frequency resonance again a quadruple coincidence of the four pairs of boron atoms. The ^{11}B NMR spectrum demonstrated the expected coupling with the boron-proton coupling constant, $^1J_{B-H}$, in the range 145-208 Hz. The ^1H NMR spectrum (**Figure 4.6**) showed the expected number of resonances in the correct integral ratio (10:2:3) due to the substituent protons (C_6H_5, OCH_2, OCH_3). No resonances due to gold-bound or free tht were observed indicating that a pure sample of **12** had been isolated. All NMR spectra are discussed in more detail in **Section 4.2.5.**

Compound **12** is analogous to PPh_3AuCl in the sense that phenyl has been replaced by carbaborane, it might therefore be expected that **12** would exhibit similar chemistry to PPh_3AuCl. However, differences in chemistry could occur in situations where the *cone angle*[114] of the phosphine is known to be important: The increased steric demands of carbaborane versus phenyl intimates that the cone angle of the phosphine carbaborane will be much larger than that of PPh_3. Nevertheless PPh_3AuCl has a varied chemistry (**Section 1.5.1**) and analogous reactions should be possible with **12**, opening up a vast new area in carbametallaborane chemistry.

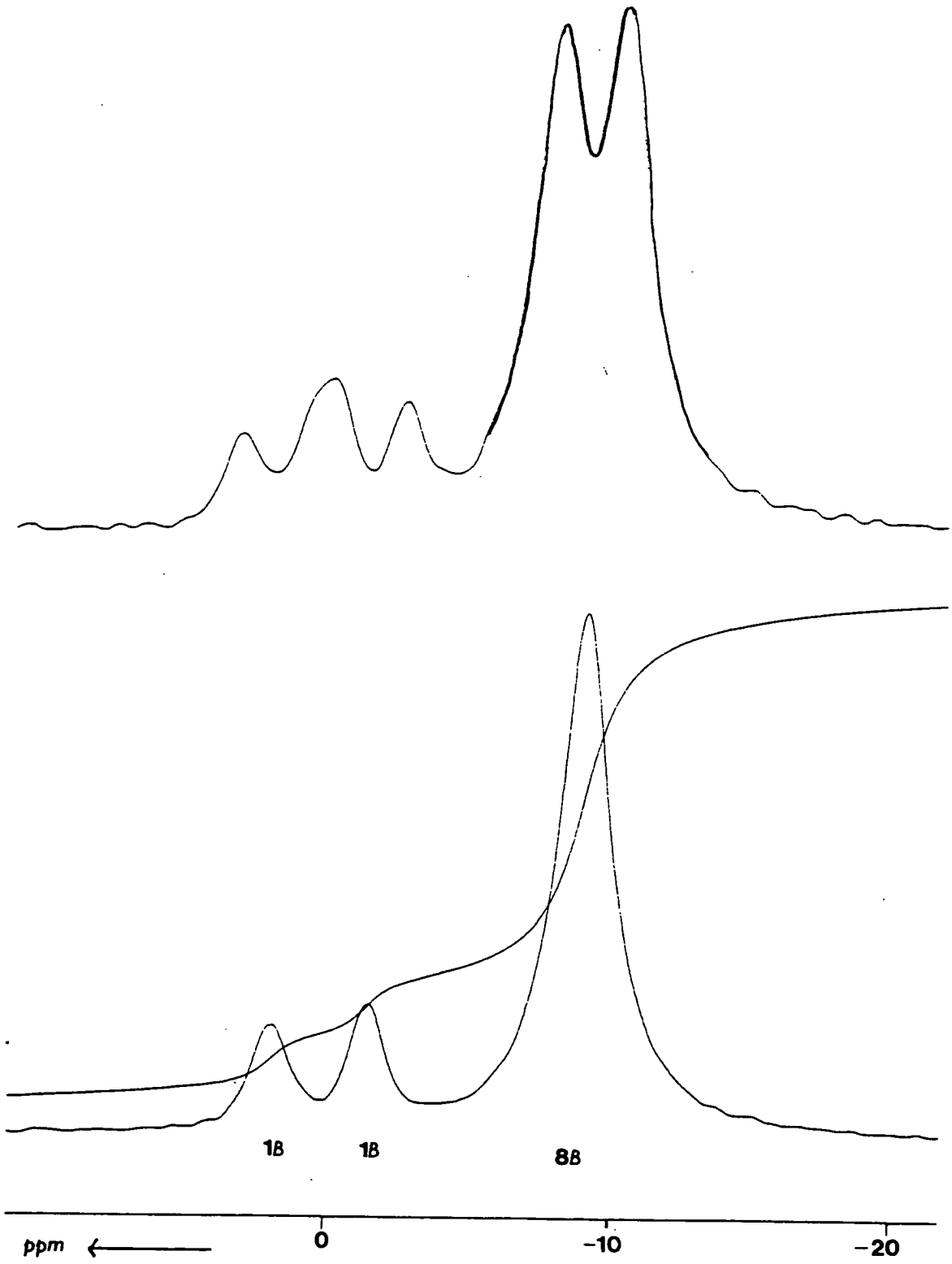

Figure 4.5 $^{11}B\{^{1}H\}/^{11}B$ NMR Spectra of **12** (64.21 MHz).

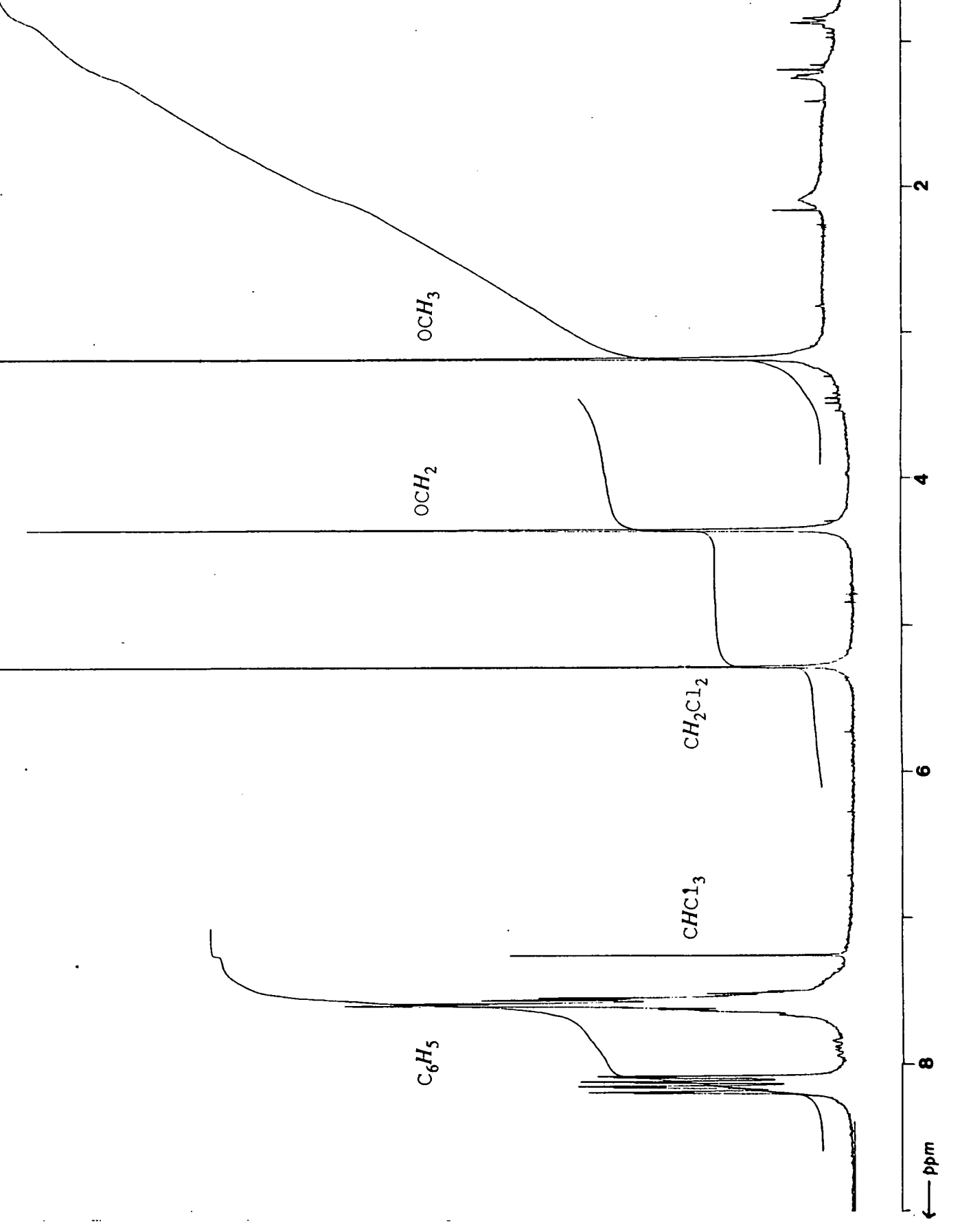

Figure 4.6 ^{1}H NMR Spectrum of **12** (200.13 MHz).

4.2.3 Synthesis and Characterisation of 1-CH_3OCH_2-2-{PPh_2AuMe}-1,2-*closo*-$C_2B_{10}H_{10}$ (**13**)

1-CH_3OCH_2-2-{PPh_2AuMe}-1,2-*closo*-$C_2B_{10}H_{10}$ (**13**) was synthesised by direct reaction of 1-CH_3OCH_2-2-{PPh_2AuCl}-1,2-*closo*-$C_2B_{10}H_{10}$ (**12**) with methyl lithium in diethyl ether at -78°C. Attempts to synthesise compound **13** by methods analogous to those described in the literature[84, 86] resulted in decomposition, with colloidal gold (Au^0) as the main product and only a small yield (<10%) of compound **13** being isolated. However, addition of methyl lithium to a cooled suspension of **12** in diethyl ether and subsequently allowing the reaction mixture to warm to room temperature, produced **13** in good yield and purity and without any appreciable decomposition.

The off-white solid recovered from diethyl ether was identified as 1-CH_3OCH_2-2-{PPh_2AuMe}-1,2-*closo*-$C_2B_{10}H_{10}$ by microanalysis and by IR and NMR spectroscopies. Microanalysis was consistent with the proposed molecular formula of $C_{17}H_{28}AuB_{10}OP$. The IR spectrum revealed the presence of B-H (ν_{max} at 2565 cm^{-1}) and CH_3OCH_2 (ν_{max} at 1438, 1379 and 1108 cm^{-1}) vibrations.

The $^{31}P\{^1H\}$ NMR spectrum exhibited the anticipated single peak, at δ 62.9 ppm. Not unexpectedly, the $^{11}B\{^1H\}$ NMR spectrum again showed three peaks of relative integral 1:1:8, the ^{11}B spectrum also showing the expected boron-hydrogen coupling ($^1J_{B-H}$ = 151-195 Hz). Resonances due to C_6H_5, OCH_2, OCH_3 and CH_3 were observed in the correct integral ratio of 10:2:3:3 respectively in the ^1H NMR spectrum of **13**. The NMR data are analysed in more detail in **Section 4.2.5**.

4.2.4 Crystallographic Study on **12**

Intensity data were collected from a single crystal of **12**, the large, well-formed colourless crystal grown by slow diffusion of *n*-hexane into a dichloromethane solution of the compound. A fraction (0.7) of CH_2Cl_2 solvate cocrystallised with one molecule of **12** and was found to be disordered in the lattice; consequently it is poorly defined. **Table 4.1** lists atomic coordinates and equivalent isotropic thermal parameters for all non-hydrogen atoms and **Table 4.2** details selected interatomic bond distances and interbond angles. **Figure 4.7** shows a perspective view of a single molecule of **12**.

The {1,2-*closo*-C_2B_{10}} cage of **12** has the expected icosahedral geometry with a C(1)-C(2) connectivity of 1.699(14) Å. This is longer than in the parent carbaborane, 1-CH_3OCH_2-1,2-*closo*-$C_2B_{10}H_{11}$ (**1**), 1.636(9) Å[20] and comparable to the corresponding distance in 1-CH_3OCH_2-2-{$CpTiCl_2$}-1,2-*closo*-$C_2B_{10}H_{10}$ (**8**), 1.699(12) Å. The orientation of the ether group is defined by the C(1)-C(101)-O-C(102) and C(2)-C(1)-C(101)-O torsion angles of 153.1(9) and -49.1(12)° respectively. The former implies a *trans* staggered arrangement of the ether group about the C(101)-O bond and is similar to that in 1-CH_3OCH_2-2-{$AsPh_3Au$}-1,2-*closo*-$C_2B_{10}H_{10}$ (**4e**; **Figure 2.12**, p72), 179.9(8)°. The latter torsion angle suggests a *cisoid* arrangement of the ether group with respect to the C(1)-C(101) bond. In 1-$C_2H_5OCH_2$-2-{MeHg}-1,2-*closo*-$C_2B_{10}H_{10}$[55] (**10**) and **8** the C(2)-C(1)-C(101)-O torsion angles are close to 0° as a result of Hg-O and Ti-O intramolecular interaction respectively. Consequently, the C(2)-C(1)-C(101)-O torsion angle and an O-Au distance of 3.343(8) Å in **12** intimate that there is no metal-oxygen intramolecular interaction.

	x	y	z	Ueq
Au	-0.05355(4)	0.52676(2)	0.41248(1)	0.0375(3)
P	0.0477(3)	0.43489(16)	0.37246(8)	0.0321(13)
Cl	-0.1483(3)	0.61861(22)	0.45528(10)	0.0642(20)
C(11)	0.1643(10)	0.3632(6)	0.3960(3)	0.033(5)
C(12)	0.1994(11)	0.3832(7)	0.4325(3)	0.045(7)
C(13)	0.2946(13)	0.3349(9)	0.4517(4)	0.063(8)
C(14)	0.3591(12)	0.2676(9)	0.4347(4)	0.064(9)
C(15)	0.3243(13)	0.2435(8)	0.3988(4)	0.058(8)
C(16)	0.2267(10)	0.2914(7)	0.3785(3)	0.044(7)
C(21)	0.1441(10)	0.4952(7)	0.3377(3)	0.034(6)
C(22)	0.0957(11)	0.5740(7)	0.3252(4)	0.046(7)
C(23)	0.1690(13)	0.6233(8)	0.3000(4)	0.059(8)
C(24)	0.2934(13)	0.5958(10)	0.2871(4)	0.068(9)
C(25)	0.3395(13)	0.5157(9)	0.2975(4)	0.064(8)
C(26)	0.2670(12)	0.4657(8)	0.3232(3)	0.052(7)
C(1)	-0.2185(10)	0.3292(7)	0.3639(3)	0.040(6)
C(2)	-0.0762(9)	0.3714(6)	0.3437(3)	0.032(5)
B(3)	-0.0900(12)	0.2587(8)	0.3482(4)	0.041(7)
B(4)	-0.2673(15)	0.2388(10)	0.3416(5)	0.056(9)
B(5)	-0.3544(13)	0.3366(10)	0.3338(4)	0.053(9)
B(6)	-0.2340(13)	0.4214(10)	0.3363(4)	0.048(8)
B(7)	-0.0295(11)	0.3072(9)	0.3055(4)	0.041(7)
B(8)	-0.1495(14)	0.2216(9)	0.3037(4)	0.048(8)
B(9)	-0.3155(14)	0.2694(9)	0.2944(5)	0.056(9)
B(10)	-0.2933(13)	0.3836(10)	0.2927(4)	0.051(8)
B(11)	-0.1178(12)	0.4080(8)	0.2982(4)	0.037(7)
B(12)	-0.1696(15)	0.3146(9)	0.2728(4)	0.049(8)
C(101)	-0.2371(11)	0.3400(8)	0.4057(3)	0.044(7)
O	-0.1213(8)	0.3164(6)	0.42495(22)	0.054(5)
C(102)	-0.1291(15)	0.3283(10)	0.4641(4)	0.077(10)
Cl(1)	-0.4656(8)	0.4595(5)	0.6028(3)	0.1089(16)
Cl(2)	-0.3893(7)	0.4096(5)	0.52638(22)	0.1089(16)
C(99)	-0.489(3)	0.3859(19)	0.5626(8)	0.1089(16)

Table 4.1 Atomic Coordinates and Equivalent Isotropic Thermal Parameters ($Å^2$) for All Non-hydrogen Atoms in **12**.

Au	- P	2.238(3)	C(2)	-B(11)	1.755(16)
Au	- Cl	2.274(3)	B(3)	- B(4)	1.782(20)
P	-C(11)	1.797(10)	B(3)	- B(7)	1.791(18)
P	-C(21)	1.811(10)	B(3)	- B(8)	1.776(19)
P	- C(2)	1.865(10)	B(4)	- B(5)	1.758(22)
C(11)	-C(12)	1.374(15)	B(4)	- B(8)	1.793(21)
C(11)	-C(16)	1.409(15)	B(4)	- B(9)	1.801(22)
C(12)	-C(13)	1.375(18)	B(5)	- B(6)	1.765(21)
C(13)	-C(14)	1.356(19)	B(5)	- B(9)	1.780(22)
C(14)	-C(15)	1.372(19)	B(5)	-B(10)	1.734(21)
C(15)	-C(16)	1.406(17)	B(6)	-B(10)	1.750(20)
C(21)	-C(22)	1.378(15)	B(6)	-B(11)	1.777(19)
C(21)	-C(26)	1.388(16)	B(7)	- B(8)	1.771(19)
C(22)	-C(23)	1.376(17)	B(7)	-B(11)	1.800(18)
C(23)	-C(24)	1.371(20)	B(7)	-B(12)	1.802(19)
C(24)	-C(25)	1.367(20)	B(8)	- B(9)	1.819(21)
C(25)	-C(26)	1.392(18)	B(8)	-B(12)	1.816(20)
C(1)	- C(2)	1.699(14)	B(9)	-B(10)	1.776(22)
C(1)	- B(3)	1.756(17)	B(9)	-B(12)	1.768(21)
C(1)	- B(4)	1.672(19)	B(10)	-B(11)	1.774(19)
C(1)	- B(5)	1.712(18)	B(10)	-B(12)	1.762(21)
C(1)	- B(6)	1.734(18)	B(11)	-B(12)	1.775(19)
C(1)	-C(101)	1.501(15)	C(101)	- O	1.374(14)
C(2)	- B(3)	1.751(16)	O	-C(102)	1.402(17)
C(2)	- B(6)	1.751(17)	Cl(1)	-C(99)	1.84(3)
C(2)	- B(7)	1.739(16)	Cl(2)	-C(99)	1.66(3)

P	- Au	- Cl	177.17(11)	C(1)	- B(4)	- B(3)	61.0(8)
Au	- P	-C(11)	112.3(3)	C(1)	- B(4)	- B(5)	59.8(8)
Au	- P	-C(21)	109.7(3)	B(3)	- B(4)	- B(8)	59.6(8)
Au	- P	- C(2)	112.9(3)	B(5)	- B(4)	- B(9)	60.0(9)
C(11)	- P	-C(21)	107.4(5)	B(8)	- B(4)	- B(9)	60.8(8)
C(11)	- P	- C(2)	110.2(5)	C(1)	- B(5)	- B(4)	57.6(8)
C(21)	- P	- C(2)	103.8(5)	C(1)	- B(5)	- B(6)	59.8(8)
P	-C(11)	-C(12)	117.3(8)	B(4)	- B(5)	- B(9)	61.2(9)
P	-C(11)	-C(16)	123.9(8)	B(6)	- B(5)	-B(10)	60.0(8)
C(12)	-C(11)	-C(16)	118.7(10)	B(9)	- B(5)	-B(10)	60.7(9)
C(11)	-C(12)	-C(13)	121.0(11)	C(1)	- B(6)	- C(2)	58.4(6)
C(12)	-C(13)	-C(14)	120.9(12)	C(1)	- B(6)	- B(5)	58.6(7)

Table 4.2 Selected Interatomic Distances (Å) and Interbond Angles (°) in **12**.

C(13)	-C(14)	-C(15)	120.2(13)	C(2)	- B(6)	-B(11)	59.7(7)
C(14)	-C(15)	-C(16)	120.1(12)	B(5)	- B(6)	-B(10)	59.1(8)
C(11)	-C(16)	-C(15)	119.1(10)	B(10)	- B(6)	-B(11)	60.4(8)
P	-C(21)	-C(22)	119.5(8)	C(2)	- B(7)	- B(3)	59.5(7)
P	-C(21)	-C(26)	122.5(8)	C(2)	- B(7)	-B(11)	59.4(7)
C(22)	-C(21)	-C(26)	118.1(10)	B(3)	- B(7)	- B(8)	59.8(7)
C(21)	-C(22)	-C(23)	121.0(11)	B(8)	- B(7)	-B(12)	61.1(8)
C(22)	-C(23)	-C(24)	120.7(12)	B(11)	- B(7)	-B(12)	59.0(7)
C(23)	-C(24)	-C(25)	119.0(13)	B(3)	- B(8)	- B(4)	59.9(8)
C(24)	-C(25)	-C(26)	120.6(13)	B(3)	- B(8)	- B(7)	60.6(8)
C(21)	-C(26)	-C(25)	120.3(11)	B(4)	- B(8)	- B(9)	59.8(8)
C(2)	- C(1)	- B(3)	60.9(6)	B(7)	- B(8)	-B(12)	60.3(8)
C(2)	- C(1)	- B(6)	61.3(7)	B(9)	- B(8)	-B(12)	58.2(8)
C(2)	- C(1)	-C(101)	118.2(8)	B(4)	- B(9)	- B(5)	58.8(8)
B(3)	- C(1)	- B(4)	62.6(8)	B(4)	- B(9)	- B(8)	59.4(8)
B(3)	- C(1)	-C(101)	118.0(9)	B(5)	- B(9)	-B(10)	58.4(8)
B(4)	- C(1)	- B(5)	62.6(8)	B(8)	- B(9)	-B(12)	60.8(8)
B(4)	- C(1)	-C(101)	121.6(10)	B(10)	- B(9)	-B(12)	59.6(8)
B(5)	- C(1)	- B(6)	61.6(8)	B(5)	-B(10)	- B(6)	60.9(8)
B(5)	- C(1)	-C(101)	120.8(9)	B(5)	-B(10)	- B(9)	60.9(9)
B(6)	- C(1)	-C(101)	117.1(9)	B(6)	-B(10)	-B(11)	60.6(8)
P	- C(2)	- C(1)	120.4(6)	B(9)	-B(10)	-B(12)	60.0(8)
P	- C(2)	- B(3)	121.5(7)	B(11)	-B(10)	-B(12)	60.2(8)
P	- C(2)	- B(6)	115.3(7)	C(2)	-B(11)	- B(6)	59.4(7)
P	- C(2)	- B(7)	123.6(7)	C(2)	-B(11)	- B(7)	58.6(7)
P	- C(2)	-B(11)	118.9(7)	B(6)	-B(11)	-B(10)	59.0(8)
C(1)	- C(2)	- B(3)	61.2(6)	B(7)	-B(11)	-B(12)	60.5(7)
C(1)	- C(2)	- B(6)	60.3(7)	B(10)	-B(11)	-B(12)	59.5(8)
B(3)	- C(2)	- B(7)	61.7(7)	B(7)	-B(12)	- B(8)	58.6(7)
B(6)	- C(2)	-B(11)	60.9(7)	B(7)	-B(12)	-B(11)	60.4(7)
B(7)	- C(2)	-B(11)	62.0(7)	B(8)	-B(12)	- B(9)	61.0(8)
C(1)	- B(3)	- C(2)	58.0(6)	B(9)	-B(12)	-B(10)	60.4(8)
C(1)	- B(3)	- B(4)	56.4(7)	B(10)	-B(12)	-B(11)	60.2(8)
C(2)	- B(3)	- B(7)	58.8(7)	C(1)	-C(101)	- O	111.1(9)
B(4)	- B(3)	- B(8)	60.5(8)	C(101)	- O	-C(102)	114.3(10)
B(7)	- B(3)	- B(8)	59.5(7)	Cl(1)	-C(99)	-Cl(2)	112.9(16)

Table 4.2 Selected Interatomic Distances (Å) and Interbond Angles (°) in **12** **(continued).**

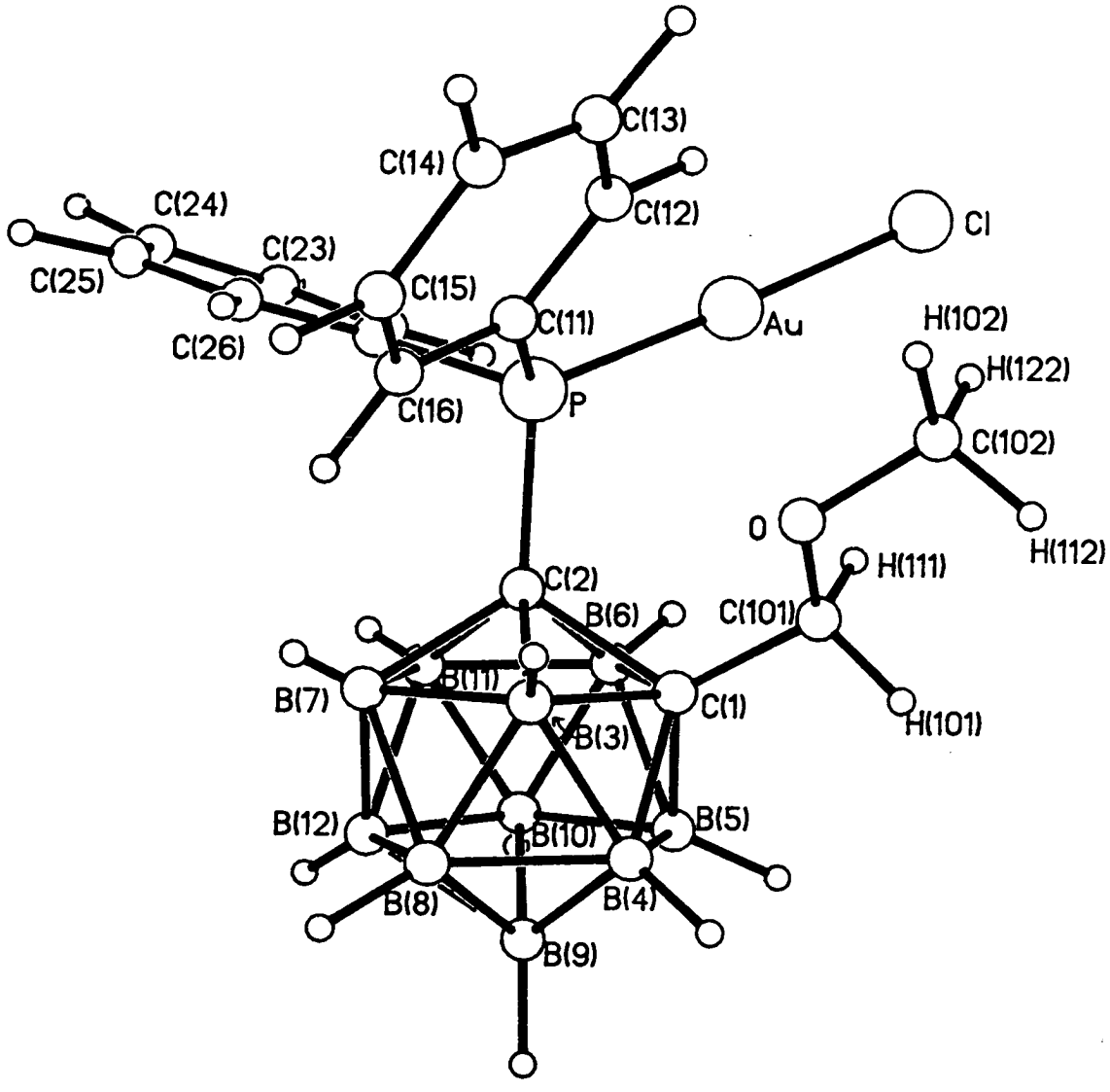

Figure 4.7 Perspective View of a Single Molecule of **12** (cage H atoms carry the same number as the B atoms to which they are bound).

The orientation of the phenyl rings is defined by the twist about the P-C(11) and P-C(21) bonds of 9 and 35° respectively, a 0° twist corresponding to a P-Au/C(11)-C(12) [or C(21)-C(22)] eclipsed arrangement. The former twist is smaller than, and the latter comparable with, those in **4e** and $AsPh_3AuMe$ (**5**) in which twists of 24, 43 and 60° and 32, 52 and 37° respectively have been measured about the As-C bonds. The orientation of the carbaborane cage relative to Au may be defined by the Au-P-C(2)-C(1) torsion angle of -43.3(8)°. It is of note that the ether group occupies the space '*cis*' to the less sterically demanding gold chloride fragment and therefore lies '*trans*' to the two phenyl rings. This is probably to minimise steric interaction between the ether and phenyl groups and not a consequence of metal-oxygen interaction.

In comparison with the connectivity distances from C(2) to adjacent atoms in **1**, the corresponding distances in **12** are all longer. This is therefore consistent with electron withdrawl from the cage system as observed in structural studies of diborane and dicarbaborane species[92, 93]: In these compounds, the connectivities to the atom at which substitution takes place are lengthened as a result of net electron density loss from the cage system (see **Section 2.3.3**). Presumably in **12**, the phosphine gold fragment is acting as a better electron withdrawer with respect to the cage than H. The corollary to this, that carbaborane is donating to phosphorus, is not inconsistent with the deductions made in **Chapter 2**, although it must be kept in mind that, strictly speaking, the current deductions and those of **Chapter 2** relate to subtly different phenomena (*i.e.* the former intimates the $\{PPh_2(AuCl)\}$ is a better electron acceptor than {H} whereas the latter concluded that $\{1\text{-}CH_3OCH_2\text{-}C_2B_{10}H_{10}\}$ is a better donor than $\{CH_3\}$). The net loss of electron density from the cage is confirmed from the $^{11}B\{^1H\}$ NMR spectrum of **12** in which the boron resonances have moved to higher frequency with respect to the corresponding resonances in **1** (*vide infra*). The observed lenghtening in **12** is in contrast to the comparison of **1** with **4e**, in which

there is no apparent trend.

The bond angles at phosphorus define the expected tetrahedral geometry, as expected. The P-Au-Cl sequence is essentially linear [177.18(11)°] as expected for a two coordinate gold(I) species, and is comparable to the P-Au-Cl angle observed in PPh_3AuCl, 179.63(8)°. The Au-P bond distance is 2.237(3) Å which is also comparable with that in PPh_3AuCl [2.235(3) Å] but shorter than those in the only other structurally characterised carbaborane gold compound so far reported, [1,2-$(PPh_2)_2${μ-$AuPPh_3$}-1,2-*closo*-$C_2B_{10}H_{10}$][ClO_4][61] (**Figure 4.4**), 2.405(1) and 2.417(1) Å, although these latter two represent bonds between P and three coordinate gold(I), and hence there is more 6*p* character in the bond. Furthermore, the Au-Cl distance in **12** is 2.274(3) Å which is also very similar to that of 2.279(3) Å in PPh_3AuCl.

It is interesting to note that, in PPh_3AuCl[103], as the twists of the phenyl rings about the P-C bonds increase beyond 30° [30, 39 and 58°], the P-C bonds increase in length [1.792(3), 1.803(13) and 1.866(12) Å respectively]. Moreover, as the twists increase the mean C-C bond lengths in the rings decrease [1.400(16), 1.396(15), 1.376(15) Å respectively]. This phenomenon is also observed in $AsPh_3AuCH_3$ (**5**): As the twists of the phenyl rings about the As-C bonds increase beyond 30° [32, 37, 57°], the As-C bond lengths also increase [1.913(10), 1.929(10) and 1.949(10) Å respectively] and the average C-C bonds shorten [1.385(18), 1.379(15) and 1.373(15) Å respectively]. Analysis of these data in **12** reveals that as the twists of the two phenyl rings increase towards 30° [9 and 35°], the P-C bonds lengthen [1.798(10) and 1.808(10) Å respectively] and the mean C-C bond shorten slightly [1.382(20) and 1.379(18) Å respectively]. It should however be noted that, in **4e**, as the twists of the phenyl rings about the As-C bonds increase [24, 43 and 60°], there is no observed progression in the As-C bonds [1.943(8), 1.9222(8) and 1.933(8) Å respectively]. The lengthening of the P/As-C bond (and shortening of the mean C-C bond) as the twists increase

might possibly be attributed to reduction in P/As *d* orbital-phenyl π system overlap: As the rings twist, the plane of the π system changes, therefore possibly altering (presumably reducing) any symmetry-allowed overlap with the *d* orbitals of P/As. However, without further detailed analysis, the reasoning for this phenomenon is unclear.

4.2.5 NMR Studies

Table 4.3 details the phosphorus chemical shifts of compounds **11**, **12**, and **13** and those of the corresponding PPh_3 compounds. The chemical shift of **11** is *ca.* 17 ppm to higher frequency than that of PPh_3 intimating that the former is less basic (donating). Consequently, electron donation to phosphorus by carbaborane must be less (smaller inductive effect) than by phenyl, resulting in less electron density around the phosphorus atom in **11** than in PPh_3. (Ether) carbaborane is therefore a poorer electron donor than phenyl, although, as previously discussed, better than methyl.

Consideration of the $^{31}P\{^1H\}$ NMR chemical shifts of PMe_3, PPh_2Me, $PPhMe_2$ and PPh_3 indicates a progressive shift in resonance from high to low frequency (at *ca.* δ 69, 47, 28, -5 ppm) respectively, intimating increased donation to phosphorus by phenyl over methyl.

	$^{31}P\{^1H\}$ (δ/ppm)	
P′ =	PPh_2Carb^*	PPh_3
P′	12.5	- 5.0
P′AuCl	54.6	33.5
P′$AuCH_3$	62.9	47.3

* PPh_2Carb = 1-CH_3OCH_2-2-PPh_2-1,2-*closo*-$C_2B_{10}H_{10}$

Table 4.3 $^{31}P\{^1H\}$ NMR Data for Analogous Phosphine Carbaborane and PPh_3 Compounds (36.46 MHz).

When PPh_3 is bound to a gold fragment, the phosphorus donates electron density to gold through the σ-bond and so a marked decrease in electron density around the phosphorus atom is experienced. This is represented in the $^{31}P\{^1H\}$ NMR spectra in which the phosphorus resonances shift to much higher frequency as compared to free phosphine. The phosphorus resonance in the NMR spectrum of PPh_3AuCl is at lower frequency than in the spectrum of PPh_3AuMe[86] because chloride is an overall better donor ligand (to gold) than methyl, this necessitating somewhat less phosphine to gold donation.

Similarily, in the $^{31}P\{^1H\}$ NMR spectra of **12** and **13** a shift of the phosphorus resonances to much higher frequency compared to that in the spectrum of **11** is observed, with the resonance due to **13** (methyl) at highest frequency. The chemical shifts are, as expected, at higher frequency than those of the corresponding PPh_3 compounds as a consequence of the decreased basicity of **11** over PPh_3. This is therefore consistent with the observation made that phenyl is a better donor to P than carbaborane. The chemical shift of **12** is also comparable to that of the related compound 1,2-$\{PPh_2AuCl\}_2$-1,2-*closo*-$C_2B_{10}H_{10}$ (δ 50.1 ppm) in which both carbaborane carbon atoms have been substituted with a $\{PPh_2AuCl\}$ fragment[61].

In the ^{31}P NMR spectrum of PPh_3AuMe, coupling of the phosphorus resonance with phenyl and methyl protons is observed, and the phosphorus-methyl proton coupling constant is large enough to allow a quartet of broad peaks (the broadening due to phosphorus-phenyl proton coupling) to be observed. However, in the $^{31}P\{^1H\}$ NMR spectrum of **13**, only one very broad peak was obtained, the (extra) broadening probably due to coupling to the boron atoms of the carbaborane.

The $^{11}B\{^1H\}$ NMR data for **11**, **12** and **13** and the parent carbaborane, 1-CH_3OCH_2-1,2-*closo*-$C_2B_{10}H_{11}$ (**1**) are outlined in **Table 4.4**. On introduction of a $\{PPh_2\}$, $\{PPh_2AuCl\}$ or $\{PPh_2AuCH_3\}$ fragment at C(2) of the ether carbaborane

there is an overall shift to higher frequency (spectrum width narrowing is only observed for **11**), intimating net electron density withdrawl from the cage. In the $^{11}B\{^1H\}$ NMR spectra of **11**, **12** and **13**, at the field strength used (64.21 MHz), the resonances due to the four pairs of boron atoms [B(3)/B(6), B(4)/B(5), B(7)/B(11), B(8)/B(10)] are indistinguishable and consequently produce a broad quadruple coincidence resonance. The two high frequency resonances of integral 1 must be due to the symmetry unique boron atoms, B(9) and B(12). Comparison with the (assigned) $^{11}B\{^1H\}$ NMR spectrum of **1** might have allowed assignment of these resonances. However, shifts in frequency of these resonances in **11**, **12** and **13** compared to those in **1** would not be unreasonable if the peaks were assigned as either B(9) and B(12) *or* as B(12) and B(9) respectively. As a result, an unequivocal assignment of these resonances cannot be made.

	$^{11}B\{^1H\}$ (δ/ppm)			
	1	**11**	**12**	**13**
1B	- 2.47	0.15	1.70	1.41
1B	- 4.23	-2.52	-1.51	-1.87
2B	- 8.47	-8.78	-9.06	-9.02
2B	-10.97	-8.78	-9.06	-9.02
4B	-12.45	-8.78	-9.06	-9.02

Table 4.4 $^{11}B\{^1H\}$ NMR Data for **1**, **11**, **12** and **13** (64.21 MHz).

However, whatever the assignment, in the $^{11}B\{^1H\}$ NMR spectra of **11**, **12** and **13** there is an overall shift to higher frequency with respect to the $^{11}B\{^1H\}$ NMR

spectrum of **1**, as previously noted. The lowest frequency resonances (of integral 8) are broad, with widths at half-height of 138 Hz (2.15 ppm), 99 Hz (1.54 ppm) and 94 Hz (1.47 ppm) respectively (compared to widths at half-height of the peaks of integral 1 of 44 and 79, 59 and 69, and 47 and 57 Hz respectively) and consequently the error for the position at which the maximum occurs will be large. Indeed, in comparison of the $^{11}B\{^1H\}$ NMR data of **11** with those of **12** and **13**, the lowest frequency resonance might have been expected to have shifted to higher frequency since, on phosphorus donation to gold, a decrease in electron density is observed at the phosphorus atom which might be compensated to some extent by electron density removal from the cage. However, in the NMR spectra of **12** and **13** the maximum of the peak of integral 8 is at slightly lower frequency than in the spectrum of **11** but, taking account of the large widths at half height, it may be assumed that these resonances are comparable.

It is the relative shifts of the resonances of integral 1 that indicate the difference the three phosphine fragments bound to C(2) have on the electron density distribution within the cage: These resonances are shifted to higher frequency in **12** and **13** (by 1.55 and 1.01 ppm in **12** and 1.26 and 0.65 ppm in **13**) compared to **11**, the small difference between the chemical shifts in **12** and **13** (0.29 and 0.36 ppm) indicating that substitution at the gold atom *trans* to phosphine does not significantly affect the carbaborane three bonds away, as expected.

The ^1H NMR spectra of **11**, **12** and **13** exhibited the expected resonances due to the phenyl and ether protons in the correct ratios. The absence of the broad peak at δ 4.00 ppm found in the ^1H NMR spectrum of **1** intimated replacement of the hydrogen atom bound to C(2) [replaced by the phosphine fragment].

On introduction of the phosphine fragment, the OCH_3 proton resonance shifts only slightly to lower frequency with respect to the corresponding resonance in the

spectrum of **1**. This is similar to the situation for compounds **4**, in which a small shift to lower frequency of the OCH_3 resonance compared to that of **1** is also observed. The OCH_2 proton resonances of **11**, **12** and **13** are shifted significantly to higher frequency of **1**, in contrast to the small (<0.2 ppm) shift observed for compounds **4**. The shifts are indicative of deshielding (electron density loss) at these protons and therefore must be a reflection of the electron density removal experienced by the cage due to phosphine substitution at C(2): The chemical shift of the hydrogen atoms bound to the carbon atom bonded directly to the cage might be expected to be affected by changes in electron density distribution within the cage.

In each spectrum the phenyl groups give two multiplet regions of relative integral 4:6 (presumably 2 and 3 respectively from each phenyl ring). The higher frequency multiplet (integral 4) is probably attributable to the hydrogen atoms bound to the carbon atoms nearest to phosphorus [C(12)/C(16) and C(22)/C(26)] because any change of shielding at phosphorus is most likely to be transmitted to these atoms. Thus, the lower frequency resonance is due to the distant hydrogen atoms bound to C(13)/C(14)/C(15) and C(23)/C(24)/C(25). This is confirmed by the fact that on bonding to gold (i.e. from **11** to **12** and **13**) the highest frequency multiplet shifts *ca.* 0.35 ppm to higher frequency whereas the integral 6 multiplet shifts only *ca.* 0.15 ppm to higher frequency indicative of the longer range effect on these latter protons.

The splitting into two sets of multiplets presumably reflects the presence of another group bound to P that is not alkyl or aryl since this is not observed in the ^1H NMR spectra of triaryl- and mixed aryl/alkyl phosphines. The observation of two distinct phenyl multiplet regions in related diphenyl phosphine carbaborane compounds has been noted but not discussed[61].

4.3 Synthesis of a Biscarbaborane Compound

4.3.1 Synthesis and Characterisation of 1-CH_3OCH_2-2-(1'-CH_3OCH_2-2'-{PPh_2Au}-1',2'-*closo*-$C_2B_{10}H_{10}$)-1,2-*closo*-$C_2B_{10}H_{10}$ (**14**)

In order to demonstrate the similarity (or, indeed, highlight any differences) between the chemistries of {PPh_3Au^I} and {1-CH_3OCH_2-2-[PPh_2Au^I]-1,2-*closo*-$C_2B_{10}H_{10}$} fragments, it was decided to attempt reactions using **12** (and **13**) that had been successful using PPh_3AuCl (PPh_3AuMe). Therefore, initially, as 1-CH_3OCH_3-2-{PPh_3Au}-1,2-*closo*-$C_2B_{10}H_{10}$ (**4a**) had been successfully synthesised in reasonable yield from PPh_3AuCl and Li[1-CH_3OCH_2-1,2-*closo*-$C_2B_{10}H_{10}$], an analogous novel biscarbaborane might be synthesised by reaction of **12** with lithium carbaborane.

The synthesis of the biscarbaborane species, compound **14**, was indeed achieved in a similar manner to that used for the synthesis of compounds **4** (**Chapter 2**): On addition of Li[1-CH_3OCH_2-1,2-*closo*-$C_2B_{10}H_{10}$] to an ethereal suspension of 1-CH_3OCH_2-2-{PPh_2AuCl}-1,2-*closo*-$C_2B_{10}H_{10}$ (**12**) most of the solid dissolved and an orange colouration, probably due to a minor Au^{III} co-product, was observed. After filtration and crystallisation of the solid recovered from the filtrate by slow diffusion of *n*-hexane into a dichloromethane solution, compound **14** was recovered as small colourless crystals in 31% yield.

14 was found to extremely stable in air and solution, though prolonged standing in solution did result in some decomposition. Characterisation was effected using the standard microanalytical and spectroscopic techniques. The crystals obtained were of reasonable quality and an X-ray structure determination was undertaken. Microanalysis of the crystals was consistent with the proposed formulation of $C_{20}H_{40}AuB_{20}O_2P$. The IR spectrum displayed a broad peak at 2580 cm^{-1} due to B-H

stretches and a number of peaks between 1438 and 1106 cm^{-1} due to (two sets of) CH_3OCH_2 vibrations.

The $^{31}P\{^1H\}$ NMR spectrum showed a sharp singlet at δ 58.8 ppm. The ^1H NMR spectrum (**Figure 4.8**) showed the two distinct multiplet regions due to phenyl protons and resonances due to OCH_2 and OCH_3 from the two (different) ether groups in the correct integral ratio of 4:6:2:2:3:3 (high to low frequency). The $^{11}B\{^1H\}$ NMR spectrum (**Figure 4.9**) showed a variety of peaks at δ 1.85, -1.08 and -8.53 ppm due to carbaborane bound to phosphorus and peaks at δ -1.68, -3.93, -7.44 and -9.48 ppm due to carbaborane bound to gold. The NMR data are discussed in more detail in **Section 4.3.3.**

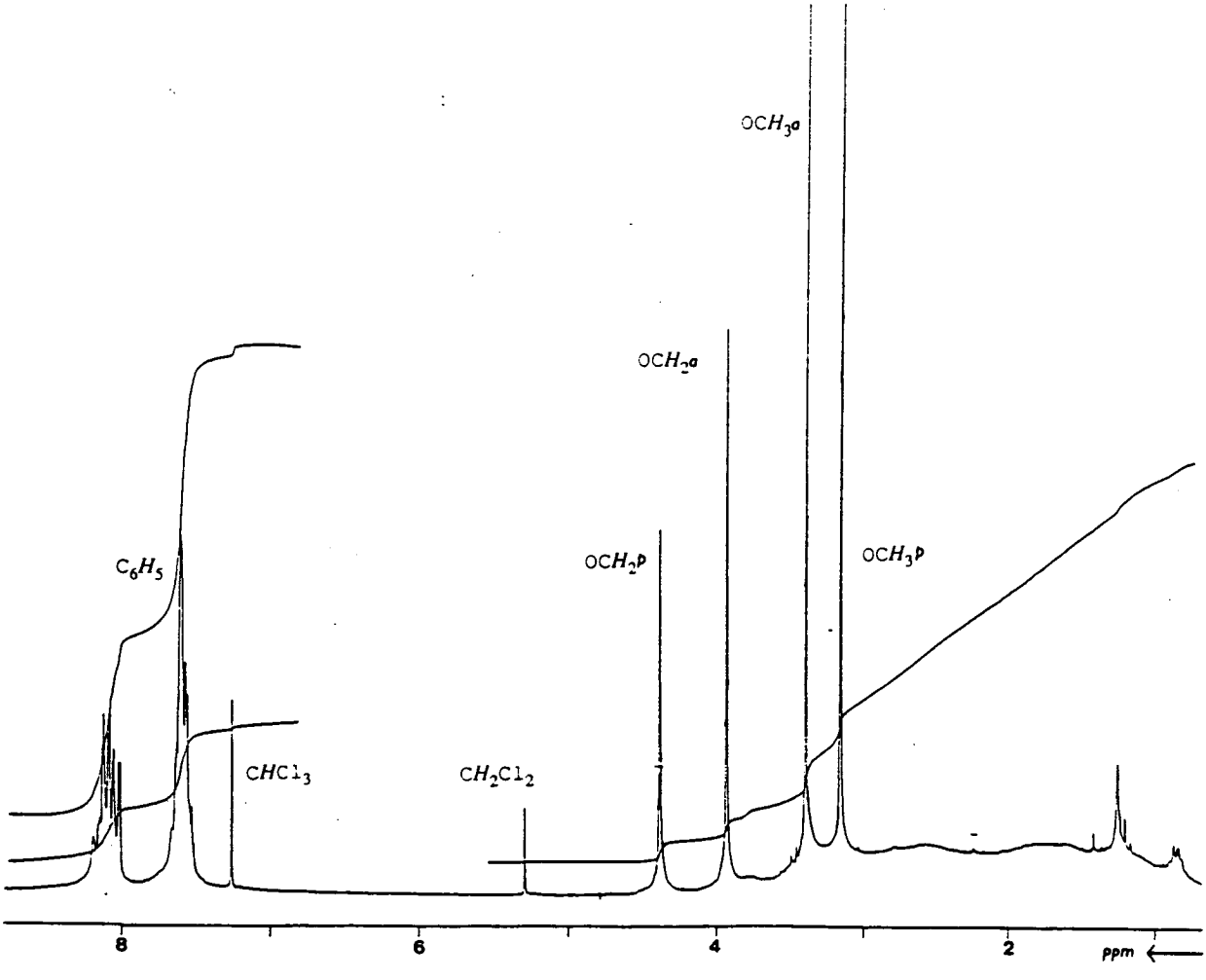

Figure 4.8 ^1H NMR Spectrum of **14** (200.13 MHz).

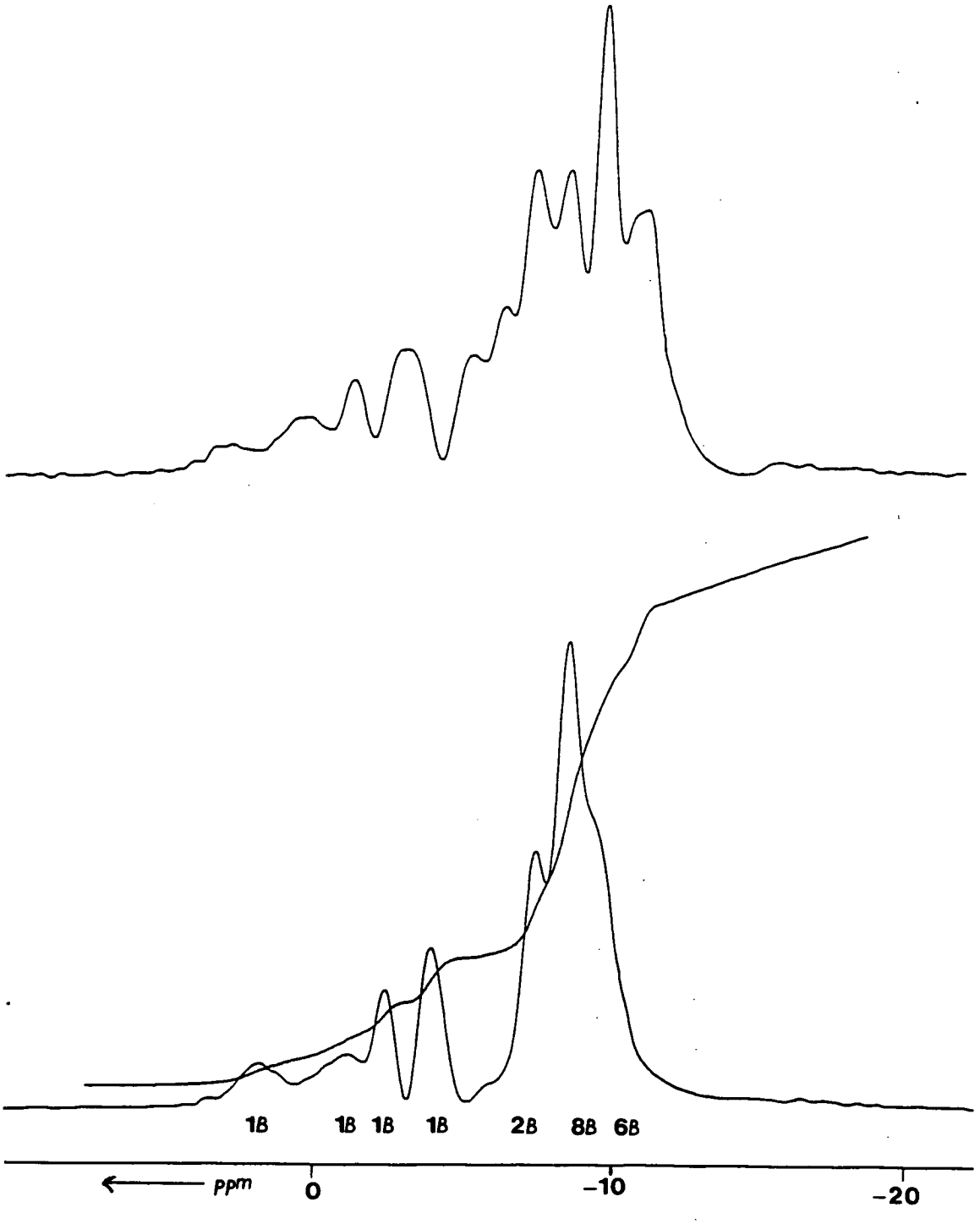

Figure 4.9 $^{11}B\{^{1}H\}/^{11}B$ NMR Spectra of **14** (64.21 MHz).

4.3.2 Crystallographic Study on **14**

Crystallisation of **14** from CH_2Cl_2/*n*-hexane yielded small but well formed colourless crystals suitable for an X-ray diffraction study. Intensity data were therefore collected from a single crystal of **14** at ambient temperature. **Table 4.5** lists atomic positions and equivalent isotropic thermal parameters for all non-hydrogen atoms and **Table 4.6** details selected interatomic distances and angles. Anisotropic thermal parameters atoms and hydrogen atom coordinates are listed in **Appendix B**. **Figures 4.10** and **4.11** illustrate alternative perspective views of a single molecule of **14**.

Both the {1,2-*closo*-C_2B_{10}} cages in **14** have the expected icosahedral geometry, with distances between corresponding antipodal atoms similar [for example C(1p)-B(12p) and C(1a)-B(12a) are 3.278(10) and 3.279(10) Å respectively, and B(3p)-B(8p) and B(3a)-B(8a) are 3.367(10) and 3.346(12) Å respectively (a represents atoms in gold-bound carbaborane; p, atoms in phosphorus bound carbaborane)]. The ether carbaborane bound to phosphorus is orientated such that it is *trans* to the ether group on carbaborane bound to gold and this is probably to minimise steric interaction between the ether carbaboranes. C(1a)-C(2a) is 1.666(8) Å and C(1p)-C(2p) is 1.681(7) Å. The former distance is comparable to the C(1)-C(2) distance of 1.667(11) Å in **4e** and longer than that in the parent *closo*-carbaborane, **1** [1.636(9) Å[20]], but not significantly so. Similarily, the C(1p)-C(2p) distance is comparable to the corresponding distance in **12** [1.699(14) Å]. Indeed, comparison of the molecular dimensions of the phosphine carbaborane fragment in **14** with those of **12** reveals that they are very similar, and this is readily illustrated by comparison of **Figure 4.7, p138 (12)** with **Figure 4.10 (14)**. This is not unexpected as the chlorine atom in **12** has been replaced by the isolobal ether carbaborane. Similarly, the molecular dimensions of the gold carbaborane fragment (see **Figure 4.11**) are

comparable to those of **4e** (see **Figure 2.12**, p72), as expected.

	x	y	z	Ueq
Au	0.31152(2)	0.17587(2)	0.10690(1)	0.0456(1)
P	0.38967(11)	0.11797(10)	0.25470(9)	0.0407(7)
C(11)	0.3184(4)	0.1453(4)	0.3493(3)	0.043(3)
C(12)	0.3564(5)	0.1287(4)	0.4506(4)	0.059(4)
C(13)	0.2925(6)	0.1481(5)	0.5151(4)	0.075(5)
C(14)	0.1899(6)	0.1832(6)	0.4793(5)	0.085(5)
C(15)	0.1514(6)	0.1993(7)	0.3806(5)	0.087(5)
C(16)	0.2159(5)	0.1814(5)	0.3140(4)	0.063(4)
C(21)	0.3611(4)	-0.0446(4)	0.2109(4)	0.045(3)
C(22)	0.3413(5)	-0.1198(5)	0.2718(5)	0.065(4)
C(23)	0.3263(7)	-0.2411(5)	0.2344(6)	0.092(6)
C(24)	0.3309(7)	-0.2870(6)	0.1363(6)	0.098(6)
C(25)	0.3485(7)	-0.2129(5)	0.0742(6)	0.086(5)
C(26)	0.3610(5)	-0.0926(5)	0.1103(4)	0.066(4)
C(1p)	0.6468(5)	0.3361(4)	0.3471(4)	0.053(3)
C(2p)	0.5688(4)	0.1879(4)	0.3283(3)	0.042(3)
B(3p)	0.6513(6)	0.2238(6)	0.2504(5)	0.058(4)
B(4p)	0.7884(6)	0.3577(6)	0.3372(6)	0.071(5)
B(5p)	0.7827(6)	0.3998(6)	0.4641(6)	0.066(5)
B(6p)	0.6416(5)	0.2935(5)	0.4579(4)	0.052(4)
B(7p)	0.6606(5)	0.1050(5)	0.3065(5)	0.058(4)
B(8p)	0.7907(6)	0.2814(6)	0.5209(5)	0.063(4)
B(9p)	0.8820(6)	0.3210(7)	0.4455(7)	0.076(5)
B(10p)	0.7999(6)	0.2115(7)	0.3130(6)	0.073(5)
B(11p)	0.6540(5)	0.1485(5)	0.4344(5)	0.058(4)
B(12p)	0.8021(6)	0.1648(6)	0.4265(6)	0.070(5)
C(11p)	0.5725(5)	0.4139(5)	0.3070(5)	0.070(4)
O(1p)	0.4816(4)	0.4075(4)	0.3495(4)	0.092(4)
C(12p)	0.4169(8)	0.4852(7)	0.3282(7)	0.115(7)
C(1a)	0.0991(5)	0.2296(5)	-0.0787(4)	0.066(4)
C(2a)	0.2439(4)	0.2226(4)	-0.0303(3)	0.049(3)
B(3a)	0.1252(7)	0.1118(6)	-0.1469(5)	0.063(4)
B(4a)	0.0340(7)	0.1862(7)	-0.2161(6)	0.074(5)
B(5a)	0.0994(9)	0.3415(7)	-0.1371(6)	0.090(6)
B(6a)	0.2299(8)	0.3613(6)	-0.0182(5)	0.074(5)
B(7a)	0.2805(7)	0.1754(7)	-0.1368(5)	0.075(5)
B(8a)	0.1486(8)	0.1524(7)	-0.2551(5)	0.077(5)
B(9a)	0.1329(7)	0.2974(7)	-0.2489(5)	0.075(5)
B(10a)	0.2543(8)	0.4054(7)	-0.1268(6)	0.084(6)
B(11a)	0.3460(7)	0.3298(7)	-0.0575(5)	0.069(5)
B(12a)	0.2861(7)	0.2891(8)	-0.2002(5)	0.082(6)
C(11a)	0.0143(7)	0.1955(9)	-0.0192(6)	0.112(7)
O(1a)	0.0674(6)	0.2670(9)	0.0881(5)	0.174(8)
C(12a)	0.0109(12)	0.3341(14)	0.1240(10)	0.241(18)

Table 4.5 Atomic Coordinates and Equivalent Isotropic Thermal Parameters ($Å^2$) for All Non-hydrogen Atoms in **14**.

Au	- P	2.2749(13)	B(8p)	-B(11p)	1.766(10)
Au	-C(2a)	2.052(5)	B(8p)	-B(12p)	1.783(10)
P	-C(11)	1.809(5)	B(9p)	-B(10p)	1.778(12)
P	-C(21)	1.820(5)	B(9p)	-B(12p)	1.769(11)
P	-C(2p)	1.875(5)	B(10p)	-B(12p)	1.761(11)
C(11)	-C(12)	1.392(7)	B(11p)	-B(12p)	1.766(10)
C(11)	-C(16)	1.380(8)	C(11p)	-O(1p)	1.388(8)
C(12)	-C(13)	1.379(9)	O(1p)	-C(12p)	1.383(10)
C(13)	-C(14)	1.374(10)	C(1a)	-C(2a)	1.666(8)
C(14)	-C(15)	1.358(10)	C(1a)	-B(3a)	1.702(9)
C(15)	-C(16)	1.405(9)	C(1a)	-B(4a)	1.696(10)
C(21)	-C(22)	1.375(8)	C(1a)	-B(5a)	1.699(11)
C(21)	-C(26)	1.396(8)	C(1a)	-B(6a)	1.692(10)
C(22)	-C(23)	1.382(10)	C(1a)	-C(11a)	1.525(11)
C(23)	-C(24)	1.383(11)	C(2a)	-B(3a)	1.715(9)
C(24)	-C(25)	1.374(11)	C(2a)	-B(6a)	1.701(9)
C(25)	-C(26)	1.378(10)	C(2a)	-B(7a)	1.708(9)
C(1p)	-C(2p)	1.681(7)	C(2a)	-B(11a)	1.705(9)
C(1p)	-B(3p)	1.725(9)	B(3a)	-B(4a)	1.756(11)
C(1p)	-B(4p)	1.694(9)	B(3a)	-B(7a)	1.743(11)
C(1p)	-B(5p)	1.701(9)	B(3a)	-B(8a)	1.745(11)
C(1p)	-B(6p)	1.722(8)	B(4a)	-B(5a)	1.756(12)
C(1p)	-C(11p)	1.518(8)	B(4a)	-B(8a)	1.744(12)
C(2p)	-B(3p)	1.723(8)	B(4a)	-B(9a)	1.761(12)
C(2p)	-B(6p)	1.735(8)	B(5a)	-B(6a)	1.763(12)
C(2p)	-B(7p)	1.730(8)	B(5a)	-B(9a)	1.742(12)
C(2p)	-B(11p)	1.720(8)	B(5a)	-B(10a)	1.737(13)
B(3p)	-B(4p)	1.776(10)	B(6a)	-B(10a)	1.770(12)
B(3p)	-B(7p)	1.765(10)	B(6a)	-B(11a)	1.753(11)
B(3p)	-B(10p)	1.757(10)	B(7a)	-B(8a)	1.757(12)
B(4p)	-B(5p)	1.756(11)	B(7a)	-B(11a)	1.749(11)
B(4p)	-B(9p)	1.760(11)	B(7a)	-B(12a)	1.760(12)
B(4p)	-B(10p)	1.772(11)	B(8a)	-B(9a)	1.789(12)
B(5p)	-B(6p)	1.770(10)	B(8a)	-B(12a)	1.769(12)
B(5p)	-B(8p)	1.764(10)	B(9a)	-B(10a)	1.754(12)
B(5p)	-B(9p)	1.761(11)	B(9a)	-B(12a)	1.764(12)
B(6p)	-B(8p)	1.763(10)	B(10a)	-B(11a)	1.771(12)
B(6p)	-B(11p)	1.764(9)	B(10a)	-B(12a)	1.764(12)
B(7p)	-B(10p)	1.753(10)	B(11a)	-B(12a)	1.766(12)
B(7p)	-B(11p)	1.775(9)	C(11a)	-O(1a)	1.379(12)
B(7p)	-B(12p)	1.759(10)	O(1a)	-C(12a)	1.311(17)
B(8p)	-B(9p)	1.780(11)			

Table 4.6 Selected Interatomic Distances (Å) and Interbond Angles (°) in **14**.

P	- Au	-C(2a)	177.28(14)	C(1p)	-B(4p)	-B(3p)	59.6(4)
Au	- P	-C(11)	113.15(16)	C(1p)	-B(4p)	-B(5p)	59.1(4)
Au	- P	-C(21)	109.39(17)	B(3p)	-B(4p)	-B(10p)	59.4(4)
Au	- P	-C(2p)	113.59(16)	B(5p)	-B(4p)	-B(9p)	60.1(4)
C(11)	- P	-C(21)	108.60(22)	B(9p)	-B(4p)	-B(10p)	60.5(4)
C(11)	- P	-C(2p)	109.68(22)	C(1p)	-B(5p)	-B(4p)	58.6(4)
C(21)	- P	-C(2p)	101.73(22)	C(1p)	-B(5p)	-B(6p)	59.4(4)
P	-C(11)	-C(12)	125.1(4)	B(4p)	-B(5p)	-B(9p)	60.1(4)
P	-C(11)	-C(16)	115.5(4)	B(6p)	-B(5p)	-B(8p)	59.9(4)
C(12)	-C(11)	-C(16)	119.3(5)	B(8p)	-B(5p)	-B(9p)	60.6(4)
C(11)	-C(12)	-C(13)	120.5(5)	C(1p)	-B(6p)	-C(2p)	58.2(3)
C(12)	-C(13)	-C(14)	120.0(6)	C(1p)	-B(6p)	-B(5p)	58.3(4)
C(13)	-C(14)	-C(15)	120.2(7)	C(2p)	-B(6p)	-B(11p)	58.9(3)
C(14)	-C(15)	-C(16)	120.8(7)	B(5p)	-B(6p)	-B(8p)	59.9(4)
C(11)	-C(16)	-C(15)	119.2(6)	B(8p)	-B(6p)	-B(11p)	60.1(4)
P	-C(21)	-C(22)	123.6(4)	C(2p)	-B(7p)	-B(3p)	59.1(3)
P	-C(21)	-C(26)	116.8(4)	C(2p)	-B(7p)	-B(11p)	58.7(3)
C(22)	-C(21)	-C(26)	119.7(5)	B(3p)	-B(7p)	-B(10p)	59.9(4)
C(21)	-C(22)	-C(23)	119.6(6)	B(10p)	-B(7p)	-B(12p)	60.2(4)
C(22)	-C(23)	-C(24)	120.4(7)	B(11p)	-B(7p)	-B(12p)	60.0(4)
C(23)	-C(24)	-C(25)	120.3(7)	B(5p)	-B(8p)	-B(6p)	60.2(4)
C(24)	-C(25)	-C(26)	119.5(7)	B(5p)	-B(8p)	-B(9p)	59.6(4)
C(21)	-C(26)	-C(25)	120.4(6)	B(6p)	-B(8p)	-B(11p)	60.0(4)
C(2p)	-C(1p)	-B(3p)	60.8(3)	B(9p)	-B(8p)	-B(12p)	59.6(4)
C(2p)	-C(1p)	-B(6p)	61.3(3)	B(11p)	-B(8p)	-B(12p)	59.7(4)
C(2p)	-C(1p)	-C(11p)	120.2(4)	B(4p)	-B(9p)	-B(5p)	59.8(4)
B(3p)	-C(1p)	-B(4p)	62.6(4)	B(4p)	-B(9p)	-B(10p)	60.1(4)
B(3p)	-C(1p)	-C(11p)	117.3(5)	B(5p)	-B(9p)	-B(8p)	59.8(4)
B(4p)	-C(1p)	-B(5p)	62.3(4)	B(8p)	-B(9p)	-B(12p)	60.3(4)
B(4p)	-C(1p)	-C(11p)	118.7(5)	B(10p)	-B(9p)	-B(12p)	59.5(4)
B(5p)	-C(1p)	-B(6p)	62.3(4)	B(3p)	-B(10p)	-B(4p)	60.4(4)
B(5p)	-C(1p)	-C(11p)	120.0(5)	B(3p)	-B(10p)	-B(7p)	60.4(4)
B(6p)	-C(1p)	-C(11p)	119.2(5)	B(4p)	-B(10p)	-B(9p)	59.4(4)
P	-C(2p)	-C(1p)	119.7(3)	B(7p)	-B(10p)	-B(12p)	60.1(4)
P	-C(2p)	-B(3p)	115.9(3)	B(9p)	-B(10p)	-B(12p)	60.0(4)
P	-C(2p)	-B(6p)	120.5(3)	C(2p)	-B(11p)	-B(6p)	59.7(3)
P	-C(2p)	-B(7p)	120.2(3)	C(2p)	-B(11p)	-B(7p)	59.3(3)
P	-C(2p)	-B(11p)	123.3(3)	B(6p)	-B(11p)	-B(8p)	59.9(4)
C(1p)	-C(2p)	-B(3p)	60.9(3)	B(7p)	-B(11p)	-B(12p)	59.6(4)
C(1p)	-C(2p)	-B(6p)	60.5(3)	B(8p)	-B(11p)	-B(12p)	60.6(4)
B(3p)	-C(2p)	-B(7p)	61.5(4)	B(7p)	-B(12p)	-B(10p)	59.7(4)
B(6p)	-C(2p)	-B(11p)	61.4(3)	B(7p)	-B(12p)	-B(11p)	60.5(4)
B(7p)	-C(2p)	-B(11p)	61.9(4)	B(8p)	-B(12p)	-B(9p)	60.1(4)

Table 4.6 Selected Interatomic Distances (Å) and Interbond Angles (°) in **14** (continued).

C(1p)	-B(3p)	-C(2p)	58.3(3)	B(8p)	-B(12p)	-B(11p)	59.7(4)
C(1p)	-B(3p)	-B(4p)	57.8(4)	B(9p)	-B(12p)	-B(10p)	60.5(4)
C(2p)	-B(3p)	-B(7p)	59.5(3)	C(1p)	-C(11p)	-O(1p)	109.0(5)
B(4p)	-B(3p)	-B(10p)	60.2(4)	C(11p)	-O(1p)	-C(12p)	114.3(6)
B(7p)	-B(3p)	-B(10p)	59.7(4)	C(2a)	-C(1a)	-B(3a)	61.2(4)
C(2a)	-C(1a)	-B(6a)	60.9(4)	C(2a)	-B(6a)	-B(11a)	59.1(4)
C(2a)	-C(1a)	-C(11a)	117.5(5)	B(5a)	-B(6a)	-B(10a)	58.9(5)
B(3a)	-C(1a)	-B(4a)	62.3(4)	B(10a)	-B(6a)	-B(11a)	60.4(5)
B(3a)	-C(1a)	-C(11a)	115.7(6)	C(2a)	-B(7a)	-B(3a)	59.6(4)
B(4a)	-C(1a)	-B(5a)	62.3(5)	C(2a)	-B(7a)	-B(11a)	59.1(4)
B(4a)	-C(1a)	-C(11a)	120.0(6)	B(3a)	-B(7a)	-B(8a)	59.8(4)
B(5a)	-C(1a)	-B(6a)	62.7(5)	B(8a)	-B(7a)	-B(12a)	60.4(5)
B(5a)	-C(1a)	-C(11a)	122.6(6)	B(11a)	-B(7a)	-B(12a)	60.4(5)
B(6a)	-C(1a)	-C(11a)	119.1(6)	B(3a)	-B(8a)	-B(4a)	60.4(5)
Au	-C(2a)	-C(1a)	122.4(3)	B(3a)	-B(8a)	-B(7a)	59.7(4)
Au	-C(2a)	-B(3a)	119.3(4)	B(4a)	-B(8a)	-B(9a)	59.8(5)
Au	-C(2a)	-B(6a)	119.2(4)	B(7a)	-B(8a)	-B(12a)	59.9(5)
Au	-C(2a)	-B(7a)	120.0(4)	B(9a)	-B(8a)	-B(12a)	59.4(5)
Au	-C(2a)	-B(11a)	120.0(4)	B(4a)	-B(9a)	-B(5a)	60.2(5)
C(1a)	-C(2a)	-B(3a)	60.4(4)	B(4a)	-B(9a)	-B(8a)	58.9(5)
C(1a)	-C(2a)	-B(6a)	60.3(4)	B(5a)	-B(9a)	-B(10a)	59.6(5)
B(3a)	-C(2a)	-B(7a)	61.2(4)	B(8a)	-B(9a)	-B(12a)	59.7(5)
B(6a)	-C(2a)	-B(11a)	61.9(4)	B(10a)	-B(9a)	-B(12a)	60.2(5)
B(7a)	-C(2a)	-B(11a)	61.7(4)	B(5a)	-B(10a)	-B(6a)	60.4(5)
C(1a)	-B(3a)	-C(2a)	58.3(4)	B(5a)	-B(10a)	-B(9a)	59.9(5)
C(1a)	-B(3a)	-B(4a)	58.7(4)	B(6a)	-B(10a)	-B(11a)	59.3(5)
C(2a)	-B(3a)	-B(7a)	59.2(4)	B(9a)	-B(10a)	-B(12a)	60.2(5)
B(4a)	-B(3a)	-B(8a)	59.8(4)	B(11a)	-B(10a)	-B(12a)	59.9(5)
B(7a)	-B(3a)	-B(8a)	60.5(4)	C(2a)	-B(11a)	-B(6a)	58.9(4)
C(1a)	-B(4a)	-B(3a)	59.0(4)	C(2a)	-B(11a)	-B(7a)	59.3(4)
C(1a)	-B(4a)	-B(5a)	58.9(5)	B(6a)	-B(11a)	-B(10a)	60.3(5)
B(3a)	-B(4a)	-B(8a)	59.8(4)	B(7a)	-B(11a)	-B(12a)	60.1(5)
B(5a)	-B(4a)	-B(9a)	59.4(5)	B(10a)	-B(11a)	-B(12a)	59.8(5)
B(8a)	-B(4a)	-B(9a)	61.4(5)	B(7a)	-B(12a)	-B(8a)	59.7(5)
C(1a)	-B(5a)	-B(4a)	58.7(5)	B(7a)	-B(12a)	-B(11a)	59.5(5)
C(1a)	-B(5a)	-B(6a)	58.5(4)	B(8a)	-B(12a)	-B(9a)	60.8(5)
B(4a)	-B(5a)	-B(9a)	60.4(5)	B(9a)	-B(12a)	-B(10a)	59.6(5)
B(6a)	-B(5a)	-B(10a)	60.8(5)	B(10a)	-B(12a)	-B(11a)	60.2(5)
B(9a)	-B(5a)	-B(10a)	60.5(5)	C(1a)	-C(11a)	-O(1a)	113.8(7)
C(1a)	-B(6a)	-C(2a)	58.8(4)	C(11a)	-O(1a)	-C(12a)	120.8(10)
C(1a)	-B(6a)	-B(5a)	58.9(5)				

Table 4.6 Selected Interatomic Distances (Å) and Interbond Angles (°) in **14** **(continued).**

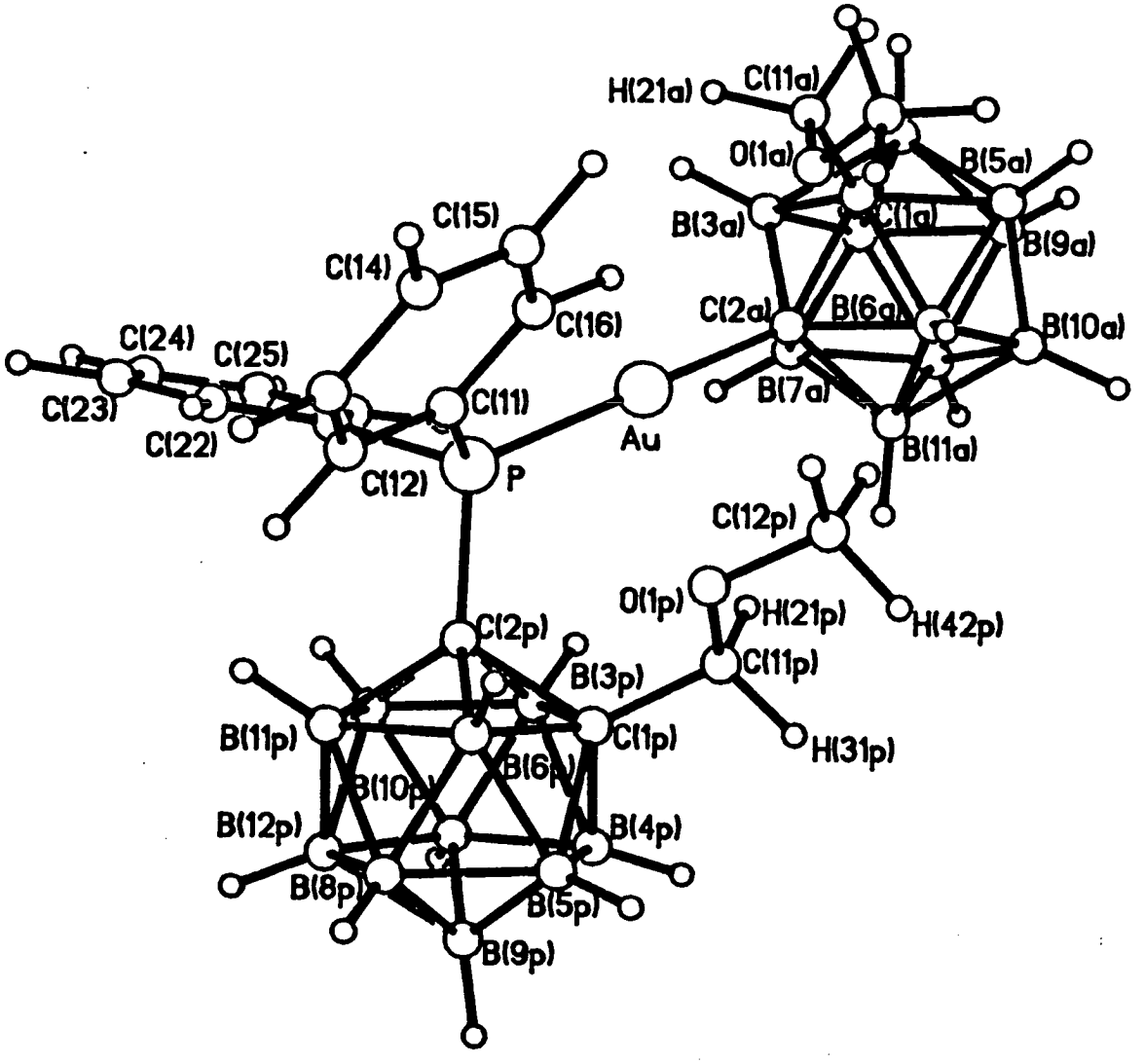

Figure 4.10 Perspective View of a Single Molecule of **14** (cage H atoms carry the same number as the B atoms to which they are bound).

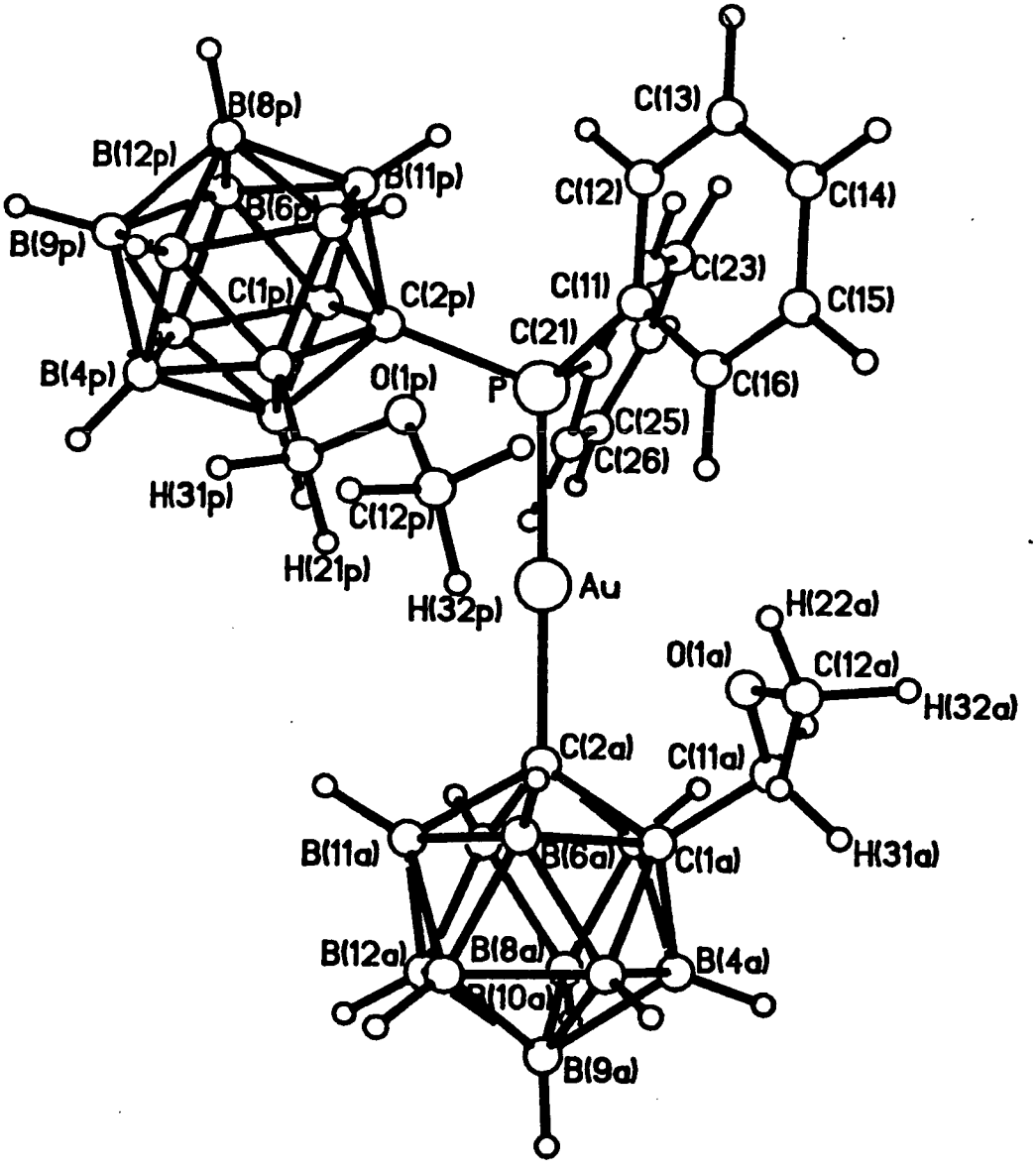

Figure 4.11 Alternative Perspective View of a Single Molecule of **14** (cage H atoms carry the same number as the B atoms to which they are bound).

The orientation of the ether group of gold-bound carbaborane is defined by the C(1a)-C(11a)-O(1a)-C(12a) and C(2a)-C(1a)-C(11a)-O(1a) torsion angles of 118.9(11) and 59.1(9)° respectively. The former indicates an eclipsed arrangement of the ether group about the C(11a)-O(1a) bond, in contrast to the corresponding angle in 1-CH_3OCH_2-2-{$AsPh_3Au$}-1,2-*closo*-$C_2B_{10}H_{10}$ (**4e**) [179.8(8)°] which represents a *trans* staggered arrangement. The eclipsed arrangement (as opposed to the expected *trans*) is probably a consequence of general steric crowding within the molecule. The latter torsion angle and an Au-O(1a) distance of 3.339(8) Å imply that there is no metal-oxygen interaction.

The ether group of phosphorus-bound carbaborane has C(1p)-C(11p)-O(1p)-C(12p) and C(2p)-C(1p)-C(11p)-O(1p) torsion angles of 173.4(6) and 54.4(7)° respectively. The former indicates a *trans* staggered arrangement as in **12** and **4e**, the latter, coupled with an Au-O(1p) distance of 3.418(5) intimates that there is no metal oxygen interaction.

Twists of 6 and 30° about the P-C(11) and P-C(21) bonds respectively define the orientation of the phenyl rings. These twists are similar to those observed in **12** and the first is close to an [C(11)/C(12)-Au/P] eclipsed arrangement (0°). The orientation of the carbaborane cage relative to Au, defined by the Au-P-C(2p)-C(1p) torsion of 41.5(4)°, is also similar to that in **12**.

The bond angles at phosphorus intimate the expected tetrahedral geometry. The P-Au-C(2a) sequence is essentially linear as expected for two-coordinate gold(I). The Au-P bond length is 2.2749(13) Å comparable to that in 1-{PPh_3Au}-1,2-*closo*-$C_2B_{10}H_{11}$ [2.271(2) Å[88]] but longer than in **12** [2.237(3) Å] and PPh_3AuCl [2.235(3) Å]. The Au-C distance is 2.052(5) Å, similar to that in **4e** and therefore presumably shorter than a Au-C_{alkyl} bond. Indeed, a single bond *trans* to 1-CH_3OCH_2-2-PPh_2-1,2-*closo*-$C_2B_{10}H_{10}$ could be expected to be *ca.* 2.12 Å by

consideration of the Au-CH_3 and Au-Cl bond lengths of 2.124(28) Å and 2.279(3) Å in PPh_3AuMe[89] and PPh_3AuCl[103] respectively and subtracting the difference from the Au-Cl bond length of 2.274(3) Å in **12**. On this basis the Au-C(2a) bond length in **14** would be anomalously short and so fully consistent with the observations and conclusions discussed in **Chapter 2.**

4.3.3 NMR Studies on **14**

The $^{31}P\{^{1}H\}$ NMR spectrum of **14** shows a singlet resonance at δ 58.75 ppm. This resonance lies between that of the corresponding gold(I) chloride (**12**) and gold(I) methyl (**13**), the $^{31}P\{^{1}H\}$ NMR spectra of which reveal single peaks at δ 54.75 and 62.8 ppm respectively (**Figure 4.12**). The relative (with respect to each other) chemical shifts of **12**, **13** and **14** are consistent with observations made from the comparison of $^{31}P\{^{1}H\}$ NMR data of PPh_3AuX, where X = Cl, Me or 1-CH_3OCH_2-1,2-*closo*-$C_2B_{10}H_{10}$: The phosphorus chemical shift of the latter (carbaborane) was found to lie between that of the former two, with the chloride at lowest frequency. The similar observation made in the comparison of the $^{31}P\{^{1}H\}$ NMR chemical shifts of **12**, **13** and **14** is therefore fully accordant with the subsequent conclusions made in **Chapter 2**: *i.e.* *closo*-carbaborane has donor properties between that of chloride (a good σ- and π-donor) and of methyl (a good σ-donor), this reflected in the relative phosphorus chemical shift (see **Section 2.3.2** and **Figure 2.6**, p57): Greater donation of electron density from the ligand *trans* to phosphine means that, overall, less is required to be donated from phosphine and, consequently, the phosphorus atom in the chloride compound has more electron density than in the carbaborane and methyl compounds respectively.

The $^{11}B\{^{1}H\}$ NMR data for **14** are compared with that for **1**[20], **4α** and **12** in **Table 4.7**. The NMR spectrum of **14** contains a variety of peaks due to the two carbaborane cages present in the molecule. Remarkably, at the field strength used (64.21 MHz) the resonances due to phosphine and gold-bound carbaboranes are mutually distinguishable: Phosphorus-bound carbaborane produces three resonances of relative integral 1:1:8 at δ 1.85, -1.08 and -8.53 ppm respectively, similar to those already observed for **11**, **12** and **13**, the resonance of integral 8 a quadruple coincidence due to the four pairs of boron atoms. Similarily, comparison with the $^{11}B\{^{1}H\}$ NMR

spectra of **11** and of **12** and **13** reveals an overall shift to higher frequency with respect to the former and only a small shift with respect to the latter, since substitution (at gold) is three bonds away.

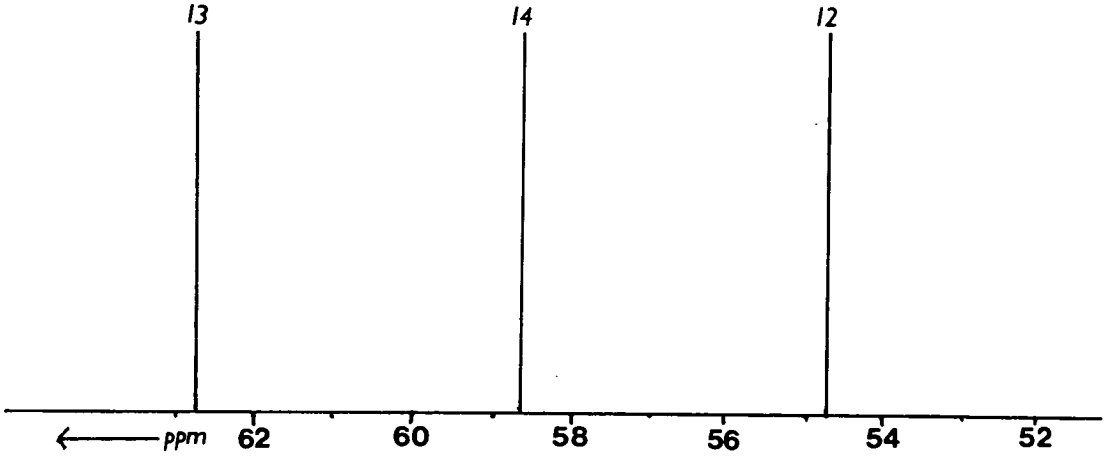

Figure 4.12 Comparison of $^{31}P\{^{1}H\}$ NMR Data of **12, 13** and **14** (36.46 MHz).

The resonances due to gold-bound carbaborane are at δ -1.68, -3.93, -7.44 and -9.48 ppm (relative integral 1:1:2:6), the low frequency resonance a triple coincidence at the field strength used (64.21 MHz). These resonances are comparable to those found in compounds **4** and are shifted overall to higher frequency with respect to the $^{11}B\{^{1}H\}$ NMR spectrum of **1**, as expected (**Section 2.3.2**).

The anticipated resonances due to the two phenyl and two ether groups in **14** were found in the ^{1}H NMR spectrum in the correct integral ratio. The absence of the broad peak, observed at δ 4.00 ppm in the ^{1}H NMR spectrum of **1**, indicated the replacement of the hydrogen atom bound to C(2a). The chemical shifts of the ether protons in **14** are compared with those of **1**[20], **4a** and **12** in **Table 4.8**. This allowed assignment of these resonances to the correct ether group: The resonances at δ 3.93 and 3.39 ppm (relative integral 2:3) are due to OC(11a)H_2 and OC(12a)H_3 respectively (similar to those in **4a**) while the resonances at δ 4.38 and 3.15 ppm (2:3)

are due to OC(11p)H_2 and OC(12p)H_3 respectively (similar to those in **12**). As observed with compounds **4**, the OC(11a)H_2 resonance has slightly shifted to high frequency, and the OC(12a)H_3 experiences only a small shift with respect to the corresponding resonances in the ^{1}H NMR spectrum of **1**.

	$^{11}B\{^1H\}$ (δ/ppm)			
	1*	**4a**	**12**	**14**
1B(a)	- 2.47	-0.97	----	-1.68
1B(a)	- 4.23	-3.97	----	-3.93
2B(a)	- 8.47	-7.27	----	-7.44
2B(a)	-10.97	-9.27	----	-9.48
4B(a)	-12.45	-9.27	----	-9.48
1B(p)		----	1.70	1.85
1B(p)		----	-1.51	-1.08
8B(p)		----	-9.06	-8.53

(a) represents Au-bound carbaborane; (p) represents P-bound carbaborane.
* parent carbaborane: neither Au- nor P-bound.

Table 4.7 $^{11}B\{^1H\}$ NMR Data for **1**, **4a**, **12** and **14** (64.21 MHz).

Similarily, the OC(11p)H_2 resonance is shifted significantly to higher frequency compared to in the spectrum of **1** and the OC(12p)H_3 resonance is shifted a small amount to lower frequency. These shifts are comparable to the resonance shifts encountered in the NMR spectra of **11**, **12** and **13** when compared to that of **1** and are

therefore indubitably due to similar reasons (see **Section 4.2.5**): The hydrogen atoms bound to the carbon atom bonded directly to the cage are likely to be affected by changes in relative shielding within the cage.

	^1H (δ/ppm)			
	1*	**4a**	**12**	**14**
OCH_2(a)	3.79	3.89	----	3.93
OCH_3(a)	3.36	3.27	----	3.39
OCH_2(p)		----	4.34	4.38
OCH_3(p)		----	3.17	3.15

(a) represents Au-bound carbaborane; (p) represents P-bound carbaborane.
* parent carbaborane: neither Au- nor P-bound.

Table 4.8 Comparison of Ether Substituent Proton Resonances in the ^1H NMR Spectra of **1**, **4a**, **12** and **14**.

As observed with **11**, **12** and **13**, the phenyl groups give two distinct multiplets of relative integral 4:6. The resonances are comparable to those in **12** and the reasoning for the two distinct regions is therefore the same (**Section 4.2.5**): The resonance of integral 4 is due to H(12)/H(16) and H(22)/H(26) since, being nearest the phosphorus atom, they are most likely to be sensitive to changes in shielding at phosphorus.

4.4 Synthesis of a Carbaborane-Borane Compound

4.4.1 Introduction

Reaction of PPh_3AuMe with *nido*-$B_{10}H_{14}$[86] produces the intensely coloured 'triple cluster' illustrated in **Figure 4.13**. This is a multiple cluster of six gold atoms and two borane polyhedra comprising four $\{PPh_3Au\}$ and two $\{B_{10}H_{12}Au\}$ fragments arranged such that the $\{Au_6\}$ part consists of three face-fused tetrahedra. In contrast, reaction of PCy_3AuMe with *nido*-$B_{10}H_{14}$ affords the colourless (mono-) phosphine gold(I) borane (**Figure 4.14**) in which a bridging hydrogen atom has been (isolobally) replaced by a bridging $\{PCy_3Au\}$ fragment[24].

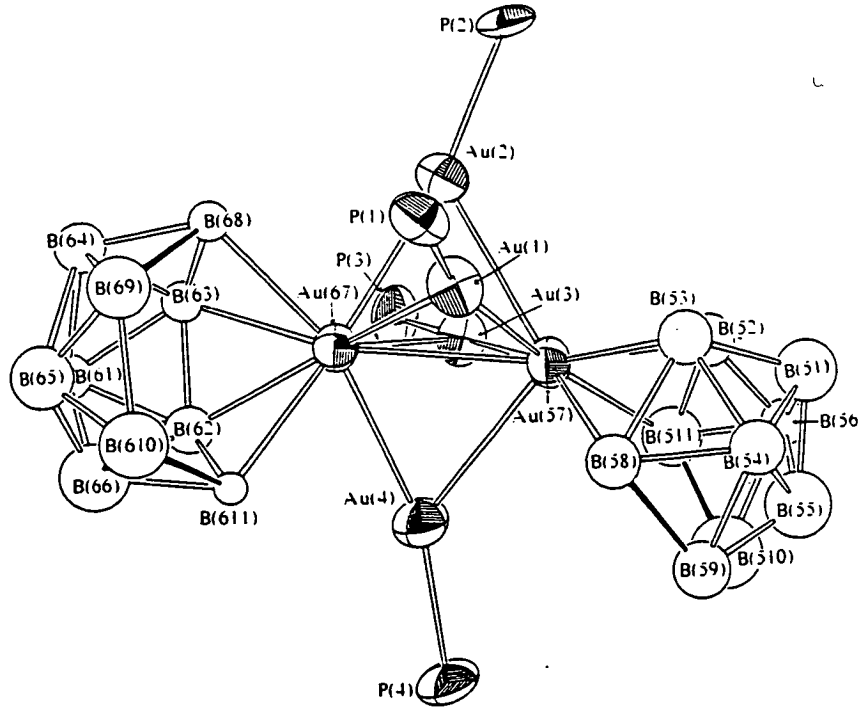

Figure 4.13 Structure of $\{(B_{10}H_{12})Au\}_2\{PPh_3Au\}_4$ (the 'triple cluster').

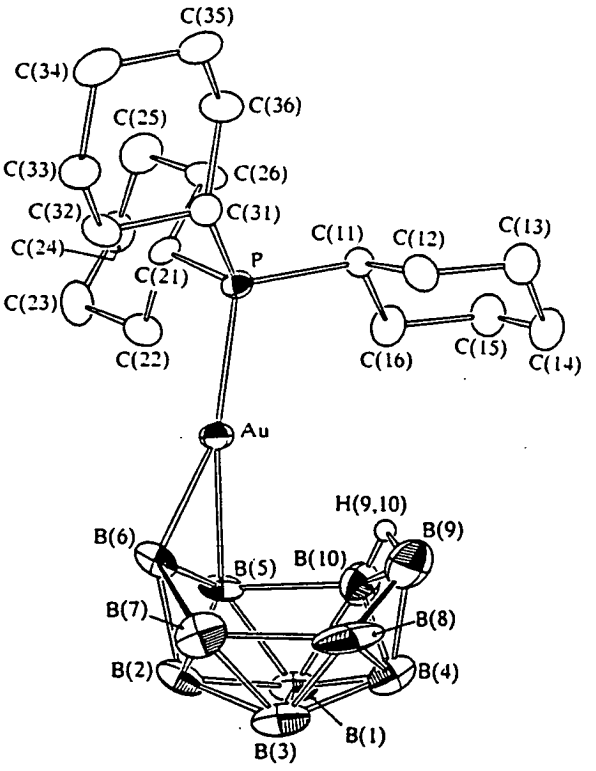

Figure 4.14 Structure of 5,6-{μ-PCy_3Au}-*nido*-$B_{10}H_{13}$.

Mechanistic studies[86] have implied that the mono-gold species are intermediates in the formation of triple clusters. PCy_3 has a much larger cone angle than PPh_3 (170 and 145° respectively[114]) and therefore the increased steric demands of PCy_3 have been attributed as the reason for the ability to isolate the mono-gold species. Consistent with this explanation, reaction of 5,6-{μ-PCy_3Au}-*nido*-$B_{10}H_{13}$ with PPh_3 affords a triple cluster identical to that formed in the reaction between PPh_3AuMe and *nido*-$B_{10}H_{14}$.

As a consequence of the increased steric demands of carbaborane over phenyl, 1-CH_3OCH_2-2-PPh_2-1,2-*closo*-$C_2B_{10}H_{10}$ **(11)** will have a much larger cone angle than PPh_3 (and PCy_3). Therefore, in contrast to PPh_3AuMe but similarly to PCy_3AuMe, reaction of 1-CH_3OCH_2-2-{PPh_2AuMe}-1,2-*closo*-$C_2B_{10}H_{10}$ **(13)** with *nido*-$B_{10}H_{14}$ should afford the mono-gold species in preference to a multi-gold cluster. This section describes the synthesis and characterisation of a phosphine carbaborane gold(I) borane.

4.4.2 Synthesis and Characterisation of 1-CH_3OCH_2-2-(5',6'-{μ-PPh_2Au}-*nido*-$B_{10}H_{13}$)-1,2-*closo*-$C_2B_{10}H_{10}$ (**15**)

Addition of *nido*-$B_{10}H_{14}$ to 1-CH_3OCH_2-2-{PPh_2AuMe}-1,2-*closo*-$C_2B_{10}H_{10}$ (**13**) in dichloromethane resulted in a transient colour change from colourless to yellow and then back to colourless again with concomitant effervescence. The absence of any intense colouration indicated that the mono-gold compound and not a 'triple cluster' had probably been produced. The resulting solid isolated from the reaction mixture was found to be a 1:5 mixture (from the $^{31}P\{^1H\}$ NMR spectrum) of **13** and (probably) 1-CH_3OCH_2-2-(5',6'-{μ-PPh_2Au}-*nido*-$B_{10}H_{13}$)-1,2-*closo*-$C_2B_{10}H_{10}$ (**15**) respectively. Since the contaminating reactant (**13**) is partially soluble in *n*-hexane it was removed by stirring the crude product in an excess of that solvent and then dissolving the solid recovered in a miniumum of CH_2Cl_2 and precipitating it out with addition of the same amount of *n*-hexane. Compound **15** was recovered as an off-white solid in 52% yield. It was found to be stable as a solid in air though solutions at room temperature became darker over *ca.* 6h indicating some decomposition.

Characterisation and identification as the (mono) gold(I) borane was effected by IR and NMR spectroscopies. The characterisation (and colour) of the product indicated that the mono-gold species had been isolated. This is in contrast to when the phosphine of PR_3AuMe is PPh_3 but comparable to when it is PCy_3 and P(*o*-tol)$_3$.

The IR spectrum displayed a broad peak, the maximum being at 2565 cm^{-1}, due to B-H stretches, and sharp peaks at 1437, 1384 and 1112 cm^{-1} due to CH_3OCH_2 vibrations. A broad peak centred at δ 69.1 ppm was observed in the $^{31}P\{^1H\}$ NMR spectrum of **15**, the broadening indicative of gold bound to boron, as previously observed in the $^{31}P\{^1H\}$ NMR spectra of gold borane compounds[24, 86]. The $^{11}B\{^1H\}$

NMR spectrum (**Figure 4.15**) exhibited a variety of peaks, those at δ 15.05, 9.55, -30.38 and -35.20 ppm due to borane, and that at δ -8.74 ppm due to carbaborane. Broad peaks with maxima at δ 1.43 and -1.19 ppm were also observed and collectively attributable to six borane and two carbaborane resonances. The ^{1}H NMR spectrum displayed the expected proton substituent resonances in the correct ratio (10:2:3).

5,6-{μ-PCy_3Au}-*nido*-$B_{10}H_{13}$ has previously been synthesised using a different synthetic route: The reaction of $[B_{10}H_{13}][NHEt_3]$ and PCy_3AuCl afforded the required (mono) gold(I) borane [24], but in lower yield. On stirring a solution of **12** with $[B_{10}H_{13}][NHEt_3]$ (prepared *in situ* from *nido*-$B_{10}H_{14}$ and NEt_3) a colour change from pale yellow to bright orange was observed, this colouration usually indicative of gold(III). The colour was not intense enough to suggest that a 'triple cluster' had formed and besides, considering the large cone angle of phosphine carbaborane, it would not be expected. A new peak was obtained in the $^{31}P\{^{1}H\}$ NMR spectrum of the (crude) reaction mixture (at δ 68.8 ppm). The $^{11}B\{^{1}H\}$ NMR spectrum showed a variety of peaks: The major peaks at δ 17.08, 15.04, 4.06 and -22.56 ppm indicated that $[(B_{10}H_{12})_2Au]^-$ had been produced[86]. The phosphorus resonance (at δ 68.8 ppm) is therefore due to the counter-ion to the gold bisborane, $[(1\text{-}CH_3OCH_2\text{-}2\text{-}PPh_2\text{-}1,2\text{-}closo\text{-}C_2B_{10}H_{10})_2Au]^+$ (*cf* δ 65.0 ppm for $[(PCy_3)_2Au]^+$). It has been reported[24] that reaction of PR_3AuCl with $[B_{10}H_{13}][NHEt_3]$ may produce the $[(B_{10}H_{12})_2Au]^-$ anion, the mechanism of the reaction probably *via* the required product, 5,6-{μ-PR_3Au}-*nido*-$B_{10}H_{13}$, this reacting with more $[B_{10}H_{13}]^-$ to give the anion.

Minor peaks, at about one-tenth of the integral of the major peaks, were also observed at δ 9.51, 1.39, -2.49, -30.43 and -35.26 ppm which implied that a small amount of the gold borane compound had been formed; these resonances being comparable with those obtained for 5,6-μ-{PCy_3Au}-*nido*-$B_{10}H_{13}$ (which has been successfully synthesised *via* this route). Attempts to separate out the small amount of

compound **15** by TLC (CH_2Cl_2 eluant) resulted in decomposition and the recovery of **11** as the only phosphorus containing product, identified by its $^{31}P\{^1H\}$ NMR spectrum.

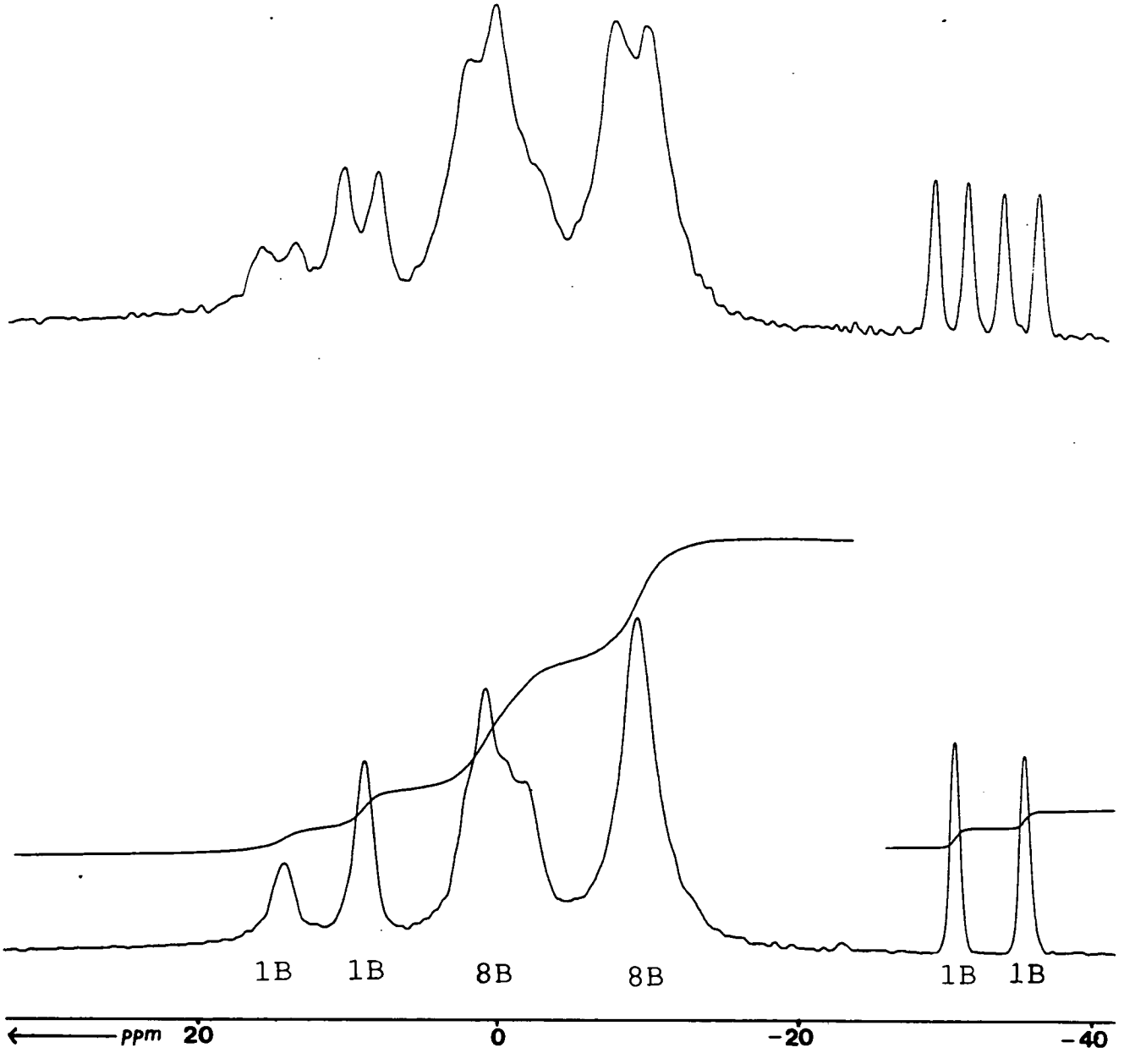

Figure 4.15 $^{11}B\{^1H\}/^{11}B$ NMR Spectra of **15** (64.21 MHz).

4.4.3 NMR Studies on **15**

A broad singlet resonance is observed at δ 69.1 ppm in the $^{31}P\{^{1}H\}$ NMR spectrum of **15** (*cf* δ 54.6 ppm for **12**), with a width at half-height of 58 Hz, in contrast to the sharp resonances observed for compounds **11-14**. The broadening has been attributed to thermal coupling to boron atoms[115] and has also been observed in related phosphineaura-[86] and phosphineplatina-boranes[116]: Broad singlet resonances have been observed at δ 26.9 and 68.9 ppm with widths at half-height of *ca.* 90 Hz in the $^{31}P\{^{1}H\}$ NMR spectra of 5,6-{μ-P(*o*-tol)$_3$Au}-*nido*-$B_{10}H_{13}$ and 5,6-{μ-PCy$_3$Au}-*nido*-$B_{10}H_{13}$ respectively (*cf* P(*o*-tol)$_3$AuCl at δ 8.55 ppm and PCy$_3$AuCl at δ 54.3 ppm). The resonance broadening and shift to higher frequency with respect to the spectrum of the corresponding chloride is therefore strong evidence for the formation of phosphine carbaborane (mono) gold(I) borane.

Table 4.9 outlines the comparison of $^{11}B\{^{1}H\}$ NMR data of **15** with **12**, *nido*-$B_{10}H_{14}$ and 5,6-{μ-P(*o*-tol)$_3$Au}-*nido*-$B_{10}H_{13}$. The resonance of integral 8 at δ -8.74 ppm is due to (phosphine) carbaborane and is is comparable to the resonances found in the $^{11}B\{^{1}H\}$ NMR spectra of **11-14**. The two resonances of integral 1 as observed in corresponding spectra of phosphine carbaboranes must form part of the broad resonance of integral 8 defined by maxima at δ 1.43 and -1.19 ppm. Similarly, this resonance of integral 8 must contain resonances due to six of the boron atoms in $\{B_{10}H_{13}\}$. The four peaks of integral 1 at highest and lowest frequency, δ 15.1 and 9.55 ppm and δ -30.4 and -35.2 ppm, are also resonances attributable to boron atoms in the $\{B_{10}H_{13}\}$ fragment. These resonances are comparable to those obtained at highest and lowest frequency in 5,6-{μ-P(*o*-tol)$_3$Au}-*nido*-$B_{10}H_{13}$ and 5,6-{μ-PCy$_3$Au}-*nido*-$B_{10}H_{13}$[24, 86]. Hence, part of the spectrum of **15** can be tentatively assigned (by ^{11}B-^{11}B COSY NMR spectroscopy) by comparison with the assigned spectrum of 5,6-(μ-P(*o*-tol)$_3$Au)-*nido*-$B_{10}H_{13}$.

$^{11}B\{^1H\}$ (δ/ppm)

	12	15	bor[a]	aubor[b]
1B	1.70	*	----	----
1B	-1.51	*	----	----
8B	-9.06	- 8.74	----	----
8B[θ]		1.43[θ]		
θ		- 1.19[θ]		
1B	----	15.05	13.72	15.13
1B	----	9.55	13.72	9.41
1B	----	*	10.79	8.34
1B	----	*	10.79	2.15
1B	----	*	1.77	1.40
3B	----	*	1.77	- 1.00
1B	----	-30.38	-35.08	-30.73
1B	----	-35.20	-35.08	-35.85

a: bor = *nido*-$B_{10}H_{14}$; b: aubor = 5,6-{μ-P(*o*-tol)$_3$Au}-*nido*-$B_{10}H_{14}$

* corresponding resonances lost under broad peak of integral 8 (defined by maxima marked θ)

Table 4.9 Comparison of $^{11}B\{^1H\}$ NMR Data of **12**, **15**, *nido*-$B_{10}H_{14}$ and 5,6-{μ-P(*o*-tol)$_3$Au}-*nido*-$B_{10}H_{13}$ (64.21 MHz).

Nido-$B_{10}H_{14}$ has C_{2v} symmetry and consequently its $^{11}B\{^1H\}$ NMR spectrum exhibits four resonances of relative integral 2:2:4:2 due to B(6)/B(9), B(3)/B(1), B(5)/B(7)/B(8)/B(10) and B(2)/B(4) respectively. On replacement of a bridging hydrogen atom [on B(5)/B(6)] with a bridging phosphine gold(I) fragment, all boron atoms become inequivalent. Thus, in the $^{11}B\{^1H\}$ NMR spectrum of 5,6-{μ-P(*o*-tol)$_3$Au}-*nido*-$B_{10}H_{13}$, the resonances of integral 2 due to B(6)/B(9), B(3)/B(1) and B(2)/B(4) split to become resonances of integral 1, as expected. The resonance of integral 4 also splits, but forms a triple coincidence and a resonance of integral 1. Similarly, comparison of the $^{11}B\{^1H\}$ NMR spectra of **15** and *nido*-$B_{10}H_{14}$ reveals that the resonance due to B(6)/B(9) of the latter at δ 13.7 ppm splits to give rise to the resonances at δ 15.05 and 9.55 ppm in **15**, and the resonance attributable to B(2)/B(4) at δ -35.1 ppm in *nido*-$B_{10}H_{14}$ splits to give rise to resonances at δ -30.38 and -35.20 ppm in **15**. The other {$B_{10}H_{13}$} resonances are part

of the broad resonance of integral 8 and consequently their actual chemical shifts are not apparent.

From the ^{11}B NMR spectrum, the boron-proton coupling constant (where it can be measured) for the $\{B_{10}H_{13}\}$ fragment is 140-153 Hz and for the carbaborane fragment it is 128 Hz. Coupling to bridging hydrogen atoms [found in the borane fragment only: H(6',7'), H(8',9') and H(9',10')] is small and produces only broadening of the resonances. In the ^{11}B NMR spectrum of **15**, resonances due to three of the boron atoms carrying bridges, B(8'), B(10') and B(7'), are part of the broad resonance of integral 8 and no obvious couplings are observed. However, the highest frequency resonance has been speculatively assigned as due to B(9'), this atom carrying two bridging and one terminal hydrogen atoms [H(8',9'), H(9',10') and H(9')]. In the ^{11}B NMR spectrum, this resonance is split by coupling to H(9'). However, the resonances are broader with an average width at half-height of 145 Hz compared to a half-height width of 103 Hz for the resonance in the proton-decoupled spectrum, indicating possible additional coupling to bridging hydrogen atoms.

The ^{1}H NMR spectrum of **15** contained the expected proton resonances attributable to the phenyl and ether group protons in the correct integral ratio. The resonances are comparable with those in the ^{1}H NMR spectra of **11-14**, as expected: The OCH_2 resonance is shifted to much higher frequency and the OCH_3 resonance to slightly lower frequency as compared to the corresponding resonances in the ^{1}H NMR spectrum of **1**. The phenyl groups produce two distinct multiplet regions of relative integral 4:6 as before (**Section 4.2.5**). Resonances due to terminal and bridging cage hydrogen atoms were not observed at the field strength used (200.13 MHz) but perhaps could be located at higher field strength and assigned by $^{1}H\{^{11}B\}$ selective NMR spectroscopy if required. However, the spectrum is likely to be complex due to the presence of two different boron cage systems.

4.5 Attempted Syntheses of New BNCT Reagents

4.5.1 Introduction

Two of the problems with the current BNCT reagent, $Na_2[B_{12}H_{11}SH]$ (BSH) are that it is not tumour specific and that it is only surface active: BSH is useful in the treatment of only brain tumours because the reagent cannot cross the blood-brain barrier. Since a tumour breaches this barrier, it can specifically bind to the surface of the tumour (*via* a disulphide link) and not with healthy brain cells on the other side of the barrier. However, in general, there is an even distribution of the reagent in other (healthy) organs and so BSH is not particularily tumour specific. The surface activity of BSH means that to irradicate the tumour completely, the (traumatic) process of treatment must be repeated several times, each destroying a further layer of tumour cells. Consequently, the ideal reagent should be tumour specific and be able to penetrate the tumour resulting in distribution throughout.

One possible way to achieve tumour specificity and penetration that has been identified is *via* boronated analogues of amino-acids. These would be of use because the amino-acid is biologically recognised and, as the tumour is the fastest growing part of the body, would therefore be taken up in greater concentration (as it grows). Thus, upon irradiation, the tumour would be specifically destroyed, and, moreover, from within, thereby reducing the need for repetition of the treatment. Analogues of betaine[117] (by replacing CH_2 with BH_2) and of valine, leucine, isoleucine and phenylanaline[118] have been synthesised and have been found to have biological activity, but the concentration of boron per molecule is too low to be of any possible use in BNCT. Of more potential use is the analine derivative (*R*)- and (*S*)-*ortho*-carboranyl analine[119, 120] which, since it contains polyhedral carbaborane, has a much larger concentration of boron per molecule.

The ultimate compound for use in BNCT would therefore have a high concentration of boron per molecule (for example, polyhedral boron compounds) and contain an amino-acid. This section reports attempts to synthesise amino-acid carbaborane compounds by linking the two components through a metal centre. The metal used was gold because, firstly, stable gold amino-acid complexes are known[121], and, secondly, gold is biologically inert and has previously been used as a pharmaceutical (for example, rheumatoid arthritis drugs). There are added advantages of using gold and these include the possible use of electron microscopy to identify the biodistribution of the reagent, gold readily detected because of its large relative mass.

4.5.2 Attempts to Synthesise BNCT Reagents *via* thtAuCl

Two possible synthetic routes, as outlined in **Figure 4.16**, were used in attempts to link sulphur bound methionine through gold to a {1,2-*closo*-C_2B_{10}} carbaborane. These routes rely on the facile replacement of the (loosely) sulphur-bound tht by the (sulphur donating) amino-acid in either the gold(I) chloride or gold(I) carbaborane.

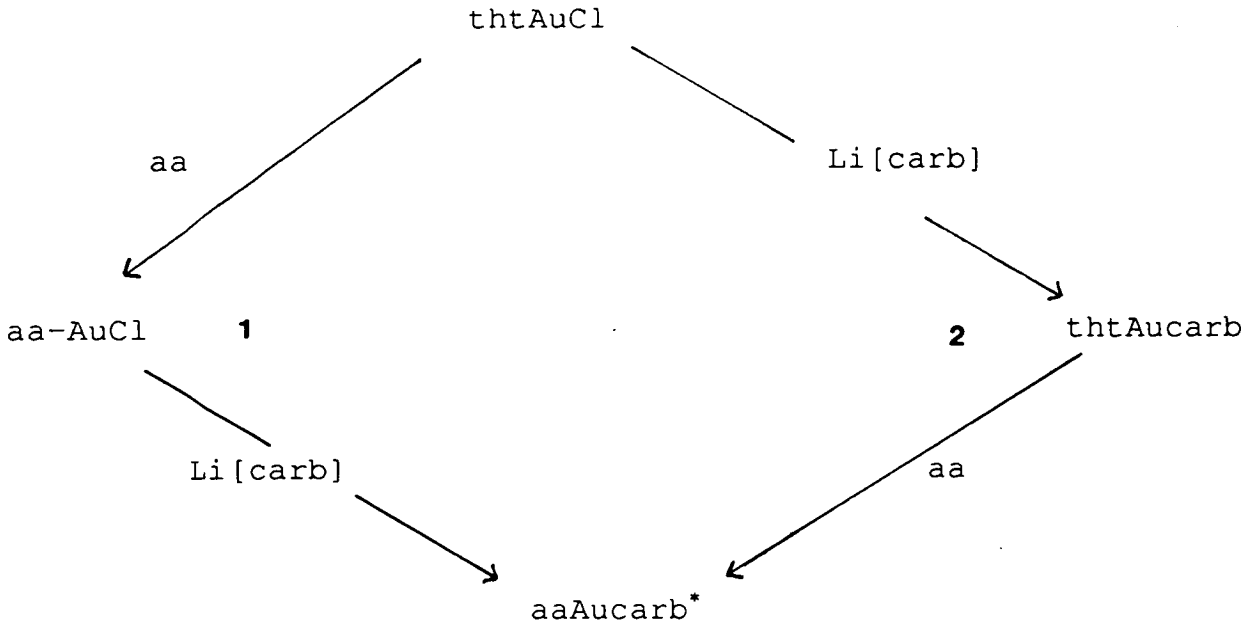

* e.g. 1-CH_3OCH_2-2-{$CH_3S(Au)CH_2CH_2CH(COOH)NH_2$}-1,2-*closo*-$C_2B_{10}H_{10}$

aa = S- containing amino-acid, for example cysteine or methionine

carb = 1-R-1,2-*closo*-$C_2B_{10}H_{10}$

Figure 4.16 Possible Synthetic Routes to Carbaborane-Amino Acid Compounds.

Route 1, *via* the amino-acid gold(I) chloride was initially promising because stirring stoichiometric amounts of thtAuCl with N-acetyl-methionine [$CH_3S(CH_2)_2CH(COOH)NHCOCH_3$] in THF afforded (after work-up) a moisture-sensitive white solid in good yield. Microanalysis and ^1H NMR data

indicated that N-acetyl S-gold(I) chloride methionine, $CH_3S(AuCl)CH_2CH_2CH(COOH)NHCOCH_3$ (**16**), had been produced: Microanalysis was accordant with the proposed formulation of $C_7H_{13}NAuClO_3S$; the ^1H NMR spectrum exhibited a variety of peaks attributable to the various amino-acid protons although solvent (THF) resonances swamped some of the expected resonances.

However, when a solution of Li[1-CH_3OCH_2-1,2-*closo*-$C_2B_{10}H_{10}$] was added to a suspension of methionine gold(I) chloride in Et_2O or benzene at various temperatures between -78°C and room temperature, and the reaction mixture subsequently stirred for 1h, decomposition occurred with colloidal solid [presumably gold(0)] but no product being recovered.

Similarly, by following route 2, decomposition to colloidal gold(0) was produced under various reaction conditions when thtAuCl was reacted with Li[1-CH_3OCH_2-1,2-*closo*-$C_2B_{10}H_{10}$]. Thus, in both routes, decompostion occurred when lithium carbaborane was added to the sulphur bound ligand gold(I) chloride and this is presumably because the gold-sulphur bond is so weak [thioether (SR_2)- gold bonds such as these are notoriously weak]: Addition of lithium carbaborane probably catalyses the cleavage of Au-S leading to subsequent decomposition to Au^0.

The synthesis of amino-acid gold carbaborane compounds was also attempted by reaction of N-acetyl S-gold(I) chloride methionine with Tl[9-SMe_2-7,8-*nido*-$C_2B_9H_{10}$] and Tl_2[1,2-$(CH_3OCH_2)_2$-1,2-*nido*-$C_2B_9H_9$] / benzyltrimethyl-ammonium chloride (by comparison with the reactions between PPh_3AuCl Tl[9-SMe_2-7,8-*nido*-$C_2B_9H_{10}$] affording 9-SMe_2-10,11-{μ-PPh_3Au}-7,8-*nido*-$C_2B_9H_{10}$[36], and between PPh_3AuCl and Tl_2[7,8-*nido*-$C_2B_9H_{11}$]/ benzyltrimethyl-ammonium chloride yielding [10-*endo*-{PPh_3Au}-7,8-*nido*-$C_2B_9H_{10}$]$^-$ [35]) but both reactions were messy producing, gold(0) and several other unidentifiable (minor) products.

4.5.3 Synthesis and Characterisation of $PPh_3AuSCH_2CH(COOMe)NH_2$ (17)

Linkage of gold to an amino-acid to form stable compounds while keeping the amino-acid functionality intact has been successfully achieved previously: It has been reported[121] that reaction of stoichiometric amounts of PPh_3AuCl and cysteine hydrochloride in ethanol, precipitates, after concentration of the solvent, a white solid characterised as $PPh_3AuSCH_2CH(COOH)NH_3^+Cl^-.HCl$. However, repetition of this reaction (for the purpose of this research) using equivalent reactant amounts and reaction conditions to those reported proved unsuccessful. It is not clear from the original paper how the HCl produced in the reaction is associated with the final product and, moreover, it seems unlikely that it would not cleave any gold-sulphur bond formed.

Since the desired product could not be isolated by the literature method, the reaction was modified: PPh_3AuCl and cysteine methyl ester hydrochloride were stirred in ethanol, but two equivalents of triethylamine were added to complex out the two equivalents of HCl produced in the reaction, thus, rendering it inactive. The desired product, $PPh_3AuSCH_2CH(COOMe)NH_2$ (**17**) was recovered by evaporating the solvent and dissolving the resultant solid in THF. The white solid (identified as NEt_3HCl from ^1H NMR spectroscopy) and the solution containing **17** were separated by filtration, and **17** was isolated in good yield (82%) and purity after trituration with Et_2O.

Characterisation of **17** was accomplished by microanalysis and by IR and $^{31}P\{^1H\}$ and ^1H NMR spectroscopies. Microanalysis was accordant with the proposed formulation of $C_{22}H_{23}NAuO_2PS$. The IR spectrum exhibited a sharp peak at 1746 cm^{-1} indicative of an organic carbonyl.

The $^{31}P\{^1H\}$ NMR spectrum showed a sharp single peak at δ 38.1 ppm. This is

shifted to high frequency compared to PPh_3AuCl and is consistent with the replacement of a good donor ligand (Cl) with a loosely bound and overall weaker donor sulphur ligand. The ^1H NMR spectrum revealed a variety of peaks due to phenyl and amino-acid proton resonances in the correct integral ratio of 15:2:1:3:2 [at δ 7.62-7.30 (m, C_6H_5), 4.23 (broad, NH_2), 3.81 (broad, CH_2CH), 3.47 (s, $COOCH_3$) and 3.37 ppm (d, CH_2CH) respectively]. The broad resonance at δ 4.23 ppm, with a width at half-height of 25 Hz, was assigned as NH_2 since N will dampen the relaxation time of these protons resulting in a broad resonance. The only resonance of integral 1 present in the spectrum was a broad peak at δ 3.81 ppm which therefore must be due to SCH_2CH: Initially this appears to be unexpected, as a triplet resonance would have been anticipated. However, on expansion of this signal, the peak develops shoulders at approximately half-height. Thus, the resonance *is* a triplet, and the broadening, due to a longer relaxation time as a consequence of the carbon atom to which this proton is bound being directly bonded to both an acid and amine group, must therefore be about equivalent to the proton-proton coupling constant of 4 Hz. The remaining singlet at δ 3.47 ppm and doublet at δ 3.37 ppm are assigned as due to $COOCH_3$ and CH_2CH respectively, as expected.

4.5.4 Reaction of 1-CH_3OCH_2-2-PPh_2AuCl-1,2-*closo*-$C_2B_{10}H_{10}$ with $HSCH_2CH(COOMe)NH_2$

The deductions made from **Section 4.2**, that 1-CH_3OCH_2-2-PPh_2-1,2-*closo*-$C_2B_{10}H_{10}$ gold(I) compounds should exhibit similar chemistry to PPh_3 gold(I) compounds (albeit account must be taken of the large difference in cone angle) has been further emphasised by the synthesis of the biscarbaborane and carbaborane-borane compounds. The aim of this part of the research was to link a carbaborane to an amino-acid through gold. **Section 4.5.3** described the linkage of PPh_3 to an amino-acid through gold; given the chemical similarity between **11** and PPh_3, it should, in theory, be possible to link a phosphine carbaborane to an amino-acid through gold.

Thus, in a similar manner to that described for the synthesis of **17**, stochiometric amounts of **11** and $HSAuCH_2CH(COOMe)NH_3Cl$ were stirred in ethanol and two equivalents of NEt_3 were added to complex out HCl. The addition of triethylamine resulted in dissolution of all the solid previously suspended. After stirring for 2h the solvent was removed and, in order to isolate the product in high purity, firstly CH_2Cl_2 was added and the mixture filtered to remove any unreacted amino-acid and, after removal of CH_2Cl_2, THF was added to the resultant solid and the mixture filtered to remove the NEt_3HCl coproduct. Analysis of the resultant off-white solid recovered from the THF solution was effected by IR and multinuclear NMR spectroscopies.

Optimisitically, the infra-red spectrum contained peaks at 2574 cm^{-1} and 1748 cm^{-1} indicative of B-H and organic C=O stretches respectively, possibly indicating the presence of a molecule containing carbaborane *and* amino-acid. However, analysis of the $^{31}P\{^1H\}$, $^{11}B\{^1H\}$ NMR and ^1H NMR spectra revealed that the solid recovered contained 1-CH_3OCH_2-2-PPh_2-1,2-*closo*-$C_2B_{10}H_{10}$, **11**, as the only phosphine-containing species. Consequently, it appears that the gold fragment has

been lost. Analysis of the solids recovered from dissolving crude compound in CH_2Cl_2 and then THF revealed that the solid insoluble in the former contained C=O but no B-H stretches in the IR spectrum. The solid insoluble in the latter was identified as NEt_3HCl (^1H NMR spectrum) only. From these analyses it is not clear what has happened to gold. It is possible that, since the NMR spectra were recorded in $CDCl_3$ (a potential source of DCl), the Au-S bond had been cleaved in solution, but recording the spectra in d_6-acetone also indicated that **11** was present in the sample.

Thus, in contrast to the synthesis of **17**, the reaction of **12** with cysteine methyl ester hydrochloride in the presence of NEt_3 does not occur, but results in decomposition to the free phosphine (carbaborane).

4.5.5 Future Work

The analogy between **12** and PPh_3AuCl has been emphasised by the similarity in their molecular structures and chemistries so far explored. Therefore, as $PPh_3AuSCH_2CH(COOMe)NH_2$ has been successfully synthesised, it would seem a promising prediction that the corresponding phosphine carbaborane gold amino-acid may be produced. Therefore, initial further work would investigate optimum reaction conditions in order for the required compound to be isolated. The determination of the mechanism for decomposition to **11** under the reaction conditions described in **Section 4.5.4** might be useful in consideration of this.

Beyond this, the compound will have to be adapted significantly if it is to be considered to be any use in BNCT. For example, the BNCT reagent needs to be soluble in water: The amino-acid function is hydrophilic but the phosphine carbaborane function is, at present, hydrophobic. Therefore, modification of the organic substituent on carbaborane and of the phosphine phenyl groups would have to be achieved to increase water solubility. Additionally, derivatisation of the amino-acid functionality may improve water solubility.

As concentration of boron in the tumour is important, it would be significant if one or both of the remaining phosphine phenyl rings could be replaced with polyhedral (carba)borane compounds. To overcome steric demands of the bulky carbaborane cage systems, carbon chains between the phosphorus atom and the cage could be inserted, or smaller cage systems could be used. In conclusion, there is a lot of potential research to be done in this area and unfortunately time constraints have prevented persual of these aims further than described.

4.6 Conclusions

The reaction of PPh_2Cl and $Li[1\text{-}CH_3OCH_2\text{-}1,2\text{-}closo\text{-}C_2B_{10}H_{10}]$ yielded a phosphine carbaborane compound (**11**) which has been successfully characterised and was found to be less basic than PPh_3: Compound **11** is analogous to PPh_3 in that (in essence) a phenyl group has been replaced by carbaborane. Compound **11** was reacted with thtAuCl, producing a phosphine carbaborane gold(I) chloride compound analogous to PPh_3AuCl. Indeed, an X-ray crystallographic study on the former has shown that phosphine carbaborane gold(I) chloride has similar molecular dimensions to PPh_3AuCl. This allowed the deduction that these two compounds could possibly have similar chemistries: PPh_3AuCl has a varied chemistry and so novel phosphine carbaborane gold(I) compounds could be envisaged starting from the chloride. Thus, initially, the phosphine carbaborane gold(I) methyl compound was synthesised (and characterised) by a similar procedure to that for PR_3AuMe.

A novel phosphine carbaborane gold(I) σ-carbaborane compound has been synthesised and structurally characterised, and was found to be similar to compounds **4** described previously (**Chapter 2**): Molecular dimensions and NMR data were fully consistent with those of compounds **4** and therefore the same conclusions to those drawn from **Chapter 2** can be made [*i.e.* that (gold-bound) carbaborane acts an electron donating ligand].

Since carbaborane is more sterically demanding than phenyl, the cone angle of phosphine carbaborane must be much larger than that of PPh_3. Therefore, it would be anticipated that, in reactions where the size of the phosphine cone angle is significant in determining the final products, reactions involving phosphine carbaborane gold(I) would possibly be different to those involving $\{PPh_3Au\}$. This has been demonstrated through the reaction of phosphine carbaborane gold(I) with

nido-decaborane(14): Reaction of *nido*-$B_{10}H_{14}$ with phosphine carbaborane gold(I) methyl yielded the mononuclear gold(I) borane compound whereas reaction with PPh_3AuMe afforded a (gold) cluster compound. The mechanism of the latter reaction has been shown[86] to proceed *via* the mono gold species and increasing the phosphine cone angle prevents cluster formation because of the increased steric demands.

Finally, it was shown that phosphine (PPh_3) could be linked to an amino-acid (cysteine) through the gold(I) centre. It was therefore anticipated that phosphine carbaborane could also be linked to an amino-acid *via* gold, and several attempts were made to do so. However, initial results were not encouraging, with either gold(0) or the original phosphine carbaborane compound (minus gold) being recovered. This area of research is still in its early stages of development and, unfortunately, time constraints did not allow further investigation. However, future aims beyond the research reported herein have been outlined.

Overall, it can be concluded that phosphine carbaborane gold(I) compounds exhibit similar chemistry to analogous tertiary aryl gold(I) compounds. Consequently, these compounds have the potential to open up a vast new area of carbametallaborane chemistry as well as being possible precursors for BNCT reagents of the future.

4.7 Overall Conclusions

The common theme in this research has been the use of lithium carbaborane containing the {1,2-*closo*-C_2B_{10}} fragment to synthesise some novel carba(metalla)borane compounds, the cage carbon atom either σ-bonded to a (transition) metal or to phosphorus. Characterisation has been successfully accomplished using a variety of (mainly spectroscopic) techniques.

The research of **Chapter 2** was undertaken in order to redress the inconsistencies that have appeared in the discussion of the ligand function of {1,2-*closo*-C_2B_{10}}: For several years this fragment has been considered as an electron withdrawing moiety because of the electron deficiency (in terms of classical electron counting rules) of such polyhedral (carba)boranes. However, the structural studies (NMR spectroscopy, X-ray crystallography and EHMO calculations) described in **Chapter 2** have indicated that, in fact, {1,2-*closo*-C_2B_{10}} acts as a σ-donating ligand. As a consequence of its better donating properties than, for example, methyl, the gold-carbon σ-bond in the carbaborane compounds has been found to be shorter and stronger than in corresponding gold(I) methyl compounds. The revelation that {1,2-*closo*-C_2B_{10}} is a better donor than methyl should not have been entirely unexpected: (Carba)boranes adopt these unusual polyhedral structures to overcome their electron 'deficiency' and are therefore not necessarily electron withdrawers; moreover, since boron is more electropositive than carbon, its atomic orbitals lie at higher energy and, consequently, it would be expected that molecular orbitals with boron character (carbaborane) would lie at higher energy than those without (methyl).

As a result of the assumption that *closo*-carbaborane is an electron withdrawer, σ-carbametallaborane chemistry has tended to concentrate on compounds containing late transition metals (d^6 configuration or greater). Such compounds have been, in

general, found to contain relatively weak metal-carbon σ-bonds. The conclusions to **Chapter 2** intimated that potentially more stable (class 3) σ-carbametallaborane compounds could be formed with early transition metal complexes. Indeed, it could generally be assumed that if the σ-alkyl compound is known then the σ-carbaborane compound could be synthesised. Therefore, the research in **Chapter 3** involved the synthesis and characterisation of titanium(IV) σ-carbaborane compounds. The conclusions that have been drawn from **Chapter 3** are that titanium(IV) σ-carbaborane compounds can be successfully synthesised and show improved thermal stability (if not air- and moisture- stability) in comparison to their methyl analogues. The increased thermal stability was not unexpected because {1,2-*closo*-C_2B_{10}} does not have any β-hydrogen atoms required in the mechanism of decomposition of many metal alkyl species. Further, the tendency for titanium(IV) to prefer a high coordination number has been demonstrated by intramolecular coordination of the oxygen atom of the carbaborane ether substituent. Future work in this area could include the synthesis of group 4 and 5, and of lanthinide and actinide class 3 σ-carbametallaboranes.

Finally, in a similar manner to the synthesis of the σ-carbametallaborane compounds, **Chapter 4** describes the synthesis of carbaboranes in which the {1,2-*closo*-C_2B_{10}} fragment is σ-bonded to phosphorus of a phosphine. This phosphine carbaborane has been found to be less basic, but with a larger cone angle, than PPh_3. It has been used as a phosphine ligand in the synthesis of analogous {PPh_3Au} compounds including a σ-carbaborane congruous to those described in **Chapter 2** and a mononuclear carbaborane-borane compound. Attempts to use phosphine carbaborane gold(I) to synthesise a carbaborane amino-acid (as a potential BNCT reagent) have been initially unsuccessful but there remains tremendous scope for future work.

Therefore, the overall aims, to synthesise and characterise some novel

carba(metalla)borane compounds from lithium carbaborane, have generally been satisfactorily met. The successful synthesis of σ-carbaborane and phosphine carbaborane metal compounds have consequently opened up potentially vast new areas in carbaborane chemistry.

CHAPTER 5
EXPERIMENTAL

5.1 Introduction

The experimental techniques employed in the synthesis, characterisation and structural analysis of the compounds described in **Chapters 2 - 4** are explained herein.

The synthetic methods used in the preparation of the compounds along with their microanalysis and IR and NMR spectral data are outlined in **Section 5.2.**

Crystallographic methods and experimental details of each structure determination are described in **Section 5.3.**

The extended Hückel molecular orbital calculation method is described in **Section 5.4.** The idealised models used in the calculations are also reported.

5.2 Synthetic Methods

5.2.1 General Techniques

All syntheses were carried out in an atmosphere of dry, oxygen-free nitrogen using standard Schlenk-line techniques, with some subsequent manipulations in air.

The solvents dichloromethane, *n*-hexane, tetrahydrofuran (THF) and ethanol were dried and distilled under nitrogen. Diethyl ether and benzene were sodium wire dried. Acetonitrile and methanol (both HPLC grade) were used as received. All solvents were degassed, either by saturating with nitrogen or by the freeze-pump-thaw method, just before use. Similarily, H_2O was distilled, deionised and degassed (nitrogen saturation) prior to use. Preparative TLC was performed using glass plates coated with Kieselgel 60 F_{254} (0.2 mm thick) which were prewashed with pure eluant.

NMR spectra were recorded at ambient temperature from $CDCl_3$ or d_6-acetone solutions on JEOL FX90Q ($^{31}P\{^1H\}$), Bruker WP200SY ($^{11}B\{^1H\}/^{11}B$ and ^1H) and Varian 600 (^{11}B-^{11}B COSY) spectrometers. Techniques for recording ^{11}B-^{11}B COSY NMR spectra have been reported previously[122]. Chemical shifts are quoted relative to external 85% H_3PO_4 ($^{31}P\{^1H\}$), $BF_3.OEt_2$ ($^{11}B\{^1H\}/^{11}B$) and $SiMe_4$ (^1H). IR spectra were obtained either as KBr pellets or as CH_2Cl_2 or THF solutions using CaF_2 plates and referenced against pure solvent on Perkin-Elmer 1600 FTIR or 598 IR spectrophometers. Microanalyses (C, H and N elemental analyses) were performed by the sporadic departmental service.

5.2.2 Synthesis of Starting Materials

PR_3AuCl[59] (R = Ph, *o*-tol, Cy and Et), thtAuCl[123] (tht = *cy*-C_4H_8S),

1-CH_3OCH_2-1,2-*closo*-$C_2B_{10}H_{11}$[20] and 1-Ph-2-{$CpFe(CO)_2$}-1,2- *closo*-$C_2B_{10}H_{10}$[48] were prepared by literature methods. The starting materials $CpTiCl_3$, Cp_2TiCl_2, 2,2'-bipyridyl, PPh_2Cl, $Tl[OOCCH_3]$, MeLi (1.4M solution in Et_2O) and *n*-BuLi (1.6M solution in hexanes) were used as received.

$AsPh_3AuCl$ was prepared in a similar way to that described[59] for PPh_3AuCl (Yield: 88%. Microanalysis: Calculated (for $C_{18}H_{15}AsAuCl$) %C 40.1; %H 2.81; Found: %C 40.3; %H 2.86.)

1-Ph-1,2-*closo*-$C_2B_{10}H_{11}$ (**2**) was synthesised in improved yield by a modified method to that reported in the literature[11]: *Nido*-$B_{10}H_{14}$ (4.0g, 32.8mmol), CH_3CN (2.7g, 65.8mmol) and PhC≡CH (3.35g, 32.8mmol) were stirred for 1h at room temperature in 45cm^3 benzene before refluxing for 70h. After cooling, the volatiles were removed *in vacuo* leaving a yellow oil. The product was extracted into *n*-pentane (5 x 20cm^3), filtered and the *n*-pentane removed *in vacuo* affording the white waxy solid of essentially pure 1-Ph-1,2-*closo*-$C_2B_{10}H_{11}$. Crystallisation from CH_3OH/H_2O (1:6) at room temperature produced colourless needle crystals of **2** in 52% yield.

Microanalysis: Calculated (for $C_8H_{16}B_{10}$): %C 43.6, %H 7.32; Found: %C 43.6, %H 7.44

IR ($CHCl_3$): ν_{max}/cm^{-1}: 2595 (B-H); 2910 (C_{cage}-H)

NMR ($CDCl_3$): $^{11}B\{^1H\}$ (δ/ppm): -1.30 (1B), -3.59 (1B), -8.18 (2B), -10.17 (4B), -12.01 (2B); $^1J_{B-H}$ = 121-149 Hz

^1H (δ/ppm): 7.58-7.33 (m, 5H, C_6H_5), 3.97 (broad, 1H, C_{cage}-*H*)

Li[1-R-1,2-*closo*-$C_2B_{10}H_{10}$] (R = CH_3OCH_2 or Ph) was synthesised by (dropwise) addition of 1 equivalent of either 1.4M LiMe in Et_2O or 1.6M *n*-BuLi in hexanes to a

stirring solution of 1-R-1,2-*closo*-$C_2B_{10}H_{11}$ in 10-20cm^3 diethyl ether at 0°C. Effervescence and clouding of the solution was generally observed. The solution of Li[1-R-1,2-*closo*-$C_2B_{10}H_{10}$] was allowed to warm to room temperature and was then used immediately.

5.2.3 Synthesis of 1-Ph-2-{PR_3Au}-1,2-*closo*-$C_2B_{10}H_{10}$ (3)

To a stirred suspension of 0.26g (0.53mmol) PPh_3AuCl in 15cm^3 Et_2O at room temperature, a 10cm^3 ethereal solution of 0.53mmol Li[1-Ph-1,2-*closo*-$C_2B_{10}H_{10}$] was added dropwise over *ca.* 5 minutes. The solution became pale orange and most of the solid dissolved. After stirring for 1h the mixture was filtered and the filtrate evaporated *in vacuo*. Crystallisation from CH_2Cl_2/*n*-hexane (1:4) at -30°C yielded 1-Ph-2-{PPh_3Au}-1,2-*closo*-$C_2B_{10}H_{10}$ (**3a**) as colourless crystals in 37% yield.

Microanalysis: Calculated (for $C_{26}H_{30}AuB_{10}P$): %C 46.3, %H 4.60; Found: %C 46.0, %H 4.46

IR (KBr): ν_{max}/cm^{-1}: 2562 (B-H)

NMR ($CDCl_3$): $^{31}P\{^1H\}$ (δ/ppm): 38.6

$^{11}B\{^1H\}$ (δ/ppm): -0.42 (1B), -3.45 (1B), -6.99 (4B), -8.34 (4B); $^1J_{B-H}$ = 146-172 Hz

^1H (δ/ppm): 7.86-7.10 (m, C_6H_5)

Similarly, the following colourless crystalline solids were prepared:

1-Ph-2-{P(*o*-tol)$_3$Au}-1,2-*closo*-$C_2B_{10}H_{10}$ (**3b**), in 36% yield.

Microanalysis: Calculated (for $C_{29}H_{36}AuB_{10}P$): %C 47.0, %H 5.06; Found: %C 48.3, %H 5.04

IR (KBr): ν_{max}/cm^{-1}: 2578 (B-H)

NMR ($CDCl_3$): $^{31}P\{^1H\}$ (δ/ppm): 16.6

$^{11}B\{^1H\}$ (δ/ppm): -0.63 (1B), -3.24 (1B), -6.92 (4B), -8.43 (4B); $^1J_{B-H}$ = 139-167 Hz

^1H (δ/ppm): 7.72-6.62 (m, 17H, aryl *H*), 2.35 (s, 9H, $C_6H_4CH_3$)

1-Ph-2-{PCy_3Au}-1,2-$C_2B_{10}H_{10}$ (**3c**), in 31% yield.

Microanalysis: Calculated (for $C_{26}H_{48}AuB_{10}P$): %C 44.4, %H 6.89; Found: %C 44.8, %H 6.95

IR (KBr): ν_{max}/cm^{-1}: 2568 (B-H)

NMR ($CDCl_3$): $^{31}P\{^1H\}$ (δ/ppm): 55.2

$^{11}B\{^1H\}$ (δ/ppm): -0.60 (1B), -3.54 (1B), -6.98 (4B), -8.45 (4B); $^1J_{B-H}$ = 152-176 Hz

^1H (δ/ppm): 7.81-7.15 (m, 5H, C_6H_5), 1.84-1.15 (m, 33H, C_6H_{11})

5.2.4 Synthesis of 1-Ph-2-{$AsPh_3Au$}-1,2-*closo*-$C_2B_{10}H_{10}$ (3e)

This was prepared in a similar way to **3a** with dropwise addition of an ethereal solution of Li[1-Ph-1,2-*closo*-$C_2B_{10}H_{10}$] to a stirring suspension of $AsPh_3AuCl$. Crystallisation yielded colourless crystals of 1-Ph-2-{$AsPh_3Au$}-1,2-*closo*-$C_2B_{10}H_{10}$ (**3e**) in 38% yield.

Microanalysis: Calculated (for $C_{26}H_{30}AsAuB_{10}$): %C 43.3, %H 4.34; Found: %C 43.2, %H 4.19

IR (KBr): ν_{max}/cm^{-1}: 2582 (B-H)

NMR ($CDCl_3$): $^{11}B\{^1H\}$ (δ/ppm): -0.27 (1B), -3.43 (1B), -6.95 (4B), -8.55 (4B); $^1J_{B-H}$ = 144-176 Hz

^1H (δ/ppm): 7.90-7.12 (m, C_6H_5)

5.2.5 Synthesis of 1-CH_3OCH_2-2-{PR_3Au}-1,2-*closo*-$C_2B_{10}H_{10}$ (4)

An ethereal solution of (10cm^3) 0.51mmol Li[1-CH_3OCH_2-1,2-*closo*-$C_2B_{10}H_{10}$] was added dropwise to a stirring suspension of 0.25g (0.51mmol) PPh_3AuCl in 15cm^3 Et_2O at room temperature. Immediately most of the solid dissolved and the solution acquired an orange tinge. The mixture was filtered after stirring for 1h and the volatiles evaporated *in vacuo*. Slow diffusion of *n*-hexane into a dichloromethane solution (4:1) at -30°C afforded colourless crystals of 1-CH_3OCH_2-2-{PPh_3Au}-1,2-*closo*-$C_2B_{10}H_{10}$ (**4a**) in 38% yield.

Microanalysis: Calculated (for $C_{22}H_{30}AuB_{10}OP$): %C 40.9, %H 4.68; Found: %C 40.3, %H 4.84

IR (KBr): ν_{max}/cm^{-1}: 2556 (B-H); 1435, 1382, 1111 (CH_3OCH_2)

NMR ($CDCl_3$): $^{31}P\{^1H\}$ (δ/ppm): 38.6

$^{11}B\{^1H\}$ (δ/ppm): (a) 64.21 MHz: -0.97 (1B), -3.97 (1B), -7.27 (2B), -9.27 (6B); $^1J_{B-H}$ = 148-183 Hz; (b) 192.63 MHz: -1.18 [1B, B(12)], -3.99 [1B, B(9)], -7.27 [2B, B(8)/B(10)], -8.62 [2B, B(4)/B(5)], -9.73 [4B, B(7)/B(11) & B(3)/B(6)]; $^1J_{B-H}$ = 141-182 Hz

^1H (δ/ppm): 7.56-7.32 (m, 15H, C_6H_5), 3.89 (s, 2H, CH_2), 3.27 (s, 3H, CH_3)

The following analogous colourless crystalline compounds were prepared in a similar way:

1-CH_3OCH_2-2-{P(*o*-tol)$_3$Au}-1,2-*closo*-$C_2B_{10}H_{10}$ (**4b**) in 37% yield.

Microanalysis: Calculated (for $C_{25}H_{36}AuB_{10}OP$): %C 43.8, %H 5.23; Found: %C 43.6, %H 5.27

IR (KBr): ν_{max}/cm^{-1} 2575 (B-H); 1446, 1384, 1108 (CH_3OCH_2)

NMR ($CDCl_3$): $^{31}P\{^1H\}$ (δ/ppm): 16.6

$^{11}B\{^1H\}$ (δ/ppm): -1.49 (1B), -3.95 (1B), -7.35 (2B), -9.68 (6B); $^1J_{B-H}$ = 145-178 Hz

^1H (δ/ppm): 7.77-6.73 (m, 12H, $C_6H_4CH_3$), 3.78 (s, 2H, OCH_2), 3.12 (s, 3H, OCH_3), 2.67 (s, 9H, $C_6H_4CH_3$)

1-CH_3OCH_2-2-{PCy_3Au}-1,2-*closo*-$C_2B_{10}H_{10}$ (**4c**) in 32% yield.

Microanalysis: Calculated (for $C_{22}H_{48}AuB_{10}OP$): %C 40.9, %H 7.47; Found: %C 39.8, %H 7.28

IR (KBr): ν_{max}/cm^{-1} 2565 (B-H); 1440, 1382, 1114 (CH_3OCH_2)

NMR ($CDCl_3$): $^{31}P\{^1H\}$ (δ/ppm): 55.6

$^{11}B\{^1H\}$ (δ/ppm): -1.36 (1B), -4.14 (1B), -7.28 (2B), -9.71 (6B); $^1J_{B-H}$ = 156-200 Hz

^1H (δ/ppm): 3.82 (s, 2H, OCH_2), 3.33 (s, 3H, OCH_3), 2.14-1.21 (m, 33H, C_6H_{11})

5.2.6 Synthesis of 1-CH_3OCH_2-2-{PEt_3Au}-1,2-*closo*-$C_2B_{10}H_{10}$ (**4d**)

This was prepared in a similar manner to **4a** except that the crude product recovered from the filtrate was purified by TLC with CH_2Cl_2 eluant, the pale orange band at R_f = 0.9 being subsequently isolated. Further purification by crystallisation from CH_2Cl_2/*n*-hexane at -30°C produced 1-CH_3OCH_2-2-{PEt_3Au}-1,2-*closo*-$C_2B_{10}H_{10}$ (**4d**) in 26% yield.

Microanalysis: Calculated (for $C_{10}H_{30}AuB_{10}OP$): %C 23.9, %H 6.02; Found: %C 23.2, %H 6.02

IR (KBr): ν_{max}/cm^{-1}: 2555 (B-H): 1433, 1381, 1106 (CH_3OCH_2)

NMR ($CDCl_3$): $^{31}P\{^1H\}$ NMR (δ/ppm): 37.2

$^{11}B\{^1H\}$ (δ/ppm): -1.48 (1B), -4.09 (1B), -7.20 (2B), -9.71 (6B); $^1J_{B-H}$ = 152-200 Hz

^1H (δ/ppm): 3.82 (s, 2H, OCH_2), 3.32 (s, 3H, OCH_3), 1.73 (t, $^3J_{H-H}$ = 22Hz, 9H, CH_2CH_3), 1.22 (q, $^3J_{H-H}$ = 22 Hz, 6H, CH_2CH_3)

5.2.7 Synthesis of 1-CH_3OCH_2-2-{$AsPh_3Au$}-1,2-*closo*-$C_2B_{10}H_{10}$ (**4e**)

Similarly to the synthesis of **4a**, reaction of $AsPh_3AuCl$ with Li[1-CH_3OCH_2-1,2-*closo*-$C_2B_{10}H_{10}$] afforded 1-CH_3OCH_2-2-{$AsPh_3Au$}-1,2-*closo*- $C_2B_{10}H_{10}$ (**4e**), after crystallisation (CH_2Cl_2/*n*-hexane [1:4] at -30°C), as colourless crystals in 31% yield.

Microanalysis: Calculated (for $C_{22}H_{30}AsAuB_{10}O$): %C 38.6, %H 4.71; Found: %C 38.3, %H 4.38

IR (KBr): ν_{max}/cm^{-1} 2562 (B-H); 1448, 1385, 1112 (CH_3OCH_2)

NMR ($CDCl_3$): $^{11}B\{^1H\}$ (δ/ppm): -1.34 (1B), -4.01 (1B), -7.28 (2B), -8.78 (6B); $^1J_{B-H}$ = 146-169 Hz

^1H (δ/ppm): 7.56-7.46 (m, 15H, C_6H_5), 3.93 (s, 2H, CH_2), 3.31 (s, 3H, CH_3)

5.2.8 Reaction of 4e with PPh_3

To a stirred solution of 0.017g (0.026 mmol) 1-CH_3OCH_2-2-{$AsPh_3Au$}-1,2-*closo*-$C_2B_{10}H_{10}$ (**4e**) in 5cm^3 CH_2Cl_2 at room temperature, a solution of 0.007g (0.026mmol) PPh_3 in 3cm^3 CH_2Cl_2 was added. After 2h the solvent was removed *in vacuo* and 5cm^3 Et_2O added. The resultant solid and solution were separated by filtration, the solid washed with a further 5cm^3 Et_2O, the washings added to the filtrate. Microanalysis of the solid indicated $AsPh_3$:

Calculated (for $C_{18}H_{15}As$): %C 70.6, %H 4.94; Found %C 69.1, %H 4.19

Solvent was evaporated from the filtrate *in vacuo* and the resultant off-white solid was identified as 1-CH_3OCH_2-2-{PPh_3Au}-1,2-*closo*-$C_2B_{10}H_{10}$ (**4a**) by IR and NMR spectroscopies:

IR (KBr): ν_{max}/cm^{-1} 2558 (B-H); 1437, 1382, 1110 (CH_3OCH_2)

NMR ($CDCl_3$): $^{31}P\{^1H\}$ (δ/ppm): 38.6

5.2.9 Synthesis of $AsPh_3AuMe$ (5)

To a stirring solution of 0.25g (0.81mmol) of $AsPh_3AuCl$ in 10cm^3 THF at 0°C, 0.75cm^3 (1.05mmol) MeLi (1.4M) in 5cm^3 Et_2O were added dropwise over *ca.* 15

minutes. A further 5cm^3 Et_2O were used to wash in any remaining MeLi. The mixture was allowed to warm to room temperature before the dropwise addition of 5cm^3 H_2O. The aqueous layer was syringed off immediately and anhydrous $MgSO_4$ was added to dry the ethereal layer. After stirring for 1h, the mixture was filtered, the magnesium sulphate washed with (2 x 15cm^3) Et_2O, and the volatiles were removed from the filtrate *in vacuo* affording a grey solid. Crystallisation from CH_2Cl_2/*n*-hexane (1:4) at -30°C produced colourless crystals of $AsPh_3AuMe$ (**5**) in 52% yield.

Microanalysis: Calculated (for $C_{19}H_{18}AsAu$): %C 44.0, %H 3.50; Found: %C 44.2, %H 3.76

NMR ($CDCl_3$): ^1H (δ/ppm): 7.46-7.38 (m, 15H, C_6H_5), 0.63 (s, 3H, CH_3)

5.2.10 Reaction of **5** with PPh_3

A solution of PPh_3 (0.01g, 0.04mmol) in 5cm^3 CH_2Cl_2 was added dropwise to a stirring solution of $AsPh_3AuMe$ (**5**; 0.02g, 0.04mmol) in 5cm^3 CH_2Cl_2 at 0°C. After 2h the solvent was removed *in vacuo* affording a white solid. Analysis of the solid by $^{31}P\{^1H\}$ NMR spectroscopy indicated only one phosphorus containing species identified, by comparison with the literature[86], as PPh_3AuMe.

NMR ($CDCl_3$): $^{31}P\{^1H\}$ (δ/ppm): 47.3

5.2.11 Attempted Deboronation of **4a**

0.05g (0.08mmol) of 1-CH_3OCH_2-2-{PPh_3Au}-1,2-*closo*-$C_2B_{10}H_{10}$ (**4a**) were suspended and 0.025g (0.45mmol; 6-fold excess) KOH were dissolved in 30cm^3 EtOH and the mixture stirred at room temperature for 1h. On heating all the solid dissolved and the mixture was refluxed for 3h. Cooling to room temperature resulted

in the precipitation of a white solid which was filtered from the ethanolic solution. Analysis of the solid indicated the recovery of **4a**:

Microanalysis: Calculated (for $C_{22}H_{30}AuB_{10}OP$): %C 40.9, %H 4.68; Found: %C 39.5, %H 4.68

NMR ($CDCl_3$): $^{31}P\{^1H\}$ (δ/ppm): 38.6

Removal of EtOH *in vacuo* revealed a white solid which showed no ν(B-H) in the IR spectrum. Therefore, deboronation of **4a** had not been achieved.

5.2.12 Attempted Deboronation of 1-Ph-2-{$CpFe(CO)_2$}-1,2-*closo*-$C_2B_{10}H_{10}$

0.37g (0.94mmol) of 1-Ph-2-{$CpFe(CO)_2$}-1,2-*closo*-$C_2B_{10}H_{10}$ and a 6 fold excess of KOH (0.31g, 5.54mmol) in 35cm^3 ethanol were stirred at room temperature for 1h before refluxing for 3h. On cooling, the brown solution was filtered and the ethanol removed *in vacuo* on a high vacuum rotary evaporator. Addition of water to the resultant waxy brown solid yielded a colourless solution and a dark solid which was filtered off. To the aqueous solution, 0.49g (1.86mmol) of $Tl[OOCCH_3]$ in 10cm^3 H_2O were added revealing a copious amount of an intense yellow precipitate which was filtered and washed with EtOH (3 x 15cm^3) and Et_2O (3 x 15cm^3). The yellow solid was identified as Tl_2[7-Ph-7,8-*nido*-$C_2B_9H_{10}$] and the brown solid as $[CpFe(CO)_2]_2$ indicating cleavage of Fe-C_{cage} σ-bond and subsequent deboronation of the carbaborane compound.

Yellow Solid:

Microanalysis: Calculated (for $C_8H_{15}B_9Tl_2$): %C 15.6, %H 2.45; Found: %C 15.8, %H 2.56

IR (KBr): ν_{max}/cm^{-1} 2502, 2439, 2379 (B-H)

Brown solid:

Microanalysis: Calculated (for $C_{14}H_{10}Fe_2O_4$): %C 47.5, %H 2.85; Found: %C 46.6, % H 2.77

IR (CH_2Cl_2): ν_{max}/cm^{-1} 1994, 1960 (C≡O) 1772 (μ-C≡O)

5.2.13 Synthesis of 1-CH_3OCH_2-2-{$TiCl_3$}-1,2-*closo*-$C_2B_{10}H_{10}$ (6)

1.0cm^3 of a 1M $TiCl_4$ (1.0mmol) solution in CH_2Cl_2 was added to a frozen solution (-196°C) of Li[1-CH_3OCH_2-1,2-*closo*-$C_2B_{10}H_{10}$] (1.0mmol) in Et_2O (10cm^3). The reaction mixture was allowed to warm slowly to room temperature and a colour change from brown to yellow-green was observed. The mixture was stirred for 1h at room temperature before filtering through 1cm of Celite®. Removal of the volatiles of the filtrate *in vacuo* afforded a green-yellow oil which was triturated with *n*-hexane and dried *in vacuo* overnight. The crystalline green solid obtained was found to be air- and moisture-sensitive. Yield: 44%

Microanalysis: Calculated (for $C_4H_{15}B_{10}Cl_3OTi$): %C 14.1, %H 4.43: Found: %C 13.2, %H 4.43

IR (Et_2O): ν_{max}/cm^{-1} 2590 (B-H); 1445, 1377, 1114 (CH_3OCH_2)

NMR (d_6-acetone): $^{11}B\{^1H\}$ (δ/ppm): -1.98 (1B), -3.47 (1B), -5.03 (2B), -8.88 (2B), -10.67 (2B), -12.24 (2B); $^1J_{B-H}$ = 142-190 Hz

^1H (δ/ppm): 4.48 (s, 2H, CH_2), 4.08 (s, 3H, CH_3)

5.2.14 Synthesis of 1-CH_3OCH_2-2-{(bipy)$TiCl_3$}-1,2-*closo*-$C_2B_{10}H_{10}$ (7)

To a stirring Et_2O ($10cm^3$) solution of 0.05g (0.15mmol) 1-CH_3OCH_2-2-{$TiCl_3$}-1,2-*closo*-$C_2B_{10}H_{10}$ (**6**) at room temperature, was added 0.03g (0.19mmol) 2,2'-bipyridyl in $5cm^3$ Et_2O. Immediate precipitation of an off-white solid was observed. After stirring for 0.5h the solid was recovered by filtration and then purified by stirring with $50cm^3$ *n*-hexane for 1h (to remove any excess 2,2'-bipyridyl). The pale-pink solid was filtered, washed with Et_2O (2 x $15cm^3$) and dried *in vacuo*. The solid, identified as 1-CH_3OCH_2-{(bipy)$TiCl_3$}-1,2-*closo*-$C_2B_{10}H_{10}$ (**7**), and found to be insensitive to air and moisture, was obtained in 76% yield.

Microanalysis: Calculated (for $C_{14}H_{23}N_2B_{10}Cl_3OTi$): %C 33.8, %H 4.66 %N 5.63; Found: %C 35.1, %H 4.95, %N 6.08;

IR (KBr): ν_{max}/cm^{-1}: 2591 (B-H); 1442, 1394, 1135 (CH_3OCH_2)

5.2.15 Synthesis of 1-CH_3OCH_2-2-{$CpTiCl_2$}-1,2-*closo*-$C_2B_{10}H_{10}$ (8)

0.46 mmol of Li[1-CH_3OCH_2-1,2-*closo*-$C_2B_{10}H_{10}$] in $10cm^3$ Et_2O were added dropwise to a stirring suspension of $CpTiCl_3$ (0.10g, 0.46mmol) in $15cm^3$ Et_2O. The mixture immediately turned orange and was stirred for a further 1h. The partially ether-soluble orange product was filtered and the solid recovered was dissolved in CH_2Cl_2 and added to the solid obtained by removing Et_2O *in vacuo*. A spot TLC (CH_2Cl_2 eluant) indicated a single (and therefore pure) compound. The product was crystallised by the slow diffusion of *n*-hexane into a dichloromethane solution (4:1) at -30°C, producing small orange platelets in 49% yield.

Microanalysis: Calculated (for $C_9H_{20}B_{10}Cl_2OTi$): %C 29.1, %H 5.43; Found: %C 29.5, %H 5.49

IR (KBr): ν_{max}/cm^{-1} 2585 (B-H); 1483, 1407, 1119 (CH_3OCH_2)

NMR ($CDCl_3$): $^{11}B\{^1H\}$ (δ/ppm): -2.41 (1B), -3.53 (1B), -5.19 (2B), -8.52 (2B), -10.82 (2B), -12.41 (2B); $^1J_{B-H}$ = 133-198

^1H (δ/ppm): 6.92 (s, 5H, C_5H_5), 4.23 (s, 2H, CH_2), 3.71 (s, 3H, CH_3)

5.2.16 Reactions of Cp_2TiCl_2 with Li[1-CH_3OCH_2-1,2-*closo*-$C_2B_{10}H_{10}$]

1:1 Reaction

A 10cm^3 diethyl ether (or benzene) solution of (2.0 mmol) Li[1-CH_3OCH_2-1,2-*closo*-$C_2B_{10}H_{10}$] was added dropwise to a stirring suspension (or solution) of 0.50g (2.0 mmol) Cp_2TiCl_2 in 10cm^3 Et_2O (or C_6H_6). No immediate change was observed but after stirring for 4h (1h) at room temperature, an orange solid had been produced. Filtration followed by crystallisation of the solid from CH_2Cl_2/*n*-hexane (1:4) yielded small orange crystals. Both these orange crystals and the pale orange solid recovered from the filtrate were analysed, the former found to be Cp_2TiCl (**9**) which had cocrystallised with one molecule of CH_2Cl_2 and the latter found to contain 1-CH_3OCH_2-1,2-*closo*-$C_2B_{10}H_{11}$ (**1**) among other (unidentified) species.

Orange crystals

Microanalysis: Calculated (for $C_{10}H_{10}ClTi.CH_2Cl_2$): %C 44.3, %H 4.05; Found: %C

44.1, %H 4.23

NMR ($CDCl_3$): ^1H (δ/ppm): 6.30 (s, 10H, C_5H_5), 5.25 (s, 2H, CH_2Cl_2)

Pale orange solid

NMR ($CDCl_3$): ^1H (δ/ppm): 4.00 (broad, 1H, C_{cage}-*H*), 3.79 (s, 2H, OCH_2), 3.36 (s, 3H, OCH_3)

1:2 Reaction

To a stirring solution of 0.50g (2.0 mmol) Cp_2TiCl_2 in $10cm^3$ benzene, a solution of 4.0 mmol Li[1-CH_3OCH_2-1,2-*closo*-$C_2B_{10}H_{10}$] in $10cm^3$ Et_2O was added dropwise. No reaction was initially observed and the reaction mixture was stirred for 24h at room temperature. An air-sensitive green solution and an orange solid were obtained. The mixture was filtered and the solvent removed from the filtrate to reveal a green oil which, after *ca.* 1h, had decomposed (under an atmosphere of dry oxygen-free nitrogen) to an orange oil. Both the orange solid and orange oil were analysed. The former was found to be Cp_2TiCl, compound **9**, and the latter was shown to contain, among other species, a mixture of compound **9** and 1-CH_3OCH_2-1,2-*closo*-$C_2B_{10}H_{11}$ (**1**).

Orange solid

NMR ($CDCl_3$): ^1H (δ/ppm): 6.30 (s, C_5H_5)

Orange oil

NMR ($CDCl_3$): ^1H (δ/ppm): 6.58 (s, relative integral [RI] 3.2, C_5H_5), 6.53 (s, RI 0.4, C_5H_5), 6.30 (s, RI 0.9, C_5H_5), 4.00 (broad, RI 1, $C_{cage}H$), 3.79 (s, RI 2, OCH_2), 3.36 (s, RI 3, OCH_3)

5.2.17 Synthesis of 1-CH_3OCH_2-2-PPh_2-1,2-*closo*-$C_2B_{10}H_{10}$ (**11**)

4.0cm^3 (6.40mmol) of *n*-BuLi (1.6M in hexanes) were added dropwise to a stirring solution of 1.0g (5.32mmol) 1-CH_3OCH_2-1,2-*closo*-$C_2B_{10}H_{11}$ in 20cm^3 benzene at 0°C. The mixture was warmed to room temperature and after *ca.* 5 minutes a white precipitate was observed. After stirring for 0.5h at room temperature, 1.17g (5.32mmol) of pale yellow liquid PPh_2Cl were added, dropwise, producing an orange colouration in the reaction mixture. The reaction mixture was stirred for 1h at room temperature before refluxing for 3h. After allowing to cool, the mixture was filtered and the volatiles removed *in vacuo* revealing a pale yellow oil. Addition of 20cm^3 *n*-hexane precipitated an off-white, waxy solid. The solid was washed with a further (10cm^3) portion of *n*-hexane before drying *in vacuo*. 1-CH_3OCH_2-2-PPh_2-1,2-*closo*-$C_2B_{10}H_{10}$ (**11**) was obtained in 57% yield.

Microanalysis: Calculated (for $C_{16}H_{25}B_{10}OP$): %C 51.6, %H 6.77; Found: %C 52.5, %H 7.05

IR (KBr): ν_{max}/cm^{-1} 2582 (B-H); 1458, 1383, 1115 (CH_3OCH_2)

NMR ($CDCl_3$): $^{31}P\{^1H\}$ (δ/ppm): 12.5

$^{11}B\{^1H\}$ (δ/ppm): 0.15 (1B), -2.52 (1B), -8.78 (8B); $^1J_{B-H}$ = 141-164 Hz

^1H (δ/ppm): 7.89-7.80 (m, 4H, $C_6H_2H_3$), 7.46-7.38 (m, 6H, $C_6H_2H_3$), 4.19 (s, 2H, OCH_2), 3.39 (s, 3H, OCH_3)

5.2.18 Reaction of **11** with $HAuCl_4.3H_2O$

0.25g (0.67 mmol) of 1-CH_3OCH_2-2-PPh_2-1,2-*closo*-$C_2B_{10}H_{10}$ (**11**) in 10cm^3

EtOH were added to a stirring solution of 0.13g (0.33mmol) $HAuCl_4.3H_2O$ in $25cm^3$ EtOH at 0°C. After *ca.* 5 minutes the solution changed colour from yellow to green and a small amount of a purple-black solid (colloidal gold) had precipitated out. After 4h copious amounts of the dark solid had been produced indicating reduction of Au^{III} to Au^0. The reaction was not pursued.

5.2.19 Synthesis of 1-CH_3OCH_2-2-{PPh_2AuCl}-1,2-*closo*-$C_2B_{10}H_{10}$ (12)

To a cooled (0°C) solution of thtAuCl (0.43g, 1.34mmol) in $40cm^3$ CH_2Cl_2, a solution of 1-CH_3OCH_2-2-PPh_2-1,2-*closo*-$C_2B_{10}H_{10}$ (0.50g, 1.34mmol in $10cm^3$ CH_2Cl_2) was added dropwise. The solution slowly turned black due to some decomposition. The mixture was allowed to warm to room temperature before being stirred for 20 minutes. The solvent was then reduced to $5cm^3$ *in vacuo* and precipitation of the product was achieved by addition of $10cm^3$ *n*-hexane. The off-white solid produced was filtered and washed with $10cm^3$ *n*-hexane. Cooling the filtrate yielded further product. Crystallisation from CH_2Cl_2/*n*-hexane (1:3) at -30°C afforded colourless crystals of 1-CH_3OCH_2-2-{PPh_2AuCl}-1,2-*closo*-$C_2B_{10}H_{10}$ (**12**) in 89% yield.

Microanalysis: Calculated (for $C_{16}H_{25}AuB_{10}ClOP$): %C 31.8, %H 4.13; Found: %C 31.7, %H 4.21

IR (KBr): ν_{max}/cm^{-1}: 2577 (B-H) 1435, 1384, 1110 (CH_3OCH_2)

NMR ($CDCl_3$): $^{31}P\{^1H\}$ (δ/ppm): 54.6

$^{11}B\{^1H\}$ (δ/ppm): 1.68 (1B), -1.51 (1B), -9.06 (8B); $^1J_{B-H}$ = 145-208 Hz

^1H (δ/ppm): 8.19-8.05 (m, 4H, $C_6H_2H_3$), 7.66-7.43 (m, 6H, $C_6H_2H_3$), 4.34 (s, 2H,

OCH_2), 3.17 (s, 3H, OCH_3)

5.2.20 Synthesis of 1-CH_3OCH_2-2-{PPh_2AuMe}-1,2-*closo*-$C_2B_{10}H_{10}$ (13)

To 1.4g (2.32 mmol) of 1-CH_3OCH_2-2-{PPh_2AuCl}-1,2-*closo*-$C_2B_{10}H_{10}$ (**12**) suspended in 20cm^3 Et_2O and cooled to -78°C, 1.75cm^3 (2.45 mmol) of ethereal MeLi were added dropwise. The mixture was allowed to warm to room temperature during which time the solution adopted an orange tinge and most of the solid dissolved. Once at room temperature, the mixture was filtered through 2cm Celite® and the solvent removed from the pale yellow filtrate *in vacuo*. The off-white solid of 1-CH_3OCH_2-2-{PPh_2AuMe}-1,2-*closo*-$C_2B_{10}H_{10}$ (**13**) was recovered in 63% yield.

Microanalysis: Calculated (for $C_{17}H_{28}AuB_{10}OP$): %C 34.9, %H 4.83; Found %C 34.5, %H 4.90

IR (KBr): ν_{max}/cm^{-1}: 2565 (B-H); 1438, 1379, 1108 (CH_3OCH_2)

NMR ($CDCl_3$): $^{31}P\{^1H\}$ (δ/ppm): 62.9

$^{11}B\{^1H\}$ (δ/ppm): 1.41 (1B), -1.87 (1B), -9.02 (8B); $^1J_{B-H}$ = 151-195 Hz

^1H (δ/ppm): 8.26-8.15 (m, 4H, $C_6H_2H_3$), 7.56-7.49 (m, 6H, $C_6H_2H_3$), 4.56 (s, 2H, OCH_2), 3.24 (s, 3H, OCH_3), 0.63 (s, 3H, CH_3)

5.2.21 Synthesis of 1-CH_3OCH_2-2-(1'-CH_3OCH_2-2'-{PPh_2Au}-1',2'-*closo*-$C_2B_{10}H_{10}$)-1,2-*closo*-$C_2B_{10}H_{10}$ (14)

A solution of Li[1-CH_3OCH_2-1,2-*closo*-$C_2B_{10}H_{10}$] (0.32mmol) in 10cm^3 was added dropwise with stirring to a suspension of 0.20g (0.32mmol)

1-CH_3OCH_2-2-{PPh_2AuCl}-$C_2B_{10}H_{10}$ in 15cm^3 Et_2O. A pale orange solution and a dark precipitate were formed immediately. The mixture was stirred at room temperature for 0.5h before separating the solid from the orange solution by filtration through 1cm Celite®. The solid was washed with a further 10cm^3 Et_2O, the washings added to the filtrate. Removal of solvent *in vacuo* revealed an orange oil which, when triturated with *n*-hexane, produced an orange solid. Colourless crystals of 1-CH_3OCH_2-2-(1'-CH_2OCH_3-2'-PPh_2Au-1',2'-*closo*-$C_2B_{10}H_{10}$)-1,2-*closo*-$C_2B_{10}H_{10}$ (**14**) were obtained by slow diffusion of *n*-hexane into a dichloromethane solution (4:1) at -30°C in 31% yield.

Microanalysis: Calculated (for $C_{20}H_{40}AuB_{20}O_2P$): %C 31.8, %H 5.33; Found: %C 32.6, %H 5.57

IR (KBr): ν_{max}/cm^{-1}: 2580 (B-H); 1438, 1436, 1384, 1380, 1112, 1106 (CH_3OCH_2)

NMR ($CDCl_3$): $^{31}P\{^1H\}$ (δ/ppm): 58.8

$^{11}B\{^1H\}$ (δ/ppm): 1.85 (1B), -1.08 (1B), -8.53 (8B) [P-bound carbaborane], -1.68 (1B), -3.95 (1B), -7.44 (2B), -9.48 (6B) [Au-bound carbaborane]

^1H (δ/ppm): 8.18-8.01 (m, 4H, $C_6H_2H_3$), 7.66-7.51 (m, 6H, $C_6H_2H_3$), 4.38 (s, 2H, OCH_2 [P-bound]), 3.93 (s, 2H, OCH_2 [Au-bound]), 3.39 (s, 3H, OCH_3 [Au-bound]), 3.15 (s, 3H, OCH_3 [P-bound])

5.2.22 Synthesis of 1-CH_3OCH_2-2-(5',6'-{μ-PPh_2Au}-*nido*-$B_{10}H_{13}$}-1,2-*closo*-$C_2B_{10}H_{10}$ (**15**)

A solution of 0.10g (0.82 mmol) *nido*-$B_{10}H_{14}$ in 5cm^3 CH_2Cl_2 was added dropwise to a solution of 1-CH_3OCH_2-2-{PPh_2AuMe}-1,2-*closo*-$C_2B_{10}H_{10}$ (0.48g;

0.82 mmol) in 10cm^3 CH_2Cl_2. A pale yellow colouration and effervescence were initially observed but after *ca.* 2 minutes both had faded. The mixture was stirred for 30 minutes before removing the solvent *in vacuo* and recovering a pale orange solid. The product was purified firstly by stirring the solid with *n*-hexane for 30 minutes and then, after decanting off the *n*-hexane, by redissolving it in a minimum of CH_2Cl_2 and precipitating it out with 10cm^3 *n*-hexane. Filtration and washing with 10cm^3 *n*-hexane afforded compound **15** in reasonable yield (52%).

IR (KBr): 2565 (B-H); 1437, 1384, 1112 (CH_3OCH_2)

NMR ($CDCl_3$): $^{31}P\{^1H\}$ (δ/ppm): 69.1

$^{11}B\{^1H\}$ (δ/ppm): 15.05 (1B), 9.55 (1B), -30.38 (1B), -35.20 (1B); $^1J_{B-H}$ = 140-153 Hz [$B_{10}H_{13}$], -8.74 (8B); $^1J_{B-H}$ = 128 Hz [$C_2B_{10}H_{10}$], 1.43 & -1.19 (8B) [6B from $B_{10}H_{13}$ and 2B from $C_2B_{10}H_{10}$]

^1H (δ/ppm): 8.01-7.90 (m, 4H, $C_6H_2H_3$), 7.66-7.55 (m, 6H, $C_6H_2H_3$), 4.27 (s, 2H, OCH_2), 3.17 (s, 3H, OCH_3)

5.2.23 Reaction of 1-CH_3OCH_2-2-{PPh_2AuCl}-1,2-*closo*-$C_2B_{10}H_{10}$ with [$NHEt_3$][*nido*-$B_{10}H_{13}$]

To 0.11g (0.90 mmol) *nido*-$B_{10}H_{14}$ in 5cm^3 CH_2Cl_2 at room temperature, 0.04g (0.93 mmol) NEt_3 were added dropwise with stirring. The resultant pale yellow solution was then added dropwise to a solution of 0.54g (0.89 mmol) 1-CH_3OCH_2-2-{PPh_2AuCl}-1,2-*closo*-$C_2B_{10}H_{10}$ in 15cm^3 CH_2Cl_2. The solution slowly turned bright orange. After 1h the volatiles were removed *in vacuo* revealing an orange oil which was dried by trituration with *n*-hexane. The crude solid was analysed by NMR spectroscopy and found to contain a small amount of the desired

product (compound **15**). In order to recover this product, prepartive TLC using, initially, CH_2Cl_2 eluant followed by acetone elution was performed. Elution with CH_2Cl_2 produced an orange band at R_f = 0.95 which, from its $^{31}P\{^1H\}$ NMR spectrum contained 1-CH_3OCH_2-2-PPh_2-1,2-*closo*-$C_2B_{10}H_{10}$ as the only phosphorus-containing compound. Acetone elution revealed a further orange band at R_f = 0.8 which was found to contain no phosphorus ($^{31}P\{^1H\}$ NMR spectroscopy).

Crude Compound

NMR ($CDCl_3$): $^{11}B\{^1H\}$ (δ/ppm): 17.08 (Relative Integral (RI) 3), 15.04 (RI 2), 4.81 (RI 1), 1.29 (RI 2), -22.56 (RI 2) [$\{(B_{10}H_{12})_2Au\}^-$], -9.03 (RI 7.2) [compound **12**], 9.51 (RI 0.27), -30.43 (RI 0.27), -35.26 (RI 0.27) [compound **15**], 0.13 (RI 1.8), -2.49 (RI 1.5) [unassigned]

Orange band (CH_2Cl_2 eluant)

NMR ($CDCl_3$): $^{31}P\{^1H\}$ (δ/ppm): 12.5

5.2.24 Synthesis of $CH_3S(AuCl)CH_2CH_2CH(COOH)NHCOCH_3$ (**16**)

A solution of 0.61g (3.2 mmol) N-acetyl-methionine in 10cm^3 THF was added, with stirring, to a suspension of thtAuCl (1.0g; 3.2 mmol) in 10cm^3 THF. The solid immediately dissolved and the mixture was stirred for 30 minutes before reducing the volume of solvent to *ca.* 3cm^3. Addition of 10cm^3 *n*-hexane precipitated out a fine white solid which was allowed to settle. The solution was decanted off and the solid was washed with 2 x 10cm^3 *n*-hexane followed by 3 x 10cm^3 Et_2O. The hygroscopic white solid of N-acetyl S-gold(I) chloride methionine (**16**) was recovered in 78% yield.

Microanalysis: Calculated (for $C_7H_{13}NAuClO_3S$): %C 19.9, %H 3.09, %N 3.31;

Found: %C 21.1, %H 3.39, %N 3.27

IR (THF): ν_{max}/cm^{-1}: 1743, 1680 (C=O)

NMR (D_2O): ^1H (δ/ppm): 3.86 (s, 3H, CH_3S), 3.30 (t, $^3J_{H-H}$ = 3 Hz, SCH_2), 2.17 (s, 3H, CH_3CON). Resonances due to O*H* and C*H* lost under THF solvent resonances.

5.2.25 Reaction of Thallium Carbaboranes with N-acetyl S-gold(I) Chloride Methionine

$Tl[9\text{-}SMe_2\text{-}7,8\text{-}nido\text{-}C_2B_9H_{10}] + CH_3S(AuCl)(CH_2)_2CH(COOH)NHCOCH_3$

A mixture of 0.10g (0.24 mmol) N-acetyl S-gold(I) chloride methionine and 0.10g (0.25 mmol) $Tl[9\text{-}SMe_2\text{-}7,8\text{-}nido\text{-}C_2B_9H_{10}]$ in 25cm^3 THF was allowed to warm to room temperature from -196°C. During this time the mixture went through several colour changes (from colourless to yellow to green) before finally producing a black solid [gold(0)] and brown solution. Once at room temperature the mixture was filtered and the volume of the filtrate reduced to *ca.* 3cm^3. Preparative TLC (CH_2Cl_2 eluant) revealed a brown band at R_f = 0.9 but no other (colourless) bands. Analysis (IR spectroscopy) of the brown solid recovered indicated the presence of borane and the absence of carbonyl. No other products could be isolated from the crude reaction mixture.

$Tl_2[7,8\text{-}(CH_3OCH_2)_2\text{-}7,8\text{-}nido\text{-}C_2B_9H_9] +$
$CH_3S(AuCl)(CH_2)_2CH(COOH)NHCOCH_3$

Similarly, a mixture of 0.10g (0.24 mmol) N-acetyl S-gold(I) chloride methionine, 0.15g (0.24

mmol) $Tl_2[7,8\text{-}(CH_3OCH_2)_2\text{-}7,8\text{-}nido\text{-}C_2B_9H_9]$ and 0.045g (0.24 mmol) benzyl-trimethylammonium chloride in 25cm^3 THF was allowed to warm from -196°C. At *ca.* 0°C, the solution became dark red and a black solid [gold(0)] was deposited. After filtration and reduction of the volume of the filtrate to *ca.* 3cm^3, part of the solution was chromatographed through a Florisil column (mesh 100-200, 2 x 10cm, THF eluant). Only a pink product was recovered which, when analysed by IR spectroscopy, was found to contain neither borane nor carbonyl. Various attempts (spot TLC, trial columns) to separate out any other products were unsuccessful.

5.2.26 Synthesis of $PPh_3AuSCH_2CH(COOMe)NH_2$ (17)

0.50g (1.0 mmol) PPh_3AuCl and 0.17g (0.99 mmol) cysteine methyl ester hydrochloride, $HSCH_2CH(COOMe)NH_3^+Cl^-$, were suspended in 40cm^3 ethanol and 0.09g (2.1 mmol) NEt_3 were added dropwise with stirring. Most of the solid immediately dissolved. The reaction mixture was stirred at room temperature for 1h before the volatiles were removed *in vacuo* revealing a white solid. To remove contaminating NEt_3HCl (identified from ^1H NMR spectrum acquired in $CDCl_3$: δ 3.05 [q, $^3J_{H\text{-}H}$ = 7 Hz, C*H*$_2$] & 1.36 (t, $^3J_{H\text{-}H}$ = 7 Hz, C*H*$_3$]), 15cm^3 THF were added and the colourless solution separated from the fine white precipitate by filtration through 2cm Celite®. THF was evaporated from the filtrate yielding a colourless oil which, on repeated trituration with diethyl ether, afforded a white solid (**17**) in 82% yield.

Microanalysis: Calculated (for $C_{22}H_{23}NAuO_2PS$): %C 44.5, %H 3.91, %N 2.36; Found: %C 43.7, %H 3.88, %N 2.45

IR (THF): ν_{max}/cm^{-1}: 1746 (C≡O)

NMR ($CDCl_3$):$^{31}P\{^1H\}$ (δ/ppm): 38.1

^1H (δ/ppm): 7.62-7.30 (m, 15H, C_6H_5), 4.23 (broad, 2H, NH_2), 3.81 (broad, 1H, SCH_2CH), 3.47 (s, 3H, $COOCH_3$), 3.37 (d, $^2J_{H-H}$ = 4 Hz, 2H, SCH_2CH)

5.2.27 Reaction of 1-CH_3OCH_2-2-{PPh_2AuCl}-1,2-*closo*-$C_2B_{10}H_{10}$ with $HSCH_2CH(COOMe)NH_3^+Cl^-$ / NEt_3

To a suspension of 0.35g (0.58 mmol) 1-CH_3OCH_2-2-{PPh_2AuCl}-1,2-*closo*-$C_2B_{10}H_{10}$ and 0.10g (0.58 mmol) cysteine methyl ester hydrochloride stirring at room temperature in 40cm^3 EtOH, 0.05g (1.16 mmol) NEt_3 were added dropwise. Most of the solid dissolved and the reaction mixture was stirred for a further 2h. The small amount of fine green precipitate was then separated from the colourless solution by filtration through 2cm Celite® and the solvent removed *in vacuo*. The off-white solid obtained was dissolved in CH_2Cl_2 (to remove any unreacted amino-acid), filtered and the solvent evaporated. The solid was then dissolved in THF (to remove NEt_3HCl), filtered, and on removal of THF, a white solid was recovered and identified as containing compound **11**.

White solid (CH_2Cl_2 insoluble)

IR (KBr): ν_{max}/cm^{-1}: 1756 (C≡O)

White solid (THF insoluble)

NMR ($CDCl_3$): ^1H (δ/ppm): 3.06 (q, $^3J_{H-H}$ = 7 Hz. CH_2), 1.36 (t, $^3J_{H-H}$ = 7 Hz, CH_3)

White solid (THF soluble)

IR (THF): ν_{max}/cm^{-1}: 2574 (B-H); 1748 (C≡O)

NMR ($CDCl_3$): $^{31}P\{^1H\}$ (δ/ppm): 12.5

$^{11}B\{^1H\}$ (δ/ppm): 0.14 (1B), -2.56 (1B), -8.79 (8B); $^1J_{B-H}$ = 139-165 Hz

^1H (δ/ppm): 7.86-7.77 (m, 4H, $C_6H_2H_3$), 7.54-7.36 (m, 6H, $C_6H_2H_3$), 4.18 (s, 2H, OCH_2), 3.37 (s, 3H, OCH_3)

5.3 Crystallographic Methods

5.3.1 Introduction

The experimental procedures used in the crystallographic determination of the solid state molecular structures presented in **Chapters 2-4** are described in this section. Obtaining molecular structures from a single crystal involves data collection from a diffraction quality crystal, data processing (reduction) followed by structure solution and refinement, finding the best fit of a model of the compound to the processed data. All X-ray data measurements were made using an Enraf-Nonius CAD4 diffractometer operating with graphite-monochromated Mo-K_α X-radiation [λ_{bar} = 0.71069 Å] and equipped with a ULT-1 low temperature device (N_2 cooling stream). Diffraction quality crystals of **4a, 4e, 5, 8, 12, 14** were obtained as described in the previous section.

5.3.2 General Techniques

Initially, unit cell parameters and orientation matrices were obtained by least-squares refinement of the setting angles of 25 strong, high angle reflections. Data were collected by ω-2θ scans in 96 steps (ω scan width = 0.8 + 0.34tanθ) at variable scan speeds. The collected data were corrected for Lorentz and polarisation effects and, if necessary, for crystal decay during data collection (CADABS[124]). Heavy atoms (Au, Ti) were located either by automatic direct methods (SHELX86[125]) or by Patterson syntheses (SHELX76[126]). Iterative full-matrix least squares refinement and ΔF syntheses (SHELX76) were used for subsequent atom location (As, P, B O, C, H, Cl). Atomic scattering factors for P, B, O, C, H, Cl were inlaid in SHELX76/86 while those for Au, Ti and As were obtained from

International Tables[127].

After refinement of all non-hydrogen atoms to isotropic convergence, data were corrected empirically for absorption (DIFABS[128]). Phenyl, cyclopentadienyl, methyl and methylene hydrogen atoms were introduced into idealised positions. In general, during the final stages of refinement, all non-hydrogen atoms were refined with anisotropic thermal parameters. After anisotropic convergence, data were weighted according to $w^{-1} = [\sigma^2(F) + g(F)^2]$ where g is variable. Finally, specific data where $F_{obs} > 2\sigma(F)$ were omitted and the structure refined by full-matrix least squares to convergence.

The computer programs CALC[129] and SHELXTL[130] were used, respectively, to obtain geometric data (interatomic distances, angles and torsions) and to draw the figures of the molecular structures.

The isotropic thermal parameter is given by the expression, $U_{iso} = \exp[-8\pi^2 U(\sin^2\theta/\lambda^2)]$.

The anisotropic thermal parameter is given by: $U_{ij} = \exp[-2\pi^2(U_{11}a^{*2}h^2 + U_{22}b^{*2}k^2 + U_{33}c^{*2}l^2 + 2U_{23}b^*c^*kl + 2U_{13}a^*c^*hl + 2U_{12}a^*b^*hk)]$.

The equivalent isotropic parameter, $U_{eq} = [\Sigma_i\Sigma_j U_{ij}a_i^*a_j^*\mathbf{a}_i.\mathbf{a}_j]/3$

1-CH_3OCH_2-2-{PPh_3Au}-1,2-*closo*-$C_2B_{10}H_{10}$ (**4a**)

Crystal Data

$C_{22}H_{30}B_{10}PAuO.CH_2Cl_2$, M = 731.45, triclinic, a = 9.711(7) Å, b = 12.640(7) Å, c = 12.813(22) Å, α = 94.53(9)°, β = 97.03(10)°, γ = 103.23(6)°, V = 1510.2 Å^3, from least squares refinement of 25 centred reflections ($13 \leq \theta \leq 15°$) at 291±1 K, Z = 2, D_c = 1.608 gcm^{-3}, μ(Mo-K_α) = 51.10 cm^{-1}, F(000) = 712 e.

Data collection and reduction

Significant crystal decay (>50%) after 536 reflections, presumably due to loss of loosely bound solvent (crystals became opaque). Therefore, full data set was not acquired.

1-CH_3OCH_2-2-{$AsPh_3Au$}-1,2-*closo*-$C_2B_{10}H_{10}$ (**4e**)

Crystal Data

$C_{22}H_{30}B_{10}AsAuO.CH_2Cl_2$, M = 775.40, triclinic, space group *P*bar1, a = 9.6664(22)Å, b = 12.706(8) Å, c = 12.787(4) Å, α = 93.78(4)°, β = 97.282(23)°, γ = 102.32(4)°, V = 1514.8(12) Å^3, from least squares refinement of 25 centred reflections ($9 \leq \theta \leq 15$) at 185±1K, Z = 2, D_c = 1.700 gcm^{-3}, μ(Mo-K_α) = 61.24 cm^{-1}, F(000) = 748 e.

Data collection and reduction

Variable scan speeds between 0.92-2.35 °min^{-1}. 5713 independent reflections measured ($1 \leq \theta \leq 25°$; $0 \leq h \leq 11$, $-15 \leq k \leq 15$, $-15 \leq l \leq 15$) of which 4814 had $F \geq 2.0\sigma(F)$. No significant crystal decay or movement noted over period of data collection (120h).

Structure solution and refinement

Au from Patterson syntheses. As, B, C, O, H_{cage}, Cl_{solv} from full-matrix least squares refinement/ΔF syntheses. Cage H atoms refined positionally subject to a single B-H distance of 1.20(5) Å. Phenyl, methyl and methylene H atoms set in idealised positions (C-H = 1.08 Å). Empirical absorption correction applied after isotropic convergence. Thereafter all non-H atoms (except those of disordered solvate [CH_2Cl_2]) allowed anisotropic thermal motion. H atoms refined with a common thermal parameter (cage H and non-cage H treated separately), $U_{cage\ H}$ = 0.083(11) Å^2 and $U_{noncage\ H}$ = 0.093(9) Å^2 at convergence. g = 0.001280, R = 0.0524, R_w = 0.0670, S = 1.132, number of variables = 374. Maximum shift/esd = 0.50 (disordered solvate). Maximum and minimum residues in final ΔF map = 2.29 (close to Au) and -3.32 eÅ^{-3} respectively.

$AsPh_3AuMe$ (5)

Crystal Data

$C_{19}H_{18}AsAu$, M = 518.24, monoclinic, space group $P2_1/c$, a = 9.0168(24) Å, b = 11.3808(21) Å, c = 17.413(4) Å, β = 104.563(18)°, V = 1729.4(7) Å^3, from least squares refinement of 25 centred reflections ($12 \leq \theta \leq 14$) at 291±1K, Z = 4, D_c = 1.990 gcm^{-3}, μ(Mo-K_α) = 103.78 cm^{-1}, F(000) = 976 e.

Data collection and reduction

Variable scan speeds between 0.92-2.35 °min^{-1}. 3463 independent reflections measured ($1 \leq \theta \leq 25°$; $0 \leq h \leq 10$, $0 \leq k \leq 13$, $-20 \leq l \leq 20$) of which 2459 had $F \geq 2.0\sigma(F)$. Data corrected for 30% crystal decay over period of data collection (76h), though no crystal movement was observed.

Structure solution and refinement

Au from Patterson syntheses. As, C from full-matrix least squares refinement/ΔF syntheses. Phenyl and methyl H atoms set in idealised positions (C-H = 1.08 Å). Empirical absorption correction applied after isotropic convergence. Thereafter Au, As and C atoms allowed anisotropic thermal motion. H atoms refined with a common thermal parameter, U_H = 0.102(10) Å^2 at convergence. g = 0.000260, R = 0.0462, R_w = 0.0431, S = 1.165, number of variables = 191. Maximum shift/esd = 0.01. Maximum and minimum residues in final ΔF map = 0.92 and -1.06 eÅ^{-3} respectively.

1-CH_3OCH_2-2-{$CpTiCl_2$}-1,2-*closo*-$C_2B_{10}H_{10}$ (**8**)

Crystal Data

$C_9H_{20}B_{10}Cl_2TiO$, M = 371.16, monoclinic, space group $P2_1/c$, a = 10.133(3) Å, b = 12.732(2) Å, c = 14.128(2) Å, β = 108.586(18)°, V = 1727.5(7) $Å^3$, from least squares refinement of 25 centred reflections ($9 \leq \theta \leq 12$) at 291±1K, Z = 4, D_c = 1.427 gcm^{-3}, μ(Mo-K_α) = 7.92 cm^{-1}, F(000) = 752 e.

Data collection and reduction

Variable scan speeds between 0.92-2.35 $°min^{-1}$. 1079 independent reflections measured ($1 \leq \theta \leq 25°$; $0 \leq h \leq 9$, $0 \leq k \leq 12$, $-13 \leq l \leq 13$) of which 1074 had $F \geq 2.0\sigma(F)$. No significant crystal movement noted, but data corrected for slight crystal decay (*ca.* 2%) over period of data collection (36h).

Structure solution and refinement

Ti from direct methods (SHELX86). B, C, O, Cl, H_{cage} from full-matrix least squares refinement/ΔF syntheses. Cage H atoms refined positionally subject to a single B-H distance of 1.20(5) Å except H(5B)-H(9B) which were set in idealised positions because of poor positional refinement. Cyclopentadienyl, methyl and methylene H atoms set in idealised positions (C-H = 1.08 Å). Cyclopentadienyl carbon atoms set in idealised positions within regular pentagon such that C-C = 1.42 Å and internal angles = 108.0°. Empirical absorption correction applied after isotropic convergence. Thereafter only Ti and Cl atoms allowed anisotropic thermal motion. H atoms refined with a common thermal parameter, U_H = 0.055(11) $Å^2$ at convergence. g = 0.000601, R = 0.1001, R_w = 0.0826, S = 1.239, number of variables = 116. Maximum shift/esd = 0.01. Maximum and minimum residues in final ΔF map = 0.64 (close to Au) and -0.63 $eÅ^{-3}$ respectively.

1-CH_3OCH_2-2-{PPh_2AuCl}-1,2-*closo*-$C_2B_{10}H_{10}$ (12)

Crystal Data

$C_{16}H_{25}B_{10}AuClPO.0.7CH_2Cl_2$, M = 604.87, orthorhombic, space group *Pbca*, a = 9.8172(16) Å, b = 15.433(3) Å, c = 35.424(4) Å, V = 5367.1(14) Å^3, from least squares refinement of 25 centred reflections ($9 \leq \theta \leq 14$) at 291±1K, Z = 8, D_c = 1.497 gcm^{-3}, μ(Mo-K_α) = 56.37 cm^{-1}, F(000) = 2320e. (M, D_c, μ(Mo-K_α) and F(000) all assume no solvate).

Data collection and reduction

Variable scan speeds between 0.92-2.35 °min^{-1}. 4722 independent reflections measured ($1 \leq \theta \leq 25°$; $0 \leq h \leq 11$, $0 \leq k \leq 18$, $0 \leq l \leq 42$) of which 3517 had $F \geq 2.0\sigma(F)$. No significant crystal movement noted but data were corrected for crystal decay of *ca.* 4% over period of data collection (108h).

Structure solution and refinement

Au from Patterson syntheses. P, B, C, O, Cl, H_{cage}, from full-matrix least squares refinement/ΔF syntheses. Cage H atoms refined positionally subject to a single B-H distance of 1.00(5) Å. Phenyl, methyl and methylene H atoms set in idealised positions (C-H = 1.08 Å). Empirical absorption correction applied after isotropic convergence. Thereafter all non-H atoms (except of disordered solvate [CH_2Cl_2]) allowed anisotropic thermal motion. All H atoms refined with a common thermal parameter, U_H = 0.083(9) Å^2 at convergence. 0.7 of dichloromethane solvate included in final model (C and Cl atoms only) with common isotropic thermal parameter U_{solv} = 0.1089(16) Å^2 at convergence. g = 0.001719, R = 0.00546, R_w = 0.0714, S = 1.006, number of variables = 313. Maximum shift/esd = 0.01. Maximum and minimum residues in final ΔF map = 2.063 [close to solvate Cl(1)] and -0.95 eÅ^{-3} respectively.

1-CH_3OCH_2-(1'-CH_3OCH_2-2'-{PPh_2Au}-1',2'-*closo*-$C_2B_{10}H_{10}$)-1,2-*closo*-$C_2B_{10}H_{10}$ **(14)**

Crystal Data

$C_{20}H_{40}B_{20}PAuO$, M = 740.68, triclinic, space group *P*bar1, a = 11.9407(22) Å, b = 11.996(3) Å, c = 13.8171(7) Å, α = 101.45(4)°, β = 109.53(3)°, γ = 106.22(2)°, V = 1695.8(12) Å^3, from least squares refinement of 25 centred reflections ($13 \leq \theta \leq 14$) at 291±1K, Z = 2, D_c = 1.451 gcm^{-3}, μ(Mo-K_α) = 43.94 cm^{-1}, F(000) = 724 e.

Data collection and reduction

Variable scan speeds between 0.92-2.35 °min^{-1}. 5553 independent reflections measured ($1 \leq \theta \leq 25°$; $0 \leq h \leq 14$, $-14 \leq k \leq 14$, $-16 \leq l \leq 16$) of which 5547 had $F \geq 2.0\sigma(F)$. No significant crystal decay or movement noted over period of data collection (124h).

Structure solution and refinement

Au from Patterson syntheses. P, B, C, O, H_{cage} from full-matrix least squares refinement/ΔF syntheses. Cage H atoms in both carbaborane moieties positionally refined subject to a single B-H distance of 1.05(5) and 1.10(5) Å for P-bound and Au-bound carbaborane respectively. Phenyl, methyl and methylene H atoms set in idealised positions (C-H = 1.08 Å). Empirical absorption correction applied after isotropic convergence. Thereafter all non-H atoms allowed anisotropic thermal motion. H atoms refined with a common thermal parameter, U_H = 0.0833(3) Å^2 at convergence. g = 0.000416, R = 0.0315, R_w = 0.0323, S = 1.113, number of variables = 460. Maximum shift/esd = 0.01. Maximum and minimum residues in final ΔF map = 1.95 (close to Au) and -1.45 eÅ^{-3} respectively.

5.4 Extended Hückel Molecular Orbital Calculations

5.4.1 Introduction

In order to analyse general structural problems and to predict structural possibilities, extended Hückel molecular orbital (EHMO) calculations can be used[131, 132]. In organometallic chemistry EHMO calculations have been widely used to accurately predict preferred conformations and rotational barriers. Results of calculations reflect maximum orbital overlap criteria and electronegativity trends but the absolute molecular orbital energies obtained can occasionally be inaccurate and, consequently, such results are only valid when considering relative energies.

5.4.2 EHMO Theory

The extended Hückel method is based on the linear combination of atomic orbitals (LCAO) in which the molecular orbitals of a model compound, defined by coordinates in orthogonal Ångstrom space and with a basis set of atomic orbital parameters for all elements in the model, are derived by linear combination of the relevant atomic orbitals:

$$\Psi = c_i\Psi_i + c_j\Psi_j$$

where Ψ is the mathematical function for an MO, Ψ_i and Ψ_j are the corresponding mathematical wavefunctions for the AO's and c_i and c_j are the AO coefficients.

For each AO, Slater type orbitals are used, these being represented mathematically as follows:

$$\Psi_{lmn} = r^{n-1}\exp^{-\zeta r}Y_{ml}(\theta, \phi)$$

$$\zeta = (Z - \sigma)/n$$

where n is related to the principal quantum number, $Y_{ml}(\theta, \phi)$ are spherical harmonics, ζ is the orbital exponent (related to effective nuclear charge), Z is the nuclear charge and σ is a screening constant.

The orbital energies are evaluated from a set of secular equations using the Hamiltonian operators H_{ii} and H_{ij} and overlap integrals S_{ij}:

$$\Sigma c_{ij}(H_{ij} - S_{ij}E) = 0$$

(E = energy)

$$H_{ii} = \Psi_i H \Psi_i$$

$$H_{ij} = \Psi_i H \Psi_j = \Psi_j H \Psi_i$$

$$S_{ij} = \Psi_i \Psi_j$$

H_{ii}'s used are the valence shell ionisation energies (VSIE's) which can be optimised by charge iteration. H_{ij}'s are calculated using a modified version of the Wolfsberg-Helmholtz formula[133]:

$$H_{ij} = K' S_{ij}(H_{ii} + H_{jj})/2$$

$$K' = K + \Delta + \Delta^2 + \Delta^4(1 - K)$$

$$\Delta = (H_{ii} - H_{ij})/(H_{ii} + H_{ij})$$

Optimisation of H_{ii} is achieved by charge iteration methods:

$$H_{ii} = -VSIE(Q)$$

$$VSIE(Q) = AQ^2 + BQ + C$$

where the parameters A, B and C are derived from multiconfigurational spectral data on atoms and their charged ions[134].

Other results predicted by EHMO calculations include:

(1) Net atomic charge:

$$q_i = \Sigma_j \Sigma_n (N c_{in}^2 + N c_{in} c_{jn} S_{ij})$$

where N = the number of electrons in the orbital and c_{in} (c_{jn}) is the coefficient of Ψ_i (Ψ_j) in the n^{th} MO.

If the atomic number is Z and q is the overall atomic charge [see (2)], then:

$$q_i = Z - q$$

(2) Overall atomic charge:

$$q = \Sigma_i q_i$$

(3) Bond overlap population (measure of bond strength between atoms r and s):

$$P_{rs} = 2\Sigma_{ij}\Sigma_n N c_{in} c_{jn} S_{ij}$$

5.4.3 EHMO Calculations on I - IV

EHMO calculations were performed on model compounds 2-{AsH_3Au}-1,2-*closo*-$C_2B_{10}H_{11}$ (I), AsH_3AuCH_3 (II), [1,2-*closo*-$C_2B_{10}H_{11}$]$^-$ (III) and [CH_3]$^-$ (IV). All calculations were performed using a locally modified version of ICON8[135] such that (where appropriate) As-H = 1.50 Å, As-Au = 2.38 Å, Au-C = 2.08 Å, C-C = C-B = B-B = 1.75 Å, B-H = C-H_{cage} = 1.20 Å and C-H_{methyl} = 1.08 Å with linear Au geometries and tetrahedral angles at C_{methyl}. As-Au-C sequences were set to lie along the *z*-axis and in **I** and **III**, C(1) was set to lie in the *yz* plane. Atomic coordinates and atomic orbital parameters for **I** and **II** are given in **Table 5.1** and **Table 5.2** respectively. The atomic coordinates and atomic orbital parameters for **III** and **IV** were obtained by removal of {AsH_3Au}$^+$ fragment from **I** and **II** respectively.

H_{ii}'s and ζ values for As, C, B and H were those inlaid in ICON8. H_{ii}'s for Au were optimised at the highest level of charge iteration available using nine VSIE(Q) functions for gold with metal *d* orbitals described by the double-zeta expansion. The results of these calculations are discussed in **Section 2.3.4** and a summary of the pertinent results is presented in **Table 2.13** (p80).

LABEL	X	Y	Z	-------S-------			-------P-------			-------D-------			CONTRACTED D		
				N	EXP	COUL	N	EXP	COUL	N	EXPD1	COUL	C1	C2	EXPD2
H91	0.00000	1.41420	6.62440	1	1.300	-13.600									
H92	1.22470	-0.70710	6.62440	1	1.300	-13.600									
H93	-1.22470	-0.70710	6.62440	1	1.300	-13.600									
H1	0.00000	2.56200	-1.28100	1	1.300	-13.600									
H2	0.00000	0.00000	-2.86440	1	1.300	-13.600									
H3	-2.43660	0.79170	-1.28100	1	1.300	-13.600									
H4	-1.50590	2.07270	1.28100	1	1.300	-13.600									
H5	1.50590	2.07270	1.28100	1	1.300	-13.600									
H6	2.43660	0.79170	-1.28100	1	1.300	-13.600									
H7	-1.50590	-2.07270	-1.28100	1	1.300	-13.600									
H8	-2.43660	-0.79170	1.28100	1	1.300	-13.600									
H10	2.43660	-0.79170	1.28100	1	1.300	-13.600									
H11	1.50590	-2.07270	-1.28100	1	1.300	-13.600									
H12	0.00000	-2.56200	1.28100	1	1.300	-13.600									
B1	0.00000	1.48860	-0.74440	2	1.300	-15.200	2	1.300	-8.500						
B2	0.00000	0.00000	-1.66440	2	1.300	-15.200	2	1.300	-8.500						
B3	-1.41580	0.46000	-0.74430	2	1.300	-15.200	2	1.300	-8.500						
B4	-0.87500	1.20440	0.74430	2	1.300	-15.200	2	1.300	-8.500						
B5	0.87500	1.20440	0.74430	2	1.300	-15.200	2	1.300	-8.500						
B6	1.41580	0.46000	-0.74430	2	1.300	-15.200	2	1.300	-8.500						
B7	-0.87500	-1.20440	-0.74430	2	1.300	-15.200	2	1.300	-8.500						
B8	-1.41580	-0.46000	0.74430	2	1.300	-15.200	2	1.300	-8.500						
C9	0.00000	0.00000	1.66440	2	1.625	-21.400	2	1.625	-11.400						
B10	1.41580	-0.46000	0.74430	2	1.300	-15.200	2	1.300	-8.500						
B11	0.87500	-1.20440	-0.74430	2	1.300	-15.200	2	1.300	-8.500						
C12	0.00000	-1.48860	0.74440	2	1.625	-21.400	2	1.625	-11.400						
AU	0.00000	0.00000	3.74440	6	2.602	-9.440	6	2.584	-4.646	5	6.163	-12.150	0.64418	0.53558	2.794
AS	0.00000	0.00000	6.12440	4	2.230	-16.220	4	1.890	-12.160						

Table 5.1 Atomic Coordinates and Atomic Orbital Parameters for I.

LABEL	X	Y	Z	-------S-------			-------P-------			-------D-------			CONTRACTED D		
				N	EXP	COUL	N	EXP	COUL	N	EXPD1	COUL	C1	C2	EXPD2
H91	0.00000	1.41420	6.62440	1	1.300	-13.600									
H92	1.22470	-0.70710	6.62440	1	1.300	-13.600									
H93	-1.22470	-0.70710	6.62440	1	1.300	-13.600									
H81	0.00000	-1.01820	1.30440	1	1.300	-13.600									
H82	0.88180	0.50910	1.30440	1	1.300	-13.600									
H83	-0.88180	0.50910	1.30440	1	1.300	-13.600									
C9	0.00000	0.00000	1.66440	2	1.625	-21.400	2	1.625	-11.400						
AU	0.00000	0.00000	3.74440	6	2.602	-9.440	6	2.584	-4.646	5	6.163	-12.150	0.64418	0.53558	2.794
AS	0.00000	0.00000	6.12440	4	2.230	-16.220	4	1.890	-12.160						

Table 5.2 Atomic Coordinates and Atomic Orbital Parameters for II.

References

1. A. Stock, "*Hydrides of Boron and Silicon*", Cornell University Press, Ithaca, New York, 1936.

2. R. Hoffmann and W.N. Lipscomb, *J. Chem. Phys.*, 1962, **36**, 3489.

3. W.N. Lipscomb, *Proc. Nat. Acad. Sci. U.S.*, 1961, **47**, 1791.

4. **a**: C.D. Good, I. Shapiro and R.E. Williams, *J. Am. Chem. Soc.*, 1962, **84**, 3837. **b**: C.D. Good, B. Keilin, I. Shapiro and R.E. Williams, *J. Am. Chem. Soc.*, 1963, **85**, 3167.

5. M.F. Hawthorne, P.A. Wegner and D.C. Young, *J. Am. Chem. Soc.*, 1965, **87**, 1818.

6. W.N. Lipscomb, "*Boron Hydrides*", Benjamin, New York, 1963.

7. K. Wade, *Adv. Inorg. Chem. Radiochem.*, 1976, **18**, 1.

8. R.E. Williams, *Adv. Inorg. Chem. Radiochem.*, 1976, **18**, 67.

9. W.N. Lipscomb and E.I. Tolpin, *Inorg. Chem.*, 1973, **12**, 2257.

10. A.J. Welch and A. J. Wynd, *J. Chem. Soc., Dalton Trans.*, 1990, 2803.

11. J.W. Ager, S.L. Clark, H.L. Goldstein, T.L. Heying, M. Hillman, D.J. Mangold, R.J. Polak and J.W. Szymanski, *Inorg. Chem.*, 1963, **2**, 1089.

12. J. Bobinski, M.S. Cohen, M. Fein, N. Mayers and N.N. Schwartz, *Inorg. Chem.*, 1963, **2**, 1111.

13. R.N. Grimes, "*Carboranes*", Academic Press, New York, 1970; and references

therein.

14. T. Onak in "*Comprehensive Organometallic Chemistry*", Eds. G. Wilkinson, F.G.A. Stone and E.W. Abel, Pergamon Press, 1981, Section 5.4.

15. **a**: A.V. Grebennikov, A.V. Kazuntsev and L.I. Zakharkin, *Izv. Akad. Nauk. SSSR, Ser. Khim.*, 1967, 2079. **b**: V.A. Brattsev, Yu. A. Chapovskii, A.I. Klimova, O.Yu. Okhlobystin, A.A. Ponomanenko, V.I. Stanko and L.I. Zakharkin, *Dokl. Akad. Nauk. SSSR*, 1964, **155**, 1119.

16. "*Gmelin Handbuch der Anorganischen Chemie, Boron Compounds*", 1980, **1**, 1st Supplement.

17. F. Teixidor, R.W. Rudolph and C. Vinas, *Inorg. Chem.*, 1986, **25**, 3339.

18. R.N. Grimes, W.C. Hutton and T.L. Venable, *J. Am. Chem. Soc.*, 1982, **104**, 4716.

19. R.K. Bohn and M.D. Bohn, *Inorg. Chem.*, 1971, **10**, 350.

20. K.F. Shaw and A.J. Welch, *Polyhedron*, 1992, **11**, 157.

21. K.F. Shaw, PhD Thesis, University of Edinburgh, 1992; and references therein.

22. **a**: R.N. Grimes in "*Comprehensive Organometallic Chemistry*", Eds. G. Wilkinson, F.G.A. Stone and F.W. Abel, Pergamon Press, 1981, Section 5.5. **b**: L.J. Todd, *ibid.*, Section 5.6. **c**: "*Metal Interactions with Boron Clusters*", Ed. R.N. Grimes, Plenum Press, New York, 1982.

23. C.E. Briant, D.N. Cox, M.P. Garcia, M. Green, D.M.P. Mingos, R.G. Somerville, F.G.A. Stone and A.J. Welch, *J. Chem. Soc., Dalton Trans.*, 1985, 2343.

24. A.J. McLennan, D. Reed, A.J. Welch and A.J. Wynd, *J. Chem. Soc., Dalton*

Trans., 1987, 2761.

25. D.M.P. Mingos, *J. Chem. Soc., Dalton Trans.*, 1977, 602.

26. T.P. Hanusa, *Polyhedron*, 1982, **1**, 663.

27. **a**: ref. 23. **b**: M.I. Forsyth, D.M.P. Mingos and A. J. Welch, *J. Chem. Soc., Chem. Commun.*, 1977, 605.

28. **a**: H.M. Colquohoun, T.J. Greenhough and M.G.H Wallbridge, *J. Chem. Soc., Chem. Commun.*, 1976, 1019. **b**: *idem.*, *Acta Cryst.*, 1977, **B33**, 3604.

29. **a**: Z. Hanousek, S. Hermanek and J. Plesek, *Collect. Czech. Chem. Commun.*, 1978, **43**, 2862. **b**: J. Cowie, E.J.M. Hamilton, J.C.V. Laurie and A.J. Welch, *Acta Cryst.*, 1988, **C44**, 1648.

30. J. Cowie, E.J.M. Hamilton, J.C.V. Laurie and A.J. Welch, *J. Organometal. Chem.*, 1990, **394**, 1.

31. M. Bown, X.L.R. Fontaine, N.N. Greenwood, J.D. Kennedy, J. Plesek, B. Stibr and M. Thornton-Pett, *Acta Cryst.*, 1990, **C46**, 995.

32. Z.G. Lewis and A.J. Welch, *J. Chem. Soc., Dalton Trans.*, 1992, 731.

33. Z.G. Lewis and A.J. Welch, in press.

34. B.D. Reid, K.F. Shaw and A.J. Welch, in preparation.

35. E.J.M. Hamilton and A.J. Welch, *Acta Cryst.*, 1990, **C46**, 1228.

36. E.J.M. Hamilton and A.J. Welch, *Polyhedron*, 1990, **9**, 2407.

37. J. Casabo, C. Miravitlles, J. Ruis, F. Teixidor and C. Vinas, *Inorg. Chem.*, 1990, **29**, 149.

38. J.R. Fernandez, G.F. Helm, J.A.K. Howard, M.U. Pilotti and F.G.A. Stone, *J. Chem. Soc., Dalton Trans.*, 1990, 1747.

39. **a**: M.U. Pilotti, F.G.A. Stone and I. Topaloglu, *J. Chem. Soc., Dalton Trans.*, 1991, 1355. **b**: *idem., ibid.*, 1991, 1621.

40. R.E. Cochoy, R.W. Rudolph and R.L. Voorhees, *J. Am. Chem. Soc.*, 1970, **92**, 3351.

41. F.R. Fronczec, G.W. Halstead and K.N. Raymond, *J. Am. Chem. Soc.*, 1977, **99**, 1769.

42. V.I. Bregadze, *Chem. Rev.*, 1992, **92**, 209.

43. S. Bresadola in "*Metal Interactions with Boron Clusters*", Ed. R.N. Grimes, Plenum Press, New York, 1982.

44. E.L. Muetterties, "*Boron Hydride Chemistry*", Academic Press, New York, 1975; and references therein.

45. D.A. Brown, S.J. Bryan, W. Clegg and K. Wade, *Polyhedron*, 1984, **3**, 307.

46. **a**: R.P. Alexander, T.L. Heying, S. Papetti, H. Schroeder and J.F. Sieckhaus, *Inorg. Chem.*, 1969, **8**, 2444. **b**: A. Yu. Aleksandrov, V.I. Bregadze, V.I. Gol'danskii, V.V. Krapov, O. Yu.Oklobystin and L.I. Zakharkin, *Dokl. Akad. Nauk. SSSR*, 1965, **165**, 593.

47. S. Bresadola, P. Rigo and A. Turco, *J. Chem. Soc., Chem. Commun.*, 1968, 1205.

48. P.M. Garrett, M.F. Hawthorne, D.A. Owen and J.C. Smart, *J. Am. Chem. Soc.*, 1971, **93**, 1362.

49. V.N. Kalinin, L.S. Podvisotskaya and L.I. Zarkharkin, *Izv. Akad. Nauk. SSSR,*

Ser. Khim., 1968, 679.

50. S. Bresadola and B. Longato, *Inorg. Chem.*, 1974, **13**, 539.

51. G. Allegra, M. Calligaris, R. Furlanetto, G. Nardin and L. Randaccio, *Cryst. Struct. Commun.*, 1974, **3**, 69.

52. M. Bottrill, P.D. Gavens, J.W. Kelland and J. McMeeking in "*Comprehensive Organometallic Chemistry*", Eds. G. Wilkinson, F.G.A. Stone and E.W. Abel, Pergamon Press, 1981, Section 22.4; and references therein.

53. A.I. Kovredov and L.I. Zakharkin, *Zh. Obshch. Khim.*, 1974, **44**, 1832.

54. I.S. Savel'eva and L.I. Zakharkin, *Izv. Akad. Nauk. SSSR, Ser. Khim.*, 1979, 1381.

55. V.N. Kalinin, Yu.T. Struchkov, A.I. Yanovskii, L.I. Zakharkin and O.M. Zurlova, *Zh. Struct. Khim.*, 1981, **22**, 120.

56. **a**: L.V. Orlova and L.I. Zakharkin, *Izv. Akad. Nauk. SSSR, Ser. Khim.*, 1970, 2417. **b**: L.A. Fedorov, B.V. Lokshin, L.V. Orlova and L.I. Zakharkin, *J. Organometal. Chem.*, 1972, **40**, 15.

57. **a**: R.J. Puddephatt in "*Comprehensive Organometallic Chemistry*", Eds. G. Wilkinson, F.G.A. Stone and E.W. Abel, Pergamon Press, 1981, Section 15. **b**: R.J. Puddephatt, "*The Chemistry of Gold*", Elsevier, Amsterdam, 1978.

58. E. Bordignon, L. Cattalini, G. Natile and A. Scatturin, *J. Chem. Soc., Chem. Commun.*, 1973, 879; and references therein.

59. M.I. Bruce, B.K. Nicholson and O. Bin Shawkataly, *Inorg. Synth.*, 1989, **26**, 324.

60. A. Laguana and R. Uson, *Organomet. Synth.*, 1986, **3**, 322.

61. O. Crespo, M.C. Gimeno, P.G. Jones and A. Laguna, *J. Chem. Soc., Dalton Trans.*, 1992, 1601.

62. P.L. Bellon. M. Manaserro and M. Sansoni, *J. Chem. Soc., Dalton Trans.*, 1973, 2423.

63. D.M.P. Mingos, *J. Chem. Soc., Dalton Trans.*, 1976, 1163.

64. D.G. Evans and D.M.P. Mingos, *J. Organometal. Chem.*, 1982, **232**, 171.

65. For example: M. Elian and R. Hoffmann, *Inorg. Chem.*, 1975, **14**, 1058.

66. G.L. Locher, *Amer. Jour. Roentgenol., Radium Therapy*, 1936, **36**, 1.

67. V.P. Bond, *I.E.E.E. Trans. Nucl. Sci.*, 1982, **NS-29-1**, 24.

68. H. Hatanaka, K. Amano, H. Kanemitsu, I. Ikeuchi and T. Yoshizaki in "*BNCT for Tumours*", Ed. H. Hatanaka, Japan, 1986, chapter 5; and references therein.

69. A. Kaczmarczyk, E.I. Tolpin, A.H. Soloway and G.R. Wellum, *Inorg. Chem.*, 1977, **16**, 2120.

70. J. Plesek, *Chem. Rev.*, 1992, **92**, 269.

71. **a**: T. Jelinek, J. Plesek and B. Stibr, *Polyhedron*, 1984, **3**, 1351. **b**: S. Hermanek, T. Jelinek, J. Plesek and B. Stibr, *Collect. Czech. Chem. Commun.*, 1986, **51**, 819.

72. D.M. Adams, F. Alam, B. Bapat, R.F. Barth and A.H. Soloway, *Basic Life Sci.*, 1989, **50**, 107.

73. F. Alam, R.F. Barth and A.H. Soloway, *Appl. Radiat. Isot.*, 1987, **38**, 503.

74. M.F. Hawthorne, E.A. Nizusawa and M.R. Thompson, *Inorg. Chem.*, 1985, **22**, 1911.

75. M.F. Hawthorne, *Pure Appl. Chem.*, 1991, **63**, 327.

76. R.F. Barth, R.G. Fairchild and A.H. Soloway, *Sci. Am.*, 1990, **263**, 68.

77. J. Morris, *Chemistry in Britain*, 1991, **27**, 331.

78. **a**: S. Bresadola, A. Frigo, B. Longato and G. Rigatti, *Inorg. Chem.*, 1973, **12**, 2788. **b**: S. Bresadola, B. Longato and F. Morandini, *J. Organometal. Chem.*, 1977, **128**, C5. **c**: S. Bresadola, N. Bresciani-Pahor and B. Longato, *ibid.*, 1979, **179**, 73.

79. M.F. Hawthorne, C.B. Knobler and X. Yang, *Angew. Chem. Int. Ed. Engl.*, 1991, **30**, 1507.

80. C.M. Mitchell and F.G.A. Stone, *J. Chem. Soc., Chem Commun.*, 1970, 1263.

81. **a**: B.J. Gregory and C.K. Ingold, *J. Chem. Soc. (B)*, 1969, 276. **b**: A.J. Carty and A. Efraty, *Inorg. Chem.*, 1969, **8**, 543.

82. For example: P.M. Garrett, M.F. Hawthorne and J.C. Smart, *J. Am. Chem. Soc.*, 1969, **91**, 4767.

83. C.E. Briant, D.N. Cox, M.P. Garcia, M. Green, D.M.P. Mingos, R.G. Somerville, F.G.A. Stone and A.J. Welch, *J. Chem. Soc., Dalton Trans.*, 1985, 2343.

84. H. Schmidbaur, T. Pollock, R. Herr, F.E. Wagner, R. Bau, J.Riede and G. Muller, *Organometallics*, 1986, **5**, 566.

85. G. Calvin, G.E. Coates and P.S. Dixon, *Chem. Ind. (London)*, 1959, 1628.

86. A.J. Wynd, PhD Thesis, University of Edinburgh, 1988.

87. A. Earnshaw and N.N. Greenwood, "*The Chemistry of the Elements*", Pergamon Press, Oxford, 1982.

88. T.V. Baukova, L.G. Kuz'mina, N.V. Dvortsova, M.A. Porai-Koshits, D.N. Kravtsov and E.G. Perevalova, *Metalorg. Khim*, 1989, **2**, 1098.

89. P.D. Gavens, J.J. Guy, M.J. Mays and G.M. Sheldrick, *Acta Cryst.*, 1977, **B33**, 137.

90. P.F. Barron, L.M. Englehardt, P.C. Healy, J. Oddy and A.H. White, *Aust. J. Chem.*, 1987, **40**, 1545.

91. F.W.B. Einstein and R. Restivo, *Acta Cryst.*, 1975, **B31**, 624.

92. P. Brain, D.Phil. Thesis, University of Oxford, 1990.

93. S.K. Boocock, N.N. Greenwood, J.D. Kennedy, W.S. McDonald and J. Staves, *J. Chem. Soc., Dalton Trans.*, 1980, 790.

94. "*Comprehensive Organometallic Chemistry*", Eds. G. Wilkinson, F.G.A. Stone and E.W. Abel, Pergamon Press, 1981, Sections 22-28; and references therein.

95. **a**: D.F. Herman and W.K. Nelson, *J. Am. Chem. Soc.*, 1953, **75**, 3877. **b**: K.-H. Thiele and K. Jacob, *Z. Anorg. Allg. Chem.*, 1968, **356**, 195. **c**: R.J.H. Clark and M.A. Cole, *Inorg. Synth.*, 1976, **16**, 120.

96. H.J. Berthold and G. Groh, *Angew. Chem.*, 1963, **75**, 576.

97. M. Basso-Bert and D. Gervais, *J. Organometal. Chem.*, 1979, **165**, 209; and references therein.

98. **a**: J.E. Bercaw and H.H. Brintzinger, *J. Am. Chem. Soc.*, 1969, **91**, 7301. **b**: G.J. Erskine, D.A. Wilson and J.D. McCowan, *J. Organometal. Chem.*, 1976, **114**, 119.

99. H. Köpf and P. Köpf-Maier, *Angew. Chem., Int. Ed. Engl.*, 1979, **18**, 477.

100. M.R. Collier, M.F. Lappert and R. Pearce, *J. Chem. Soc., Dalton Trans.*, 1973, 445.

101. J.L. Atwood, G.K. Barker, J. Holton, W.E. Hunter, M.F. Lappert and R. Pearce, *J. Am. Chem. Soc.*, 1977, **90**, 6645.

102. M.F. Lappert, D.S. Patil and J.B. Pedley, *J. Chem. Soc., Chem. Commun.*, 1975, 830.

103. N.C. Baenziger, W.E. Bennett and D.M. Soboroff, *Acta Cryst.*, 1976, **B32**, 962.

104. A.C. Skapski and P.G.H Troughton, *Acta Cryst.*, 1970, **B26**, 716.

105. R.D. Gorsich, *J. Am. Chem. Soc.*, 1960, **82**, 4211.

106. J. Schiemann, E. Weiss, F. Näumann and D. Rehder, *J. Organometal. Chem.*, 1982, **232**, 219.

107. J.G. Reynolds, A. Zalkin and D.H. Templeton, *Inorg. Chem.*, 1977, **16**, 3357.

108. Y.V. Roberts, PhD Thesis, University of Edinburgh, 1991.

109. M. Sullivan and M. Schröder, unpublished results.

110. For example, **a**: R.P. Alexander and H.A. Schroeder, *Inorg. Chem.*, 1963, **2**, 1107. **b**: L.I. Zakharkin, V.I. Bregadze and O. Yu. Okhlobystin, *Izv. Akad. Nauk SSSR, Ser. Khim.*, 1964, 1539.

111. H.D. Smith, *J. Am. Chem. Soc.*, 1965, **87**, 1817.

112. L.I. Zakharkin and G.G. Zhigareva, *Izv. Akad. Nauk SSSR, Ser. Khim.*, 1965, 932.

113. L.I. Zakharkin, V.I. Bregadze and O. Yu. Okhlobystin, *J. Organometal. Chem.*,

1965, **4**, 211.

114. C.A. Tolman, *Chem. Rev.*, 1977, **77**, 313.

115. J.D. Kennedy and J. Staves, *Zeit. Naturforsch., Teil B*, 1979, **34**, 808.

116. S.K. Boocock, N.N. Greenwood, J.D. Kennedy, W.S. McDonald and J. Staves, *J. Chem. Soc., Dalton Trans.*, 1981, 2573.

117. B.F. Spielvogel, L. Wojniwich, M.K. Das, A.J. McPhail and K.D. Hargrave, *J. Am. Chem. Soc.*, 1976, **98**, 5702.

118. L.J. Todd, W.J. Mills, C.H. Sutton and M.W. Baize, *Inorg. Chem.*, 1991, **30**, 1046.

119. P. Lindstrom and S. Sjoberg, *Research Report*, Division of Organic Chem., Uppsala University, 1990.

120. O. Leukart, M. Cavlezel, A. Eberle, E. Escher, A. Tun-Kyi and R. Schwyzer, *Helv. Chim. Acta*, 1976, **59**, 2184.

121. For example: D.H. Brown, G.C. McKinley and W.E. Smith, *J. Chem. Soc., Dalton Trans.*, 1978, 199.

122. T.L. Venable, W.C. Hutton and R.N. Grimes, *J. Am. Chem. Soc.*, 1984, **106**, 29.

123. **a**: ref 60. **b**: R. Uson, A. Laguna and M. Laguna, *Inorg. Synth.*, 1989, **26**, 86.

124. CADABS: R.O. Gould and D.E. Smith, University of Edinburgh, 1986.

125. SHELX86: G.M. Sheldrick, University of Göttingen, 1986.

126. SHELX76: G.M. Sheldrick, University of Cambridge, 1976.

127. "*International Tables for X-Ray Crystallography*", Kynoch Press, Birmingham,

1974, **4**, 99.

128. DIFABS: N.G. Walker and D. Stuart, *Acta Cryst.*, 1983, **A39**, 158.

129. CALC: R.O. Gould and P. Taylor, University of Edinburgh, 1986.

130. SHELXTL: G.M. Sheldrick, University of Göttingen, 1985.

131. R. Hoffmann and W.N. Lipscomb, *J. Chem. Phys.*, 1962, **36**, 2179.

132. R. Hoffmann, *ibid.*, 1963, **39**, 1397.

133. J.H. Ammeter, H.-B. Bürgi, J.C. Thibeault and R. Hoffmann, *J. Am. Chem. Soc.*, 1978, **100**, 3686.

134. C.J. Ballhousen and H.B. Gray, "*Molecular Orbital Theory*", Benjamin Press, New York, 1965.

135. ICON8: J. Howell, A. Rossi, D. Wallace, K. Haraki and R. Hoffmann, *Quantum Chemistry Program Exchange*, University of Indiana, No. 344.

APPENDIX A

SYNTHESIS OF π-CARBARUTHENABORANES

A.1 Introduction

The synthesis and chemistry of π-carbametallaborane compounds, in which a metal either occupies the final vertex of a *closo*-polyhedron (class 1 carbametallaborane) or bridges a polyhedral edge of a *nido*-carbaborane anion (class 2 carbametallaborane), is an extensively researched area and continues to be of great interest in organometallic chemistry. The rapid development of π-carbametallaborane compounds has been the result of the analogy between the bonding capabilities of $[C_2B_9H_{11}]^{2-}$ and Cp^-, first recognised by Hawthorne and co-workers[A1] (see **Section 1.4.1**).

Since the synthesis of the ferrocene analogue, $[(C_2B_9H_{11})_2Fe]^{2-}$ [A1], numerous sandwich complexes either containing $\{C_2B_9\}^{2-}$ alone or both $\{C_2B_9\}^{2-}$ and Cp^- ligands have been reported[A2]. It is only relatively recently[A3, A4, A5] that species in which polyenes other than Cp^- have been used to act as *exo*-polyhedral ligands to carbametallaboranes. The first example of such a complex, 1,2-Me_2-3-(η^4-C_4Ph_4)-3,1,2-*closo*-$PdC_2B_9H_9$, was reported by Hawthorne *et al*[A6] in 1968, but it was not until 1981 that Stone and co-workers[A7] reported the first η^6-arene carbametallaborane compound, 1-(η^6-C_6H_5Me)-2,4-Me_2-1,2,4-*closo*-$FeC_2B_9H_9$. The impact of this paper was such that it subsequently lead to much interest in arene carbametallaborane sandwich complexes: Compounds of the type [(η^6-arene)M(carbaborane)], where M = Fe^{II}, Ru^{II} or Os^{II}, were considered to be of potential interest since, as 18-electron diamagnetic neutral compounds, they might have interesting derivative chemistry including, for example, loss of the neutral arene ligand. Since the initial research[A7],

several arene carbametallaborane compounds have been synthesised: **Figure A.1** illustrates an example of an 18-electron arene ruthenium(II) carbaborane[A8] and **Figure A.2** is an example of a similar arene iron(II) carbaborane[A8].

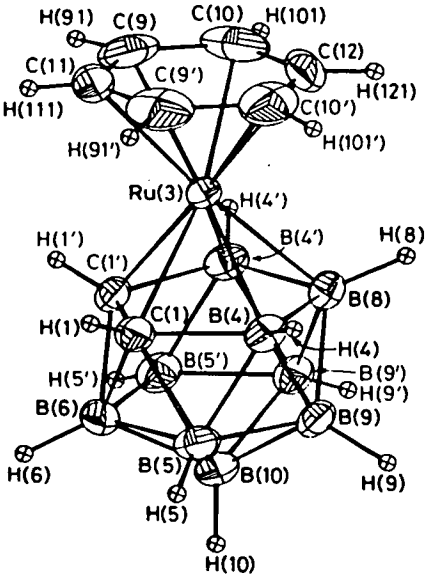

Figure A.1 Molecular Structure of 3-(η^6-C_6H_6)-3,1,2-*closo*-$RuC_2B_9H_{11}$.

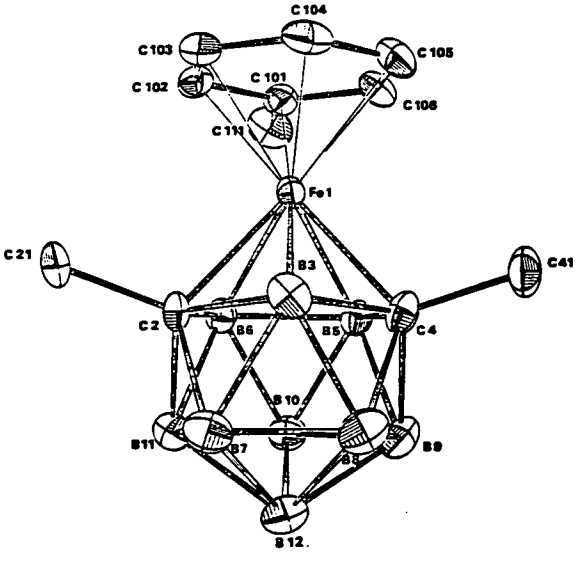

Figure A.2 Molecular Structure of 1-(η^6-C_6H_5Me)-2,4-Me_2-1,2,4-*closo*-$FeC_2B_9H_9$.

More recent research has concentrated on indenyl and fluorenyl ligand carbametallaborane sandwich compounds[A4, A5, A9], for example 3-(η^5-C_9H_7)-3,1,2-*closo*-$CoC_2B_9H_{11}$, and on steric interactions between the *exo*-polyhedral ligand and the carbaborane carbon substituents. In some cases these interactions have produced unusual distortions in cage geometry, as in 1,2-Ph_2-3-(η^6-*p*-cym)-3,1,2-$RuC_2B_9H_9$[A10] where C(1)-C(2) is essentially non-bonding.

The d^6 arene ruthenium(II) carbaboranes are unslipped *closo*-carbametallaborane compounds and molecular geometries are consistent with PSEP theory predictions (see **Section 1.2**). "Slippage" describes the scenario in which the metal atom is not positioned centrally above the carbaborane (C_2B_3) face. The slip parameter, Δ, is defined as the displacement of the metal atom from the central position (Δ = 0 Å represents an (ideally) unslipped carbametallaborane). It is the distance between the projection of the metal onto the lower pentagonal ring [B(5)-B(6)-B(11)-B(12)-B(9)] and the centroid of that ring (**Figure A.3**). The centroid of the lower five-membered ring is used as the point of reference as it has been recognised[A11, A12] that the lower ring is more planar than the open C_2B_3 face in most carbametallaboranes. In its simplest form, slippage occurs so that the metal atom avoids the adoptance of an unfavourable electron configuration (usually more than 18 electrons). Thus, metals with a d^n configuration between 3 and 7 have small slip parameters while metals with a d^n configuration of greater than 8 have slips (Δ) of, on average, *ca.* 0.5 Å. *Endo-nido*-carbametallaboranes, formed by the (σ-bonding) interaction of one orbital donor fragments such as $\{PPh_3Au\}^+$, $\{Ph_3Sn\}^+$ and $\{PPh_3Hg\}^{2+}$ with the *nido*-carbaborane anion, could be considered as extreme cases of slippage and values of 0.92 and 1.26 Å have been reported for the slip parameters of 10-*endo*-$\{PPh_3Hg\}$-7,8-*nido*-$C_2B_9H_{11}$[A13] and [10-*endo*-$\{Ph_3Sn\}$-10-μ-H-7,8-*nido*-$C_2B_9H_{10}]^-$ [A14] respectively.

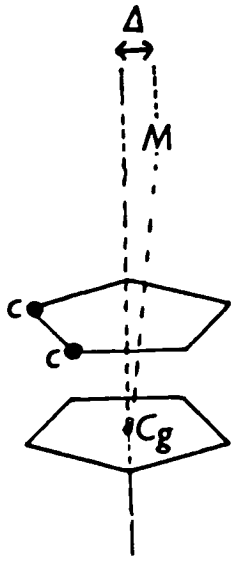

C_g = centroid of lower pentagonal belt

Figure A.3 Measurement of the Slip Parameter (Δ).

The synthesis of *closo-* (and *endo-nido-*) carbametallaboranes is best achieved by reaction of a metal fragment halide with a salt of $\{7,8\text{-}nido\text{-}C_2B_9\}^{2-}$ [A1, A15, A16]. For example, the reaction of $Tl_2[7,8\text{-}nido\text{-}C_2B_9H_{11}]$ and $[(\eta^6\text{-}C_6H_6)RuCl_2]_2$ affords $3\text{-}(\eta^6\text{-}C_6H_6)\text{-}3,1,2\text{-}closo\text{-}RuC_2B_9H_{11}$ (and TlCl) in reasonable yield[A8].

Thallium carbaborane compounds were recognised[A17] as good precursors to transition metal carbaborane compounds because of the high affinity of thallium for chloride and the insolubility of the resulting thallium chloride. This meant that reaction with (transition) metal halides occurred readily at (or below) room temperature, with the precipitation of TlCl the driving force of the reaction. Consequently, facile displacement of thallium by other metals offers a convenient route for the syntheses of new carbametallaborane compounds.

This appendix reports the syntheses of mono-carbon substituted *closo*-carbaruthenaborane species and represents work done in the early part of the author's research. These mono-carbon substituted compounds were initially synthesised so that they could be lithiated at C(2) and a σ-bonded metal introduced (as described in **Chapters 2** and **3**) to produce dimetal species. However, initial results were not encouraging and so details of that work are not reported. The synthesis and characterisation of *closo*-carbaruthenaborane compounds are reported in **Section A.2.** Structural studies, including an X-ray crystallographic study and NMR studies are also described in **Section A.2.** Finally, **Section A.3** details the conclusions, **Section A.4** outlines the experimental procedures used and **Section A.5** lists the references for this appendix.

A.2 Synthesis and Characterisation of π-Carbametallaboranes

A.2.1 Thallium Carbaborane Compounds (**18** and **19**)

Tl_2[7-Ph-7,8-*nido*-$C_2B_9H_{10}$] (**18**) was synthesised in a similar manner to that reported for Tl_2[7,8-*nido*-$C_2B_9H_{11}$][A8]: Refluxing six equivalents of potassium hydroxide with the parent *closo*-carbaborane, 1-Ph-1,2-*closo*-$C_2B_{10}H_{11}$ (**2**), in ethanol for 3 hours yielded the dipotassium salt of the *nido*-carbaborane anion. This was converted to the thallium salt by metathesis: Addition of thallium(I) acetate to an aqueous solution of potassium carbaborane afforded the bright yellow solid Tl_2[7-Ph-7,8-*nido*-$C_2B_9H_{10}$] (**18**) in good yield. Compound **18** was found to be mildly light sensitive, turning grey on prolonged exposure to natural light.

As with other dithallium carbaborane compounds[A8, A17, A18], **18** is very insoluble in most solvents and, as a result, characterisation was accomplished by infra-red spectroscopy and microanalysis only: The insolubility meant that solution NMR spectroscopy could not be used. The infra-red spectrum was recorded from a KBr pellet of **18** and exhibited bands at 2509, 2443 and 2381 cm^{-1} corresponding to B-H stretches. The peaks at 2509 and 2443 cm^{-1} may be assigned as the stretching of 5-coordinate and 4 coordinate (C_2B_3 facial) *B*-H bonds respectively by analogy with 3,3,3,3-$(THF)_4$-3,1,2-*closo*-$SmC_2B_9H_9D_2$[A19]. Similarily, the band at 2381 cm^{-1} intimates interaction between B-*H* and Tl as observed in [PPN][Tl{7,8-*nido*-$C_2B_9H_{11}$}][A20]. Microanalysis was accordant with the proposed formulation of $C_8H_{15}B_9Tl_2$.

Tl_2[1-CH_3OCH_2-1,2-*nido*-$C_2B_9H_{10}$] (**19**) was synthesised and characterised according to the literature[A18], using methods which are similar to those described above.

A.2.2 1-CH_3OCH_2-3-(η^6-*p*-cym)-3,1,2-*closo*-$RuC_2B_9H_{10}$ (**20**)

The reaction of Tl_2[7-CH_3OCH_2-7,8-*nido*-$C_2B_9H_{10}$] (**19**) and [(η^6-*p*-cym)$RuCl_2$]$_2$ (*p*-cym = 1-CH_3-4-$(CH_3)_2CH$-C_6H_4) in CH_2Cl_2 afforded crude compound **20** which was purified by TLC: The synthesis of **20** is not a clean reaction and consequently a low yield of product is retrieved. Preparative TLC with CH_2Cl_2 eluant separated four products from the reaction mixture: The pale brown band at R_f = 1.0 was identified as compound **20**, while the yellow (R_f= 0.8), pink (R_f = 0.7) and orange (R_f = 0.6) bands were found to be non-boron containing. The low yield and absence of carbaborane in these products resulted in them being deemed not to be of current interest and so they were not analysed further. Compound **20**, isolated as pale yellow crystals (from CH_2Cl_2/*n*-hexane [1:4] at -30°C), was identified as 1-CH_3OCH_2-3-(η^6-*p*-cym)-3,1,2-*closo*-$RuC_2B_9H_{10}$ by microanalysis and by infra-red and ^1H and $^{11}B\{^1H\}/^{11}B$ NMR spectroscopies.

Microanalysis was congruous with the proposed formulation of $C_{14}H_{29}RuB_9O$. The IR spectrum showed the expected broad band at 2542 cm^{-1} indicative of B-H stretches and sharp peaks were also observed at 1449, 1382 and 1124 cm^{-1} due to the various CH_3OCH_2 vibrations.

The expected variety of peaks due to the *p*-cymene group and the carbaborane carbon substituent with integrals in the required ratios was noted in the ^1H NMR spectrum (**Figure A.4**). The resonances with relative integral (high to low frequency) of 4:1:2:3:1:3:6 were observed as a multiplet between δ 5.88-5.78 ppm (C_6H_4), a broad peak at δ 3.97 ppm (C_{cage}-*H*), an apparent singlet at δ 3.69 ppm (OCH_2), a singlet at δ 3.32 ppm (OCH_3), a heptet at δ 2.87 ppm ($^3J_{H\text{-}H}$ = 7 Hz, Me_2CH-C_6H_4Me), a singlet at δ 2.31 ppm ($Me_2CHC_6H_4$-CH_3) and a doublet at δ 1.29 ppm ($^3J_{H\text{-}H}$ = 7 Hz, $(CH_3)_2CH$-C_6H_4-Me), respectively.

The aryl hydrogen atoms, H(2'), H(6'), H(3') and H(5'), are chemically (and

magnetically) inequivalent resulting in a complex second order resonance pattern in the ^{1}H NMR spectrum. The OCH_2 hydrogen atoms are also magnetically inequivalent and so would be expected to yield an AB resonance pattern. However, a doublet with a very small coupling (J = 1 Hz) is observed. These protons must therefore have very similar chemical shifts and the H-H coupling constant must presumably be greater than the chemical shift difference between them. All other resonances and couplings are as expected.

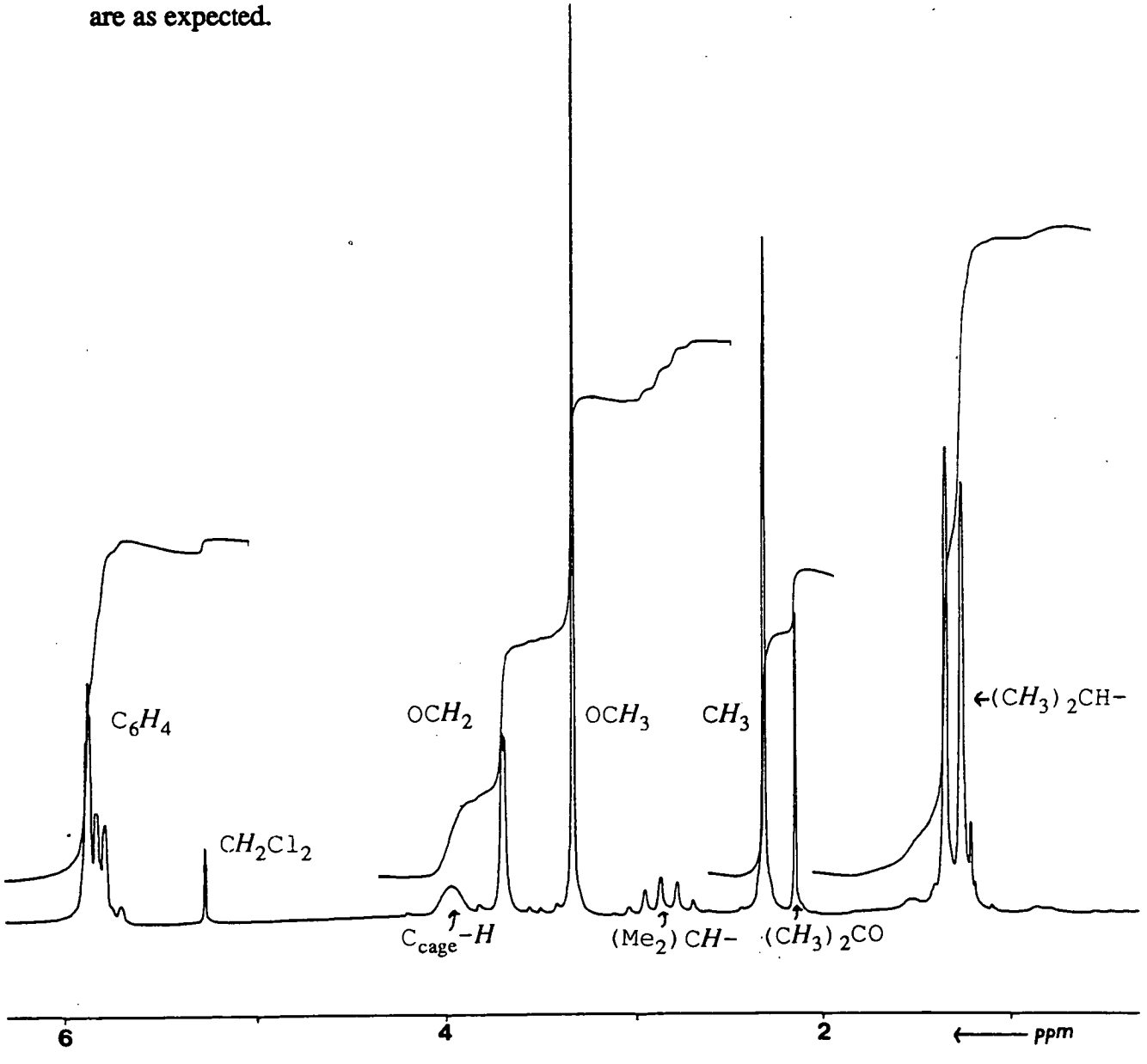

Figure A.4 ^{1}H NMR Spectrum of **20** (200.13 MHz).

The $^{11}B\{^1H\}$ NMR spectrum (**Figure A.5**) showed seven peaks of relative integral 2:1:1:2:1:1:1, the two peaks of integral 2 being double coincidences as the symmetry of the molecule results in all boron atoms being unique. The ^{11}B NMR spectrum indicated the expected coupling with the bound hydrogen atoms.

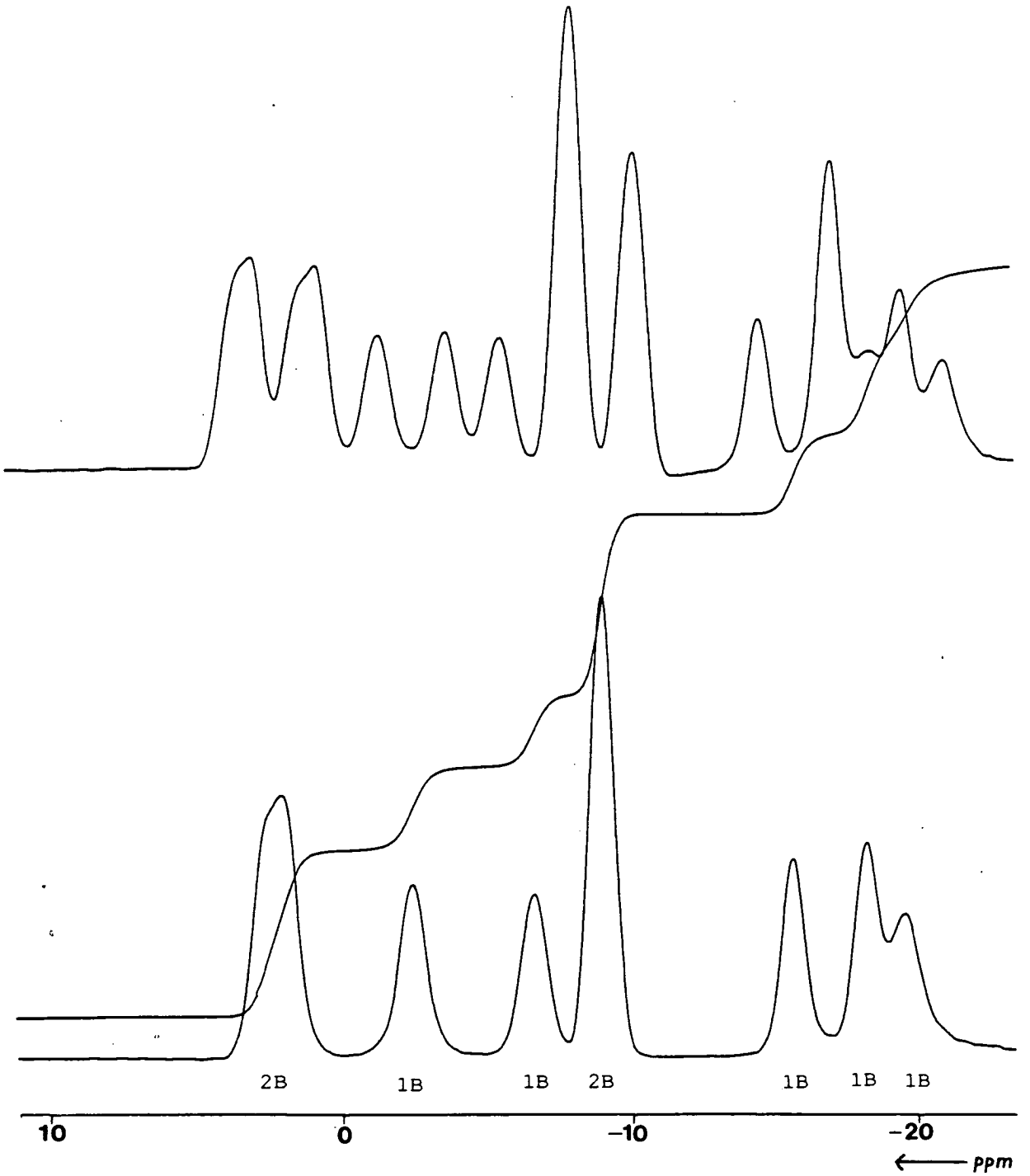

Figure A.5 $^{11}B\{^1H\}/^{11}B$ NMR Spectra of **20** (64.21 MHz).

The assignment of the $^{11}B\{^1H\}$ NMR spectrum of 1,2-$(CH_3OCH_2)_2$-3-(η^6-*p*-cym)-3,1,2-*closo*-$RuC_2B_9H_9$[A21] (**21**) was accomplished by comparison with the assigned (by ^{11}B-^{11}B COSY NMR experiments) spectrum of 3-(η^6-C_6Me_6)-3,1,2-*closo*-$RuC_2B_9H_{11}$[A22] (**22**) and by assuming that the connectivity pattern in these species is the same as that in the corresponding {1,2-*closo*-C_2B_{10}} species. This is a valid assumption since {arene Ru} fragments are isolobal with {BH} and so the changes in relative shielding (electron density distribution) on introduction of electron withdrawing CH_3OCH_2 groups may be considered similar in {3,1,2-*closo*-RuC_2B_9} compounds as in {1,2-*closo*-C_2B_{10}} compounds (as outlined in **Section 1.3.4**).

Similarily, the $^{11}B\{^1H\}$ NMR spectrum of **20** (**Figure A.5**) has been tentatively assigned by comparison with the (assigned) $^{11}B\{^1H\}$ NMR spectra of compounds **21** and **22** (**Table A.1**), the assignment being detailed in **Figure A.6**. The important difference between compounds **21** and **22** and compound **20** is that the former two have C_s symmetry (assuming symmetrical orientation of the *p*-cymene group in **21**) while **20**, being mono-carbon substituted, only has C_1 symmetry. In the un- and di-(carbon) substituted {3,1,2-*closo*-MC_2B_9} compounds, B(5) and B(11), B(9) and B(12) and B(4) and B(7) are symmetry related boron atom pairs [related by a plane of symmetry perpendicular to the C(1)-C(2) bond and bisecting B(6), B(8) and B(10)] but in mono-carbon substituted compounds they become inequivalent as there is no longer a plane of symmetry.

On etheration at C(1), the resonance due to B(6) would be expected to shift to higher frequency compared to the corresponding resonance in (unsubstituted) 3-(η^6-C_6Me_6)-3,1,2-*closo*-$RuC_2B_9H_{11}$ (**22**) and consequently gives rise to the peak of integral 1 at δ -19.5 ppm in the $^{11}B\{^1H\}$ NMR spectrum of **20**, representing a shift of 4.5 ppm to higher frequency. B(5) and B(11), inequivalent in **20**, produce the resonances at δ -15.6 and -18.2 ppm, the resonance due to B(5) probably shifting to

higher frequency (by 4.2 ppm to δ -15.6 ppm) than the B(11) resonance (1.6 ppm to δ -18.2 ppm) because B(5) is directly connected to C(1), the atom at which ether substitution takes place. In the $^{11}B\{^1H\}$ NMR spectrum of **21** the resonances become equivalent again, shifting overall to higher frequency to yield the resonance of integral 2 at δ -16.1 ppm.

	$^{11}B\{^1H\}$ (δ/ppm)		
Atom	**22**	**20**	**21**
B(8)	4.2	2.11	2.05
B(10)	- 2.3	2.11	2.05
B(4)	- 5.4	- 2.38	- 2.86
B(7)	- 5.4	- 6.60	- 2.86
B(9/12)	- 9.5	- 8.93	- 8.73
B(5)	-19.8	-15.62	-16.11
B(11)	-19.8	-18.19	-16.11
B(6)	-24.0	-19.51	-19.34

Table A.1 Comparison of $^{11}B\{^1H\}$ NMR Data of **20, 21** and **22.**

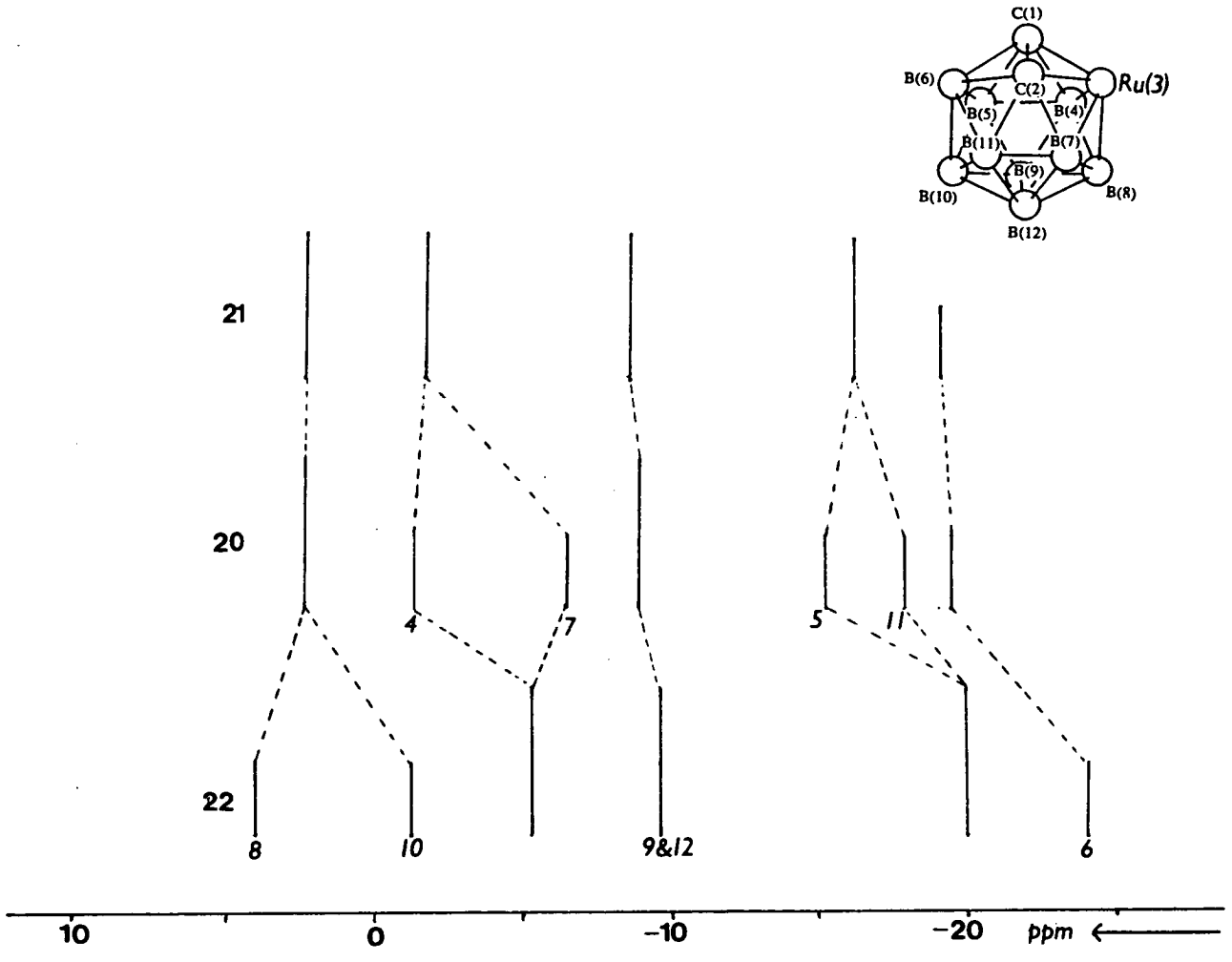

Figure A.6 Assignment of $^{11}B\{^1H\}$ NMR Spectrum of **20**.

As with the resonance due to B(5)/B(11), the B(4)/B(7) resonance in the spectrum of **22** splits to give two resonances of integral 1, one shifted to higher frequency, the other to lower, in the $^{11}B\{^1H\}$ NMR spectrum of **20**. The resonance shifted to higher frequency (by 3.0 ppm to δ -2.4 ppm) is presumably due to B(4) [closer to point of etheration], the lower frequency resonance due to B(7). The shift to lower frequency is probably a consequence of the antipodal effect: B(5), the antipodal atom of B(7), produces a marked shift in resonance to higher frequency (decrease in electron density) resulting in an increase in electron density (and so shift to lower frequency) at B(7), the effect of which is greater than the electron withdrawing effect of the ether group two connectivities away. Similarily, the resonance due to B(8) moves to lower

frequency (by 2.1 ppm to δ 2.1 ppm) since it is antipodal to B(6), the resonance of which exhibits a marked shift to higher frequency as a result of being directly bonded to the atom from which the greatest electron withdrawl takes place [C(1)]. From these observations, it can be deduced that when the shift to higher frequency is greater than *ca.* 4 ppm for one atom then the antipodal effect is the dominant factor in determining the resonance shift of the antipodal atom.

The resonance attributable to B(10) in the spectrum of **20** shifts 4.4 ppm (to contribute to the resonance of integral 2 at δ 2.1 ppm) with respect to the corresponding resonance in the spectrum of **22**. Since B(10) is two connectivities away from the point of substitution, this shift is larger than expected. However, it should be noted that B(10) is antipodal to Ru and the *exo*-polyhedral ligand at ruthenium is different in **20** and **22**. Also, B(10) is directly connected to B(5) and B(6), both of which experience a large decrease in electron density as a consequence of being directly connected to C(1). These factors could possibly affect the relative electron density at B(10) [and, to some extent, at other atoms in the cage] more in **20** than in **22**.

Furthermore, the larger than expected decrease in electron density at B(10) could affect atoms to which it is connected, resulting in possible anomalous shifts: The resonance at δ -8.93 ppm is due to B(9) and B(12) and, at the field strength used (64.21 MHz), does not distinguish between these inequivalent boron positions. However, a slight shift (0.57 ppm) to higher frequency compared to the corresponding (integral 2) resonance in the spectrum of **22** is observed. The shift is somewhat unexpected as B(12) is antipodal to C(1) and because C(1) experiences a large decrease in electron density as a consequence of being directly bound to an electron withdrawing group, a complementary increase in electron density at B(12) [antipodal effect] might have been expected.

It is interesting to note that in the molecular structure of **21** the orientation of the *p*-cymene group with respect to carbaborane results in C_1 molecular symmetry[A21]. However, the $^{11}B\{^1H\}$ NMR spectrum of **21** intimates C_s molecular symmetry with the plane of symmetry perpendicular to the C(1)-C(2) vector: Therefore, in solution, the molecule must have time averaged mirror symmetry and this can only occur if the *p*-cymene group is rotating over the cage about the Ru(3)...B(10) axis. However, in **20**, rotation of *p*-cymene will not alter the (C_1) symmetry of the molecule and so cannot be deduced from the $^{11}B\{^1H\}$ NMR spectrum. The barrier to rotation of arene functions is generally small and, as there are no increased steric restrictions in **20** as compared to **21**, it may be assumed that, in solution, *p*-cymene also rotates in **20**.

A.2.3 1-Ph-3-(η^6-mes)-3,1,2-*closo*-$RuC_2B_9H_{10}$ (23)

1-Ph-3-(η^6-mes)-3,1,2-*closo*-$RuC_2B_9H_{10}$ (**23**; mes = $C_6H_3Me_3$-1,3,5), one of the few examples of a mesitylene carbaruthenaborane compound, was synthesised by reaction between Tl_2[7-Ph-7,8-*nido*-$C_2B_9H_{10}$] (**18**) and the mesitylene ruthenium(II) dimer, [(η^6-$C_6H_3Me_3$-1',3',5')$RuCl_2]_2$, in dichloromethane and was purified by TLC. As with the synthesis of compound **20**, the reaction between thallium carbaborane and mesitylene ruthenium(II) dimer only proceeds with moderate yield; the reaction is not clean and other products are synthesised: TLC revealed two other (non-boron containing) products. With dichloromethane eluant on silica plates, TLC produced a pale yellow band at R_f = 1.0 (compound **23**), a purple band at R_f = 0.5 and a yellow band at R_f = 0.3. ^1H NMR spectra of both the purple and yellow products revealed resonances due to protons in the mesitylene group and other unassigned resonances, but no resonances due to phenyl protons indicating that carbaborane was not present in either product. Crystallisation of the solid recovered from the band at R_f = 1.0 (in CH_2Cl_2/*n*-hexane) produced yellow crystals of **23** in moderate yield.

Both **20** and **23** were synthesised so that the hydrogen atom bound to C(2) could be abstracted with alkyl lithium reagents and a σ-bonded metal introduced as discussed previously for *closo*-carbaborane compounds (**Chapters 2** and **3**). On addition of *n*-BuLi to cooled dimethoxyethane solutions of **20** and **23** respectively, colour changes from yellow to orange were observed. However, results from reaction of these lithiated carbaruthenaboranes with metal fragments such as $CpFe(CO)_2I$ and $Mn(CO)_5Br$ were not encouraging and this line of research has been temporarily discontinued.

Characterisation of **23** was effected by microanalysis and by infra-red and ^1H and $^{11}B\{^1H\}/^{11}B$ NMR spectroscopies. A single crystal X-ray diffraction study was also undertaken and the solid state structure consequently obtained.

The IR spectrum exhibited a broad peak with maximum absorbance at 2520 cm^{-1} corresponding to B-H stretches. Microanalysis of crystals of **23** was consistent with the proposed molecular formula, $C_{17}H_{27}B_9Ru$.

The ^1H NMR spectrum (**Figure A.7**) showed the expected three sets of peaks due to the phenyl and mesitylene groups with integrals in the correct ratio (5:3:9) at δ 7.28-7.04 ppm (multiplet, C_6H_5), δ 5.23 ppm (singlet, $C_6H_3Me_3$) and δ 2.04 ppm (singlet, $C_6H_3(CH_3)_3$) respectively. Also present was a broad peak of integral 1 at δ 4.32 ppm assigned to C_{cage}-*H*. The resonances due to mesitylene aryl protons and methyl substituent protons are singlets in the ^1H NMR spectrum. This intimates that on the NMR timescale the mesitylene is rotating over the C_2B_3 face: Six peaks in total would be expected if rotation was not occurring. The barrier to rotation is likely to be small and therefore rotation is not unexpected. As with **20**, rotation will not impose time averaged mirror symmetry on the molecule and so the $^{11}B\{^1H\}$ NMR spectrum remains asymmetric.

The $^{11}B\{^1H\}$ NMR spectrum (**Figure A.8**) exhibited seven resonances of relative integral 1:1:1:1:2:1:2, the two peaks of integral 2 being double coincidences. The $^{11}B\{^1H\}$ NMR spectrum of **23** was tentatively assigned in a similar way to that of **20**: The resonances were compared with the (assigned[A22]) boron resonances obtained for the related (unsubsitituted) compound, 3-(η^6-C_6Me_6)-3,1,2-*closo*-$RuC_2B_9H_{11}$, **22**, (**Table A.2**) and assigned by comparison, taking account of the assumptions made previously in the assignment of the spectrum of **20** (*i.e.* that {arene Ru} is isolobal with {BH} and so resonance shifts in carbaruthenaboranes on (carbon) substitution should be similar to those observed in the parent *closo*-carbaboranes). Thus, on phenyl substitution at C(1), an overall shift to higher frequency and spectrum width narrowing is observed compared to the unsubstituted species and consistent with the removal of electron density from the cage.

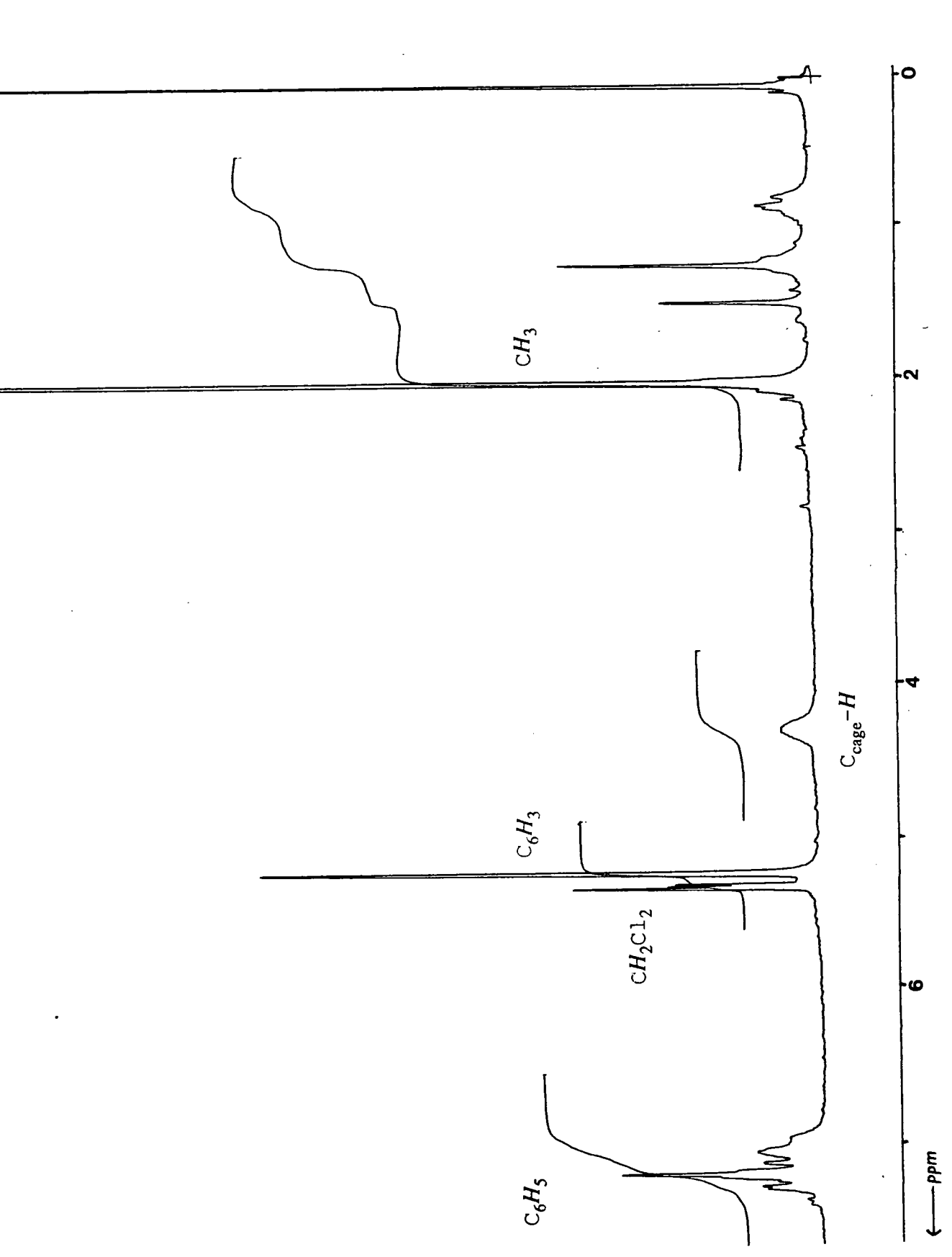

Figure A.7 ^{1}H NMR Spectrum of **23** (200.13 MHz).

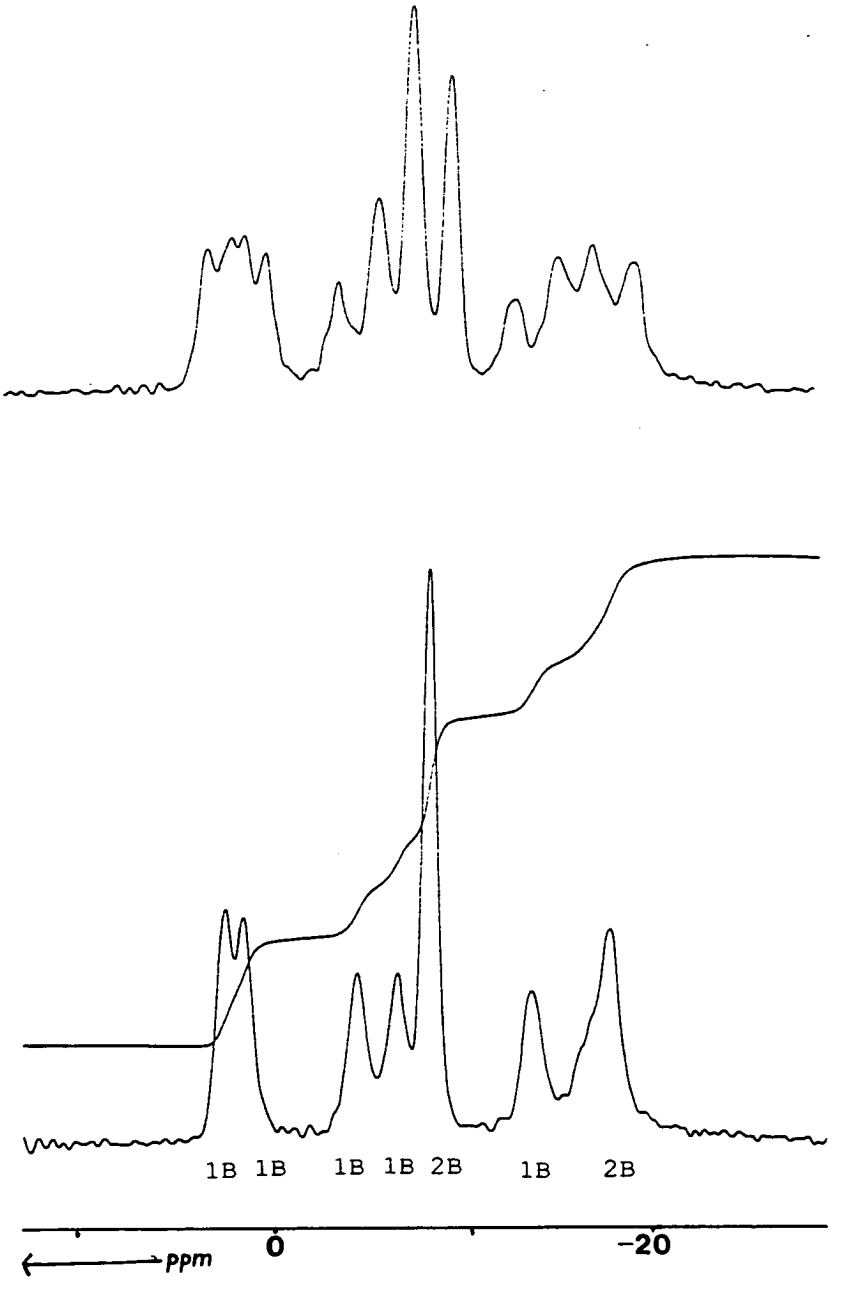

Figure A.8 $^{11}B\{^{1}H\}/^{11}B$ NMR Spectra of **23** (64.21 MHz).

	$^{11}B\{^1H\}$ (δ/ppm)		
Atom	**22**	**23**	diphenyl*/#
B(8)	4.2	3.19	30.32
B(10)	- 2.3	2.17	15.58
B(4)	- 5.4	- 4.25	15.58
B(7)	- 5.4	- 6.51	12.57
B(9/12)	- 9.5	- 8.35	- 0.45
B(5)	-19.8	-14.13	- 1.41
B(11)	-19.8	-18.70	- 1.41
B(6)	-24.0	-18.70	-20.13

Resonances not assigned. Listed from high to low frequency.

Table A.2 Comparison of $^{11}B\{^1H\}$ NMR Data of **22**, **23** and 1,2-Ph_2-3-(η^6-*p*-cym)-3,1,2-*pseudocloso*-$RuC_2B_9H_9$.

The boron atoms affected the most (in terms of electron density distribution) by introduction of an electron withdrawing group at C(1) would be B(4), B(5) and B(6) since they are only one connectivity away from C(1). Thus, B(6) gives the resonance at δ -18.7 ppm in the $^{11}B\{^1H\}$ NMR spectrum of **23**, shifting 5.3 ppm to higher

frequency compared to the corresponding resonance in the spectrum of **22**. Similarily, the resonance due to B(5) shifts 5.7 ppm and the B(4) resonance shifts 1.1 ppm to higher frequency to give integral 1 resonances at δ -14.1 and -4.3 ppm respectively.

The resonances due to the atoms antipodal to B(6) and B(5), B(8) and B(7) respectively, exhibit shifts to lower frequency (by 1.0 ppm to δ 3.2 ppm and 1.1 ppm to δ -6.5 ppm respectively) as a consequence of the (expected) antipodal effect, this dominant over the electron withdrawing effect of the phenyl group for these atoms. B(11), no longer equivalent to B(5) and further from the point of substitution, shifts 1.1 ppm to higher frequency to contribute to the integral 2 resonance at δ -18.7 ppm.

The shift in the B(10) resonance with respect to that in the spectrum of **22** (by 4.5 ppm to δ 2.2 ppm) is larger than expected. As noted in the comparison of **20** and **22**, the *exo*-polyhedral ligand at the atom antipodal to B(10) [Ru] is different. Also, two of the atoms to which B(10) is connected [B(5) and B(6)] experience a decrease in electron density as a result of being directly connected to C(1). These factors could affect the relative shielding at B(10) differently to that expected. Furthermore, these could also anomalously affect atoms connected to B(10): As observed in the spectrum of **20**, the inequivalent atoms B(9) and B(12) give a double coincidence resonance at the field strength used (64.21 MHz), and this shifts slightly (1.2 ppm) to higher frequency. Again, this is unexpected as B(12) is antipodal to C(1) and a shift to lower frequency might have been predicted.

It is of note that comparison of the $^{11}B\{^1H\}$ NMR spectra of the related *closo* parent carbaboranes, 1,2-*closo*-$C_2B_{10}H_{12}$[A18], 1-Ph-1,2-*closo*-$C_2B_{10}H_{11}$ and 1,2-Ph_2-1,2-*closo*-$C_2B_{10}H_{10}$[A23] indicates a general overall resonance shift to higher frequency and spectrum width narrowing on progressive introduction of a phenyl group (**Section 1.3.4**). These trends are also apparent from the comparison of the $^{11}B\{^1H\}$

NMR spectra of **22** and **23**. However, comparison of these spectra with that of 1,2-Ph_2-3-(η^6-arene)-3,1,2-$RuC_2B_9H_9$ (arene = *p*-cymene, C_6H_6, C_6Me_6)[A10, A23] reveals a vast difference with a general shift of the resonances of the latter compounds to much higher frequency as a result of the cage distortions imposed by the steric repulsions of the two phenyl groups. Thus, in contrast to the comparisons observed for (ether carbaruthenaboranes) **20**, **21** and **22**, the NMR spectra of diphenyl carbaruthenaborane compounds would not have been readily predicted.

Large, well formed, yellow crystals of 1-Ph-3-($C_6H_3Me_3$-1',3',5')-3,1,2-*closo*-$RuC_2B_9H_{10}$ (**23**) were produced when *n*-hexane diffused into a dichloromethane (or chloroform) solution at -30°C. An X-ray diffraction study was undertaken to ascertain the overall geometry of the molecule. Intensity data were collected from a single crystal of **23** at ambient temperature. **Table A.3** details atomic positions and equivalent isotropic thermal parameters for all non-hydrogen atoms and **Table A.4** lists selected bond distances and interbond angles. All other relevant data (anisotropic thermal parameters and hydrogen atom coordinates) are given in **Appendix B**. A perspective view of a single molecule of **23** is presented in **Figure A.9**.

The solid state molecular structure of **23** shows it to be a *closo*-carbametallaborane as would be predicted by PSEP theory (*n* + 1 SEP; see **Section 1.2**). The overall cage geometry is that of an unslipped MC_2B_9 icosahedron as expected for a d^6 metal η-bonded to a {*nido*-C_2B_9} fragment. The slip parameter as defined in **Section A.1** (of 0.036 Å) is negligible. The C_2B_3 face, the lower B_5 ring defined by B(6)-B(5)-B(9)-B(12)-B(11) and the aryl ring are all planar with only small estimated standard deviations from planarity (least squares planes) of 0.030, 0.032 and 0.015 Å respectively.

Figure A.10 shows a plan view of a single molecule of **23** with B(5), B(6), B(9),

B(10), B(11) and B(12) and corresponding hydrogen atoms removed for clarity and illustrates the orientation of the phenyl ring with respect to the cage and mesitylene ligand. The conformation of the phenyl substituents in dicarbaborane compounds may be defined in terms of an angle θ, this being a measure of the deviation of the phenyl group from a 90° torsion about the C(1)-C(11) [and, where appropriate, C(2)-C(21)] bond. In **23** the torsion angle C(2)-C(1)-C(11)-C(12) is 158.3(4)° [and C(2)-C(1)-C(11)-C(16) is -21.9(6)°] defining a twist, θ, of 68°. The twists of the two phenyl substituents in the parent *closo*-carbaborane, 1,2-Ph_2-1,2-*closo*-$C_2B_{10}H_{10}$, are 1° and 3° [A24]

	x	y	z	Ueq
Ru(3)	0.57101(3)	0.46432(2)	-0.05340(2)	0.0177(2)
C(1)	0.6556(4)	0.5716(3)	-0.14189(24)	0.0200(18)
C(11)	0.5327(4)	0.6180(3)	-0.1890(3)	0.0240(19)
C(12)	0.4572(5)	0.6929(3)	-0.1499(3)	0.0365(22)
C(13)	0.3362(5)	0.7331(3)	-0.1919(3)	0.0421(25)
C(14)	0.2951(6)	0.7018(4)	-0.2710(3)	0.046(3)
C(15)	0.3712(5)	0.6308(4)	-0.3144(3)	0.046(3)
C(16)	0.4896(6)	0.5885(4)	-0.2729(3)	0.0356(22)
C(31)	0.4960(5)	0.3477(3)	0.0316(3)	0.0291(19)
C(32)	0.4519(5)	0.4340(3)	0.0682(3)	0.0255(19)
C(33)	0.3693(5)	0.5013(3)	0.0209(3)	0.0290(21)
C(34)	0.3314(5)	0.4793(4)	-0.0671(3)	0.0314(22)
C(35)	0.3724(4)	0.3928(3)	-0.1058(3)	0.0287(21)
C(36)	0.4563(5)	0.3282(3)	-0.0572(3)	0.0284(20)
C(311)	0.5844(6)	0.2802(3)	0.0838(4)	0.044(3)
C(331)	0.3227(7)	0.5899(4)	0.0628(4)	0.044(3)
C(351)	0.3299(6)	0.3707(4)	-0.2006(4)	0.043(3)
C(2)	0.7069(5)	0.4638(3)	-0.1684(3)	0.0301(21)
B(12)	0.9430(6)	0.4788(5)	-0.0519(4)	0.031(3)
B(11)	0.8918(6)	0.4581(4)	-0.1620(3)	0.0318(24)
B(4)	0.6918(5)	0.5955(3)	-0.0341(3)	0.0243(20)
B(6)	0.8079(5)	0.5601(4)	-0.2043(3)	0.0305(24)
B(5)	0.7990(6)	0.6435(3)	-0.1193(3)	0.0308(23)
B(7)	0.7873(5)	0.4096(3)	-0.0773(3)	0.0246(21)
B(9)	0.8817(6)	0.5935(4)	-0.0240(3)	0.0300(24)
B(10)	0.9526(6)	0.5739(4)	-0.1292(4)	0.036(3)
B(8)	0.7820(5)	0.4945(4)	0.0108(3)	0.0280(23)

Table A.3 Atomic Positions and Equivalent Isotropic Thermal Parameters ($Å^2$) for All Non-hydrogen Atoms in **23**.

Ru(3) - C(1)	2.181(4)	C(33) -C(34)	1.419(7)
Ru(3) -C(31)	2.215(4)	C(33) -C(331)	1.476(7)
Ru(3) -C(32)	2.196(4)	C(34) -C(35)	1.414(7)
Ru(3) -C(33)	2.251(5)	C(35) -C(36)	1.413(6)
Ru(3) -C(34)	2.248(5)	C(35) -C(351)	1.527(7)
Ru(3) -C(35)	2.253(4)	C(2) -B(11)	1.724(7)
Ru(3) -C(36)	2.210(4)	C(2) - B(6)	1.748(7)
Ru(3) - C(2)	2.157(5)	C(2) - B(7)	1.752(7)
Ru(3) - B(4)	2.196(5)	B(12) -B(11)	1.763(8)
Ru(3) - B(7)	2.188(5)	B(12) - B(7)	1.793(7)
Ru(3) - B(8)	2.232(5)	B(12) - B(9)	1.779(8)
C(1) -C(11)	1.501(5)	B(12) -B(10)	1.793(8)
C(1) - C(2)	1.656(6)	B(12) - B(8)	1.788(8)
C(1) - B(4)	1.706(6)	B(11) - B(6)	1.768(7)
C(1) - B(6)	1.713(6)	B(11) - B(7)	1.753(7)
C(1) - B(5)	1.714(6)	B(11) -B(10)	1.810(8)
C(11) -C(12)	1.407(6)	B(4) - B(5)	1.771(7)
C(11) -C(16)	1.402(7)	B(4) - B(9)	1.773(7)
C(12) -C(13)	1.414(7)	B(4) - B(8)	1.796(7)
C(13) -C(14)	1.338(7)	B(6) - B(5)	1.755(7)
C(14) -C(15)	1.398(7)	B(6) -B(10)	1.776(8)
C(15) -C(16)	1.404(7)	B(5) - B(9)	1.787(7)
C(31) -C(32)	1.408(6)	B(5) -B(10)	1.745(8)
C(31) -C(36)	1.427(6)	B(7) - B(8)	1.804(7)
C(31) -C(311)	1.491(7)	B(9) -B(10)	1.752(8)
C(32) -C(33)	1.421(6)	B(9) - B(8)	1.766(7)

C(1) -Ru(3) -C(31)	175.72(15)	C(36) -Ru(3) - B(8)	127.16(18)
C(1) -Ru(3) -C(32)	146.89(15)	C(2) -Ru(3) - B(7)	47.56(18)
C(1) -Ru(3) -C(33)	116.53(16)	B(4) -Ru(3) - B(8)	47.85(18)
C(1) -Ru(3) -C(34)	103.54(16)	B(7) -Ru(3) - B(8)	48.15(18)
C(1) -Ru(3) -C(35)	113.18(15)	Ru(3) - C(1) -C(11)	109.1(3)
C(1) -Ru(3) -C(36)	140.39(16)	Ru(3) - C(1) - C(2)	66.81(21)
C(1) -Ru(3) - C(2)	44.90(16)	Ru(3) - C(1) - B(4)	67.55(20)
C(1) -Ru(3) - B(4)	45.89(16)	C(11) - C(1) - C(2)	120.7(3)
C(1) -Ru(3) - B(7)	79.33(16)	C(11) - C(1) - B(4)	121.4(3)
C(1) -Ru(3) - B(8)	79.50(17)	C(11) - C(1) - B(6)	114.1(3)
C(31) -Ru(3) -C(32)	37.22(16)	C(11) - C(1) - B(5)	115.2(3)
C(31) -Ru(3) -C(33)	67.64(16)	C(2) - C(1) - B(6)	62.5(3)
C(31) -Ru(3) -C(34)	79.21(17)	B(4) - C(1) - B(5)	62.4(3)
C(31) -Ru(3) -C(35)	67.06(16)	B(6) - C(1) - B(5)	61.6(3)
C(31) -Ru(3) -C(36)	37.63(16)	C(1) -C(11) -C(12)	120.7(4)
C(31) -Ru(3) - C(2)	130.88(17)	C(1) -C(11) -C(16)	121.3(4)
C(31) -Ru(3) - B(4)	135.93(17)	C(12) -C(11) -C(16)	117.9(4)
C(31) -Ru(3) - B(7)	96.90(17)	C(11) -C(12) -C(13)	120.8(4)
C(31) -Ru(3) - B(8)	99.55(17)	C(12) -C(13) -C(14)	119.9(5)
C(32) -Ru(3) -C(33)	37.23(16)	C(13) -C(14) -C(15)	121.3(5)
C(32) -Ru(3) -C(34)	66.22(17)	C(14) -C(15) -C(16)	119.6(5)
C(32) -Ru(3) -C(35)	78.18(16)	C(11) -C(16) -C(15)	120.3(4)
C(32) -Ru(3) -C(36)	66.86(16)	Ru(3) -C(31) -C(32)	70.67(25)
C(32) -Ru(3) - C(2)	167.48(17)	Ru(3) -C(31) -C(36)	71.0(3)
C(32) -Ru(3) - B(4)	108.18(17)	Ru(3) -C(31) -C(311)	128.2(3)
C(32) -Ru(3) - B(7)	122.26(17)	C(32) -C(31) -C(36)	117.8(4)

Table A.4 Selected Interatomic Distances (Å) and Interbond Angles (°) in **23**.

C(32)	-Ru(3)	- B(8)	96.52(17)	C(32)	-C(31)	-C(311)	120.8(4)
C(33)	-Ru(3)	-C(34)	36.76(17)	C(36)	-C(31)	-C(311)	121.4(4)
C(33)	-Ru(3)	-C(35)	66.39(16)	Ru(3)	-C(32)	-C(31)	72.1(3)
C(33)	-Ru(3)	-C(36)	79.35(17)	Ru(3)	-C(32)	-C(33)	73.5(3)
C(33)	-Ru(3)	- C(2)	153.57(17)	C(31)	-C(32)	-C(33)	123.0(4)
C(33)	-Ru(3)	- B(4)	99.27(17)	Ru(3)	-C(33)	-C(32)	69.28(25)
C(33)	-Ru(3)	- B(7)	158.82(17)	Ru(3)	-C(33)	-C(34)	71.5(3)
C(33)	-Ru(3)	- B(8)	117.91(18)	Ru(3)	-C(33)	-C(331)	131.3(4)
C(34)	-Ru(3)	-C(35)	36.62(17)	C(32)	-C(33)	-C(34)	117.6(4)
C(34)	-Ru(3)	-C(36)	66.53(17)	C(32)	-C(33)	-C(331)	121.0(4)
C(34)	-Ru(3)	- C(2)	120.39(18)	C(34)	-C(33)	-C(331)	121.4(4)
C(34)	-Ru(3)	- B(4)	116.05(18)	Ru(3)	-C(34)	-C(33)	71.7(3)
C(34)	-Ru(3)	- B(7)	158.39(18)	Ru(3)	-C(34)	-C(35)	71.9(3)
C(34)	-Ru(3)	- B(8)	153.31(18)	C(33)	-C(34)	-C(35)	121.1(4)
C(35)	-Ru(3)	-C(36)	36.88(16)	Ru(3)	-C(35)	-C(34)	71.5(3)
C(35)	-Ru(3)	- C(2)	101.10(17)	Ru(3)	-C(35)	-C(36)	69.9(3)
C(35)	-Ru(3)	- B(4)	148.14(17)	Ru(3)	-C(35)	-C(351)	129.7(3)
C(35)	-Ru(3)	- B(7)	122.32(17)	C(34)	-C(35)	-C(36)	119.8(4)
C(35)	-Ru(3)	- B(8)	164.00(17)	C(34)	-C(35)	-C(351)	120.0(4)
C(36)	-Ru(3)	- C(2)	104.96(17)	C(36)	-C(35)	-C(351)	120.1(4)
C(36)	-Ru(3)	- B(4)	173.45(17)	Ru(3)	-C(36)	-C(31)	71.4(3)
C(36)	-Ru(3)	- B(7)	97.35(17)	Ru(3)	-C(36)	-C(35)	73.2(3)
C(31)	-C(36)	-C(35)	120.7(4)	C(1)	- B(5)	- B(4)	58.6(3)
Ru(3)	- C(2)	- C(1)	68.30(21)	C(1)	- B(5)	- B(6)	59.1(3)
Ru(3)	- C(2)	- B(7)	67.13(22)	B(4)	- B(5)	- B(9)	59.8(3)
C(1)	- C(2)	- B(6)	60.3(3)	B(6)	- B(5)	-B(10)	61.0(3)
B(11)	- C(2)	- B(6)	61.2(3)	B(9)	- B(5)	-B(10)	59.5(3)
B(11)	- C(2)	- B(7)	60.6(3)	Ru(3)	- B(7)	- C(2)	65.31(22)
B(11)	-B(12)	- B(7)	59.1(3)	Ru(3)	- B(7)	- B(8)	67.22(22)
B(11)	-B(12)	-B(10)	61.2(3)	C(2)	- B(7)	-B(11)	58.9(3)
B(7)	-B(12)	- B(8)	60.5(3)	B(12)	- B(7)	-B(11)	59.6(3)
B(9)	-B(12)	-B(10)	58.7(3)	B(12)	- B(7)	- B(8)	59.6(3)
B(9)	-B(12)	- B(8)	59.3(3)	B(12)	- B(9)	-B(10)	61.0(3)
C(2)	-B(11)	- B(6)	60.1(3)	B(12)	- B(9)	- B(8)	60.6(3)
C(2)	-B(11)	- B(7)	60.5(3)	B(4)	- B(9)	- B(5)	59.7(3)
B(12)	-B(11)	- B(7)	61.3(3)	B(4)	- B(9)	- B(8)	61.0(3)
B(12)	-B(11)	-B(10)	60.2(3)	B(5)	- B(9)	-B(10)	59.1(3)
B(6)	-B(11)	-B(10)	59.5(3)	B(12)	-B(10)	-B(11)	58.6(3)
Ru(3)	- B(4)	- C(1)	66.56(20)	B(12)	-B(10)	- B(9)	60.2(3)
Ru(3)	- B(4)	- B(8)	67.12(22)	B(11)	-B(10)	- B(6)	59.1(3)
C(1)	- B(4)	- B(5)	59.0(3)	B(6)	-B(10)	- B(5)	59.8(3)
B(5)	- B(4)	- B(9)	60.6(3)	B(5)	-B(10)	- B(9)	61.5(3)
B(9)	- B(4)	- B(8)	59.3(3)	Ru(3)	- B(8)	- B(4)	65.03(22)
C(1)	- B(6)	- C(2)	57.2(3)	Ru(3)	- B(8)	- B(7)	64.63(22)
C(1)	- B(6)	- B(5)	59.2(3)	B(12)	- B(8)	- B(7)	59.9(3)
C(2)	- B(6)	-B(11)	58.7(3)	B(12)	- B(8)	- B(9)	60.1(3)
B(11)	- B(6)	-B(10)	61.4(3)	B(4)	- B(8)	- B(9)	59.7(3)
B(5)	- B(6)	-B(10)	59.2(3)				

Table A.4 Selected Interbond Angles (°) in **23** (continued).

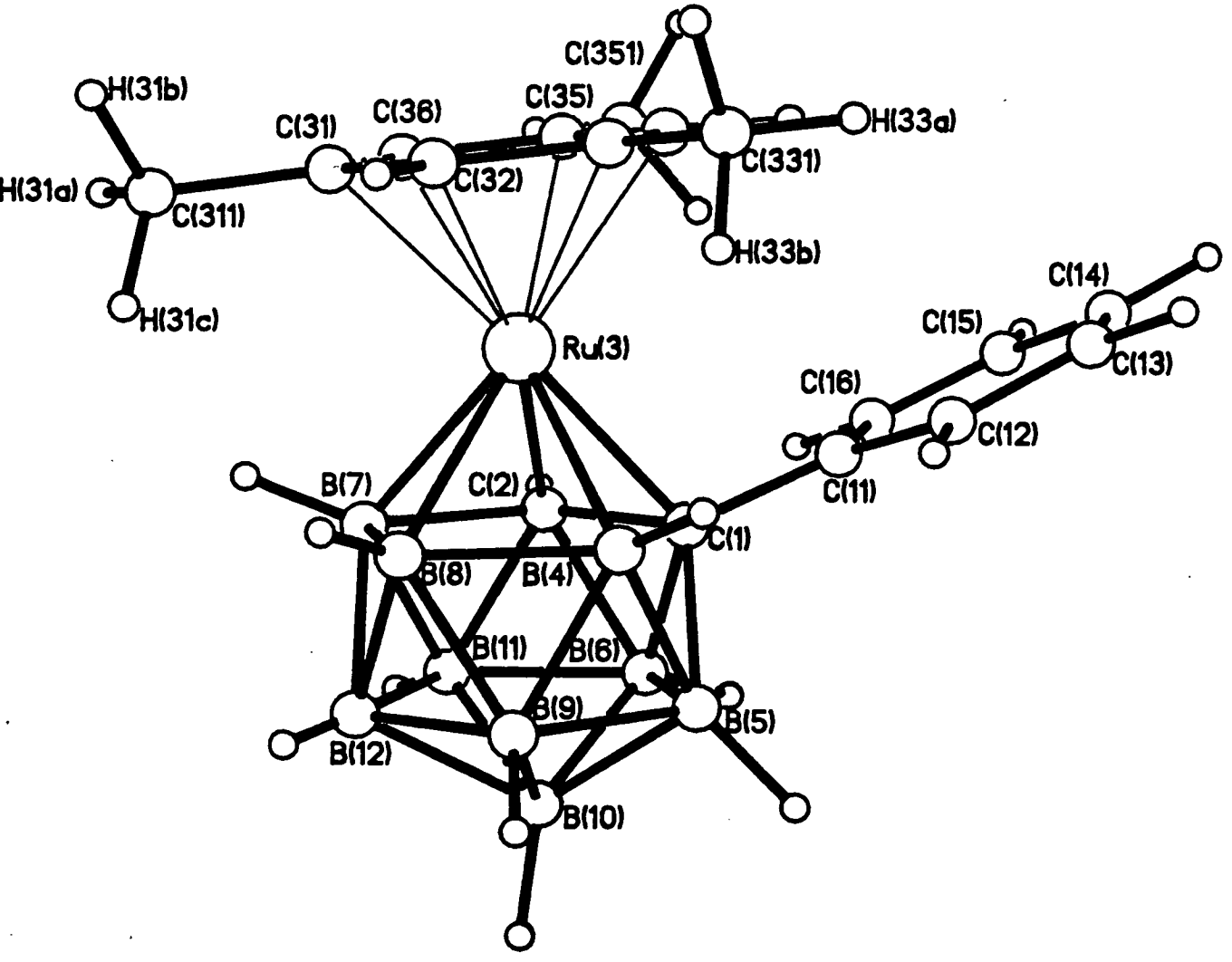

Figure A.9 Perspective View of a Single Molecule of **23** (cage H atoms carry the same number as the [B & C] atoms to which they are bound).

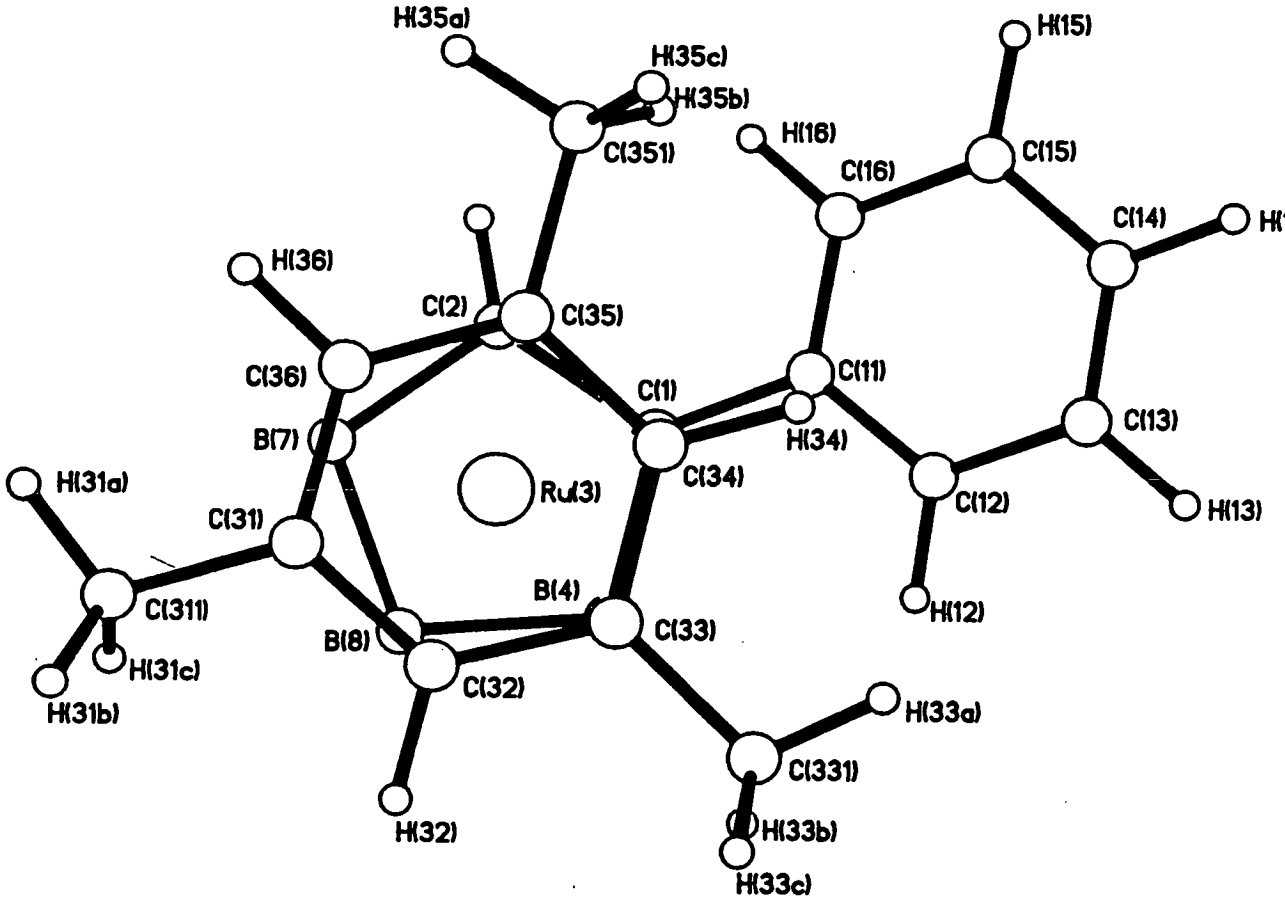

Figure A.10 Plan View of a Single Molecule of **23** With B(5), B(6), B(9), B(10), B(11) and B(12) Removed for Clarity.

Analysis of possible interactions in **23** between the phenyl group and mesitylene and carbaborane intimates that the phenyl group has probably adopted such a twist in order to minimise sterically unfavourable interactions between the groups: The mesitylene group and the phenyl ring are orientated such that the phenyl group lies between two methyl groups with the C(34)-H(34) bond almost eclipsing the C(1)-C(31) bond. The distance between H(35B) [mesitylene] and H(16) [phenyl] is

2.432(7) Å and between H(33A) [mesitylene] and H(12) [phenyl] it is 2.940(7) Å. Also, the distance between between H(4B) [carbaborane] and H(12) [phenyl] is 2.04(7) Å and between H(2C) [carbaborane] and H(16) [phenyl] it is 2.44(9) Å. The H(2C)-H(16) and H(35B)-H(16) distances are just longer and the H(4B)-H(12) distance is shorter than the sum of the van der Waals' radii of two hydrogen atoms (2.4 Å[A25]), though it should be noted that the phenyl (and methyl) hydrogen atoms have been set in idealised positions. Consequently, these distances are (possibly) not absolute values, but they do give an indication of likely H...H interactions. Therefore, these short H...H distances suggest that the orientation of the phenyl group is a compromise in order to minimise steric interactions of phenyl with both mesitylene and carbaborane: Any greater twist might relieve the unfavourable interactions between H(4B) and H(12) and between H(35B) and H(16) but is likely to increase those between H(2C) and H(16) and between H(12) and H(33A).

It is of note that the twist of the phenyl ring is similar to that observed in related species with two phenyl rings on the adjacent cage carbon atoms as, for example, in 1,2-Ph_2-3-(η^6-*p*-cym)-3,1,2-*pseudocloso*-$RuC_2B_9H_9$[A10] where $\theta = 66°$ and 44° and in 1,2-Ph_2-3-(η^6-C_6H_6)-3,1,2-*pseudocloso*-$RuC_2B_9H_9$[A10] where $\theta = 61°$. These twists of the phenyl rings with respect to the cage have been attributed to the steric influence of the arene and the phenyl groups, the phenyl rings twisting to minimise steric interactions with the arene and with each other. Additionally, the presence of three sterically demanding ligands has resulted in distortion of the icosahedron with essentially non-bonding C(1)-C(2) distances of 2.455(6) Å in the former and 2.486(6) Å in the latter. The C(1)-C(2) bond length in **23** is 1.656(6) Å which is longer than that in the related (unsubstituted) species 3-(η^6-C_6H_6)-3,1,2-*closo*-$RuC_2B_9H_{11}$ [C(1)-C(2) = 1.626 (5) Å] and similar to that in 3-(η^6-C_6Me_6)-3,1,2-$RuC_2B_9H_{11}$[A27] [C(1)-C(2) = 1.657(10) Å] but significantly shorter than that in the distorted compounds described above. Thus, the steric influences of the mesitylene and phenyl

groups in **23** do not affect the overall geometry as observed in the diphenyl carbaruthenaborane compounds.

The plane of the mesitylene group is tilted with respect to the lower pentagonal belt by 5.5° about an axis lying almost perpendicular to the C(35)-C(36) and C(32)-C(33) vectors and away from the phenyl ring: C(31), C(32) and C(36) lie between 0.03 and 0.05 Å closer to the ruthenium atom than do C(33), C(34) and C(35), these atoms lying above C(2), C(1) and B(4) respectively. The corresponding tilting angle for 3-(η^6-C_6Me_6)-3,1,2-*closo*-$RuC_2B_9H_{11}$[A26] (**22**) is 3.2° and for 1,2-$(CH_3OCH_2)_2$- 3-(η^6-*p*-cym)-3,1,2-*closo*-$RuC_2B_9H_9$[A21] (**21**) is 7.0°, the arenes in both species tilting away from C(1) and C(2). The tilt in the former has been explained[A8] by the (assumedly) stronger *trans* influence arising from the stronger bonding of ruthenium to boron [B(4), B(7), B(8)] versus carbon [C(1) and C(2)] while, in the latter, steric repulsion has been attributed as the dominant factor[A21]. The tilt observed in **23** is presumably a consequence of the two factors since there is some steric interaction observed.

A.3 Conclusions

Mesitylene and *p*-cymene mono-carbon substituted carbaruthenaborane compounds, 1-CH_3OCH_2-3-(η^6-*p*-cym)-3,1,2-*closo*-$RuC_2B_9H_{10}$ (**20**) and 1-Ph-3-(η^6-$C_6H_3Me_3$-1',3',5')-3,1,2-*closo*-$RuC_2B_9H_{10}$ (**23**), have been successfully synthesised and characterised, the two compounds synthesised in low yield from the appropriate thallium carbaborane and arene ruthenium(II) dimer. Microanalysis, infra-red and ^1H NMR data were consistent with the proposed formulations.

The $^{11}B\{^1H\}$ NMR spectra of **20** and **23** have been assigned by comparison with (assigned) spectra of related species and by accounting for factors described previously (**Section 1.3.4**), in particular, taking note that {arene Ru} is isolobal with {BH}. On introduction of an electron withdrawing group (Ph or CH_3OCH_2), net electron withdrawal from the carbaborane cage is observed as manifested in the shifts of boron resonances to higher frequency compared to corresponding resonances in the spectrum of a related unsubstituted carbaruthenaborane compound.

An X-ray diffraction study of a single crystal of **23** confirmed it to be a carbaruthenaborane with the anticipated *closo* geometry, the metal 'unslipped' as expected for a d^6 metal η-bonded to a {*nido*-C_2B_9} fragment. The twist (θ) of the phenyl ring with respect to the carbaborane cage is comparable to the twists observed in related diphenyl carbaruthenaborane compounds (for example, 1,2-Ph_2-3-(η^6-*p*-cym)-3,1,2-*pseudocloso*-$RuC_2B_9H_9$) implying that there is some steric repulsion between the phenyl and mesitylene (and carbaborane) groups, but not enough to cause distortion of the polyhedron as observed consistently in diphenyl species.

These mono-carbon substituted carbaruthenaborane compounds were initially synthesised so that the hydrogen atom bound to C(2) could be replaced with an isolobal metal fragment to form dimetal carbaborane compounds. Successful

lithiation appears to have occurred but introduction of the metal fragment has so far proved elusive. It is possible that steric repulsion between the carbaborane substituents ({arene Ru} and Ph/CH_3OCH_2) and the incoming metal fragment prevents formation of the dimetal species. Consequently, sterically undemanding metal fragments and substituents may be required for reaction to take place. This remains a field of research with great potential and would complement current work by Stone *et al*[A27] where dimetal species with one metal η-bonded to a *nido*-carbaborane and the second metal fragment σ-bonded to a cage boron atom have been reported (see **Section 1.4.1** and **Figure 1.17**, p24).

A.4 Experimental

A.4.1 General Techniques

The general experimental techniques and conditions, solvents and instruments used in the preparation of the following compounds were as those described in **Section 5.2.1.**

A.4.2 Starting Materials

1-Ph-1,2-*closo*-$C_2B_{10}H_{11}$ (**Section 5.2.2**), Tl_2[7-CH_3OCH_2-7,8-*nido*-$C_2B_9H_{10}$][A18] (**19**), [(η^6-mes)$RuCl_2$]$_2$[A28] (mes = $C_6H_3Me_3$-1,3,5) and [(η^6-*p*-cym)$RuCl_2$]$_2$[A29] (*p*-cym = 1-CH_3-4-$(CH_3)_2$CH-C_6H_4) were synthesised by literature methods. Tl[$OOCCH_3$] and KOH (pellets) were used as received.

A.4.3 Synthesis of Tl_2[7-Ph-7,8-*nido*-$C_2B_9H_{10}$] (**18**)

A mixture of 1.76g (8.0 mmol) 1-Ph-1,2-*closo*-$C_2B_{10}H_{11}$ and 2.69g (48 mmol) KOH were dissolved in 20cm^3 EtOH and stirred at room temperature for 30 minutes before refluxing for 3h. After cooling, EtOH was removed *in vacuo* revealing a waxy white solid, K_2[7-Ph-7,8-*nido*-$C_2B_9H_{10}$]. This was dissolved in 15cm^3 H_2O, filtered, and to the solution 4.21g (16 mmol) Tl[$OOCCH_3$] in 10cm^3 H_2O was added dropwise. The bright yellow solid of Tl_2[7-Ph-7,8-*nido*-$C_2B_9H_{10}$] which precipitated out was recovered by filtration and washed with 3 x 15cm^3 EtOH and 3 x 15cm^3 Et_2O. The solid (81% yield) was dried *in vacuo* in the dark.

Microanalysis: Calculated (for $C_8H_{15}B_9Tl_2$): %C 15.6, %H 2.45; Found: %C 15.0, %H 2.18

IR (KBr): ν_{max}/cm^{-1}: 2509, 2443, 2381 (B-H)

A.4.4 Synthesis of 1-CH_3OCH_2-3-(η^6-*p*-cym)-3,1,2-*closo*-$RuC_2B_9H_{10}$ (20)

A mixture of 1.07g (1.75 mmol) $[(\eta^6\text{-}p\text{-cym})RuCl_2]_2$ and 2.05g (3.5 mmol) $Tl_2[7\text{-}CH_3OCH_2\text{-}7,8\text{-}C_2B_9H_{10}]$ (**19**) were cooled to -196° before addition of $10cm^3$ CH_2Cl_2. The mixture was allowed to warm to room temperature with stirring and a colour change in the solution from red/brown to deep red and precipitation of a grey solid were observed. After stirring for 1h at room temperature the solution was filtered and the volume of filtrate reduced to *ca.* $2cm^3$. The required product was isolated by preparative TLC with CH_2Cl_2 eluant: The pale brown band at R_f = 1.0 was collected and afforded a yellow solid. Crystallisation from CH_2Cl_2/*n*-hexane at -30°C produced large, well formed crystals of **20** in 29% yield.

Microanalysis: Calculated (for $C_{14}H_{29}B_9ORu$): %C 40.8, %H 7.10; Found %C 40.4, %H 6.92

IR (CH_2Cl_2): ν_{max}/cm^{-1}: 2542 (B-H); 1449, 1382, 1124 (CH_3OCH_2)

NMR (CD_2Cl_2): $^{11}B\{^1H\}$ (δ/ppm): 2.11 [2B, B(8)/B(10)], -2.38 [1B, B(4)], -6.60 [1B, B(7)], -8.93 [2B, B(9)/B(12)], -15.62 [1B, B(5)], -18.19 [1B, B(11)], -19.51 [1B, B(6)]; $^1J_{B\text{-}H}$ = 86-160 Hz

^1H (δ/ppm): 5.88-5.78 (m, 4H, C_6H_4), 3.97 (broad, 1H, C_{cage}-*H*), 3.69 (apparent d, J = 1 Hz, 2H, OCH_2), 3.32 (s, 3H, OCH_3), 2.87 (heptet, $^3J_{H\text{-}H}$ = 7 Hz, 1H, $Me_2CHC_6H_4Me$), 2.31 (s, 3H, $Me_2CHC_6H_4CH_3$), 1.29 (d, $^3J_{H\text{-}H}$ = 7 Hz, 6H, $(CH_3)_2CHC_6H_4Me$)

A.4.5 Synthesis of 1-Ph-3-(η^6-mes)-3,1,2-*closo*-$RuC_2B_9H_{10}$ (23)

Compound **23** was synthesised in a similar manner to that described for **20**: A mixture of $[(\eta^6\text{-mes})RuCl_2]_2$ (0.88g; 1.5 mmol) and Tl_2[7-Ph-7,8-*nido*-$C_2B_9H_{10}$] (1.85g; 3.0 mmol) were allowed to warm from -196° in 10cm^3 CH_2Cl_2, and then stirred for 30 minutes at room temperature. The orange solution was filtered from the grey solid and the volume of the filtrate reduced to *ca.* 2cm^3 *in vacuo*. Preparative TLC (CH_2Cl_2 eluant) revealed several bands of which the yellow band at R_f = 1.0 was collected. Further purification was achieved by crystallisation from CH_2Cl_2/*n*-hexane at -30° which afforded yellow crystals of **23** in 26% yield.

Microanalysis: Calculated (for $C_{17}H_{27}B_9Ru$): %C 47.5, %H 6.33; Found: %C 47.1, %H 6.04

IR (CH_2Cl_2): ν_{max}/cm^{-1}: 2522 (B-H)

NMR ($CDCl_3$): $^{11}B\{^1H\}$ (δ/ppm): 3.19 [1B, B(8)], 2.17 [1B, B(10)], -4.25 [1B, B(4)], -6.51 [1B, B(7)], -8.35 [2B, B(9)/B(12)], -14.13 [1B, B(5)], -18.70 [2B, B(11)/B(6)]; $^1J_{B\text{-}H}$ = 79-158 Hz

^1H (δ/ppm): 7.28-7.04 (m, 5H, C_6H_5), 5.23 (s, 3H, $C_6H_3Me_3$), 4.32 (broad, 1H, C_{cage}-*H*), 2.04 (s, 9H, $C_6H_3(CH_3)_3$)

A.4.6 Crystallographic Data for 23

The experimental techniques used in the crystallographic determination of the molecular structure of **23** were as those described in **Section 5.3**.

Crystal Data

$C_{17}H_{27}B_9Ru$, M = 429.76, orthorhombic, space group $P2_12_12_1$, a = 9.300(4) Å, b =

14.217(5) Å, c = 15.1943(4) Å, V = 2009.0(14) Å^3, from least squares refinement of 25 centred reflections ($14 \leq \theta \leq 15$) at 291±1K, Z = 4, D_c = 1.421 gcm^{-3}, μ(Mo-K_α) = 7.64 cm^{-1}, F(000) = 872 e.

Data collection and reduction

Variable scan speeds between 0.92-2.35 °min^{-1}. 2044 independent reflections measured ($1 \leq \theta \leq 25°$; $0 \leq h \leq 11$, $0 \leq k \leq 16$, $0 \leq l \leq 18$) of which 2021 had $F \geq 2.0\sigma(F)$. No significant crystal movement noted but data corrected for crystal decay (10%) over period of data collection (47h).

Structure solution and refinement

Ru from Patterson syntheses. B, C, H_{cage} from full-matrix least squares refinement/ΔF syntheses. Cage H atoms refined positionally subject to a single B-H distance of 1.10(5) Å. Phenyl and methyl H atoms set in idealised positions (C-H = 1.08 Å). Empirical absorption correction applied after isotropic convergence. Thereafter all non-H atoms allowed anisotropic thermal motion. H atoms refined with a common thermal parameter (cage H and non-cage H treated separately), $U_{cage\ H}$ = 0.058(6) Å^2 and $U_{noncage\ H}$ = 0.081(6) Å^2 at convergence. g = 0.000280, R = 0.0295, R_w = 0.0355, S = 0.972, number of variables = 278. Maximum shift/esd = 0.10. Maximum and minimum residues in final ΔF map = 0.58 and -0.61 eÅ^{-3} respectively.

A.5 References

A1. M.F. Hawthorne, D.C. Young and P.A. Wegner, *J. Am. Chem. Soc.*, 1965, **87**, 1818.

A2. T. Onak in "*Comprehensive Organometallic Chemistry*", Eds. G. Wilkinson, F.G.A. Stone and E.W. Abel, Pergamon Press, 1981, Section 5.4.

A3. R.G. Swisher, E. Sinn and R.N. Grimes, *Organometallics*, 1984, **3**, 599.

A4. D.E. Smith and A.J. Welch, *Organometallics*, 1986, **5**, 760.

A5. Z.G. Lewis, D. Reed and A.J. Welch, *J. Chem. Soc., Dalton Trans.*, 1992, 731.

A6. M.F. Hawthorne, D.C. Young, T.D. Andrews, D.V. Howe, R.L. Pilling, A.D. Pitts, M. Reintjes, L.F. Warren Jr. and P.A. Wegner, *J. Am. Chem. Soc.*, 1968, **90**, 879.

A7. M.P. Garcia, M. Green, F.G.A. Stone, R.G. Somerville and A.J. Welch, *J. Chem. Soc., Chem. Commun.*, 1981, 871.

A8. M.P. Garcia, M. Green, F.G.A. Stone, R.G. Somerville, A.J. Welch, C.E. Briant, D.N. Cox and D.M.P Mingos, *J. Chem. Soc., Dalton Trans.*, 1985, 2343.

A9. Z.G. Lewis and A.J. Welch, *Acta Cryst.*, 1992, **C48**, 53.

A10. J. Cowie and A.J. Welch, unpublished results.

A11. H.M. Colquohoun, T.J. Greenhough and M.G.H. Wallbridge, *J. Chem. Soc., Chem. Commun.*, 1976, 1019.

A12. *idem.*, *Acta Cryst.*, 1977, **B33**, 3604.

A13. *idem.*, *J. Chem. Soc., Dalton Trans.*, 1979, 619.

A14. J. Kim, S. Kim and Y. Do, *J. Chem. Soc., Chem. Commun.*, 1992, 938.

A15. R.N. Grimes in "*Comprehensive Organometallic Chemistry*", Eds. G. Wilkinson, F.G.A. Stone and E.W. Abel, Pergamon Press, 1981, Section 5.5.

A16. M.F. Hawthorne, *J. Organometal. Chem.*, 1975, **100**, 97.

A17. J.L. Spencer, M. Green and F.G.A. Stone, *J. Chem. Soc., Chem. Commun.*, 1972, 1178.

A18. K.F. Shaw and A.J. Welch, *Polyhedron*, 1992, **11**, 157.

A19. M.J. Manning, C.B.Knobler and M.F. Hawthorne, *Inorg. Chem.*, 1991, **30**, 2009.

A20. *idem.*, *ibid.*, 1991, **30**, 3589.

A21. K.F. Shaw, PhD Thesis, University of Edinburgh, 1992.

A22. M. Bown, J. Plesek, K. Base, B. Stibr, X.L.R Fontaine, N.N. Greenwood and J.D. Kennedy, *Mag. Reson. Chem.*, 1989, **27**, 947.

A23. Z.G. Lewis, PhD Thesis, University of Edinburgh, 1991.

A24. Z.G. Lewis and A.J. Welch, *Acta Cryst.*, in press (1992).

A25. A. Earnshaw and N.N. Greenwood, "*The Chemistry of the Elements*", Pergamon Press, Oxford, 1982.

A26. M. Bown, J. Plesek, B. Stibr, X.L.R. Fontaine, N.N. Greenwood, J.D. Kennedy

and M. Thornton-Pett, *Acta Cryst.*, 1990, **C46**, 995.

A27. **a**: S.A. Brew, N. Carr, M.D. Mortimer and F.G.A. Stone, *J. Chem. Soc., Dalton Trans.*, 1991, 811; **b**: M.U. Pilotti, F.G.A. Stone and I. Topaloglu, *ibid.*, 1991, 1355; **c**: *idem., ibid.*, 1991, 1621; **d**: S.A. Brew and F.G.A. Stone, *ibid.*, 1992, 867.

A28. M.A. Bennett and A.K. Smith, *J. Chem. Soc., Dalton Trans.*, 1974, 233.

A29. M.A. Bennett, T.-N. Huang, T.W. Mathieson and A.K. Smith, *Inorg. Synth.*, 1982, **21**, 75.

APPENDIX B

SUPPLEMENTARY CRYSTALLOGRAPHIC DATA

	x	y	z
H(12)	0.1688(10)	0.4431(8)	0.0219(8)
H(13)	0.2323(10)	0.3887(10)	-0.1501(8)
H(14)	0.1595(12)	0.2003(9)	-0.2254(8)
H(15)	-0.0034(14)	0.0657(9)	-0.1336(8)
H(16)	-0.0710(11)	0.1237(8)	0.0357(8)
H(22)	0.2139(10)	0.2313(7)	0.2943(9)
H(23)	0.2028(13)	0.0663(8)	0.3841(9)
H(24)	-0.0341(14)	-0.0494(8)	0.4027(8)
H(25)	-0.2502(12)	-0.0073(8)	0.3160(8)
H(26)	-0.2380(10)	0.1563(7)	0.2238(8)
H(32)	-0.1863(12)	0.3830(8)	0.3219(7)
H(33)	-0.4308(12)	0.4195(9)	0.2984(7)
H(34)	-0.5688(13)	0.4049(9)	0.1200(8)
H(35)	-0.4666(12)	0.3520(9)	-0.0308(8)
H(36)	-0.2201(10)	0.3233(8)	-0.0136(6)
H(101)	0.106(13)	0.775(10)	0.414(10)
H(111)	0.059(14)	0.689(10)	0.321(11)
H(102)	-0.1089(11)	0.5691(9)	0.5352(9)
H(112)	-0.1419(11)	0.5886(9)	0.3998(9)
H(122)	-0.1054(11)	0.7002(9)	0.4965(9)
H(3B)	0.307(11)	0.590(7)	0.528(7)
H(6B)	0.239(10)	0.730(8)	0.189(6)
H(7B)	0.566(10)	0.573(8)	0.349(8)
H(8B)	0.608(10)	0.721(8)	0.578(6)
H(12B)	0.708(8)	0.711(8)	0.353(9)
H(11B)	0.495(12)	0.620(8)	0.194(7)
H(5B)	0.303(10)	0.920(6)	0.361(9)
H(9B)	0.599(11)	0.941(5)	0.476(8)
H(10B)	0.569(10)	0.874(7)	0.249(8)
H(4B)	0.337(11)	0.831(11)	0.557(11)

Table B.1 Atomic Coordinates for All Hydrogen Atoms in 1-CH_3OCH_2-2-{$AsPh_3Au$}-1,2-*closo*-$C_2B_{10}H_{10}$ (**4e**).

	U11	U22	U33	U23	U13	U12
Au	0.0408(2)	0.0352(2)	0.0396(2)	0.0006(1)	0.0043(1)	0.0063(1)
As	0.0367(5)	0.0353(4)	0.0408(4)	0.0016(3)	0.0066(3)	0.0077(3)
C(11)	0.033(4)	0.044(4)	0.045(4)	-0.001(3)	0.006(3)	0.012(3)
C(12)	0.042(5)	0.058(5)	0.062(5)	0.012(4)	0.018(4)	0.008(4)
C(13)	0.035(5)	0.102(8)	0.055(5)	0.022(5)	0.023(4)	0.009(5)
C(14)	0.058(6)	0.094(8)	0.056(5)	0.011(5)	0.023(5)	0.037(6)
C(15)	0.085(8)	0.063(6)	0.058(6)	-0.004(5)	0.029(6)	0.009(5)
C(16)	0.056(6)	0.057(5)	0.060(5)	-0.002(4)	0.023(5)	0.002(5)
C(21)	0.036(4)	0.043(4)	0.036(4)	-0.001(3)	0.006(3)	0.013(3)
C(22)	0.045(6)	0.047(5)	0.089(7)	0.010(5)	-0.017(5)	0.014(4)
C(23)	0.074(8)	0.063(6)	0.086(7)	0.012(5)	-0.023(6)	0.028(6)
C(24)	0.097(9)	0.052(5)	0.054(5)	0.012(4)	0.014(5)	0.038(6)
C(25)	0.061(7)	0.052(5)	0.078(6)	0.019(5)	0.029(5)	0.021(5)
C(26)	0.034(5)	0.058(5)	0.070(6)	0.018(4)	0.027(4)	0.017(4)
C(31)	0.053(5)	0.037(4)	0.044(4)	0.004(3)	0.010(4)	0.025(4)
C(32)	0.071(7)	0.080(7)	0.046(5)	-0.019(4)	-0.006(5)	0.047(6)
C(33)	0.077(8)	0.096(8)	0.049(5)	-0.005(5)	0.008(5)	0.063(7)
C(34)	0.079(8)	0.084(7)	0.054(5)	0.008(5)	0.003(5)	0.058(6)
C(35)	0.062(7)	0.094(8)	0.049(5)	0.019(5)	-0.003(5)	0.038(6)
C(36)	0.054(6)	0.077(6)	0.032(4)	0.009(4)	0.010(4)	0.021(5)
C(101)	0.032(5)	0.055(5)	0.095(7)	0.029(5)	0.029(5)	0.024(4)
O	0.033(3)	0.088(5)	0.095(5)	0.037(4)	0.030(3)	0.037(3)
C(102)	0.045(6)	0.093(7)	0.082(7)	0.032(6)	0.033(5)	0.033(5)
C(1)	0.023(4)	0.038(4)	0.049(4)	-0.003(3)	0.008(3)	0.021(3)
C(2)	0.043(5)	0.026(3)	0.035(4)	-0.001(3)	0.008(3)	0.007(3)
B(3)	0.028(4)	0.040(4)	0.036(4)	0.010(3)	0.009(3)	0.017(3)
B(6)	0.033(5)	0.038(4)	0.047(5)	0.012(4)	0.006(4)	0.014(4)
B(7)	0.026(5)	0.050(5)	0.053(5)	0.006(4)	0.014(4)	0.024(4)
B(8)	0.028(5)	0.072(6)	0.048(5)	0.002(5)	0.004(4)	0.014(5)
B(12)	0.026(5)	0.061(6)	0.073(7)	0.020(5)	0.017(5)	0.007(4)
B(11)	0.042(5)	0.050(5)	0.036(4)	0.007(4)	0.021(4)	0.021(4)
B(5)	0.043(6)	0.036(4)	0.078(7)	0.002(4)	0.013(5)	0.020(4)
B(9)	0.040(6)	0.052(6)	0.075(7)	-0.006(5)	0.000(5)	0.003(5)
B(10)	0.038(5)	0.049(5)	0.055(5)	0.018(4)	0.011(4)	0.010(4)
B(4)	0.049(6)	0.045(5)	0.047(5)	-0.010(4)	0.013(4)	0.014(4)

Table B.2 Anisotropic Thermal Parameters ($Å^2$) for All Non-Hydrogen Atoms in **4e**.

	x	y	z
H(12)	0.53527(10)	0.34895(8)	-0.05847(7)
H(13)	0.4272(12)	0.4101(9)	-0.1950(6)
H(14)	0.1602(14)	0.3655(9)	-0.2607(6)
H(15)	0.0050(12)	0.2460(11)	-0.1918(7)
H(16)	0.1153(10)	0.1786(9)	-0.0533(6)
H(22)	0.2355(13)	0.4529(9)	0.0087(7)
H(23)	0.1465(14)	0.6148(10)	0.0861(9)
H(24)	0.2215(15)	0.6162(12)	0.2285(9)
H(25)	0.3633(14)	0.4588(12)	0.3023(7)
H(26)	0.4541(12)	0.2959(10)	0.2318(7)
H(32)	0.6470(12)	0.0516(11)	0.0600(7)
H(33)	0.9262(14)	0.0646(13)	0.0741(8)
H(34)	1.0649(14)	0.2465(14)	0.1218(8)
H(35)	0.9204(13)	0.4237(13)	0.1364(8)
H(36)	0.6423(12)	0.4160(10)	0.1177(7)
H(101)	0.2511(10)	-0.1838(7)	0.1111(5)
H(102)	0.1042(10)	-0.1029(7)	0.1372(5)
H(103)	0.2809(10)	-0.1243(7)	0.2073(5)

Table B.3 Atomic Coordinates for All Hydrogen Atoms in $AsPh_3AuMe$ (**5**).

	U11	U22	U33	U23	U13	U12
Au(1)	0.0479(2)	0.0475(2)	0.0490(3)	0.0031(2)	0.0114(2)	-0.0076(2)
As(1)	0.0407(5)	0.0463(6)	0.0478(6)	0.0023(5)	0.0116(5)	-0.0065(4)
C(11)	0.052(6)	0.050(6)	0.046(6)	-0.006(5)	0.018(5)	-0.013(5)
C(12)	0.058(6)	0.057(6)	0.051(7)	-0.001(5)	0.019(5)	-0.011(5)
C(13)	0.063(7)	0.065(7)	0.044(7)	-0.003(6)	0.012(5)	-0.020(6)
C(14)	0.095(9)	0.065(7)	0.035(6)	0.004(5)	0.015(6)	-0.007(7)
C(15)	0.046(6)	0.098(9)	0.055(8)	0.001(7)	0.000(6)	0.001(6)
C(16)	0.040(6)	0.070(7)	0.049(7)	0.011(5)	0.004(5)	0.002(5)
C(21)	0.041(6)	0.046(5)	0.053(7)	0.008(5)	0.012(5)	-0.001(4)
C(22)	0.071(7)	0.054(6)	0.062(7)	0.002(6)	0.027(6)	-0.003(6)
C(23)	0.072(8)	0.057(7)	0.100(11)	0.000(7)	0.034(8)	0.005(6)
C(24)	0.074(8)	0.079(9)	0.073(9)	-0.025(8)	0.027(7)	-0.008(7)
C(25)	0.074(8)	0.092(9)	0.053(7)	-0.018(8)	0.024(6)	-0.016(8)
C(26)	0.060(7)	0.065(7)	0.059(8)	-0.005(6)	0.017(6)	-0.011(6)
C(31)	0.031(5)	0.060(6)	0.054(7)	0.004(5)	0.012(5)	-0.004(5)
C(32)	0.060(7)	0.074(8)	0.067(8)	-0.014(7)	0.019(6)	-0.002(6)
C(33)	0.052(7)	0.100(10)	0.095(10)	-0.006(9)	0.028(7)	0.020(7)
C(34)	0.045(7)	0.135(13)	0.081(10)	0.019(9)	0.020(7)	0.008(8)
C(35)	0.042(6)	0.106(10)	0.088(10)	-0.013(8)	-0.001(6)	-0.025(7)
C(36)	0.050(6)	0.070(8)	0.090(9)	-0.011(7)	0.018(6)	-0.013(6)
C(1)	0.048(5)	0.031(5)	0.043(6)	0.013(4)	0.011(4)	-0.018(4)

Table B.4 Anisotropic Thermal Parameters ($Å^2$) for All Non-Hydrogen Atoms in **5**.

	x	y	z
H(11)	0.2695(11)	-0.0053(8)	0.5078(9)
H(12)	0.0306(11)	0.0663(8)	0.3776(9)
H(13)	-0.0791(11)	0.2073(8)	0.4730(9)
H(14)	0.0919(11)	0.2229(8)	0.6622(9)
H(15)	0.3074(11)	0.0916(8)	0.6837(9)
H(101)	0.3835(14)	0.4870(12)	0.5849(11)
H(111)	0.3969(14)	0.4594(12)	0.7100(11)
H(102)	0.0475(14)	0.3873(12)	0.5870(11)
H(112)	0.1362(14)	0.4996(12)	0.5658(11)
H(122)	0.1648(14)	0.4541(12)	0.6887(11)
H(3B)	0.481(11)	0.374(9)	0.468(6)
H(4B)	0.649(12)	0.478(5)	0.665(8)
H(10B)	0.576(12)	0.157(9)	0.470(6)
H(11B)	0.782(11)	0.319(9)	0.526(8)
H(12B)	0.794(11)	0.111(6)	0.660(9)
H(5B)	0.65965	0.38425	0.81427
H(6B)	0.45035	0.21985	0.75910
H(7B)	0.88382	0.32706	0.74386
H(8B)	0.73607	0.16654	0.81585
H(9B)	0.54204	0.05816	0.64741

Table B.5 Atomic Coordinates for All Hydrogen Atoms in 1-CH_3OCH_2-2-{$CpTiCl_2$}-1,2-*closo*-$C_2B_{10}H_{10}$ (**8**).

	U11	U22	U33	U23	U13	U12
Ti	0.033(2)	0.028(2)	0.036(2)	0.002(2)	0.015(1)	-0.002(2)
Cl(1)	0.058(3)	0.073(4)	0.039(3)	-0.014(3)	0.020(3)	-0.014(3)
Cl(2)	0.053(3)	0.050(3)	0.051(3)	0.010(3)	-0.002(3)	0.004(3)

Table B.6 Anisotropic Thermal Parameters ($Å^2$) for Titanium and Chlorine Atoms in **8**.

	x	y	z
H(12)	0.1516(11)	0.4378(7)	0.4463(3)
H(13)	0.3181(13)	0.3506(9)	0.4807(4)
H(14)	0.4385(12)	0.2331(9)	0.4496(4)
H(15)	0.3715(13)	0.1875(8)	0.3860(4)
H(16)	0.2000(10)	0.2736(7)	0.3500(3)
H(22)	-0.0009(11)	0.5976(7)	0.3355(4)
H(23)	0.1278(13)	0.6842(8)	0.2903(4)
H(24)	0.3539(13)	0.6369(10)	0.2690(4)
H(25)	0.4329(13)	0.4909(9)	0.2855(4)
H(26)	0.3065(12)	0.4036(8)	0.3320(3)
H(3B)	-0.009(9)	0.236(8)	0.360(4)
H(4B)	-0.297(13)	0.196(7)	0.360(3)
H(5B)	-0.403(12)	0.349(9)	0.356(3)
H(6B)	-0.263(14)	0.473(6)	0.349(4)
H(7B)	0.054(8)	0.321(9)	0.295(4)
H(8B)	-0.115(12)	0.170(5)	0.290(4)
H(9B)	-0.374(11)	0.243(8)	0.276(3)
H(10B)	-0.361(11)	0.423(7)	0.281(4)
H(11B)	-0.074(12)	0.455(6)	0.286(4)
H(12B)	-0.185(12)	0.329(8)	0.2463(19)
H(101)	-0.3207(11)	0.2998(8)	0.4149(3)
H(111)	-0.2600(11)	0.4071(8)	0.4117(3)
H(102)	-0.0344(15)	0.3084(10)	0.4770(4)
H(112)	-0.2115(15)	0.2898(10)	0.4753(4)
H(122)	-0.1474(15)	0.3959(10)	0.4703(4)

Table B.7 Atomic Coordinates for All Hydrogen Atoms in 1-CH_3OCH_2-2-{PPh_2AuCl}-1,2-*closo*-$C_2B_{10}H_{10}$ (**12**).

	U11	U22	U33	U23	U13	U12
Au	0.0372(3)	0.0371(3)	0.0383(3)	-0.0071(2)	0.0065(2)	0.0010(2)
P	0.029(1)	0.035(1)	0.033(1)	-0.003(1)	0.000(1)	0.003(1)
Cl	0.059(2)	0.066(2)	0.068(2)	-0.028(2)	0.022(2)	0.000(2)
C(11)	0.031(5)	0.033(5)	0.034(6)	0.006(5)	0.002(5)	0.010(4)
C(12)	0.046(6)	0.043(6)	0.047(7)	-0.004(6)	-0.013(5)	-0.002(5)
C(13)	0.078(9)	0.076(9)	0.034(7)	0.009(7)	-0.001(6)	0.010(8)
C(14)	0.041(7)	0.082(10)	0.070(10)	0.011(8)	-0.006(7)	0.027(7)
C(15)	0.059(8)	0.054(7)	0.063(9)	0.005(7)	0.003(7)	0.024(6)
C(16)	0.042(6)	0.051(6)	0.040(7)	-0.007(5)	-0.001(5)	0.008(5)
C(21)	0.025(5)	0.043(6)	0.035(6)	0.001(5)	-0.001(4)	0.004(4)
C(22)	0.046(6)	0.034(6)	0.057(8)	0.009(6)	0.009(6)	0.004(5)
C(23)	0.060(8)	0.053(7)	0.063(9)	0.024(7)	-0.001(7)	-0.006(6)
C(24)	0.058(8)	0.081(10)	0.064(10)	0.020(8)	0.007(7)	-0.009(7)
C(25)	0.047(7)	0.075(9)	0.070(10)	0.023(8)	0.027(7)	0.015(7)
C(26)	0.039(6)	0.059(7)	0.056(8)	0.000(7)	0.009(6)	0.014(6)
C(1)	0.032(5)	0.049(6)	0.038(7)	-0.002(5)	0.011(5)	0.003(5)
C(2)	0.029(5)	0.033(5)	0.033(6)	0.002(5)	0.014(4)	0.007(4)
B(3)	0.035(7)	0.037(7)	0.050(9)	0.000(6)	-0.002(6)	-0.001(5)
B(4)	0.047(8)	0.055(9)	0.067(11)	-0.015(8)	-0.007(8)	-0.017(7)
B(5)	0.030(7)	0.069(9)	0.059(10)	-0.007(8)	-0.008(6)	-0.013(7)
B(6)	0.029(6)	0.062(9)	0.052(9)	0.000(8)	0.000(6)	0.010(6)
B(7)	0.026(6)	0.052(7)	0.044(8)	-0.011(6)	-0.005(5)	0.005(5)
B(8)	0.040(7)	0.052(8)	0.053(9)	-0.014(7)	-0.005(6)	-0.009(6)
B(9)	0.040(8)	0.049(8)	0.079(12)	-0.009(8)	-0.001(7)	-0.009(6)
B(10)	0.038(7)	0.065(9)	0.049(9)	-0.009(7)	-0.006(6)	0.017(7)
B(11)	0.028(6)	0.048(7)	0.035(7)	0.005(6)	-0.003(5)	0.006(5)
B(12)	0.056(8)	0.057(8)	0.033(8)	-0.013(7)	-0.012(7)	0.020(7)
C(101)	0.042(6)	0.056(7)	0.036(7)	0.004(5)	0.007(5)	-0.008(5)
O	0.047(5)	0.083(6)	0.031(4)	0.002(4)	0.009(4)	-0.010(4)
C(102)	0.087(10)	0.084(10)	0.059(10)	0.024(8)	-0.015(8)	-0.018(9)

Table B.8 Anisotropic Thermal Parameters ($Å^2$) for All Non-Hydrogen Atoms in **12**.

	x	y	z
H(12)	0.4366(5)	0.1005(4)	0.4788(4)
H(13)	0.3232(6)	0.1356(5)	0.5938(4)
H(14)	0.1398(6)	0.1979(6)	0.5298(5)
H(15)	0.0702(6)	0.2262(7)	0.3530(5)
H(16)	0.1856(5)	0.1957(5)	0.2361(4)
H(22)	0.3376(5)	-0.0843(5)	0.3483(5)
H(23)	0.3108(7)	-0.3003(5)	0.2820(6)
H(24)	0.3206(7)	-0.3815(6)	0.1084(6)
H(25)	0.3525(7)	-0.2487(5)	-0.0022(6)
H(26)	0.3708(5)	-0.0351(5)	0.0602(4)
H(3p)	0.596(6)	0.206(6)	0.171(4)
H(4p)	0.820(6)	0.429(5)	0.304(5)
H(5p)	0.801(6)	0.494(4)	0.506(5)
H(6p)	0.578(5)	0.320(6)	0.487(5)
H(7p)	0.609(5)	0.017(4)	0.257(4)
H(8p)	0.832(6)	0.309(6)	0.606(3)
H(9p)	0.983(4)	0.373(5)	0.483(5)
H(10p)	0.845(6)	0.178(6)	0.270(5)
H(11p)	0.597(6)	0.080(5)	0.458(5)
H(12p)	0.846(6)	0.104(5)	0.456(5)
H(21p)	0.5253(5)	0.3798(5)	0.2195(5)
H(31p)	0.6374(5)	0.5079(5)	0.3333(5)
H(22p)	0.3485(8)	0.4744(7)	0.3640(7)
H(32p)	0.3672(8)	0.4630(7)	0.2415(7)
H(42p)	0.4845(8)	0.5789(7)	0.3624(7)
H(3a)	0.082(6)	0.026(4)	-0.137(5)
H(4a)	-0.066(4)	0.139(5)	-0.259(5)
H(5a)	0.040(6)	0.396(5)	-0.133(5)
H(6a)	0.230(6)	0.412(5)	0.060(4)
H(7a)	0.333(6)	0.115(5)	-0.133(5)
H(8a)	0.126(6)	0.094(5)	-0.338(4)
H(9a)	0.095(6)	0.315(5)	-0.319(4)
H(10a)	0.295(6)	0.502(4)	-0.126(5)
H(11a)	0.445(4)	0.374(5)	0.001(4)
H(12a)	0.353(5)	0.307(6)	-0.244(5)
H(21a)	-0.0036(7)	0.1011(9)	-0.0227(6)
H(31a)	-0.0752(7)	0.2051(9)	-0.0602(6)
H(22a)	0.0672(12)	0.3829(14)	0.2096(10)
H(32a)	-0.0834(12)	0.2759(14)	0.1114(10)
H(42a)	0.0024(12)	0.3991(14)	0.0807(10)

Table B.9 Atomic Coordinates for All Hydrogen Atoms in 1-CH_3OCH_2-2-(1'-CH_3OCH_2-2'-{PPh_2Au}-1',2'-*closo*-$C_2B_{10}H_{10}$)-1,2-*closo*-$C_2B_{10}H_{10}$ **(14).**

	U11	U22	U33	U23	U13	U12
Au	0.0409(1)	0.0405(1)	0.0400(1)	0.0145(1)	0.0165(1)	0.0158(1)
P	0.0343(6)	0.0342(5)	0.0404(5)	0.0130(4)	0.0172(5)	0.0124(5)
C(11)	0.032(2)	0.035(2)	0.045(2)	0.011(2)	0.017(2)	0.009(2)
C(12)	0.055(3)	0.052(3)	0.054(3)	0.023(2)	0.029(2)	0.021(2)
C(13)	0.076(4)	0.074(4)	0.057(3)	0.028(3)	0.041(3)	0.029(3)
C(14)	0.067(4)	0.096(5)	0.073(4)	0.027(3)	0.047(3)	0.035(4)
C(15)	0.058(4)	0.106(5)	0.077(4)	0.031(4)	0.037(3)	0.045(4)
C(16)	0.048(3)	0.071(3)	0.053(3)	0.021(2)	0.027(2)	0.030(3)
C(21)	0.035(2)	0.031(2)	0.052(2)	0.010(2)	0.016(2)	0.011(2)
C(22)	0.058(3)	0.043(3)	0.071(3)	0.021(2)	0.028(3)	0.016(2)
C(23)	0.098(5)	0.043(3)	0.103(5)	0.029(3)	0.043(4)	0.025(3)
C(24)	0.105(6)	0.041(3)	0.106(5)	0.007(3)	0.037(5)	0.026(3)
C(25)	0.083(5)	0.052(3)	0.086(4)	-0.003(3)	0.038(4)	0.018(3)
C(26)	0.060(3)	0.046(3)	0.067(3)	0.009(2)	0.032(3)	0.014(2)
C(1p)	0.044(3)	0.031(2)	0.066(3)	0.017(2)	0.026(2)	0.007(2)
C(2p)	0.035(2)	0.029(2)	0.048(2)	0.013(2)	0.019(2)	0.009(2)
B(3p)	0.042(3)	0.057(3)	0.057(3)	0.019(3)	0.027(3)	0.015(3)
B(4p)	0.042(3)	0.062(4)	0.086(4)	0.033(3)	0.032(3)	0.007(3)
B(5p)	0.052(4)	0.039(3)	0.074(4)	0.008(3)	0.018(3)	-0.001(3)
B(6p)	0.040(3)	0.040(3)	0.049(3)	0.004(2)	0.013(2)	0.004(2)
B(7p)	0.038(3)	0.043(3)	0.074(4)	0.012(3)	0.026(3)	0.015(2)
B(8p)	0.038(3)	0.062(4)	0.060(4)	0.016(3)	0.009(3)	0.006(3)
B(9p)	0.039(3)	0.059(4)	0.098(5)	0.025(4)	0.025(3)	0.005(3)
B(10p)	0.042(3)	0.069(4)	0.085(5)	0.022(3)	0.033(3)	0.020(3)
B(11p)	0.040(3)	0.048(3)	0.065(3)	0.026(3)	0.017(3)	0.014(3)
B(12p)	0.037(3)	0.053(3)	0.094(5)	0.027(3)	0.021(3)	0.016(3)
C(11p)	0.062(3)	0.038(3)	0.089(4)	0.029(3)	0.035(3)	0.019(2)
O(1p)	0.076(3)	0.065(3)	0.115(3)	0.038(2)	0.051(3)	0.043(2)
C(12p)	0.115(6)	0.082(5)	0.119(6)	0.034(4)	0.054(5)	0.067(5)
C(1a)	0.047(3)	0.070(3)	0.063(3)	0.027(3)	0.023(3)	0.027(3)
C(2a)	0.045(3)	0.049(3)	0.037(2)	0.016(2)	0.017(2)	0.016(2)
B(3a)	0.060(4)	0.046(3)	0.051(3)	0.011(3)	0.010(3)	0.009(3)
B(4a)	0.051(4)	0.076(5)	0.059(4)	0.027(3)	0.005(3)	0.011(3)
B(5a)	0.097(6)	0.075(5)	0.076(4)	0.036(4)	0.030(4)	0.055(5)
B(6a)	0.096(5)	0.041(3)	0.054(3)	0.017(3)	0.020(4)	0.027(3)
B(7a)	0.071(4)	0.075(4)	0.061(4)	0.022(3)	0.037(3)	0.040(4)
B(8a)	0.086(5)	0.068(4)	0.048(3)	0.017(3)	0.022(3)	0.025(4)
B(9a)	0.070(4)	0.073(4)	0.054(4)	0.030(3)	0.018(3)	0.019(4)
B(10a)	0.087(5)	0.056(4)	0.066(4)	0.032(3)	0.011(4)	0.004(4)
B(11a)	0.048(4)	0.074(4)	0.053(3)	0.025(3)	0.012(3)	0.001(3)
B(12a)	0.065(4)	0.099(5)	0.054(4)	0.036(4)	0.027(3)	0.018(4)
C(11a)	0.073(5)	0.146(7)	0.095(5)	0.056(5)	0.050(4)	0.057(5)
O(1a)	0.105(5)	0.291(10)	0.083(4)	0.047(5)	0.052(4)	0.110(6)
C(12a)	0.161(12)	0.339(21)	0.157(11)	0.030(12)	0.062(9)	0.177(14)

Table B.10 Anisotropic Thermal Parameters ($Å^2$) for All Non-Hydrogen Atoms in **14.**

	x	y	z
H(12)	0.4920(5)	0.7200(3)	-0.0870(3)
H(13)	0.2771(5)	0.7890(3)	-0.1601(3)
H(14)	0.2013(6)	0.7319(4)	-0.3020(3)
H(15)	0.3391(5)	0.6086(4)	-0.3795(3)
H(16)	0.5478(6)	0.5331(4)	-0.3060(3)
H(32)	0.4823(5)	0.4498(3)	0.1352(3)
H(34)	0.2699(5)	0.5292(4)	-0.1052(3)
H(36)	0.4905(5)	0.2633(3)	-0.0876(3)
H(31A)	0.6069(6)	0.2187(3)	0.0445(4)
H(31B)	0.5262(6)	0.2598(3)	0.1422(4)
H(31C)	0.6843(6)	0.3135(3)	0.1024(4)
H(33A)	0.2617(7)	0.6309(4)	0.0160(4)
H(33B)	0.4159(7)	0.6293(4)	0.0836(4)
H(33C)	0.2562(7)	0.5742(4)	0.1192(4)
H(35A)	0.3706(6)	0.3022(4)	-0.2186(4)
H(35B)	0.3748(6)	0.4233(4)	-0.2440(4)
H(35C)	0.2141(6)	0.3711(4)	-0.2062(4)
H(2C)	0.696(10)	0.424(7)	-0.220(6)
H(12B)	0.009(8)	0.465(5)	-0.017(5)
H(11B)	0.943(6)	0.402(5)	-0.212(4)
H(4B)	0.626(8)	0.647(5)	-0.005(5)
H(6B)	0.801(7)	0.584(5)	-0.280(4)
H(5B)	0.843(7)	0.715(4)	-0.151(4)
H(7B)	0.797(7)	0.331(5)	-0.056(4)
H(9B)	0.946(7)	0.642(5)	0.014(5)
H(10B)	1.077(6)	0.592(5)	-0.150(4)
H(8B)	0.786(8)	0.478(5)	0.070(5)

Table B.11 Atomic Coordinates for All Hydrogen Atoms in 1-Ph-3-(η^6-mes)-3,1,2-*closo*-$RuC_2B_9H_{10}$ **(23).**

	U11	U22	U33	U23	U13	U12
Ru(3)	0.0140(2)	0.0193(2)	0.0198(2)	-0.0003(1)	0.0003(1)	-0.0002(1)
C(1)	0.023(2)	0.022(2)	0.015(2)	0.001(1)	0.011(2)	-0.005(2)
C(11)	0.023(2)	0.022(2)	0.027(2)	0.005(2)	0.005(2)	-0.005(2)
C(12)	0.039(2)	0.030(2)	0.040(2)	0.012(2)	0.001(2)	0.011(2)
C(13)	0.034(2)	0.039(2)	0.053(3)	0.022(2)	0.003(2)	0.008(2)
C(14)	0.030(2)	0.061(3)	0.047(3)	0.031(2)	-0.009(2)	-0.001(2)
C(15)	0.028(2)	0.064(3)	0.044(3)	0.010(2)	-0.024(2)	-0.010(3)
C(16)	0.029(2)	0.045(2)	0.033(2)	0.009(2)	-0.004(2)	-0.005(2)
C(31)	0.026(2)	0.031(2)	0.031(2)	0.004(2)	0.007(2)	-0.002(2)
C(32)	0.026(2)	0.028(2)	0.023(2)	0.001(2)	0.015(2)	-0.004(2)
C(33)	0.017(2)	0.035(2)	0.035(2)	0.002(2)	0.005(2)	0.004(2)
C(34)	0.013(2)	0.037(2)	0.044(3)	0.006(2)	-0.001(2)	0.003(2)
C(35)	0.015(2)	0.037(2)	0.035(2)	0.001(2)	0.006(2)	-0.011(2)
C(36)	0.018(2)	0.030(2)	0.037(2)	-0.008(2)	0.000(2)	-0.010(2)
C(311)	0.041(3)	0.031(2)	0.060(3)	0.009(2)	-0.011(3)	-0.013(2)
C(331)	0.057(3)	0.033(2)	0.043(3)	-0.005(2)	0.013(2)	0.009(2)
C(351)	0.041(3)	0.050(3)	0.038(2)	0.005(2)	-0.008(2)	-0.019(2)
C(2)	0.027(2)	0.036(2)	0.027(2)	0.002(2)	0.007(2)	0.009(2)
B(12)	0.012(2)	0.044(3)	0.038(3)	0.005(2)	0.002(2)	-0.002(2)
B(11)	0.025(2)	0.039(3)	0.032(2)	-0.002(2)	0.009(2)	0.008(2)
B(4)	0.015(2)	0.032(2)	0.026(2)	0.000(2)	-0.002(2)	-0.008(2)
B(6)	0.029(2)	0.032(2)	0.031(2)	0.003(2)	0.009(2)	-0.005(2)
B(5)	0.025(2)	0.029(2)	0.038(2)	0.003(2)	0.002(2)	-0.014(2)
B(7)	0.016(2)	0.019(2)	0.038(2)	0.000(2)	-0.004(2)	0.005(2)
B(9)	0.029(3)	0.030(2)	0.030(2)	-0.007(2)	-0.013(2)	-0.007(2)
B(10)	0.022(2)	0.047(3)	0.040(3)	0.013(2)	-0.007(2)	-0.010(2)
B(8)	0.024(2)	0.038(3)	0.022(2)	0.005(2)	-0.003(2)	-0.008(2)

Table B.12 Anisotropic Thermal Parameters ($Å^2$) for All Non-Hydrogen Atoms in **23.**

APPENDIX C

LECTURES, COURSES AND MEETINGS ATTENDED

Inorganic Medicinal Chemistry by Drs. S.K. Chapman and A.J. Welch.

EPR Spectroscopy by Dr. R.E.P Winpenny.

Computers in Chemistry by Drs. M.A.D. Fluendy, K.P. Lawley and G.S. McDougall.

Departmental Postgraduate Lectures, Research Seminars and Colloquia, 1989-1992.

Inorganic Section Meetings, 1989-1992.

B.C.A Residential Crystallography School, Aston, Birmingham, April 1991.

Intraboron X, XI and *XII*, Annual meetings of UK Boron Chemists, 1989-1992.

Waddington Graduate Symposium on Inorganic Chemistry, Durham, 1990.

University of Strathclyde Inorganic Club Meetings, 1991 and 1992.

RSC, Scottish Dalton Division Meeting, Edinburgh, 1992

1st International Conference on the Chemistry of the Copper and Zinc Triads, Edinburgh, 1992.

29th International Conference on Coordination Chemistry, Lausanne, Switzerland, 1992.